Landscape evolution modelling in large, complex braided river the Brahmaputra: A case study of Majuli Island, North-East India.

Prasujya Gogoi

Thesis submitted to the University of Nottingham for the degree of Doctor of Philosophy

May 2018

Abstract

The River Brahmaputra is one of the largest rivers, ranking ninth in terms of mean annual discharge (19, 800 m^3s^{-1}). The river has a multi-channel, braided/anastomosed planform that changes frequently and exhibits rapid transformations in channel morphology. This research was set in the context of the River Brahmaputra near Majuli Island, Assam, India. Morphologically, this part of the river is very volatile, increased braiding intensity of the river is believed by many to be responsible for severe erosion in the southern part of Majuli Island. Therefore in this research, a medium-term morphological evolution and change are investigated, in a study reach of 40 km near southern part of Majuli Island, Assam. There is a limited number of morphological models that can model the landscape evolution of braided rivers. Beside this, there is high cost and difficulty in collecting the hydrological, hydraulic, morphometric and sediment data needed to run a 2D, physics-based model in a very large, complex braided river, particularly as data for such rivers is often sensitive and therefore classified. Therefore the best alternative for modelling complex, braided rivers with limited data availability is to use a form of simplified morphological model which is known as a reduced complexity model or RCM. The rcm model CAESAR-Lisflood was used in this research to model medium term channel evolution. New indices were developed to validate the rcm model which quantify lateral shifting of the thalweg (Thalweg Migration Index, TMI), braiding intensity (Modified Plan Form Index, MPFI), cross-sectional disposition of anabranch channels (Modified Flow Geometry Index, MFGI) and change in bar area (Bar Deformation Index, BDI). Trends and changes in the four braiding indices that were forecast by the C-L + models indicated that the Brahmaputra in the study reach is likely to remain volatile morphologically for the next two decades. Deposition in this reach is very likely to continue to exceed erosion, with net deposition increasing through time due to increased sediment inputs associated with greater monsoon runoff. The River Brahmaputra may widen its primary channel in response to increased runoff and net deposition and therefore the braiding intensity will most probably intensify. The thalweg channel may remain shifting northwards towards Majuli Island. The number of sandbars is likely to increase and rates at which sandbars are

formed and deformed are likely to rise. The bank erosion and loss of floodplain may become more severe, especially in the southern part of Majuli Island.

Acknowledgment

The origin of the research work presented in this thesis lies far from the verdant campus of the University of Nottingham, in the north-eastern state of Assam in India where the mighty river Brahmaputra flows with vigour and magnificence. The incredible force with which the river flows through the region has led to the evolution of an incredibly dynamic braided network of channels and rise of the largest river island in the world, the Majuli Island. While growing up in the vicinity of this river, somewhere along my formative years the river grew on me, too. It is therefore only fitting that my passion for the river Brahmaputra culminated into this PhD based on Majuli Island.

For a body of work that spans nearly four years and two continents, I have a long list of people to thank.

First and foremost, I would like to begin by thanking my primary supervisor Prof Colin Thorne who is the reason behind this project. It all began with his enthusiastic response to my tentative enquiry that led me to undertake this project as my PhD research here at the University of Nottingham. His constant academic support to work on such a challenging project is immense and invaluable. I am grateful to him for introducing me to several people who I have benefited from, building research and institutional collaborations, and for bringing his treasure of knowledge and experience to this thesis. Without him this thesis would have simply not been possible.

In this endeavour I owe similar profound gratitude to my co-supervisor Dr Nick Mount whose insight into the subject matter forms the foundation of this research. His vast knowledge on hydro-informatics has provided me the superior technical advice that was required in my work. The thought provoking discussions that I have had with him on a wide range of topics kept me motivated throughout. His constant encouragement and faith in me is what kept me going, for I see him as much as a friend as a co-supervisor.

This research would have also not been possible without the considerable input from Prof Nayan Sharma and his research group at IIT Roorkee in India. The help I received from him and his group in collecting the hydrological data and making new braiding indices for validating the model is worthy of more than just a special mention. Without their help data collection would been very difficult for someone like myself coming from a foreign institution. His expertise on river Brahmaputra and its morphology gave me a much deeper understanding of this river to be able to build the foundation of my research. I am indebted to Prof Sharma for his sincerity in taking care of my comfort during my stay at IIT Roorkee. Despite being far away from Nottingham I never felt that he was ever more than a phone call away to discuss and resolve my problems.

I would like to express my gratitude to the Vice Chancellor of Tezpur Central University, Assam, India, for allowing me to use their geo-technical laboratory to carry out the laboratory work. In this regard, I must mention the most essential help I received during my fieldwork from Dr Jahnu Baruah, Ajit Konwar, Diganta, Neeraj Khaund for their assistance during a difficult, flood-ridden situation, and my childhood friend Navaneeta Bhuyan, who provided me a comfortable homely accommodation during my visit to Assam.

I would also like to thank Bhaskar Das, Assistant Engineer, Department of Water Resource, Guwahati, Assam, India, for providing additional discharge data, and Purusutam Das, Assistant Director, Town and Country Planning Organisation, Assam, India, for his selfless effort in collecting the data in my absence. I also appreciate Jamal Zohepur’s help and support in acquiring forecast hydrological data to run the forecasting models.

I would also like to express my sincere appreciation towards Prof Tom Coulthard (University of Hull) and Dr Tim Meadow for their timely advice while running the model. To John Milner (University of Nottingham), for providing the all-important IT resources in this journey of modelling RCM models. Without John’s support, I cannot imagine completing my simulations in the Ebdon computer lab at the School of Geography.

This research was supported by several funding bodies and I owe it to each one of them. First of all, I would like to thank the International office, University of Nottingham, for awarding me the Vice Chancellor Scholarship of Research Excellence to complete my study here at Nottingham. Additional financial support was provided by Newton Bhaba PhD Placement Award by Newton Fund in collaboration with the British Council UK and Department of Biotechnology, India. Further, I also owe my sincere gratitude towards Funds for Women Graduate and Sir Rischard Stapely Educational Trust for providing me the living and maintenance allowance while pursing my PhD.

Completing this thesis has been a long and an arduous journey and I couldn't have done it without the unflinching support I have received from my family and friends. There are no words to describe how much I owe to my dad Dandeswar Gogoi, my mom Bina Gogoi Goswami and my younger brother Ganjan Surya Gogoi, without whose emotional, financial and sometimes academic support I would have simply not been able to complete my PhD.

I also owe a lot to my aunt Renu Gogoi for being there for me whenever I wanted her talk to her, discuss with her, or just be myself.

Finally, special thanks to my dear friends Sulila, Dhamendra, Joli, Barasa ba, Parul, Debi, Games and Pratyush for keeping me going through the most difficult times and encouraging me daily. For their friendship, no words are necessary, nor will suffice.

Prasujya Gogoi

Abbreviations

ADCP: Acoustic Doppler Current Profiler

AHP: Analytic Hierarchy Process

BB: Braided Bar

BM: Measure of braiding channel

BDI: Bar Deformation Index

CAESAR: Cellular Automaton Evolutionary Slope and River

C-L: CAESAR Lisflood hindcast

C-L+: CAESAR Lisflood forecast

C.I.: Consistency Index

CFD: Computational Fluid Dynamics

CRZ: Coastal Regulation Zone

CH: Thalweg Changes and Bankline Migration

CHB: Channel Belt Area

C.S: Cross-section

CSC: Cross-sectional position

DEM: Digital Elevation Model

DPR: Detail Project Report

DHK: Dhakhinpat Sediment Sample

ETM: Enhanced Thematic Mapper

FGI: Flow Geometry Index

GIS: Geographical Information System

GLUE: Generalised Likelihood Uncertainty Estimation

GDS: Gauge Discharge Site

GHM: Global hydrological model

HTL: High Tide Line

ISIMIP: Inter- Sectoral Impact Model Inter-comparison Project

IRS LISS: Indian Remote Sensing Satellite Linear Imaging Self scanning sensor

INSAT LISS: Indian National Satellite System Linear Imaging Self scanning sensor

IIT: Indian Institute of Technology

JULES: Joint UK Land Environment Simulator

LPJmL: Lund Potsdam Jena managed Land

LEM: Landscape Evolution Model

LSM: Landsurface model

LIDAR: Light Detection and Ranging

MPFI: Modified Plan Form Index

MFGI: Modified Flow Geometry Index

MAE: Mean Absolute Error

MARE: Mean Absolute Relative Error

MSS: Multi Spectral Scanner

MRE: Mean Relative Error

MacPDM: Macro-scale probability distribution moisture model

NDVI: Normalised Difference Vegetation Index

NIR: Near Infrared

PFI: Plan Form Index

R: Red band

RCC: Roller compact concrete

RRZ: River Regulation Zone

RME: Relative Mean Error

RAE: Relative Absolute Error

R.I.: Random consistency

RCP: Representative Concentration Pathways

RCM: Reduced Complexity Model

SAC: Space Application Centre

S: Sediment Discharge

SRTM: Shuttle Radar Topography Mission

SSL_C: Suspended Sediment Load Coarse

SSL_M: Suspended Sediment Load Medium Fine

SSL_F: Suspended Sediment Load Fine

TMI: Thalweg Migration Index

TM: Thematic Mapper

TLM: Lateral Position of the Channel

USGS: United States Geological Survey

W: Channel Belt Width

WP: Wetted Perimeter

Table of Contents

List of figures:

List of tables:

Chapter 1: Introduction

1.1 Setting the scene

The Brahmaputra is one of the largest rivers on Earth, ranking ninth in terms of mean annual discharge (19, 800 m^3s^{-1}). It drains a basin usually stated as having an area of 520,000, although this has been revised to 712,035 km^2 based on recent satellite-based terrain analysis (Assam Tribune, 2011). The overall length of the Tsangpo-Brahmaputra-Padma-Meghna drainage system from its source at the Angsi Glacier in the high Himalayas to the sea at the Bay of Bengal is 5,425 km. The river carries a heavy load of sediment, varying between about 500 million and over 1 billion tonnes per year depending on the magnitude and duration of the annual monsoon flood (Sarker, 2008).

The middle course of the Brahmaputra runs through the Vale of Assam in India. In this reach, the river has a multi-channel, braided/anastomosed planform that changes almost constantly and periodically exhibits rapid transformations in channel morphology. In this research, medium-term trends of morphological evolution and change are investigated, in a study reach near Majuli Island, Assam. Majuli Island is the World's largest riverine island, though its area decreased during the twentieth century (from a reported 1,255 km^2 in 1901 to just over 420 km^2 in 2001, according to Sarma and Phukan (2004)) due to erosion by the Brahmaputra and it is proposed to make it a UNESCO World Heritage Site with a view to better protecting and conserving the island and its rich culture (TNT, 2018).

To examine the morphological changes of the river Brahmaputra researchers and investigators have used remotely sensed data. The Space Application Centre (SAC) and Brahmaputra Board (1996) have jointly studied the extent of river erosion in Majuli Island. This was undertaken in order to identify and delineate the areas of the island which have undergone changes along the bank line due to dynamic behaviour of the river Brahmaputra. Fluvial landforms are formed due to geomorphological processes operating in the river channel. The channel pattern or the landform of a river or a reach reflects the hydrodynamics of flow within the channel and the allied processes of sediment transfer and energy dissipation (Sharma et al., 2012).

In large rivers like the Brahmaputra, braiding is generally favoured by the very large and highly variable discharge, heavy sediment load (including a substantial component moving as bedload) and easily-eroded, non-cohesive river banks. In the resulting, wide, shallow channels, multiple secondary flow cells split the flow into several high velocity threads, which contribute to the formation of mid-channel bars that grow through time to divide the river into multiple anabranches (Bathurst et al., 1979; Richards, 1982: Richardson and Thorne, 2000).

Das and Saraf (2007) studied course changes in the River Brahmaputra between 1970 and 2002, and the influence of neotectonics in different reaches of the river using Landsat-MSS, TM and ETM images. For assessing the rate of erosion of the river Brahmaputra, Kotoky et al. (2005) studied selected reaches using topo-sheets (1914-1975) and IRS satellite images in the cloud-free period. In this study, they superimposed the bank lines to get the areas of erosion and deposition. However, there was lack of representation of braiding because only the outer bank lines of the river were mapped, even though braiding processes have long been recognised as primarily controlling the distributions of erosion and deposition in time and space (Thorne et al. 1993).

Sharma (2004) did measure the braiding behaviour of the Brahmaputra using Landsat images, applying a Plan Form Index (PFI) to assess and quantify braiding intensity. Nevertheless, a comprehensive study of morphological evolution and braid-channel migration in the Brahmaputra in India has not yet been undertaken.

The understanding past landscape evolution in such a large and complex river and developing the ability to forecast future morphological trends and changes over the medium-term, are key not only to understanding and explaining morpho-dynamics in great rivers like the Brahmaputra, but also to forecasting and managing the impacts of future changes in the riverine landscape on people, property and infrastructure located in and near the river.

There is an increasing demand for understanding, predicting and controlling large braided rivers (Schuurman et al., 2018). However, one-dimensional (1D) hydraulic and sediment models that are routinely used for single-channel rivers are insufficient to simulate the behaviour of braided streams due to their inability to simulate the transverse flow field. For better and more realistic representation of the flow field, two-dimensional (2D) or three dimensional (3D) numerical models are required. However, 3D models are numerically expensive for anything larger than very short river reaches and time scales. Hence, 2D models should be used for realistic hydrological and sediment modelling of braided rivers. Unfortunately, it is not currently feasible to model substantial reaches of a braided river over periods longer than a few months or years using a physics-based, two-dimensional, hydraulic and sediment model with a fully mobile bed and erodible banks.

Reduced Complexity Models (RCM) provide an alternative approach to physics-based simulation of braided rivers because they represent process-form relations in complex geomorphological systems in a simplified manner. However, the simplifications involved in RCM approaches can reduce the suitability of RCMs for making precise forecasts of, for example, the exact future locations of anabranches or bars in a braided stream. On the other hand, RCMs have been found to be able to simulate changes in overall stream morphology (e.g. channel width and braiding intensity), evolutionary trajectory (e.g. narrowing/widening and/or incision/aggradation), and sediment dynamics (e.g. sediment budget) (Ziliani et al., 2013). Hence, there are reasons to believe that RCMs could be useful in modelling gross reach-scale braided river morpho-dynamics.

Past studies have evaluated the capacity of RCMs to reproduce laboratory experiments ((Doeschl-Wilson, 2005), the topographic detail in short river reaches (Nicholas and Quine, 2007), and processes that operate over geological timescales (Coulthard, 2002). However, little attention has so far been paid to the capacity of RCMs to simulate channel behaviour in large, braided rivers at the time and space scales useful for river science, engineering and management.To address this research gap, this study evaluates the capacity of an RCM to model selected morphological indices and behaviours in the braided River Brahmaputra near Majuli Island, Assam.

1.2 Research Question

To what extent can a cellular automaton, landscape evolution model be used to simulate medium-term channel evolution in a large complex braided river? A case study of Majuli Island, in the River Brahmaputra, Northeast India.

1.3 Objectives

1. To undertake a literature review to characterise the major hydrologic, hydraulic and geomorphologic processes driving landscape evolution in Majuli Island, and also undertake a review of the literature on channel evolution modelling in very large, complex rivers.

2. To develop new braiding indices that better describe braided river morphology and that can be used to derive morphological performance metrics for validation and interpretation of numerical models.

3. To identify an appropriate modelling approach and a specific tool for simulating channel evolution processes near Majuli Island at a reach-scale and over the medium-term.

4. To understand the performance and limitations of cellular automaton models in braided river modelling.

5. To identify the data sources and pre-processing requirements for parameterisation of the CAESAR-Lisflood model and to assemble the data required for CAESAR Lisflood to undertake hindcasting of channel evolution.

6. To develop a method for calibrating CAESAR-Lisflood.

7. To assess changes in medium-term river morphological forecasts by the cellular model.

8. Compare the trends and changes forecast using the C-L + H08 model combination with the results of previous studies to assess their plausibility and validate the modelled forecasts of morphological changes responsible for medium-term landscape evolution in Majuli Island.

9. To evaluate the applicability of landscape evolution modelling and interpret research findings in the context of the future river and land management at Majuli Island.

1.4 Thesis Structure

The structure of the thesis is designed to address each of these nine research objectives in turn. Table 1. sets out the structure of this thesis.

Table 1.1. Structure of the thesis

Chapter(s)	Topic(s)
2, 3 and 4 Background, braiding indices and model selection	Description of geomorphological changes occurring in the River Brahmaputra.
	Development of new braiding indices to measure the morphological process response of the river Brahmaputra. Explanation of the need to develop medium-term landscape evolution of the River Brahmaputra near Majuli Island.
	Justification for the use of the CAESAR-Lisflood reduced complexity, cellular automaton model in this research.
5 and 6 Hindcasting	Description of model operation and data requirement.
	Changes in model parameter values and model operation
	Model evaluation criteria and model evaluation
7 Forecasting	Selection of the best fit
	Forecast of reach hydrology
	Ensemble of forecasting runs Trends of medium-term channel evolution (thalweg sub-channel behaviour, braiding intensity)
8 Discussion of contribution to knowledge	Discussion of the new knowledge in the research findings with respect to modelling and forecasting medium-term landscape evolution in the Brahmaputra and other large, braided rivers.
9 Conclusion and recommendations	Conclusions, key research findings and recommendations for future research.

Chapter 2: Study Basin

2.1 Geography

The Brahmaputra is one of the World's largest rivers. It originates as a snow-melt fed stream in the high Himalayan mountains of Southern Tibet, China, where it is named the Tsangpo. Within China, the river initially flows eastward before it turns northeast to cross a series of falls and rapids. It turns sharply south-south-west and steepens for about 500 km (Figure 1.1) before entering the Indian state of Arunachal Pradesh where it is called the Siang.

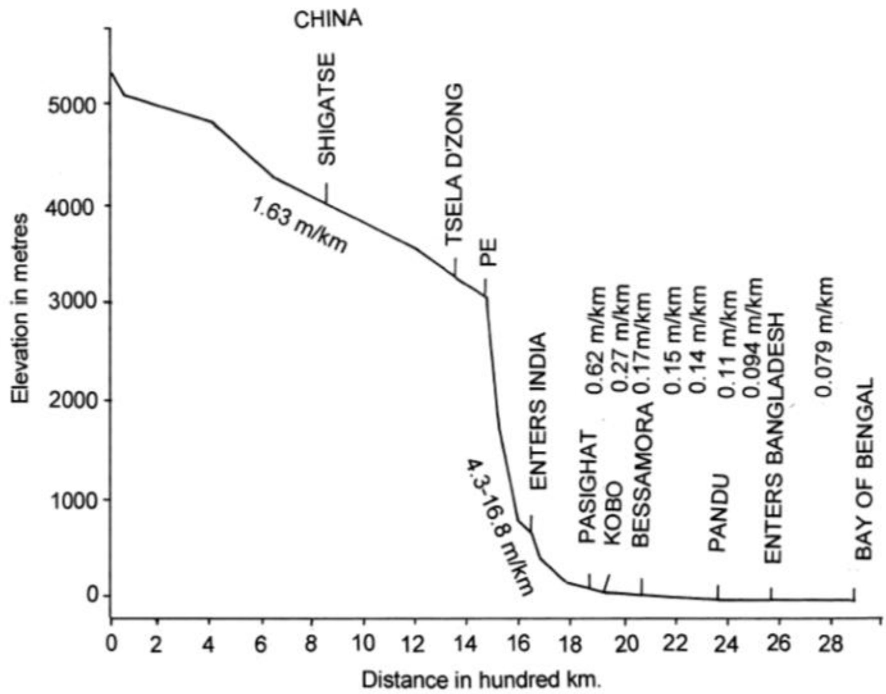

Figure 1.1. Long profile of the River Brahmaputra. Source WAPCOS (1993).

In Arunachal Pradesh, the gradient decreases markedly, as the river flows across the plains of Pasighat. The tributaries Dihang, Dibang and Lohit enter the Siang near Laikaghat, which is about 50 km downstream of Pasighat, forming the Brahmaputra (Figure 1.2). The Brahmaputra then flows through the relatively narrow Assam valley within the state of Assam (Sarma and Phukan, 2005), before it makes it way to the Bay of Bengal via Bangladesh.

The overall length of the river is 2,880 km, of which 1,625 km is in Tibet, 918 km is in India and 337 km is in Bangladesh. The drainage has an area of 520,000 km^2, of which 293,000 km^2 is in Tibet, 45,000 km^2 is in Bhutan, 195,000 km^2 is in India and 47, 000 km^2 is in Bangladesh (Sarma and Phukan, 2005). The Brahmaputra is the World’s 7th largest river, with the highest specific water and sediment yields (Thorne et al., 1993).

The 40 km study reach for the research reported in this thesis is adjacent to Majuli Island, which is near the city of Bessamora, Assam, India (Figure 1.2). Due to the marked reduction in slope downstream of where the river exits the Himalayas, sediment dynamics within the river in this reach are dominated by deposition processes, which result in a braided planform and a long-term trend for sediment accretion (Sarma and Phukan, 2005).

Majuli Island is bounded by the River Subansiri to the northwest, the Kherkatia suti (a seasonal, flood spill channel) to the northeast and the Brahmaputra to the south and southwest. Majuli is the World’s largest river island, measuring 80 km in length (east-west) and 10-15 km in width (north-south). The island ranges in elevation between 30 and 114 m above mean sea level and has an area of just over 520 km^2 (Brahmaputra Board, 2013).

The annual average discharge of the Brahmaputra is around 8,830 $m^3 s^{-1}$ at Bessamora (period 1975-1990, WAPCOS, 1993) and the annual average suspended sediment load (measured at Pandu, which is 200 km downstream of Majuli Island), is about 400 million tonnes (period 1955-1979, Goswami, 1985).

Table 2.1: Rationale description of the scale and boundaries of the study area.

Action	Justification
1. 17 years, daily simulations (1998- 2015)	• Availability of continuous daily water discharge and sediment load data for river Brahmaputra.
2. Extrapolating discharge and suspended sediment data the data by calculating the catchment area of Brahmaputra near Majuli Island form the satellite image and suspended sediment rating curve of Pandu.	• 17 years data (1998- 2015) were collected from Pandu gauge discharge, sediment site (GDS), Water Resource Department, Govt. of Assam, India. • Daily data available in Water Resource Department for this period. • Pandu is the only gauge discharge, sediment site (GDS) in river Brahmaputra in Indian counterpart. This gauge discharge site is 200 km away from Majuli Island. The other discharge site of Brahmaputra measure discharge only which is not useful for this study. • CAESAR Lisflood model has simulated both daily water discharge and suspended sediment load. • Catchment area was calculated in Arc GIS using hydrology tool.
3. Selection of the reach (40 km approximately).	• Based on the results outcome of the five newly developed indices, the research has investigated that the southern part of Majuli Island is very vulnerable in term of land degradation (Figure 1.3). • Hence it will be very significant to run the simulations for this reach and compare the modelled output with the Landsat data output.

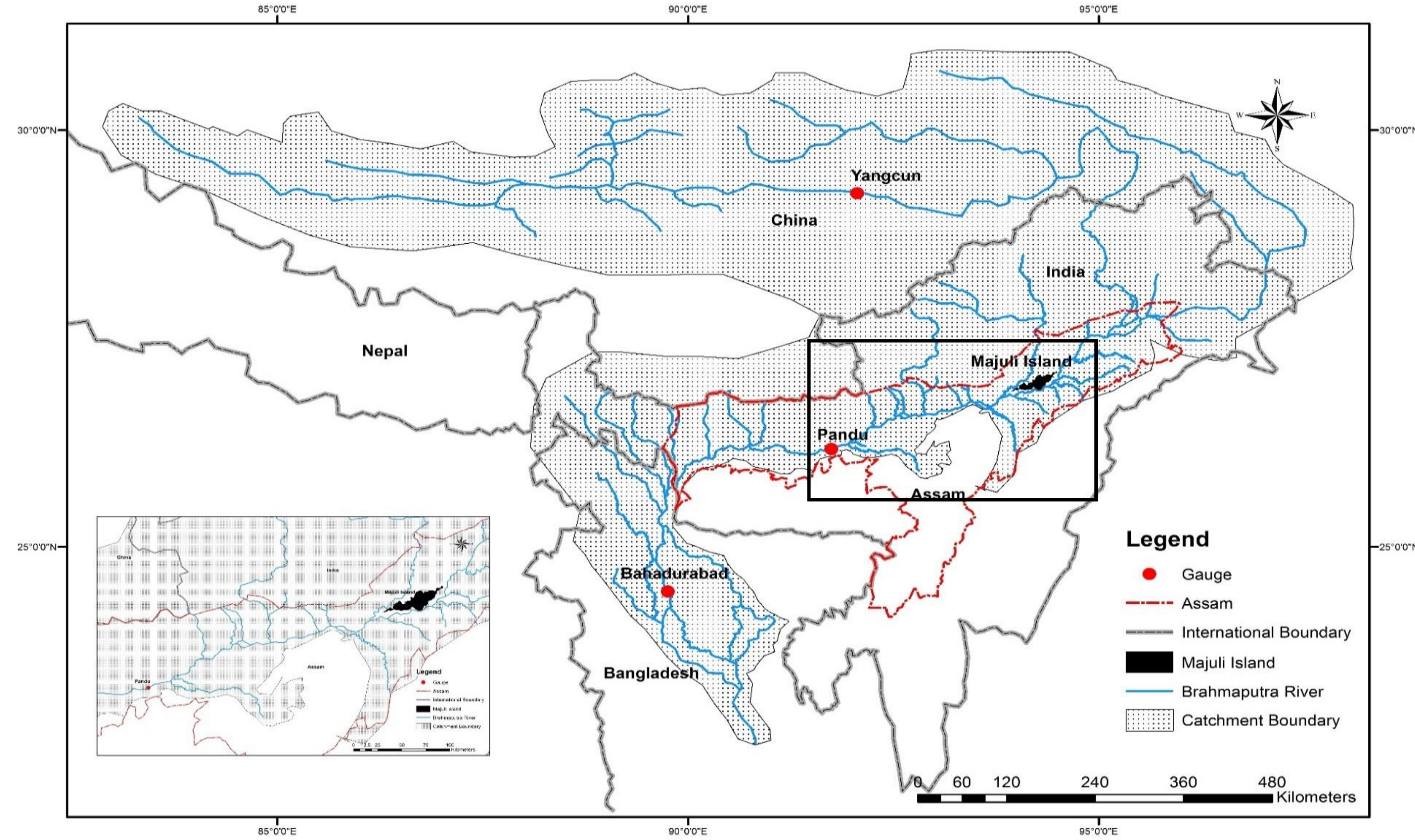

Figure 1.2. Location map of the gauge stations in the whole catchment of the River Brahmaputra, study area Majuli Island in Assam.

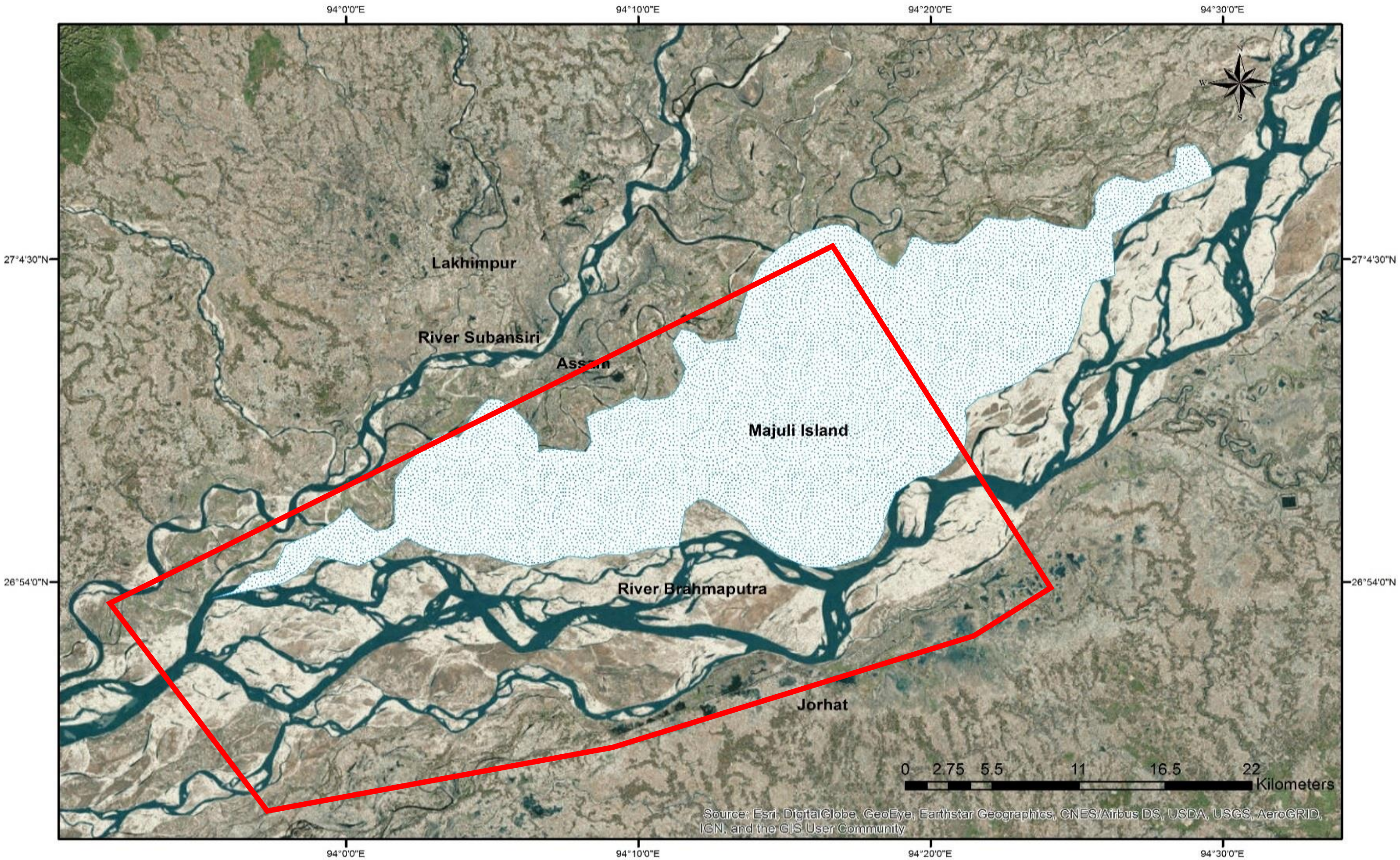

Figure 1.3. Location map of the study area Majuli Island in Assam.

Table 2.2: An overview of the combined field work, remote sensing, hydrological, sedimentological, bathymetric data, existing earth observation and modelling approach

Technique	Data and modelling approach	Purpose or Use of data and modelling approach
1. Fieldwork	1. Collected sediment samples from the floodplain, sandbar (stable and unstable) 2. River reconnaissance survey 3. Interaction with the local people, NGO, Govt. official and news media channel	1. Classify the grain sizes which were used in hydrological modelling 2. Measuring the slope of the river bank which was used in the hydrological modelling 3. Vegetation type and growth which was used in the hydrological modelling 4. Information about the level of flooding and erosion in Majuli Island 5. Mitigation measures which were undertaken by the government 6. View of the local people and NGO's about those mitigation measures and their opinion
2. Remote sensing	1. Landsat images 2. SRTM 90 m resolution	1. NDVI technique was used to classify the land-use and landcover from the Landsat images of the study area, which has helped in delineating the river channel, sandbar and floodplain to calculate the braiding pattern of the River Brahmaputra near Majuli Island 2. To create the Bathymetry of the River Brahmaputra in GIS.
3. Modelling approach	1. Reduced complexity modelling which is designed to model the long-term landscape evolution of the large fluvial system	1. Reduce complexity modelling approach was used to model 40 km reach of the River Brahmaputra for 20 years near Majuli Island.

4. Hydrological data	1. Daily discharge flow (source: Water Resource Department, Government of India). 2. Daily discharge flow (H08, JULES, LPJML and MacPDM) (source: ISIMIP, University of Potsdam)	1. Hindcasting 17 years flow model (1998-2015 March) River Brahmaputra near Majuli Island 2. Forecasting 20 years (2015 April – 2035) River Brahmaputra near Majuli Island
5. Sedimentological data	1. Daily suspended-sediment load data for three-grain size (2mm, 600 µm and 75µm). The daily suspended sediment load was extrapolated from the sediment rating curve of the River Brahmaputra.	1. The extrapolated suspended sediment load was used both for hindcasting and forecasting landscape evolution model for the River Brahmaputra.
6. Bathymetric data	1. Bathymetric data was prepared by combining SRTM 90 m DEM and measured cross-section data (source: Water Resource Department, Government of India).	1. SRTM data was used to create the floodplain and sandbars, while cross-sections data were used to create the bathymetry of the river channel (more detail in chapter 5).
7. Accessing of existing earth observation	1. Landsat images and SRTM 90 m DEM • Tracing the braiding pattern • Thalweg channel migration • Sandbar formation and deformation • Channel widening	1. Quantifying the braiding pattern, thalweg migration, sandbar formation and deformation, channel widening using newly developed braiding indices.

2.2The planform classification of the River Brahmaputra

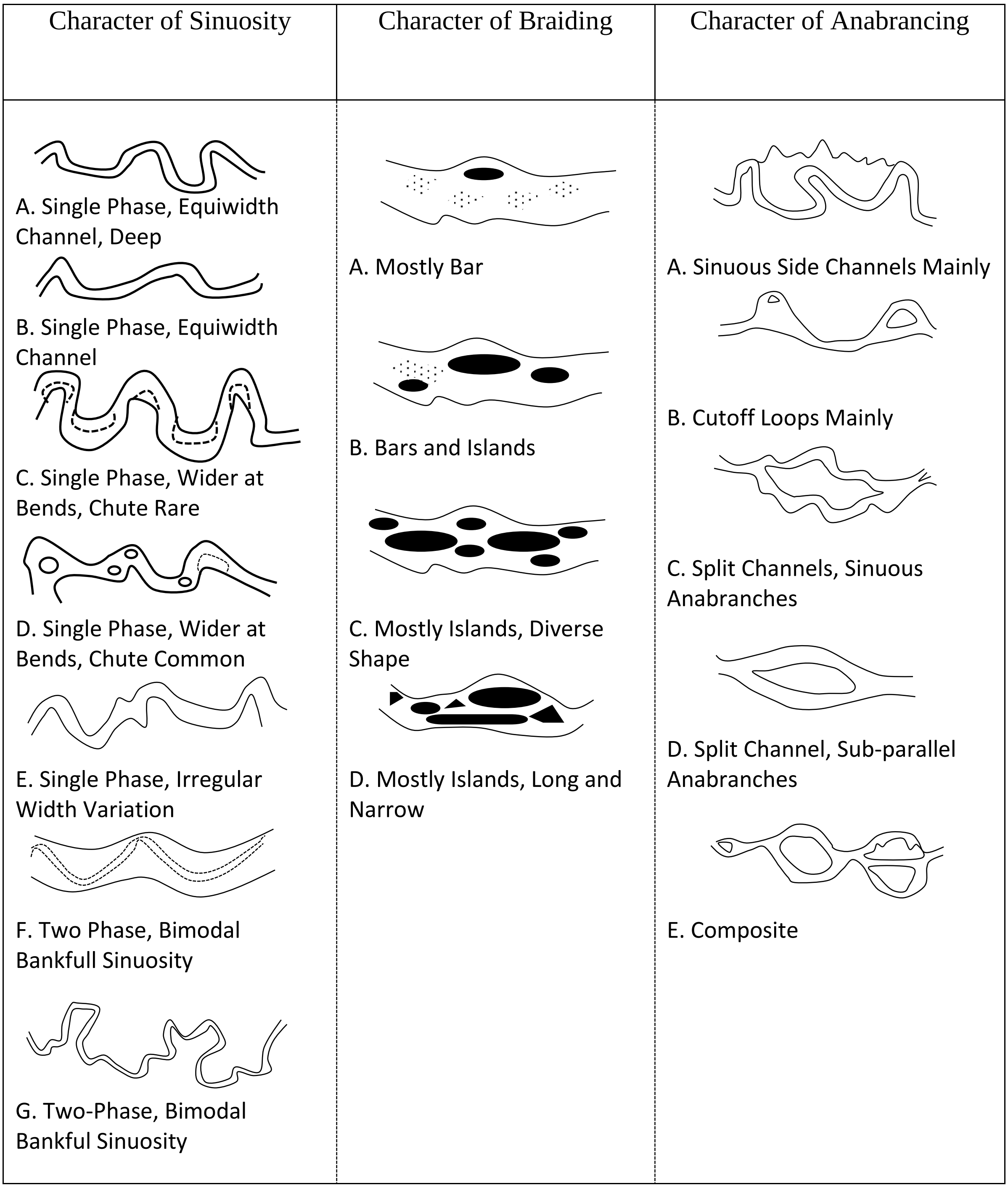

Figure 1.4: Channel pattern classification devised by Brice (1975)

The existing classification of channel morphology fails to account for dynamic adjustment or evolution of the fluvial system. Therefore geomorphologist has begun to develop a new classification of channel morphology. Brice 1975 has classified channel morphology based on the simple characteristic of river i.e. sinuosity, braiding and anabranching (Figure 1.4). In 1981 Brice has modified the classification of channel morphology based on relatively simple adjustment which has identified channels as degrading, aggrading, widening and lateral shifting.

Meandering Style	Braiding Style	Anastomosing style	Combination of all the three river style (hybrid river)

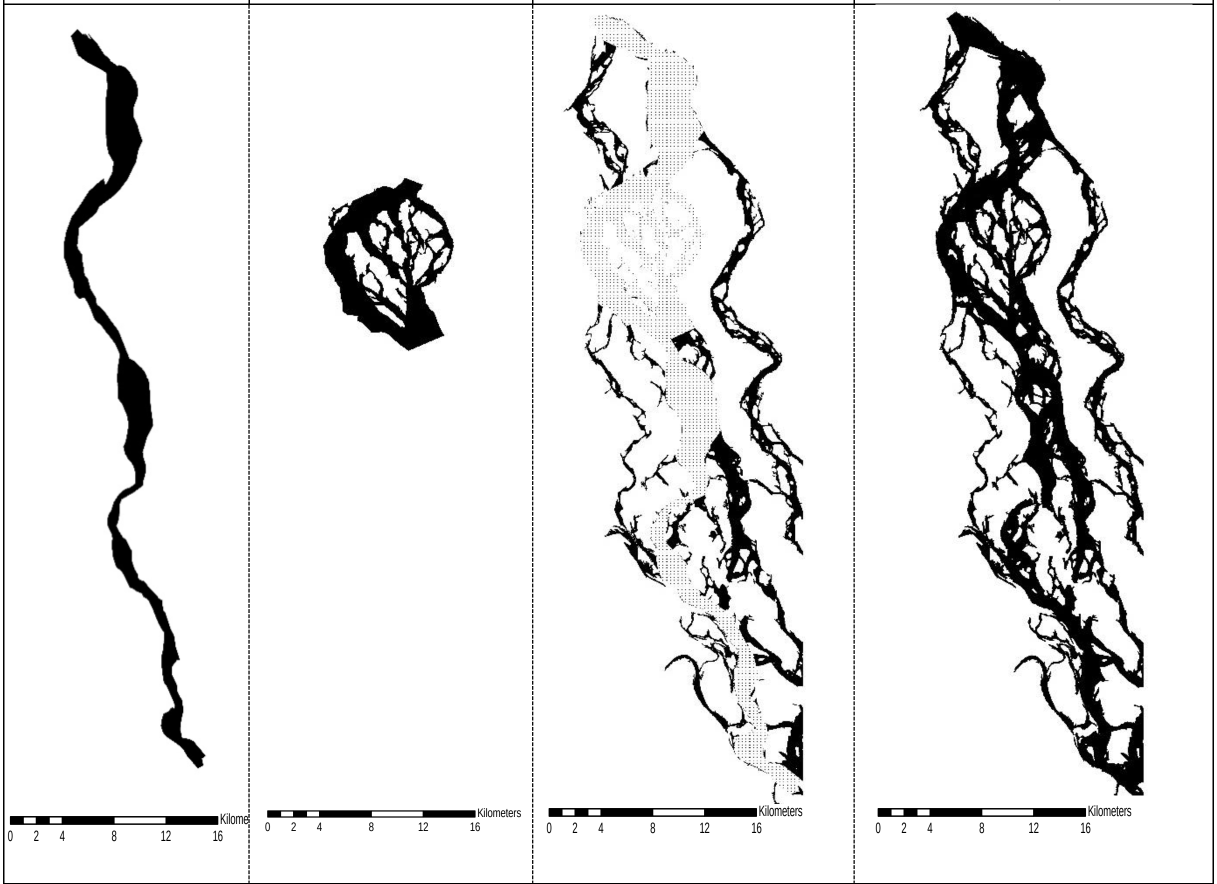

Figure 1.5: Deconstruction of planform pattern of the River Brahmaputra.

The most comprehensive system of channel classification was given by Rosgen (1994) which was based on the channel entrenchment, width-depth ratio, sinuosity, slope range and channel material.

Rivers are subjected to alter the shape and morphology when there is a change in the velocity, boundary roughness, slope, discharge, sediment grain size, sediment concentration and channel width and depth (Leopold et al., 1964). The River Brahmaputra can be classified as a complex or hybrid river system as it is composed of all the river pattern described by Brice, Rosgen etc. The River Brahmaputra has meandering, braiding and anastomosing channels pattern. In different location the pattern varies, the dominance of one pattern coexist with the other channel pattern (Figure 1.5).

2.3 Fluvial geomorphology and the influence of seismicity

The channel of the Brahmaputra near Majuli Island is wide and shallow, with multiple sub-channels through which the flow is distributed around and dissects numerous sandbars and islands in the braided planform. According to Sarma (2005) and Charlton (2008), braid bars can be divided into four categories:

1. mid-channel braid bars and islands,
2. lateral or sidebars,
3. tributary bars,
4. unit bars.

Salient features of the geology and geomorphology of the Assam Valley around Majuli Island are described in Table 2.1.

Table 2.3. Salient geological, hydrological and geomorphic features at Majuli Island.

Features	Impacts
Tectonics	Elevates river bed and increases discharge and sediment yield, causing floods and erosion.
Precipitation	Heavy rainfall during monsoon causes flooding.
Topography	Low relief (30–114 m above mean sea level) in the Island make it vulnerable to flooding during the monsoon season.
Braiding	Deposition in the river creates sandbars and islands.
Anabranching	Leads to erosion and dissection of the island fragment it into smaller islands and leads to new bars forming.
Meandering Tuni River and back watering	High stages in the Brahmaputra cause backflow in the Tuni River which floods the island and causes erosion.
Lateral shifting of Brahmaputra River	Causes of bank erosion, especially along the southern flank of the island.
Embankment failure	Breaching due to bank erosion or during floods leads to severe life risks and property damage on the Island.

Mid-channel bars are formed in areas of flow divergence and are mostly sand with little vegetation. They are elongated and either rhombic or triangular in shape, with their long-axis aligned parallel to the direction of flow. Islands are more stable mid-channel bars, covered by vegetation. However, during high flows, when and where currents breach the channel boundary, they create new sub-channels by eroding either a stable island or the floodplain. As new sub-channels are created, existing sub-channels are abandoned as their flow is diverted elsewhere, or when they become infilled with sediment (Charlton, 2008).

The Brahmaputra is able to form and reform numerous sandbars due to its abundant load of sediment, which is derived from the catchment upstream and local river bank erosion. During high flows, these braid bars are partly or wholly submerged, the sub-channels tend to merge into a single, very wide channel with few visible bars (Figure 1.3). Conversely, during low discharges, extensive numbers of bars and areas of bar surface are exposed, with the river divided into a thalweg channel and multiple, secondary and tertiary anabranches (Figures 1.4 and 1.5). Sub-channels in braided reaches of the Brahmaputra are highly dynamic, frequently changing in size and shifting in position (Figure1.6). Alterations, involving dissection and modification of existing sandbars and the genesis and growth of new bars, occur over relatively short periods (days to a year).

The presence of braid bars and islands, coupled with the large discharge and sediment load of the river generates complex patterns of flow and sudden shifts in the patterns and locations of sub-channels. Individual sub-channels may be created, abandoned and/or reoccupied within the space of a few days (Charlton, 2008). This phenomenon leads to a distinct planform type, referred to as anabranching.

Anabranches are substantial second-order sub-channels etched into the braid plain and/or the surrounding floodplain. Anabranches divide up the land into a number of large islands. This is type of planform is predominant in the Brahmaputra in Assam. In fact, anabranching is currently dissecting the southern part of Majuli Island (Figure 1.6). Unlike sub-channels, major anabranches each have their own characterises and their planforms may be straight, meandering or braided. The sinuosity of actively meandering anabranches is, however, relatively low and rarely exceeds 1.5 (Sarma and Phukan, 2004; Charlton, 2008).

Figure 1.6. Sandbar formation near Majuli Island during high flow.

Figure 1.7. Exposed sandbar near Majuli Island during low flow.

Figure 1.8. Exposed sandbar near Majuli Island during low flow.

There are also low-energy anabranches that are relatively inactive geomorphologically. In these reaches, the Brahmaputra is described as anastomosing. In contrast to braided reaches, rates of lateral channel migration are typically very low in anastomosing reaches.

While the sub-channels and even some anabranches are unstable and change frequently (especially during floods), the overall course of the Brahmaputra near Majuli Island is relatively stable. That said, it has changed historically and could do so again, depending on future flow and sediment transport conditions.

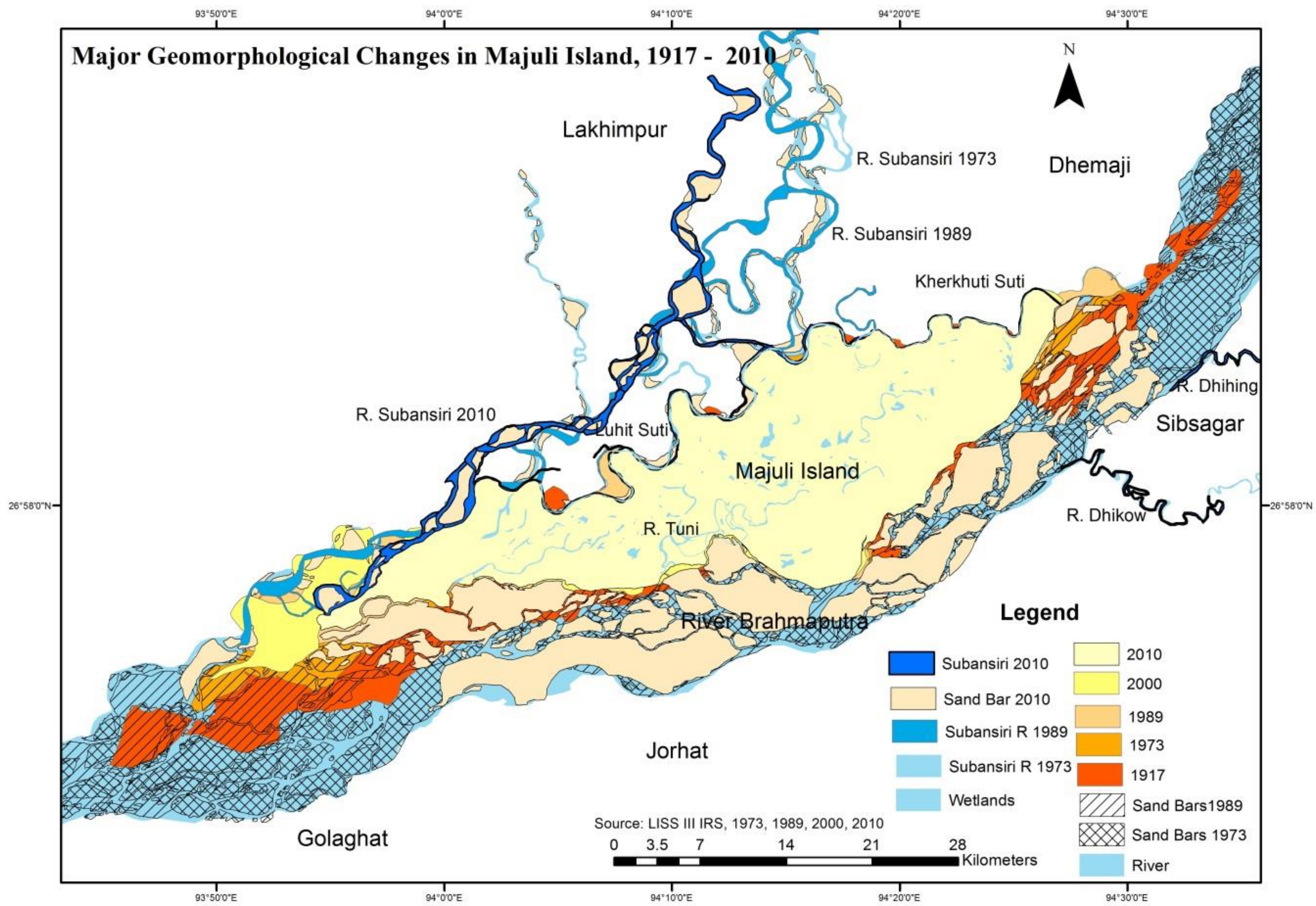

Figure 1.9. Geomorphological changes in River Brahmaputra near Majuli Island 1917 - 2010.

The shifting planform of the river, its capacity to increase in width (creating the space for the genesis, growth and movement of braid bars) depends on the existence of readily erodible river banks. A history of severe erosion and morphological change at Majuli Island demonstrates that its bank materials are highly susceptible to erosion (Figure 1.6). The fact that bank erosion is concentrated in the southwestern part of the island, near the confluence of the Brahmaputra and its tributary the Subansiri, indicates that it is these rivers that are primarily devouring the land, with the maximum long-term rate of bank retreat being on the order of 50 m y^{-1}. Sediment eroded from the southwestern part of the island is feeding bank accretion along the River Subansiri to the north, where the banks in some locations are advancing at a long-term, average rate of about 150 myr^{-1} (Sarma and Phukan, 2004). Notwithstanding these contrasting rates, erosion has dominated accretion overall. For example, the total area of Majuli Island in 1914 was 734 km^2 but this had decreased to 506 km^2 in 2008. Most of that decrease has occurred since the Assam Earthquake of 1950. In fact, the area of the island has decreased by more than 370 km^2 since 1950 alone (Singh, 2011). Recently, however, there has been an increase in the landmass of Majuli Island, which was measured to be 523 km^2 in 2013.

The severity of erosion in the area can be attributed at least in part, to its seismicity, with the 1950 Assam Earthquake being pivotal. Morphotectonic models created by Lahiri and Sinha, (2012) describe how coseismic and interseismic forces influence the morphodynamics of the Brahmaputra, including in the reach adjacent to Majuli Island. Lahiri and Sinha (2012) model depicts the pre-1950 earthquake the Brahmaputra as being highly dynamic and aggradational in the upper two units of the Assam valley (Figure1.9). Frequent avulsions in tributaries draining from the north contrast with older, meandering south bank tributaries. This reflects the influence of two different tectonic domains: namely, the Himalayan thrust belt to the north and the Naga Patkai thrust to the south.

The Great Assam earthquake of 1950 had a magnitude of 8.7, making it the most powerful recorded earthquake at that time. This event caused landslide on a huge scale in the eastern Himalayas and led to liquefaction of large areas in the Assam Valley. Massive disturbance of the landscape increased the supply of sediment to the Brahmaputra, resulting up to 3 m of bed aggradation in a very short period following the earthquake. Coseismic subsidence in the Subansiri and Lohit depressions generated further morphodynamic changes in the Brahmaputra. Aggradation occurred in the Lohit depression, destabilising the channel and accelerating rates lateral erosion in unit 1 (Figure 1.7).

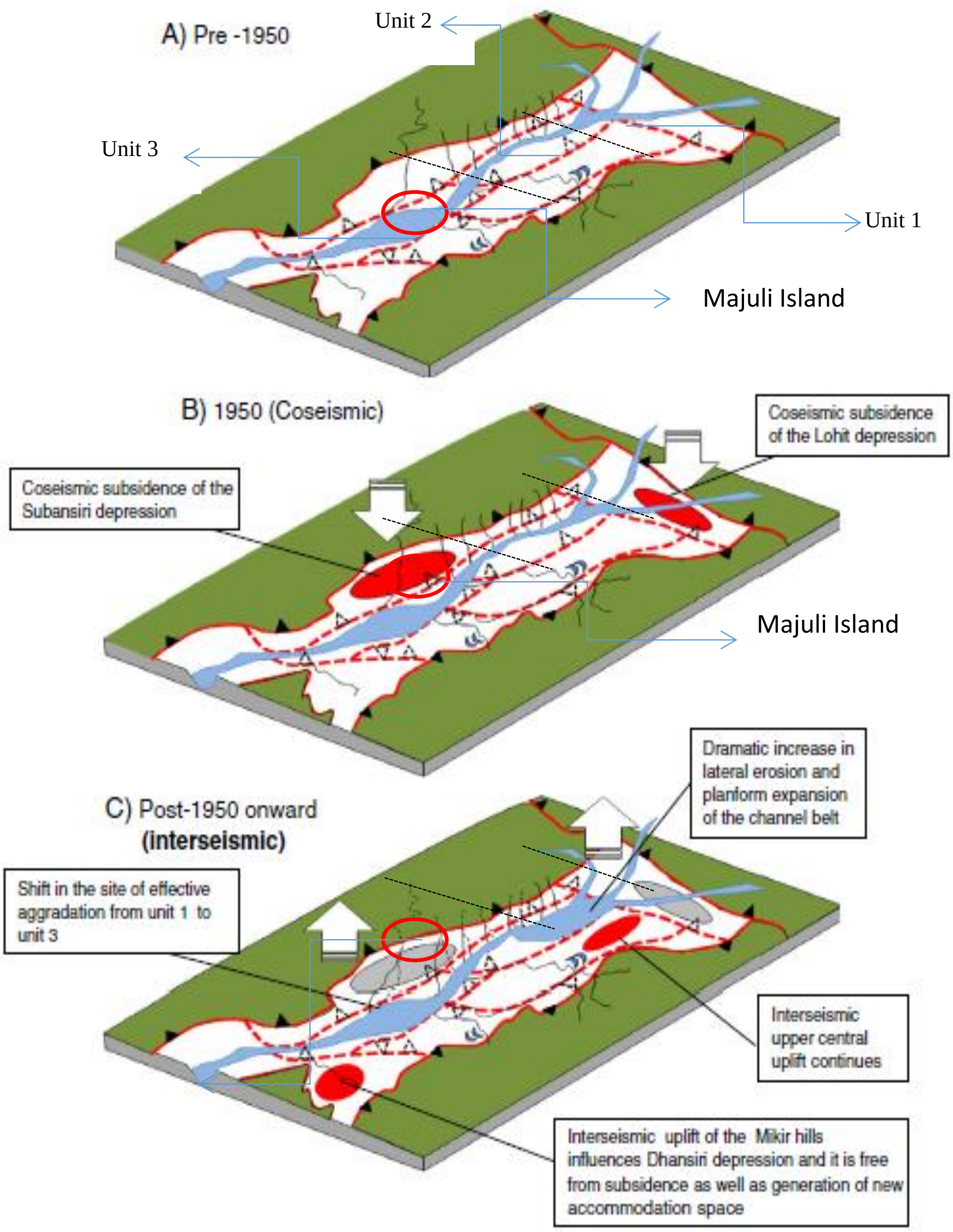

Figure 1.10. Coseismic and inter-seismic forces influencing morphodynamics in the Assam Valley. (A) Pre-1950 earthquake. (B) 1950 earthquake caused subsidence in the Subansiri and Lohit depressions which helped to generate more space for sedimentation. (C) Post-1950 earthquake to the present-day scenario. Aggradation in the Lohit depression decreased the bedload/suspended

load ratio and increased lateral erosion tremendously in unit 1. Unit 2 does not show much change in braid bar/channel area ratio. The site of effective aggradation shows a switchover from unit 1 to unit 3. Subsidence in the Subansiri depression caused a number of channels of the north bank to avulse in the southwest direction. South bank tributaries remained mostly unaffected. Source: Lahiri, and Sinha (2012).

Following the earthquake, subsidence to the north of Majuli Island continued in the Subansiri depression. This has resulted in channel widening and an increase in the amount of sediment locally supplied to the Brahmaputra after it has left the Himalayas and entered the plains, overloading the river and driving a gradually accumulating, morphodynamic trend (Goswami, 1999).

Local sediment supply is also controlled by hillslope stability, the extent and density of vegetation cover. In this case, sediment supply is the dependent variable and vegetation cover the controlling variable. Climate change affects both vegetation cover and hillslope stability, which, in turn: determine local sediment supply; influence channel pattern; affect in-stream flow dynamics, and; govern sediment transport capacity. Over long periods, it is the cumulative effects of these small-scale processes and adjustments that drive large-scale changes in the Brahmaputra.

According to the neotectonic models developed by Lahiri and Sinha (2012), Majuli Island is northward dipping due to the influence of the Main Frontal Thrust in the foothills of Himalaya. The dip slope of the island is believed to promote northward channel migration and affect patterns of valley sedimentation. Additionally, the Jorhat Fault (in the south of Majuli Island) is thought to define the southern boundary of the island.

Based on these models, Lahiri and Sinha (2012) interpreted historical trends and changes in selected fluvio-geomorphic parameters including: channel belt area (CHB), channel belt width (W), braided bar area (BB), channel area (CH), thalweg changes, and bankline migration at Majuli Island for the years 1915, 1975 and 2005. Their interpretations suggest that temporal variability in CHB, W, BB, CH, LB and RB is strongly correlated with the rate at which Majuli Island is eroded. Channel belt area (CHB) and width (W) are negatively correlated with erosion rate, while braid bar (BB) and channel (CH) areas are positively correlated, particularly in the lower half of Majuli Island. Lahiri and Sinha (2012) argue that increased erosion of the Majuli Island, particularly between 1975 and 2005, is clearly related to the increase in braid bar area observed in the lower reaches of the Brahmaputra in the study area.

Time itself is an important factor. Every drainage basin has a historical legacy resulting from past changes that have taken place. Channel changes over periods of tens to hundreds of thousands of years can materially adjust the slope of the entire valley. The current form of the Assam Valley results not only from tectonics but also from the cumulative effects of fluvial processes of sediment erosion, transport and deposition over short as well as long periods. Figures 2.6 illustrate changes in the form and features of the basin and how the evolution of the drainage networks of the Brahmaputra and Subansiri between 1917 and 2010 has changed the shape and size of Majuli Island.

2.4 Bank and bar sediments at Majuli Island

The banks of the Brahmaputra are composed of fine sand and silt in varying proportions, with the only minor amounts of clay (generally <5%) (Goswami, 1985). According to the subsoil surveys carried out by the River Research Station at various locations on Majuli Island and encompassing a depth of up to 30 m, the island is mostly underlain by grey coloured, fine to medium sized; poorly graded sand covered by light grey coloured silt mixed with clay, and; fine sand of varying thickness ranging from 1.5 to 12 m. However, there are few pockets (for example, Salmora, Dakhinpat and Bessamora, all located in the southwestern part of Majuli Island bordering the Brahmaputra), where the soil is rich in inorganic clay and the depth of clay-rich horizon is greater than 15 m (Goswami, 2001; Singh and Goswami, 2011). Field investigations conducted during this doctoral research at various locations on Majuli Island corroborate these finds, as described later in this section.

The Wentworth scale was used in this research (Table 2.2).

Table 2.2. Wentworth (1922) grain size classification

4.75 mm → Granule
2 mm → Very Coarse Sand
1 mm → Coarse Sand
600 µm → Medium Sand
425 µm → Medium Sand
300 µm → Medium Sand
212 µm → Fine Sand
150 µm → Fine Sand
75 µm → Very Fine Sand
Pan → Silt & Clay

Major morphological changes are possible in the Brahmaputra due to its great power and the high erodibility of the channel banks, which may, in turn, be attributed to the lack of cohesive materials. In detail, the hydraulics of the near-bank flow and the composition of the bank materials control the types and rates of bank failure. Generally, rapid bank retreat results from frequent failure events. As noted above, according to the literature, bank material at Majuli Island varies mostly from coarse sand to fine sand and silt.

To investigate the size distributions and properties of sediments and bank materials, in this study samples were collected from river banks and sandbars at selected locations along the Brahmaputra near Majuli Island. The locations were: Dhakhinpat (samples DHK1, 2, 3, 4, 5), and; Kamalabari (samples at the ghat, (Figure 1.10) a sandbar opposite the ghat, and the embankment (Table 2.3).

Table 2.4: Sediment sampling locations.

Location	Latitude	Longitude	Elevation m
DHK 1	26°55'58.24"N	94°13'05.93"E	86
DHK 2	26°55'07.98"N	94°14'40.16"E	87
DHK 3	26°55'24.40"N	94°17'52.86"E	87
DHK 4	26°56'47.66"N	94°18'25.71"E	89
DHK 5	26°54'24.42"N	94°16'44.67"E	88
Kamalabari	26°54'57.39"N	94°09'37.93"E	84
Sand Bar	26°54'59.20"N	94°09'38.47"E	85
Embankment	26°55'12.08"N	94°09'10.51"E	91

Samples DHK 1 and DHK 5 come from sandbars visited under low flow conditions during December 2014. These samples have a high proportion of medium sand and they are, consequently, non-cohesive. In contrast, samples DHK 2 (Figure 1.11), DHK 3 and DHK 4 are from the bank of the Brahmaputra.

These samples are more than 50% silt and clay and they are cohesive. Dakhinpat (as well as the nearby communities of Bessamora and Salmora) are in the region of Majuli Island which is less affected by erosion. Samples collected from Kamalabari ghat and a sandbar opposite contain more than 50% of silt and clay and are also cohesive. At Kamalabari ghat, a sample was also collected from the earthen embankment, which is known as the 'lifeline of Majuli Island' (Figure 1.10). The embankment mostly comprises medium sand and is non-cohesive. Due to its non-cohesive nature, the embankment is highly prone to erosion or breaching during high flows.

Figure 1.11. Sediment sampling site near Kamalabari ghat.

Figure 1.12. Sediment sample collection near Kamalabari ghat.

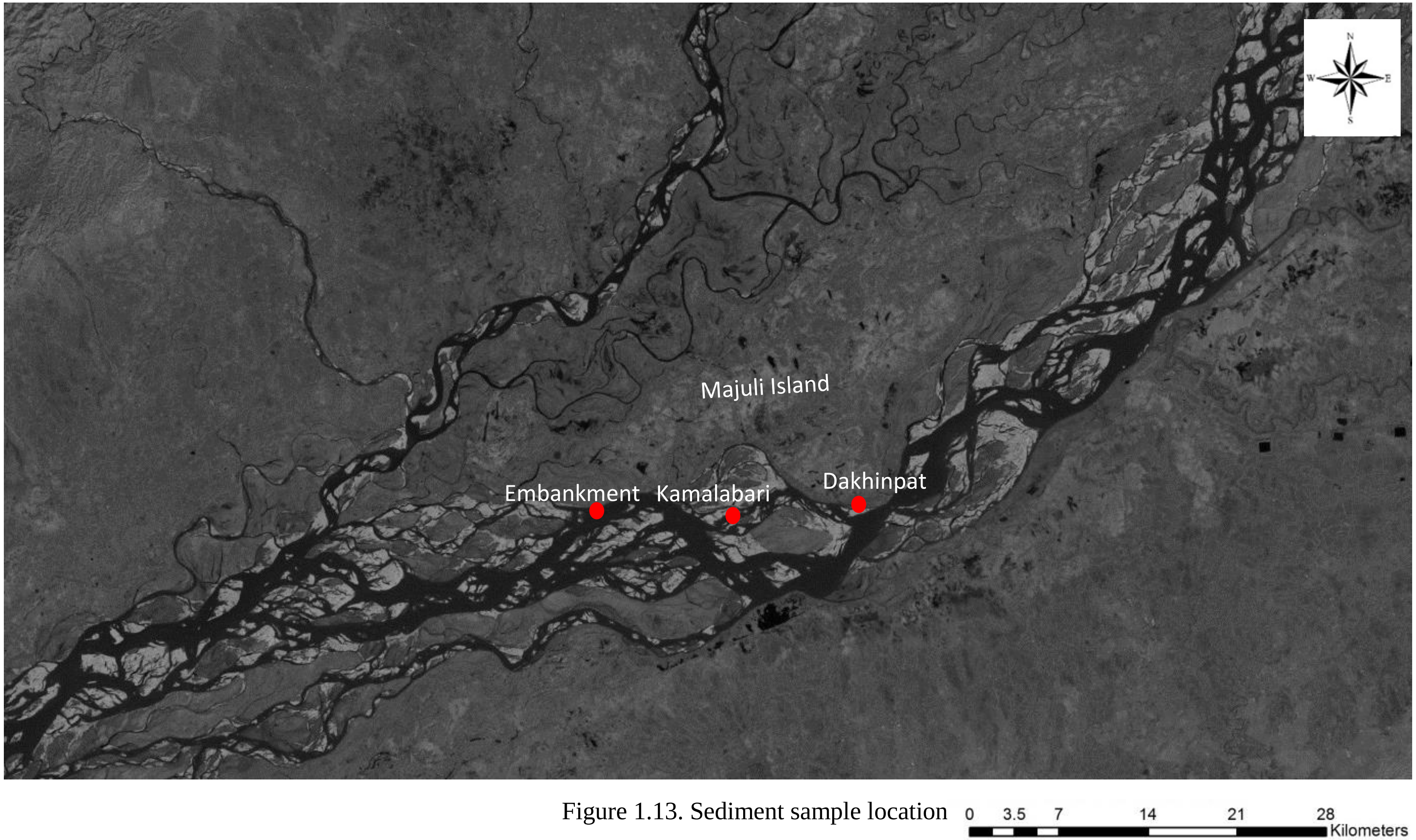

Figure 1.13. Sediment sample location

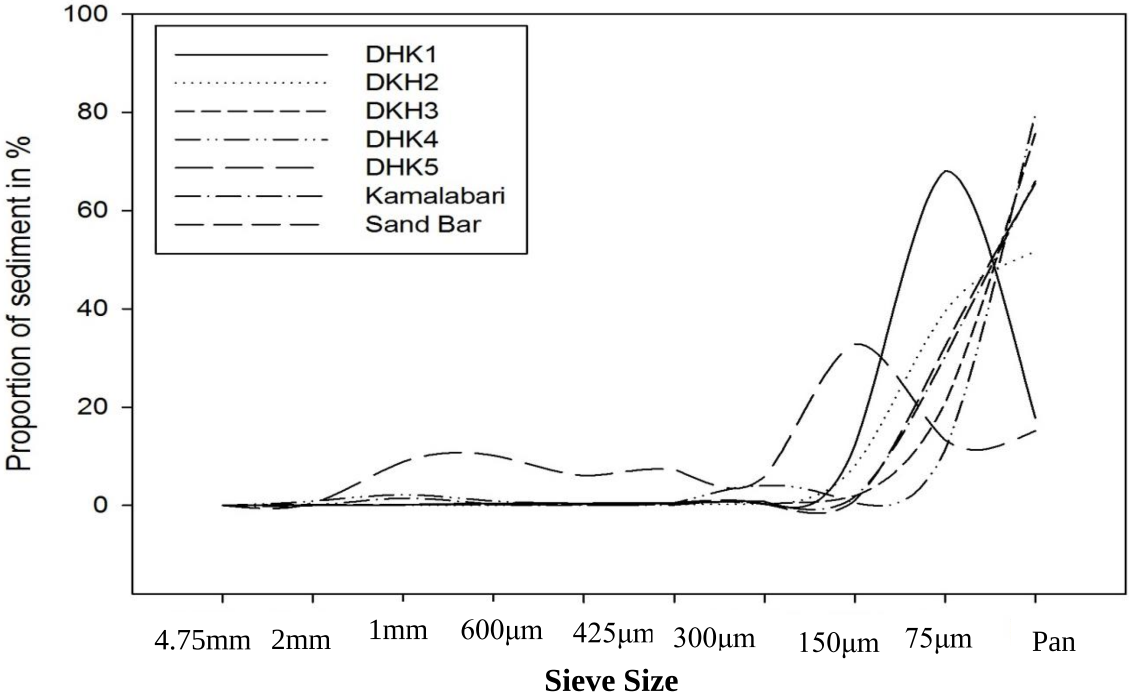

Figure 1.14. Sediment sample particle size distributions.

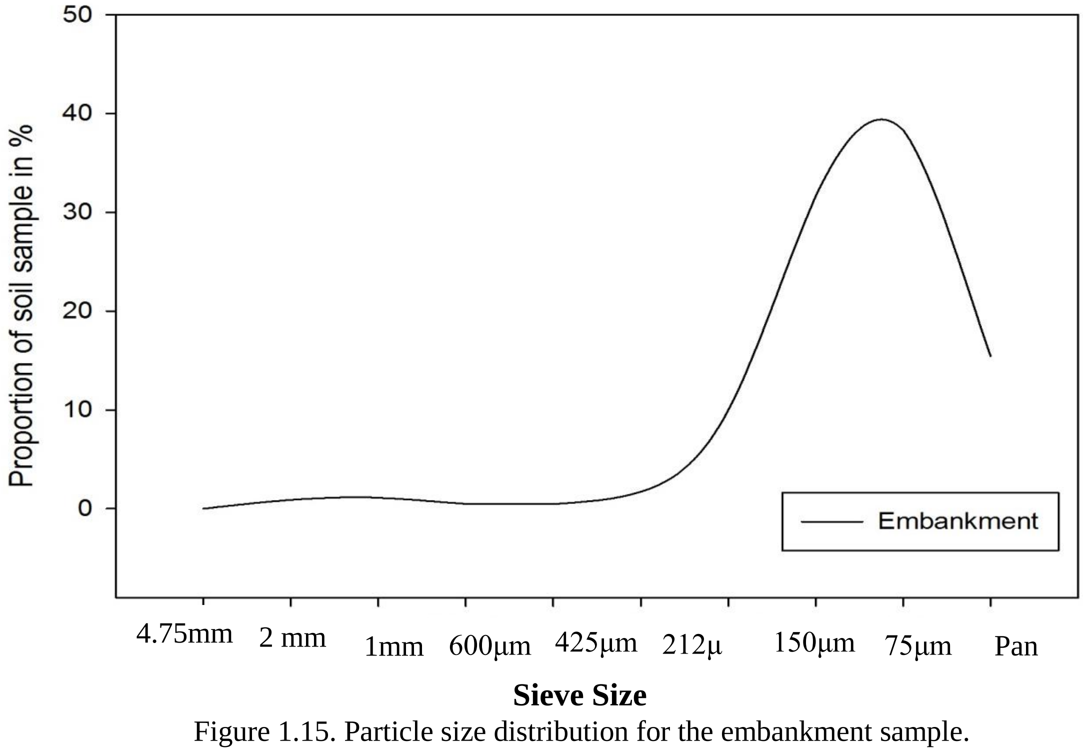

Figure 1.15. Particle size distribution for the embankment sample.

The government has constructed 155 km embankments to protect Majuli Island from flooding, including the south-east embankment (Figure 1.13), which is the longest and is known as the ‘lifeline of Majuli Island’. During floods, the Brahmaputra sometimes breaches the embankments, leading to serious flooding.

Bank retreat between 1996 and 2001 consumed land in Majuli Island at an average annual rate of 6.42 km^2yr^{-1} (Sarma and Phukan, 2004) and in areas where the bank is retreating, the embankment is also threatened by erosion. In response, the embankment has been retired along about 42 km of its length over the last 20 years. Consequently, only about 88 km of embankment still follows its original alignment. Conversely, in 2013, the Brahmaputra Board reclaimed 2.47 km^2 of land at Majuli Island by raising and strengthening 96.2 km of the embankment (Table 2.4).

Figure 1.16. The south-east embankment, the ‘lifeline of Majuli Island’.

Table 2.5: Total land area, eroded area, reclaimed area and loss area of the Majuli Island, 1914- 2013. (Source: Brahmaputra Board, Guwahati).

Year	**Area of Majuli Island in km^2**	**Area eroded in km^2**	**Area reclaim in km^2**	**The average loss of area per year in km^2**	**Source**
1914	733.79				Survey of India map
1949	708.91	24.88		0.71	Survey of India map
1963	588.79	120.12		8.58	Survey of India map
1988	513.89	74.90		2.996	IRS LISS III
1998	510.79	3.10		0.31	INSAT IC LISS III
2000	520.23		9.44		INSAT ID LISS III
2003	511.89	8.34		2.78	INSAT ID LISS III
2004	502.21	9.68		9.68	IRS P6 LISS III
2008	506.37		4.16		IRS P6 LISS III
2013	522.73	16.36	2.47	3.27	IRS P6 LISS III

2.4 Cross-sectional evolution of the Brahmaputra near Majuli Island

The Assam Department of Water Resources has established and periodically resurveys 65 cross–sections in the Brahmaputra within the state of Assam. Cross-sections in the reach adjacent to Majuli Island extend from C.S. 45 upstream to C.S. 58. These cross-sections were resurveyed in 1988, 1998 and 2007 (Figures 1.14 and 1.15)

Near Majuli Island, the width of the river varies between 9 and 18 km and cross-sections are characterised by multiple channels of varying depths that are separated by bars and islands with varying elevations. For example, in 1988, at C.S. 55 the major anabranch was in the middle of the braided channel and there were also two second-order channels and a few small sub-channels near both the north and south banks of the river. At the same cross-section (C.S. 55) in 2007, the main channel had deepened and widened while the second-order sub-channels had disappeared due to sedimentation, with a few small sub-channels remaining in the braided pattern.

Further downstream, at C.S. 54, in 1988, the main channel was close to the north bank, with two second-order channels and a few small sub-channels located towards the south bank. In 2007, the location and dimensions of the main channel remained unchanged, but the second-order channels were replaced by additional sub-channels in a more intensely braided pattern. Further downstream again, at C.S. 53, in 1988, the main channel was along the south bank with two second-order channels towards the north bank. When next resurveyed in 2007, the major anabranch had deepened and one of the second-order channels had disappeared due to sedimentation processes.

At C.S. 50 in 1988, a deep main anabranch was found slightly to the south of the centreline of the braided channel. However, in when the cross-section was resurveyed in 1998 (following the massive flood event with a record daily discharge 37,709 m^3s^{-1} and the highest recorded daily sediment load of 18,000 m^3s^{-1} the main anabranch had shallowed due to deposition of flood sediments. In 2007, C.S. 50 the main anabranch was still in the same position, though it had widened slightly, and two second-order sub-channels had formed towards the north bank.

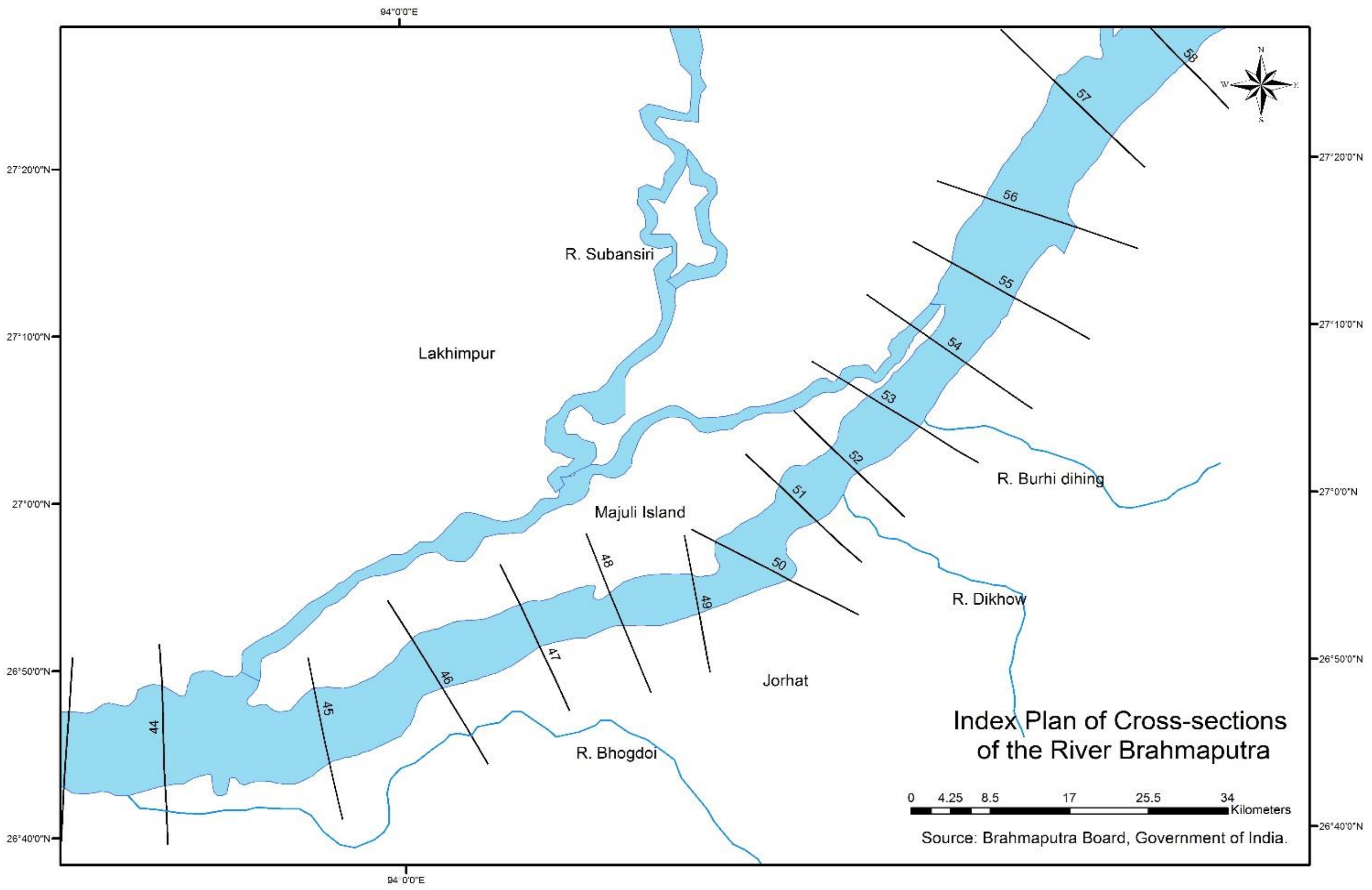

Figure 1.17. Locations of a cross-section along the Brahmaputra near Majuli Island.

Figure 1.18: Cross-section of the river Brahmaputra near Majuli Island. (Source: Water Resource Department, Govt. of Assam, India)

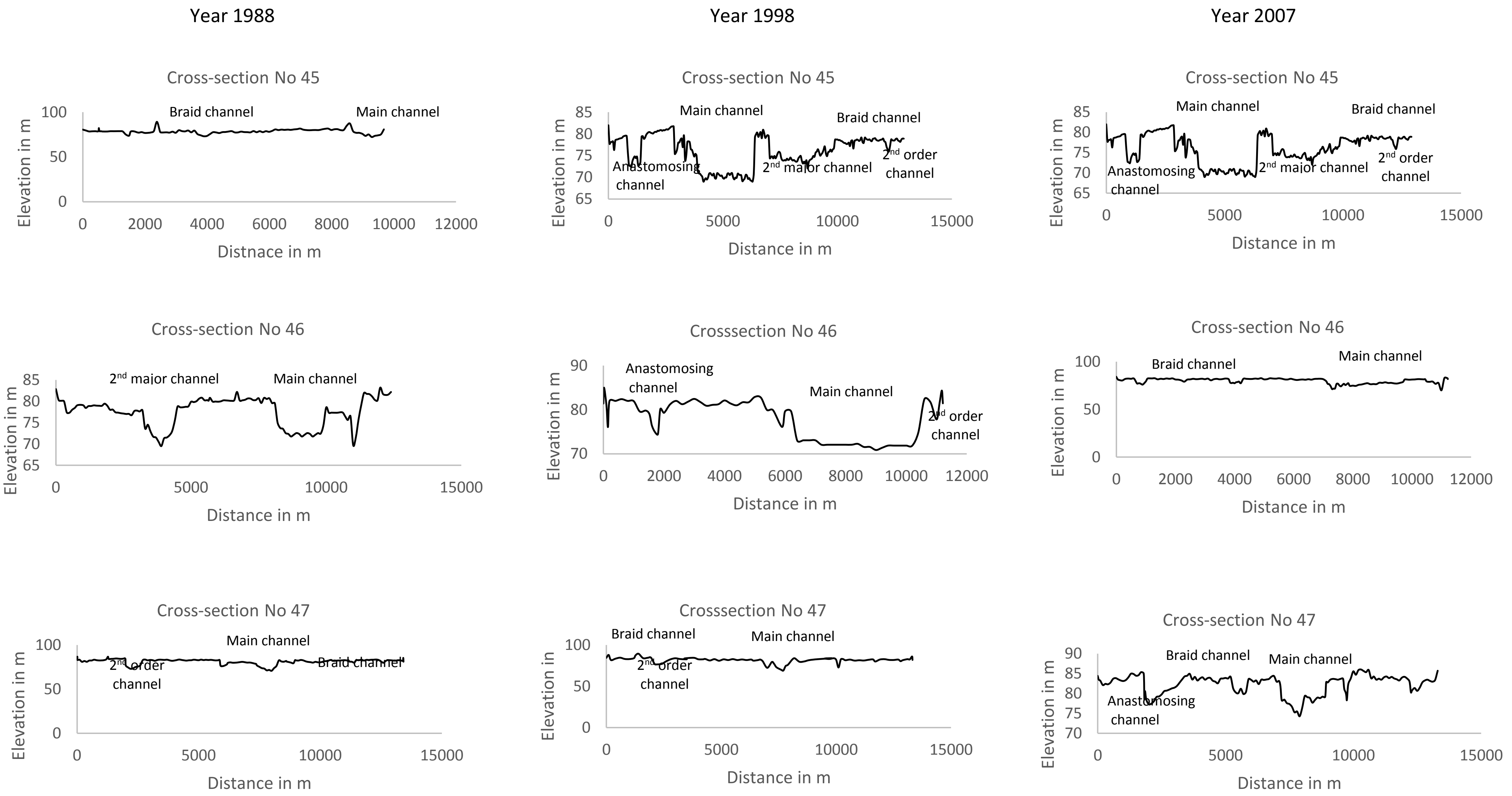

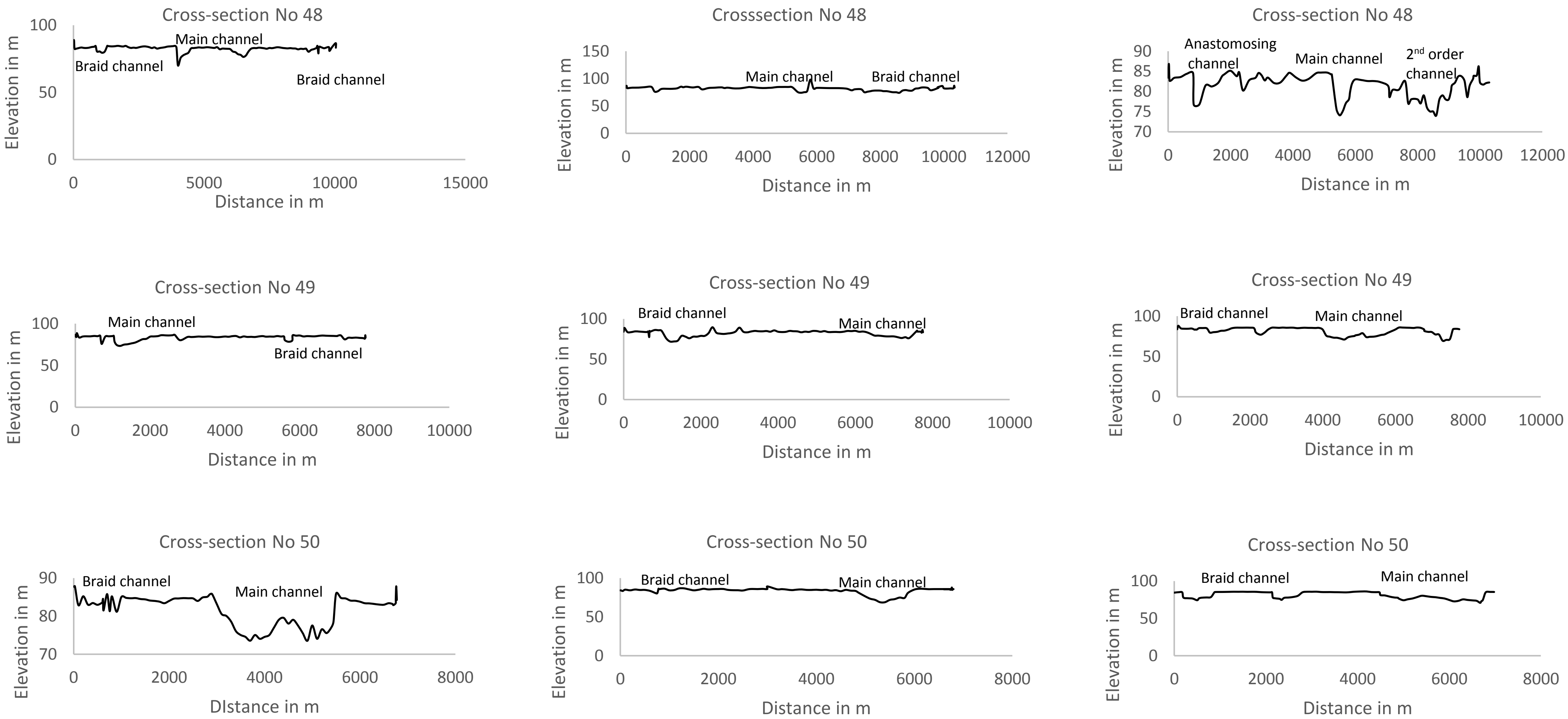
Cross-section No 48
Main channel
Braid channel
Braid channel
Elevation in m
Distance in m
Crosssection No 48
Main channel
Braid channel
Elevation in m
Distance in m
Cross-section No 48
Anastomosing channel
Main channel
2nd order channel
Elevation in m
Distance in m
Cross-section No 49
Main channel
Braid channel
Elevation in m
Distance in m
Cross-section No 49
Braid channel
Main channel
Elevation in m
Distance in m
Cross-section No 49
Braid channel
Main channel
Elevation in m
Distance in m
Cross-section No 50
Braid channel
Main channel
Elevation in m
DIstance in m
Cross-section No 50
Braid channel
Main channel
Elevation in m
Distance in m
Cross-section No 50
Braid channel
Main channel
Elevation in m
Distance in m

Year 1988

Year 1998

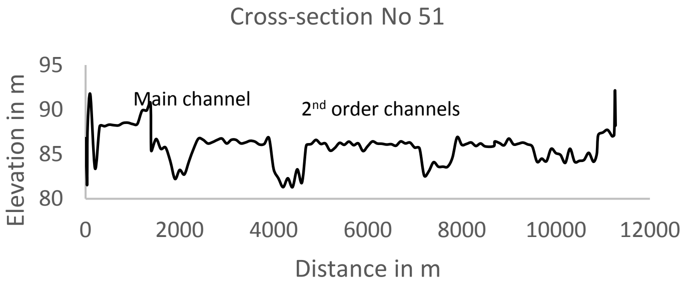

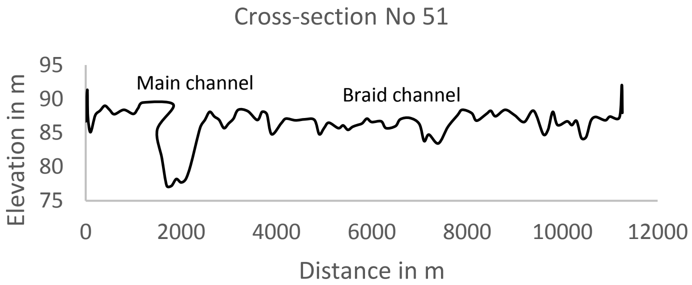

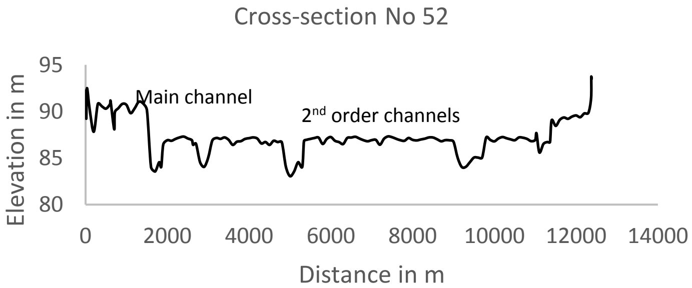

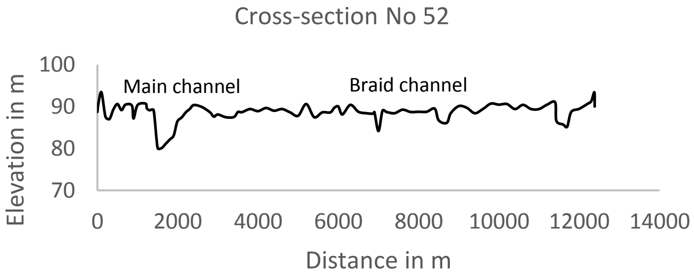

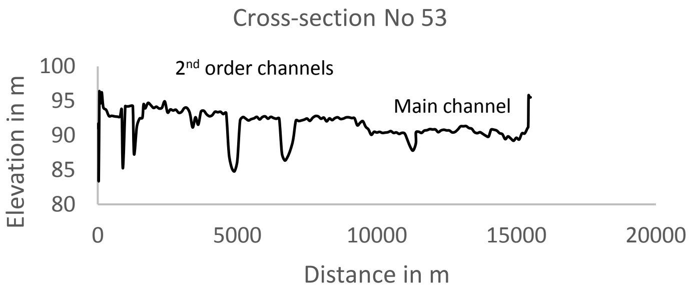

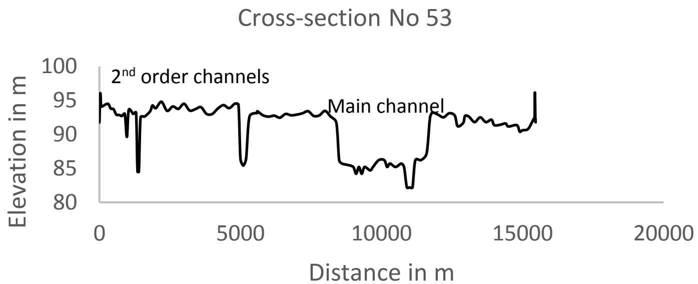

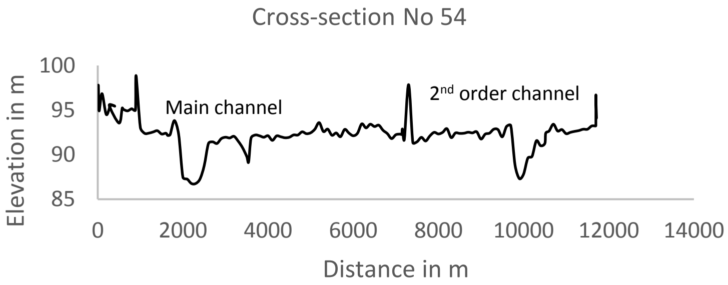
Cross-section No 54
Elevation in m
Distance in m
Main channel
2nd order channel
100
95
90
85
0
2000
4000
6000
8000
10000
12000
14000

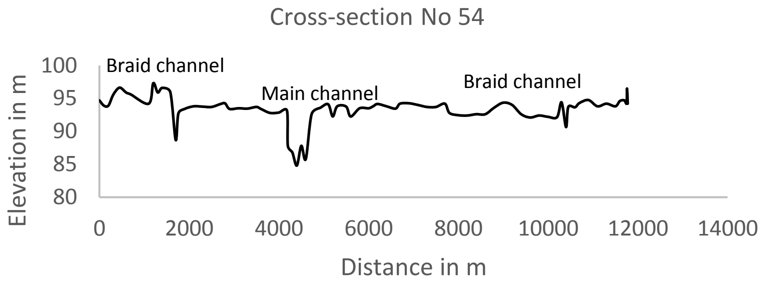
Cross-section No 54
Elevation in m
Distance in m
Braid channel
Main channel
Braid channel
100
95
90
85
80
0
2000
4000
6000
8000
10000
12000
14000

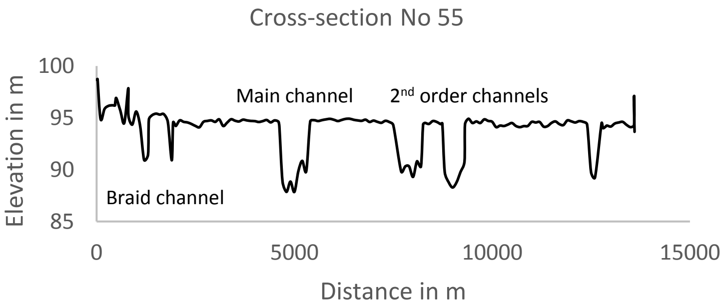
Cross-section No 55
Elevation in m
Distance in m
Main channel
2nd order channels
Braid channel
100
95
90
85
0
5000
10000
15000

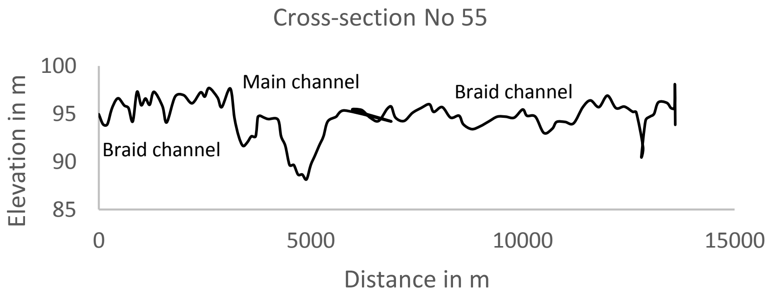
Cross-section No 55
Elevation in m
Distance in m
Main channel
Braid channel
Braid channel
100
95
90
85
0
5000
10000
15000

At cross-sections C.S. 49, 48 and 47, the major anabranch was narrow and shallow in both 1988 and 1998. However, at C.S. 48 and 47 in 2007, the major anabranch had split into two large, second-order sub-channels, one adjacent to the north bank and the other one in the middle of the braided river, together with a number of small sub-channels which had developed in these cross-sections.

At cross-sections C.S 48, 47, 46 and 45 the river seems to have evolved into a broadly anastomosing pattern within which the sub-channels remain relatively stable and in approximately the same locations between 1998 and 2007.

Notwithstanding its relative stability, some changes are still evident in the reach between C.S 48 and C.S. 45. For example, at C.S. 46 in 1988, the main anabranch was locally divided into two, second-order, sub-channels. But in 1998 (following the major flood event that summer) the second-order channel closer to the south bank widened and deepened due to erosion. Conversely, in 2007 the main channel was shallower due to sediment deposition. At C.S. 45 in 1988, the main anabranch was adjacent to the south bank. In 1998, following the flood, a new main anabranch and another second-order channel had developed closer to the north bank, while the abandoned course of the 1988 main anabranch had partially silted to form a channel complex that included one, second-order, sub-channel and a small number of lesser sub-channels, all flowing along the south bank. This pattern remained unchanged in 2007.

It is clear from consideration of cross-sectional changes observed in 1998 that the record flood event (and the associated record sediment load) had a tremendous morphological impact on the Brahmaputra adjacent to Majuli Island. Generally, the great flood simplified the multi-channel morphology, scouring shallow areas and filling deep areas. This contrasts with generalised morphological changes observed at intermediate stages and discharges when the flow is divided between a number of anabranches and sub-channels of different orders that are separated by braid bars (Sharma, 2005). Under these flows, bar growth reduces the overall cross-sectional area, concentrating flow in the anabranches and sub-channels. Sub-channel deepening, widening and lateral erosion then ensues, forming one or two large anabranches and/or multiple second-order sub-channels. In anabranches and sub-channels adjacent to the floodplain, bank retreat results in the Brahmaputra widening and/or migrating laterally, usually towards the north. Braiding is most intense in reaches where bank materials are non-cohesive and easily eroded because such banks do not restrict processes of widening or lateral migration driven high discharges that deposit a significant proportion of their heavy sediment loads. In reaches where the bank is formed in cohesive materials, for example near Dakhinpat and Bessamora on Majuli Island, bank retreat and/or lateral migration is somewhat restricted, which results in deeper channels being scoured.

Chapter 3. Quantitative analysis of morphology and process-response in braided rivers

3.1. Introduction

Braided rivers generally have higher stream powers than otherwise equivalent single-thread rivers. It follows that braided rivers must be able to dissipate the excess energy somehow, given that hydraulics in both single-thread and braided rivers approximate uniform, steady flow. Braided rivers achieve this by transporting heavy sediment loads, building multiple bars, eroding their banks, and developing very wide, shallow channels which are hydraulically less efficient than the channels of single-thread rivers. Processes of bank erosion and braid bar formation, deformation and destruction are, consequently, intertwined with the need for braided rivers to dissipate their excess stream power through morphological changes that increase flow resistance.

In a braided river, sandbars are transient and relatively unstable sediment features, while islands are relatively stable and more long-lived. Sandbars are modified almost continuously by processes of sediment erosion, transport and deposition: they respond quickly and evolve rapidly during their short lives. Vegetated islands are modified intermittently: they respond slowly and persist for decades to centuries.

Major changes in the dimensions of the braided channel take place during medium to high, in-bank flows due to rapid rates of erosion, transport and deposition facilitated by high stream power, mobile bed sediments and erodible banks. Flow in the wide, shallow channel that results in features multiple secondary flow cells that break it up into multiple flow threads, with sub-channels forming where secondary currents converge at the surface, down-well and diverge at the bed, and medial bars forming where secondary flows converge at the bed upwells and diverge at the surface.

Such is the power and sediment load of the River Brahmaputra that the processes outlined above are able to mould a channel that is huge and hugely variable, with flows that divide and rejoin to give that channel a complex and ever-changing morphology. In short, the Brahmaputra manifests braiding process-response at a scale seldom observed elsewhere. The magnitude of discharges in the river derived from snowmelt in the World's highest mountain range, coupled with rainfall in the Indian monsoon. The abundant sediment supply is attributed to erosion of actively uplifting mountains of the Himalaya together with re-entrainment of highly erodible, alluvial deposits stored in the Assam valley.

Recognising these basic facts explain why the Brahmaputra is one of the largest and most active braided rivers, globally. The extent of variability of its overall waterway ranges from its narrowest width of about 1 km, near Guwahati, to the 23 km wide braid plain about 30 km downstream in Gumi. The study reach for this research extends about 40 km along the River Brahmaputra adjacent to Majuli Island. As described in Chapter 2, this stretch of the river features sub-reaches exhibiting anastomosed, anabranched and braided channels divided by varying patterns and sizes of sandbars and islands, none of which are permanent in nature. To support systematic and quantitative analysis of the complex geomorphological traits of the study reach, it is essential to apply rationally derived and rigorously defined parameters capable of faithfully characterising and representing the nature of the river's morphology. This type of analysis is not new and a number of 'braid indices' have been developed in past studies for this specific purpose. The next section reports work undertaken to determine the suitability and utility of existing indices that led to the decision to modify selected indices to make them compatible with the objectives of this study.

3.2 Existing and Modified Braiding Indices

Generally, braiding indices fall into one of two categories. The first category considers the mean number of active channels or braid bars per transect across the channel. The second category considers the ratio of the sum of channel lengths in a reach to a measure of the reach length. Bridge (1993) presented a useful compilation of braiding indices and suggested that braiding intensity is better represented by indices in the first category because the second category actually represents a form of 'total sinuosity'. Bridge's Table provided the basis for an expanded and updated version compiled during this study (Table 1).

Table 3.1. Existing Braiding Indices. Source: Bridge (1993).	
Author	Braiding Index
Brice (1960, 1964)	*Braiding index* $= \frac{2(sum\ of\ lengths\ of\ all\ bars+islands\ in\ the\ reach)}{centreline\ length\ of\ the\ reach}$
Howard et al. (1970)	*Braid index* $=(Av.no.of\ anabranches\ per\ cross-section)-1$
Engelund and Skovgaard (1973), Parker (1976), Fujita (1989)	*Mode*$=$ $number\ of\ rows\ of\ alternate\ bars\ (and\ sinous\ flow\ paths)$ $= 2 \times the\ number\ of\ braid\ and\ side\ bars\ per\ cross-section$
Rust (1978)	*Mode*$=number\ of\ braids\ per\ meander\ wavelength$
Hong and Davies (1979)	*Total sinuosity*$= \frac{length\ of\ channel\ segments}{channel\ belt\ length}$
Mosley (1981)	*Braiding index*$=\frac{total\ length\ of\ banfull\ channels}{distance\ along\ main\ channel}$
Richards (1982)	*Total sinuosity*$=\frac{total\ active\ channel\ length}{valley\ length}$
Ashmore (1991)	$Mean\ number\ of\ active\ channel\ per\ transect, or$ $Mean\ number\ of\ active\ channel\ links\ in\ braided\ netwrok$
Friend and Sinha (1993)	*Braid Channel Ratio*$=\frac{sum\ of\ mid-channel\ lengths\ of\ all\ channels}{length\ of\ mid-line\ of\ widest\ channel}$
Sharma (2004)	*Plan Form Index*$=\frac{\frac{Flow\ top\ width(T)}{Overall\ river\ width\ (B)}\times 100}{number\ of\ braid\ channels\ (N)}$
Sharma (2004)	*Flow geometry Index*$=\frac{\sum depths\ (d_i)\times widths\ (x_i)\ of\ submerged\ sub-channel}{Hydraulics\ mean\ depth\ of\ stream(R)\times Flow\ top\ width\ of\ the\ stream(T)} \times Number\ of\ braid\ channels\ (N)$

Early braiding indices measured the sum of bar or island perimeters relative to reach length, making them very strongly flow stage dependent. For this reason, an early proponent of braiding indices, Jim Brice, abandoned this form of braiding index (see Brice, 1964 and Table 3.1) instead classified the *degree of braiding* as the proportion of the channel length in a reach that is divided by bars and islands, and the *character of braiding* in terms of (1) whether bars or islands are dominant and (2) the planform shapes of bars and islands. Subsequent indices of the first type have evolved from the early work of James Brice. The most recent entries listed in Table 3.1 are type one indices developed by Professor Nayan Sharma at the IIT in Roorkee, India (Sharma, 2004) and these provided the basis for the modified braiding indices developed in this study, which are listed in Table 3.2.

The modified braiding indices developed by the candidate under the supervision of Professor Nyan Sharma himself, during a period of study at the Indian Institute of Technology, Roorkee. They too fall in the first category of indices because they consider either the number of active sub-channels or braided bars at transects across the river. The Modified Planform Index measures the planform change in a defined node of a braided river, which includes the number of bars, braid channels their size and length. The Modified Flow Geometry Index considers local flow variability across a transect while treating the thalweg (main and deepest) channel separately. The Bar Deformation Index is a measure of the change in the size of islands or bars between two dates of observation. The Thalweg Migration Index quantifies the extent of lateral movement of the thalweg channel between two dates of observation, and whether the movement is towards the left or right bank of the river Governing equations for these modified indices are given in Table 3.2.

Table 3.2. New Braiding Indices developed during this study.	
Description	Modified Braiding Index
Modified Planform Index measures the planform change in a defined node of a braided river, which includes the number of bars, braid channels their size and length.	$\text{Modified Plan form index (MPFI)} = \frac{\frac{\sum length\ of\ the\ bar\ (LBi)}{Length\ of\ reach\ (LR)} \times \frac{Mean\ flow\ top\ width\ (\bar{T})}{Mean\ overall\ river\ width\ (B)} \times 100}{Number\ of\ braid\ channels\ (N)}$
Modified Flow Geometry Index considers local flow variability across a transect while treating the thalweg (main and deepest) channel separately.	$\text{Modified Flow Geometry index} = \frac{\sum depths\ of\ submerged\ channels\ (d_i) \times \sum widths\ of\ submerged\ channels (x_i)}{hydraulic\ mean\ depth\ of\ the\ channel (R)} \times \frac{depth\ of\ the\ thalweg\ channel (d^{th})}{hydraulic\ mean\ depth\ of\ the\ channel\ (R)}$
Bar Deformation Index is a measure of the change in the size of islands or bars between two dates of observation.	$Bar\ Deformation\ Index\ (BDI) = \frac{Changed\ Bar\ Area\ (AC)}{Reference\ Bar\ Area\ (AR)} \times 100$
Thalweg Migration Index quantifies the extent of lateral movement of the thalweg channel between two dates of observation, and whether the movement is towards the left or right bank of the river.	$Thalweg\ Migration\ Index = \frac{Changed\ offset\ of\ the\ average\ length\ from\ the\ reference\ latitude\ to\ the\ thalweg\ channel. (OLC)}{Reference\ offset\ of\ the\ average\ length\ from\ latitude\ to\ the\ thalweg\ channel. (OLR)}$

3.3 Acquisition of data needed to identify fluvio-morphological features

3.3.1 Introduction

Such is the national and international significance of the River Brahmaputra that data pertaining to it are classified in India. Consequently, access to hydrological and morphological data is strictly limited, which makes non-governmental studies centred on landform change in the Brahmaputra challenging. In this study, cross-section data used in quantitative analysis of process-response and changes in braiding intensity in the study reach near Majuli Island between 1977 and 2007 were obtained from the Water Resource Department of Guwahati and Majuli Island, Assam and the Indian Institute of Technology, Roorkee.

Application of remote sensing techniques made the use of braiding indices possible, providing a way of identifying fluvio-morphological features as necessary to quantify not only the intensity and type of braiding but also how the braided pattern has shifted and changed through time. In this study, Landsat images for the period 1987 to 2015, were obtained from the United States Geological Survey (USGS).

In Landsat images, areas of deep water in the river appear black in the near-infrared (NIR) band of the satellite imagery because of high absorbance. However, the bed surface of shallow water regions reflects back some of the incident visual and infrared light and, therefore, the reflected radiance of shallow water is different from that of the deep water. Using this concept, it is possible to distinguish deep pools from shallow areas in a braided river (Karmaker and Dutta, 2016) and that utility was used to advantage in this study.

The Landsat images used in this study were mostly taken during the low flow season (October to January). Images for the period 2003 to 2008 were found to have stripes in them, making them less than ideal for use in this study. Another limitation was related to cloud cover. Most of the images of the area around Majuli Island have some cloud cover, even during dry season. While cloud-free Landsat images are relatively rare, it proved possible to find sufficient low flow season images to provide a consistent series throughout the period 1987 - 2015.

3.3.2 NDVI classification

The Landsat images were analysed based on the Normalised Difference Vegetation Index (NDVI), using the image classification tool in Arc GIS 10.3. The NDVI data layer is defined as:

$$NDVI= (NIR-R)/ (NIR+R)$$

where NIR represents the spectral reflectance in near infrared band and R represents the red band.

NDVI values range between -1 and +1, where increasing positive values indicate green vegetation and negative values indicate non-vegetated surfaces such as water, barren land, ice, snow or cloud.

Landsat ETM images (1987 – 2015) were analysed to categorise the Landuse. Hence, based on NDVI values, a supervised classification was used to classify water bodies (active channels), sand surfaces (sandbars) and vegetated land (islands and floodplains) within the image (Figure 2.1). These three categories of Landuse were used to apply the new, modified braided indices and to establish their utility in identifying and characterising fluvial and morpho-dynamic changes in the study reach during the last 30 years.

3.3.3 Raster to vector conversion

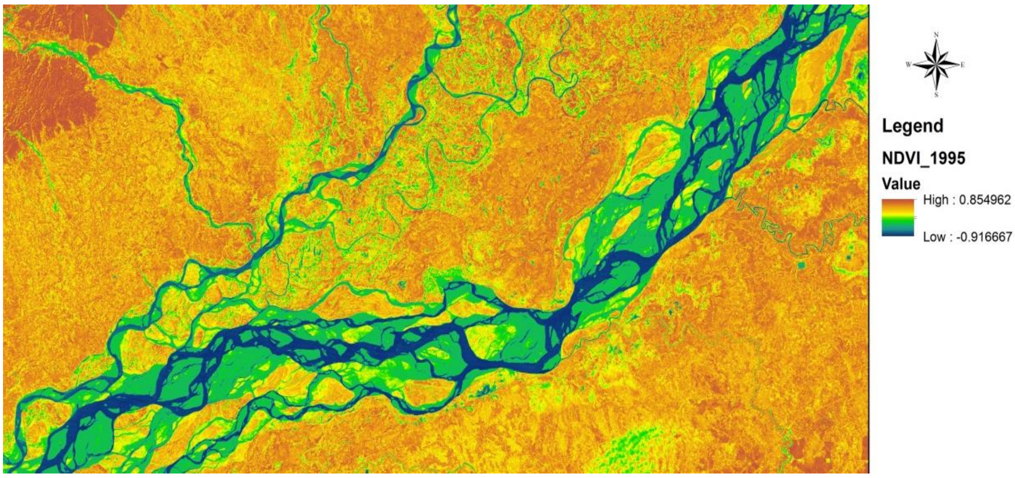

Figure 2.1: Image classification using NDVI near Majuli Island.

NDVI based classified images (Figure 2.2) were converted into vector data by using the conversion tool raster to a polygon in Arc Gis.

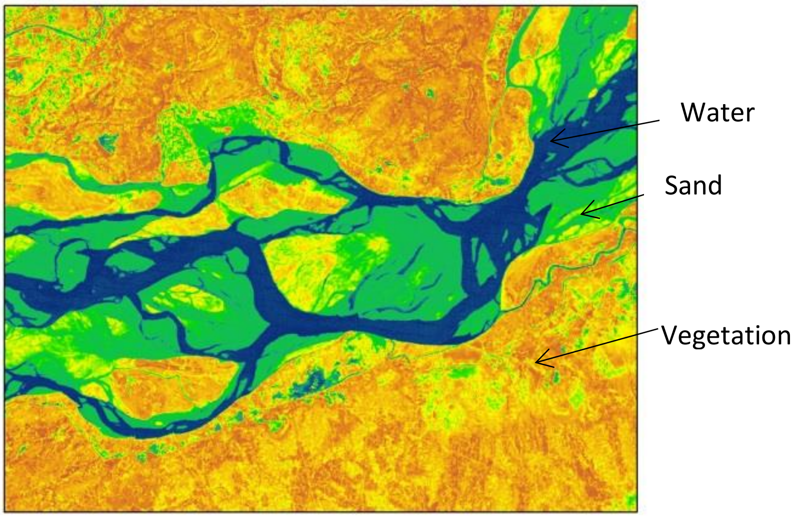

Figure 2.2: NDVI Raster image.

Method:

LandSat ETM

↓

NDVI Classification

(Supervised)

↓

Raster to Polygon using Conversion Tool in Arc Gis

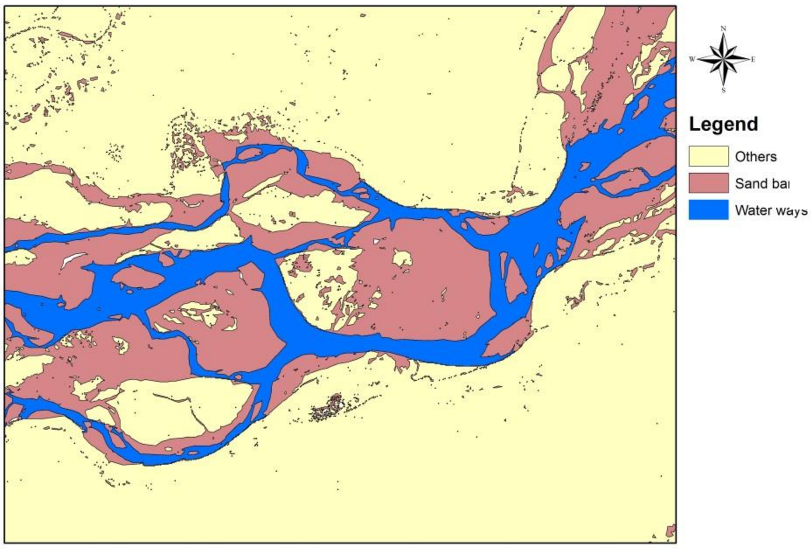

Water = (-0.4) – (-0.9)

Sand = 0.2 – 0.1

Vegetation = 0.8 – 0.3

Figure 2.3: Vector data conversion.

This technique provides a more accurate measurement of the size, shape and length of all the entities (i.e. water, sandbar and island) in the vector that could be obtained using manual digitisation (Figure 2.3). These vector data were used to apply the modified braiding indices, as reported in the remainder of this chapter.

3.4 Thalweg Migration Index (TMI)

The TMI represents the degree and direction of lateral shifting by the deepest anabranch or sub-channel in the braided planform during the period between two observations. The terms within the TMI are illustrated in Figure 2.4., 2.5 Numerically:

$$TMI = \frac{OLC}{OLR}$$

where, OLC = changed offset of the average length from the reference latitude or longitude base on the thalweg channel orientation and OLR = reference offset of the average length from latitude or longitude base on the thalweg channel orientation.

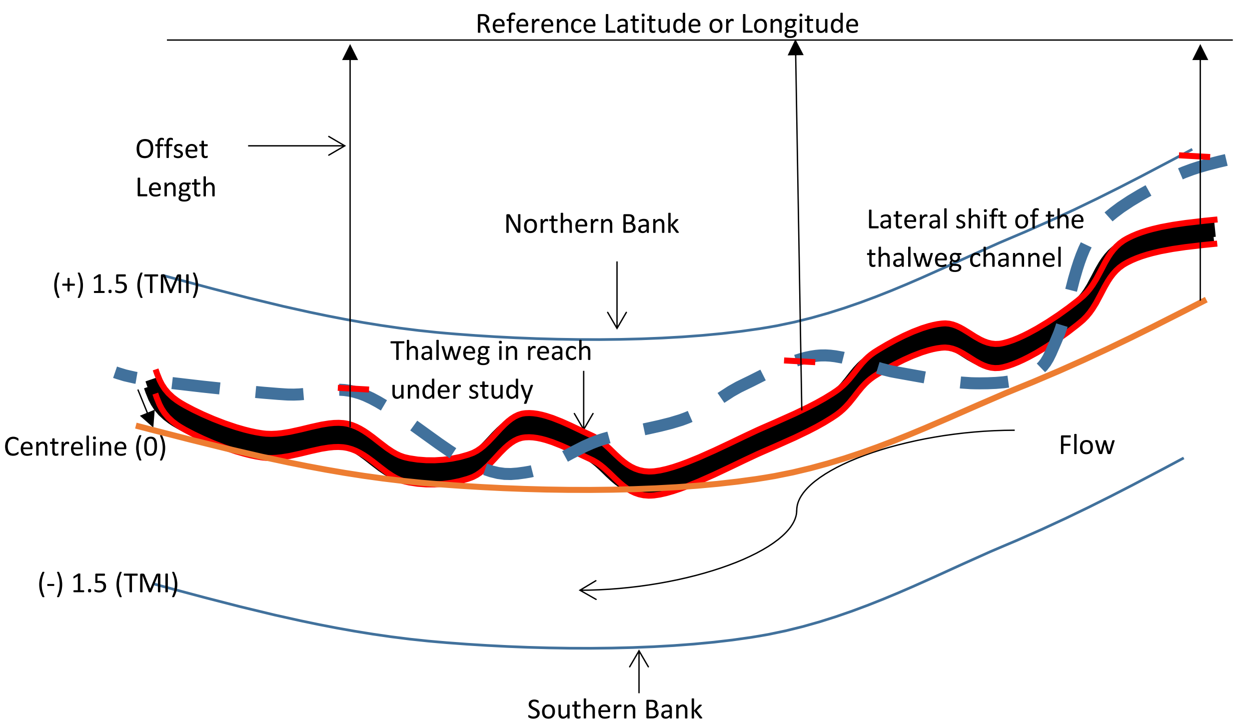

Figure 2.4: Definition sketch for OLC for OLR.

Landsat images from 1987 to 2015, were analysed in Arc GIS to calculate the TMI values as functions of space and time. These TMI values quantify the changing position of the deepest sub-channel in the river study reach (Figure

2.6). Thalweg channel offset lengths were measured for three locations were measured from the reference latitude (Figure 2.7). These offset lengths were used to quantify the thalweg channel migration using TMI (Figure 2.8).

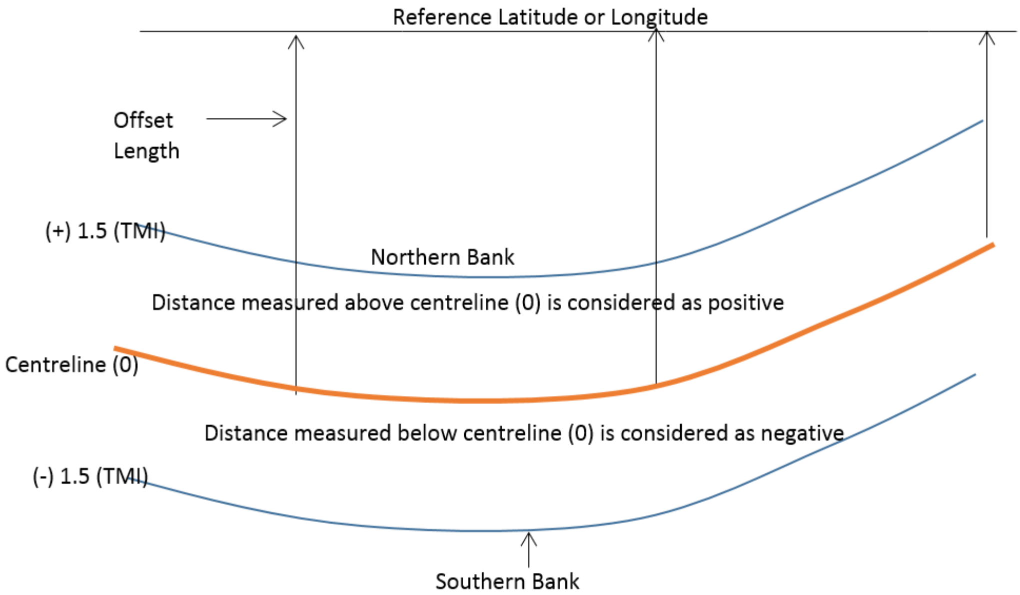

Figure 2.5: Definition sketch for OLC for OLR.

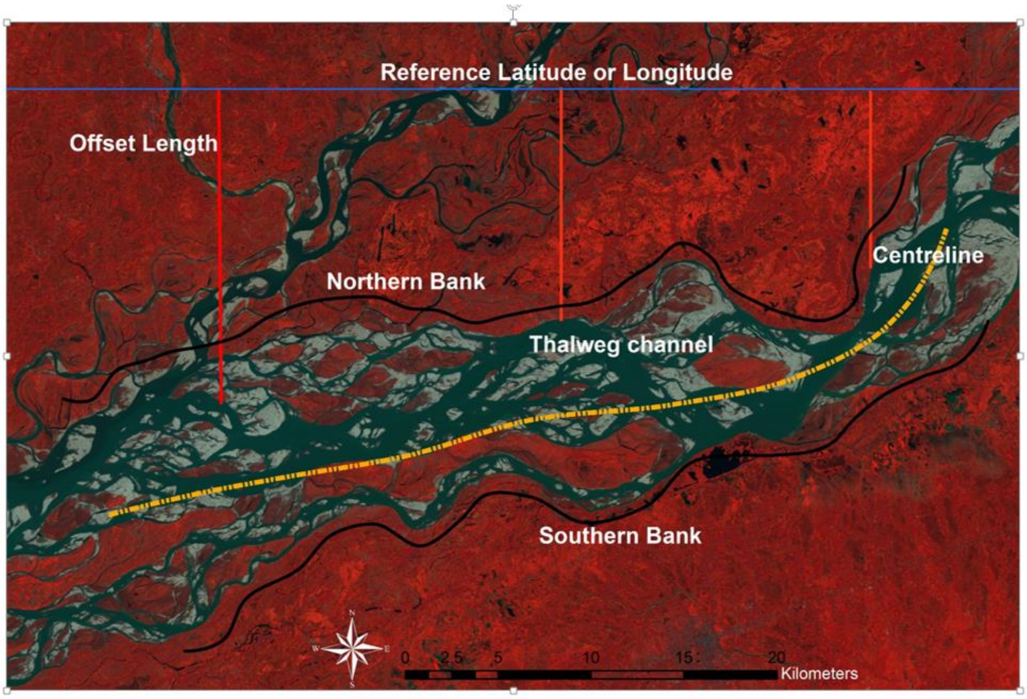

Figure 2.6. 2009 Landsat image of the 40 km study reach of the Brahmaputra adjacent to Majuli Island.

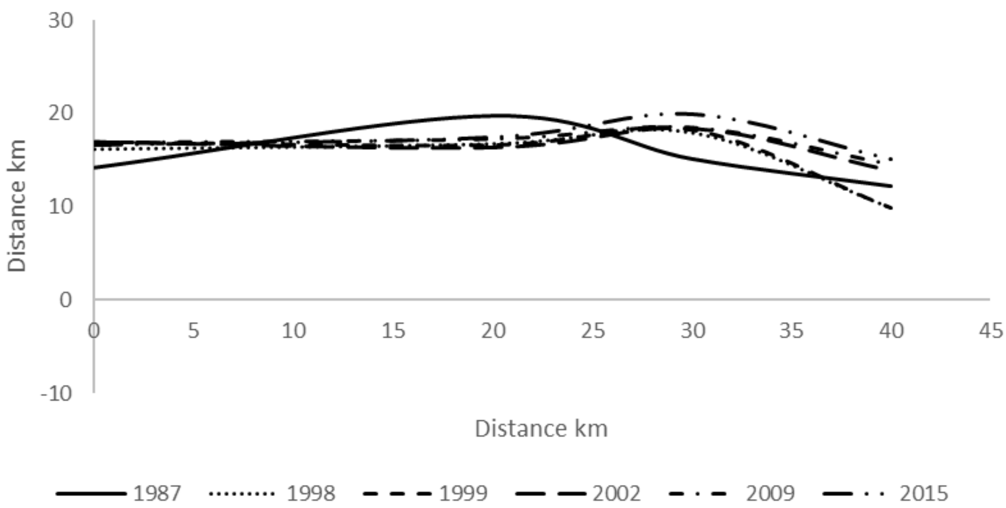

Figure 2.7. Thalweg channel migration in the study reach 1987 - 2015.

Figure 2.7 indicates that the position of the thalweg channel has changed more significantly in the downstream third of the study reach, with the position changing little in the upstream half of the study reach.

The range of TMI values measured for the river Brahmaputra near Majuli Island during the period 1987 to 2015 is -1.5 to +1.5 and the direction of change is indicated by the negative and positive signs. This range is dependent on the distance of the geographical coordinate from the thalweg channel, hence this may vary according to the lateral movement of the river from the reference coordinate at the different time period.

Migrating towards North Bank 1.5 ⟵ 0 ⟶ -1.5 Migrating towards South Bank

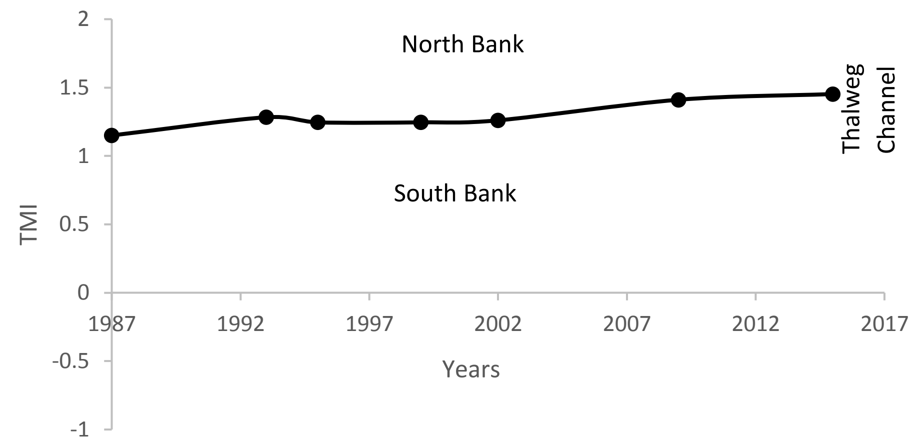

Figure 2.8: Thalweg migration index near Majuli Island.

Figure 2.8 indicates that during the period 1987 – 2015, the thalweg channel in the study reach migrated steadily northwards towards Majuli Island.

3.5. Modified Plan Form Index (MPFI)

In a braided river, the high energy fluvial environment, heavy bedload and erodible banks generate complex channel morphology that changes frequently. There is consequently a need to formulate appropriate indicators to describe these braiding phenomena and the fluvial landform patterns that result, in quantitative terms (Sharma, 2004).

Sharma (2004) proposed the Plan Form Index (PFI) for this purpose, defined as:

$$PFI = \frac{\frac{T}{B} \times 100}{N}$$

where, T = water surface width, B = overall river width and N = number of braid channels (Figure 2.9).

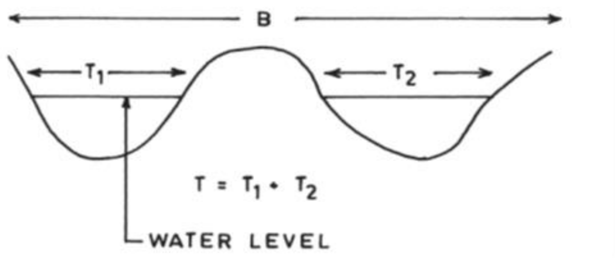

Figure 2.9. Definition of terms in the PFI developed by Sharma (2004).

In this study, the PFI has been modified to better account for the relative length of bars as well as their relative width and a threshold value of MPFI for the reach adjacent to Majuli Island has been defined. The original PFI represents the product of the actual flow width over the overall width per braid channel whereas MPFI represents the product of the actual flow width over the overall bankfull width, while also accounting for the length of the bars relative to the length of the reach, per braid. Taking the length of the node in the channel as the length of the reach, Modified Plan Form Index is calculated from:

$$MPFI = \frac{\frac{\sum length\ of\ the\ bar\ (LBi)}{Length\ of\ reach\ (LR)} \times \frac{Mean\ flow\ top\ width\ (\overline{T})}{Mean\ overall\ river\ width\ (B)} \times 100}{Number\ of\ braid\ channels\ (N)}$$

where, $\sum LBi$ = length of the bar ($\sum LBi = LB_1 + LB_2 + LB_3 + \cdots + LB_n or \sum_{i=1}^{n} LB)$, LR = length of node, $\overline{T}$ = Mean flow top width, N is the number of braid channels or multi channels.

$$\overline{T} = \frac{T_1 + T_2 + T_3 + \cdots + T_n}{n}) or\ \overline{T} = \frac{\sum_{i=1}^{n} T}{n}$$

and $\overline{B}$ = mean over all bankful river width,

$$\left(\overline{B} = \frac{B_1 + B_2 + B_3 + \cdots + B_n}{n}\right) or\ \overline{B} = \frac{\sum_{i=1}^{n} B}{n}$$

and the key dimensions are illustrated in Figure 3.9.

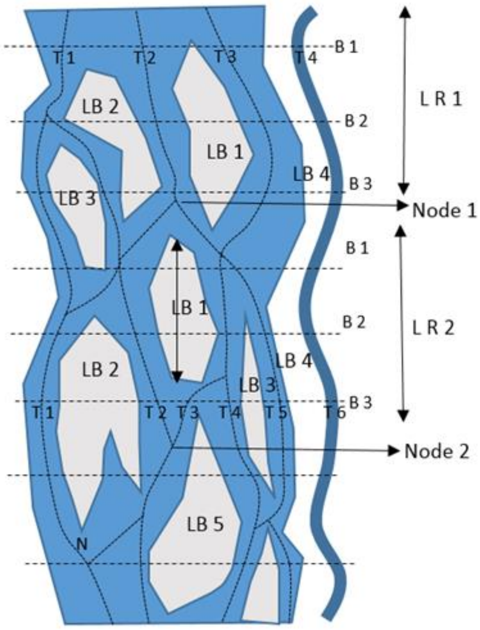

Figure 2.10. Schematic layout definition sketch for Modified Plan Form Index.

MPFI is the product of the length of the bar as a proportion of the length of the reach and means flow top width as a proportion of mean overall width divided by a number of channels (Figure 2.10). This represents the spatiotemporal dynamics of planform changes. MPFI reflects the fluvial landform disposition with respect to a given water level with lower values indicative of a higher degree of braiding.

MPFI values were calculated using the Landsat images for 1987 to 2015, with the study reach divided into sub-reaches 1 (upstream, around Kamalabari) and 2 (downstream, around Burha Chapori) (Figure 2.11). The MPFI value for sub-reach 1 in 1987 indicates moderately intense braiding (Figure 2.12). In 1993 this reach had become highly braided and it remained highly braided in 2015. In sub-reach 2, the MPFI value in 1987 indicated a high intensity of braiding. By 1993 MPFI decreased towards being high to moderate braiding. In 2009, MPFI indicates a return to highly intense braiding. This is image was taken just after the very high monsoon runoff that occurred in 2008 (Figure 2.13). Sub-reach 2 continued to be highly braided in 2015.

Contrast in braiding intensity between sub-reaches 1 and 2 indicated by their different MPFI values and trends are consistent with the hypothesis that bank cohesion (and therefore erosion resistance) is higher in the area around

Kamalabari, so that the potential for the river to widen sufficiently to accommodate highly intense braiding is lower, relative to that sub-reach 2 where the banks around Burha Chapori are non-cohesive and highly erodible, increasing the potential for river widening, anabranching and the formation of numerous braid bars and islands.

Lahiri and Singha (2014), proposed that the valley floor in the vicinity of sub-reach 2 is northward dipping, due to the topographic expression of the main Himalayan frontal thrust (see Figure 3.1 in the next Chapter). Their argument that an increase in the area of active braid bars observed in the Brahmaputra adjacent to the southern part of Majuli Island (i.e. in sub-reach 2 as defined in this study) may be driving increased erosion along the southern edge of the island due to neotectonics effects is supported by initial assessment of the record of MPFI values and their changes through time over the last 30 years.

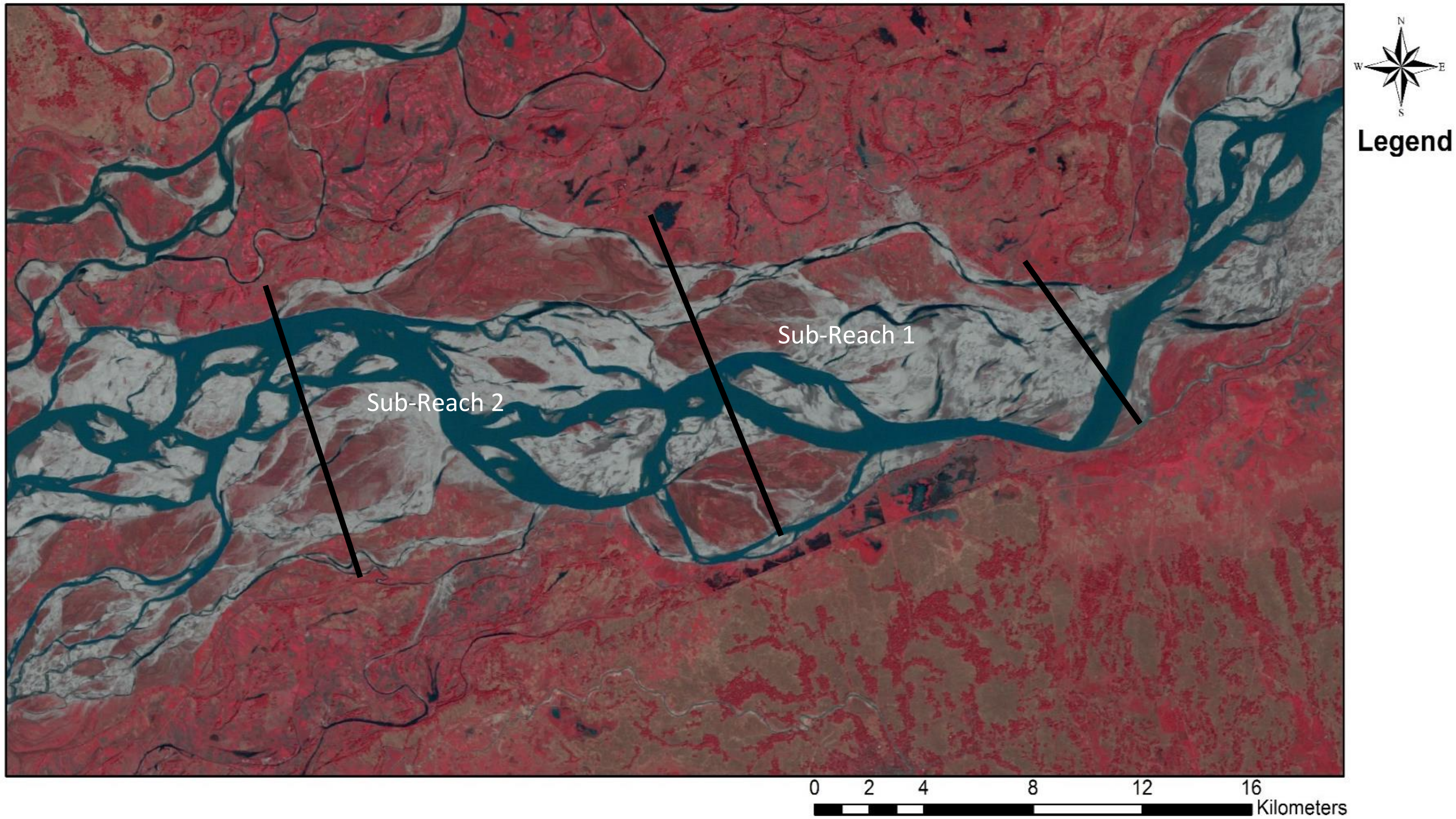

Figure 2.11. 1987 Landsat image of the study reach with sub-reach 1 (Kamalabari) and sub-reach 2 (Burha Chapori) indicated.

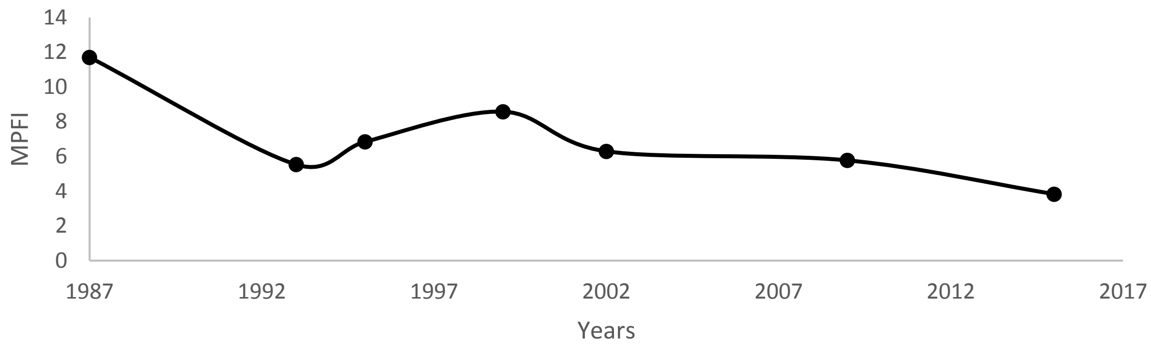

Figure 2.12. Trends in Modified Plan Form Index values in sub-reach 1.

MPFI Thresholds
MPFI < 6 – High braiding
6 > MPFI < 18 - Moderate braiding
MPFI > 18 - low braiding

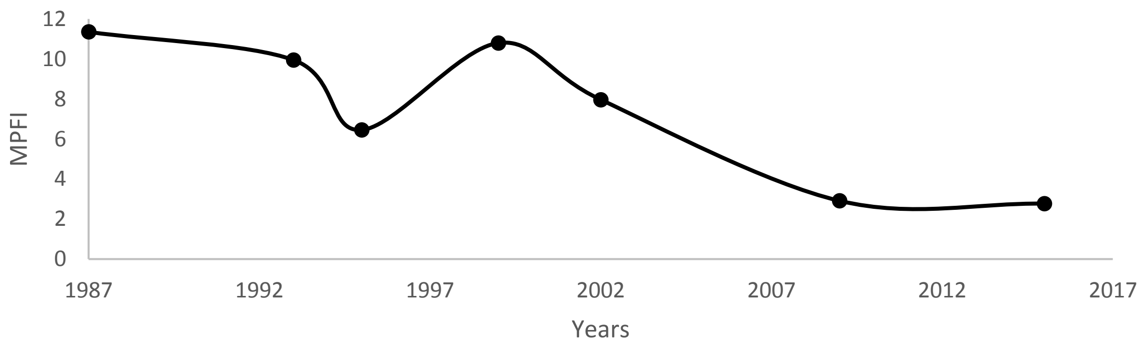

Figure 2.13. Trends in Modified Plan Form Index values in sub-reach 2.

3.6 Modified Flow Geometry Index (MFGI)

The Flow Geometry Index (FGI), developed by Sharma (2004), reflects the underwater sub-channel disposition and the hydraulic efficiency of a braided stream. Higher values indicate the occurrence of a higher intensity of braiding. This index is illustrated in Figure 2.14 and defined numerically by:

$$FGI = \frac{\sum di.xi}{R.T.} \times N$$

where, di and xi = depth and width of each of the active (i.e. wet) sub-channel, T = overall water surface width, R = overall hydraulic radius, and N = number of sub-channels.

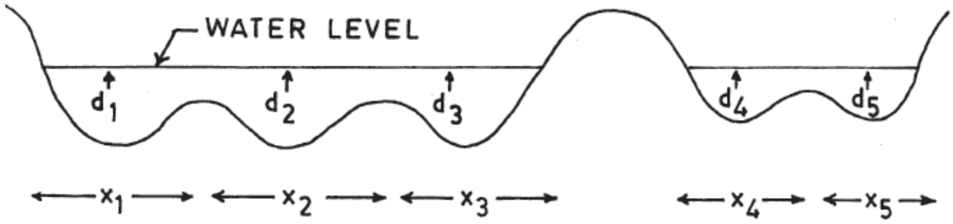

Figure 2.14. Flow geometry used to define FGI. Source: Sharma (2004).

The original, two-dimensional, FGI was modified as part of this research, to account for additional, important, fluvial parameters.

Modified Flow Geometry Index (MFGI) is a parameter that reflects the cross-sectional and planform dispositions of active (i.e. wet) sub-channels and, hence, the hydraulic (in)efficiency of the braided river. It is defined by:

$$MFGI = \frac{\sum_{i=1}^{n} d \times \sum_{i=1}^{n} x}{R} \times \frac{d^{th}}{R}$$

where, $\sum_{i=1}^{n} d = d_1 + d_2 + d_3 + \cdots + d_n$ and $\sum_{i=1}^{n} x = x_1 + x_2 + x_3 + \cdots + x_4$ are depth and width of each active (i.e. wet) sub-channel, d^{th} is the depth of the thalweg channel and $R = \frac{\sum_{i=1}^{n} d}{n}$ is the overall hydraulic radius of the braided river and the terms in the equation are illustrated in Figure 2.15.

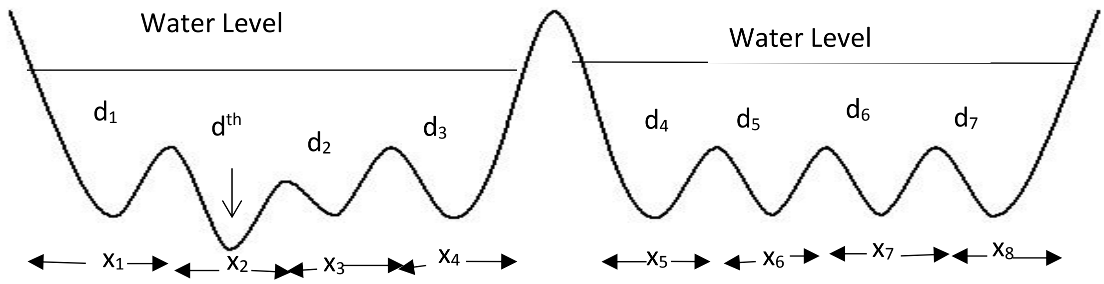

Figure 2.15. Definition sketch illustrating cross-sectional parameters in the MFGI.

MFGI is the product of two terms, each of which represents a dimensionless, morphological parameter. The first term is the product of the sums of the depths and widths of the wet parts of active sub-channels, divided by the overall hydraulic radius of all the active sub-channels. The second term is the maximum depth of the thalweg sub-channel, divided by the hydraulic overall radius of the all the active sub-channels. High values of MFGI indicate intense braiding, which tends to reduce the hydraulic efficiency of the river channel and increase the rate at which stream energy is dissipated due to high flow resistance.

MFGI values for cross sections 49-47 in the study reach have been calculated for the years 1988, 1998 and 2007 (Figure 2.16 – 2.17). These are the only cross-sections for which data are available in the study reach (see Figure 1.14). The results indicate that braiding intensity in the study reach increased between 1988 and 2007. In 2007, MFGI values suggest that braiding intensity was moderate at cross-sections 49 and 48 (in sub-reach 1) but highly intense at cross-section 47, which is in sub-reach 2. Hence, in terms of braiding intensity, these results for MFGI are consistent with those for MPFI.

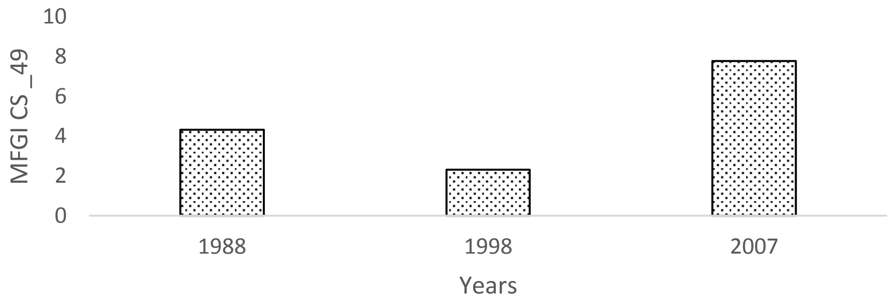

Figure 2.16. Record of MFGI values for cross-section 49 in the study reach.

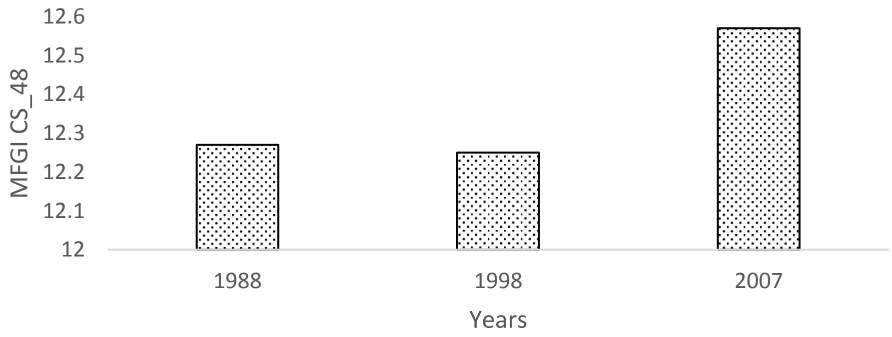

Figure 2.17. Record of MFGI values for cross-section 48 in the study reach.

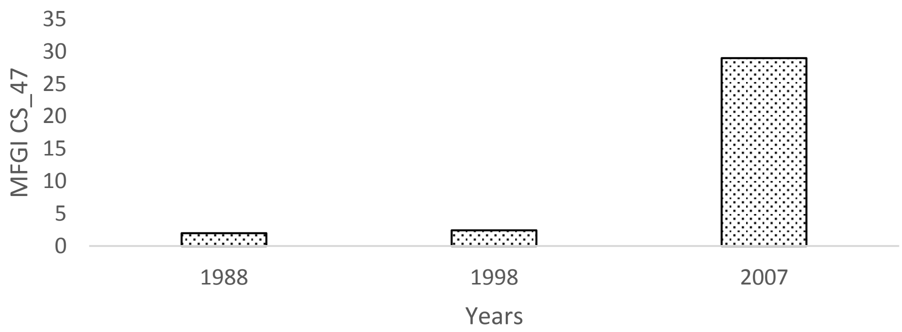

Figure 2.18. Record of MFGI values for cross-section 47 in the study reach.

MFGI Thresholds
MFGI > 5 - Low Braiding
5 > MFGI < 15 - Moderate Braiding
MFGI > 15 – High Braiding

3.7 Bar Deformation Index (BDI)

The Bar Deformation Index (BDI) developed in this research represents the change in the planform area and shape of a braid bar during the period of time between consecutive measurements. It is defined by:

$$BDI = \frac{AC}{AR} \times 100$$

where, AR = Reference Braid Bar Area at the time of the first observation, AC = Braid Bar Area at subsequent times of observation, and the terms in the equation are illustrated in Figure 2.19.

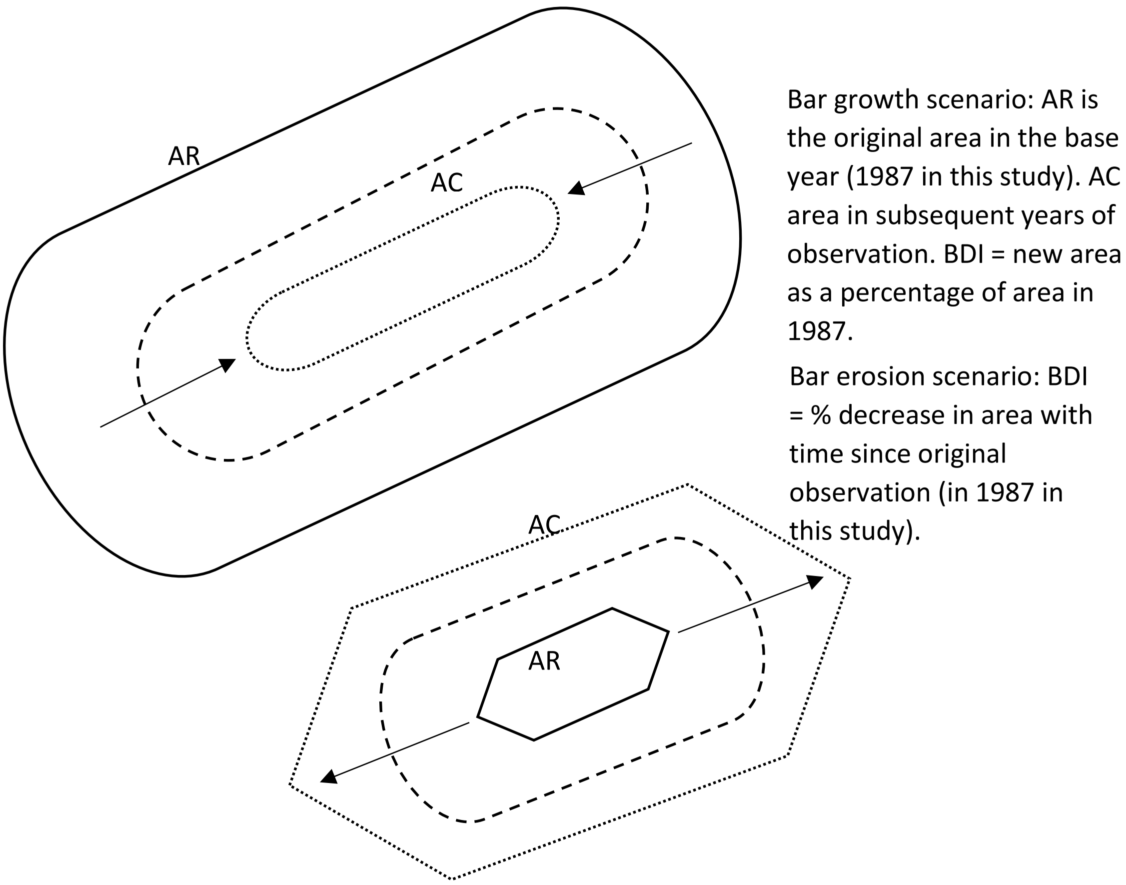

Figure 2.19. Definition sketch for AR, AC and Bar Deformation Index.

Three braid bars within the study reach were selected for BDI analysis, based on the same Landsat images (taken between 1987 and 2015) used in applying the TMI and MPFI. The bars are labelled A-1. A-2 and A-3 in Figure 2.20. A-1 was a transient, unstable, mostly unvegetated bar, A-2 was a smaller, stable, vegetated bar that was occupied by people, and A-3 was a larger, stable bar with dense vegetation cover (Figure 2.20). 1987 was the reference year. The braid bars were categorised into micro, meso and macro-bar size classes with the categories defined as follows:

Micro-Bar: 1 - 15 km^2
Meso-Bar: 15 - 30 km^2
Macro-Bar: > 30 km^2

Changes to the areas, lengths and width of the three selected braid bars that took place between 1987 and 2015 are complex in both sequence and nature. For this reason, they are chronicled and described in detail in Table 3.4.

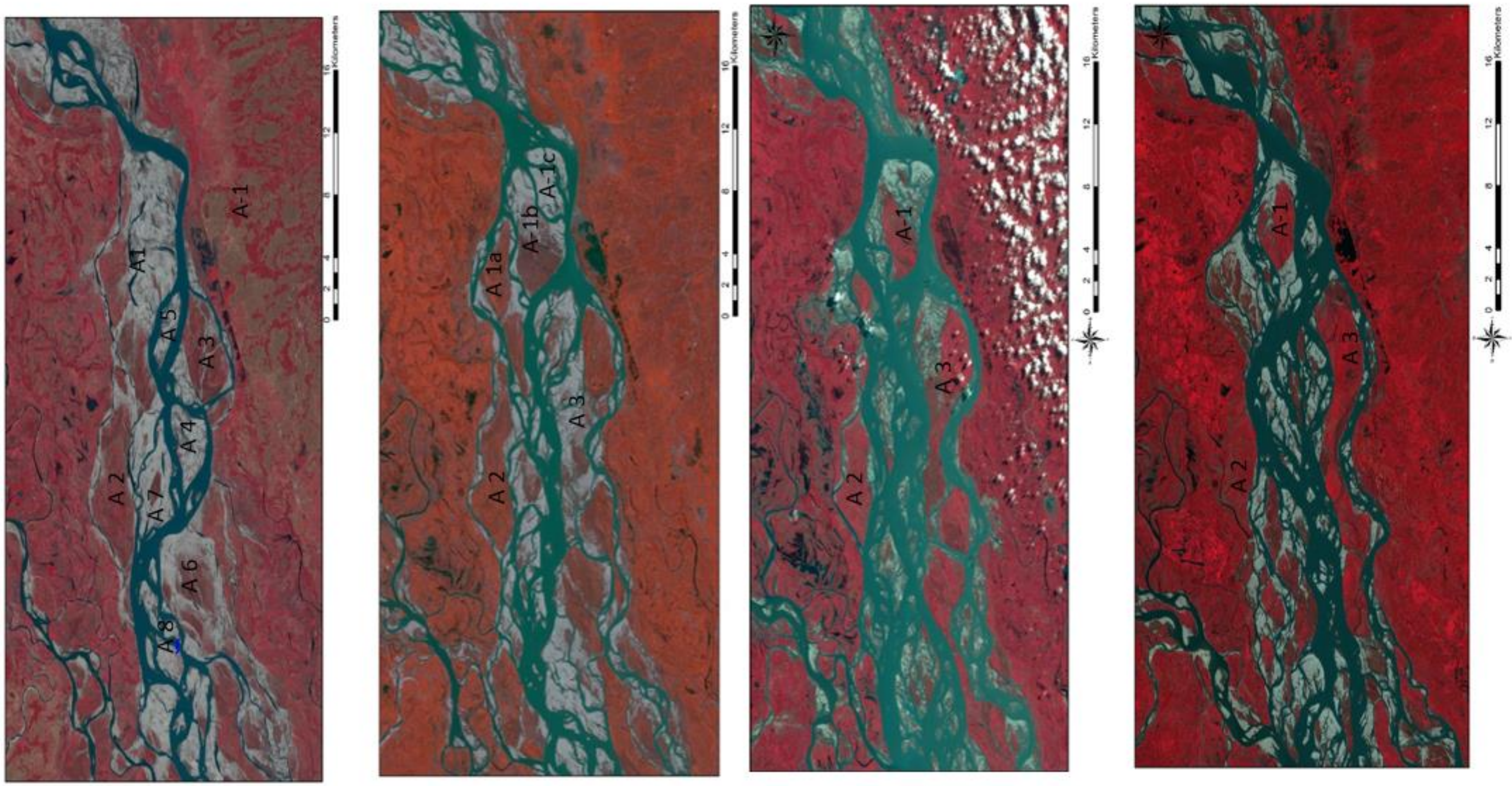

Figure 2.20. Braid bars selected for BDI analysis of the same study area (Figure 1.3) (date of the image are 1987, 1993, 1999 and 2015).

Table 3.4. Observed Braid Bar dimensions and changes 1987 - 2015						
Image Date	Bar Size Class	Bar code	Area (km^2)	Length (km)	Width (km)	Remarks
19.12.1987	Macro	A-1	68.07	17.64	7.48	Base Year
	Meso	A-2	18.25	6.68	4.80	
	Meso	A-3	24.99	16.69	3.55	
01.11.1993	Meso	A-1a	18.86	10.86	3.76	Transformed into two Meso-Bars (a+b) & one Micro-bar (c) by dissection
	Meso	A-1b	18.15	7.63	5.02	
	Micro	A-1c	4.90	3.76	2.57	
	Meso	A-2	21.13	11.66	3.04	Transformed into a Meso Bar
	Transformed into Macro	A-3	43.71	18.85	4.78	Transformed into Macro-bar by merging of A4, A5, A6, A7 and A8
07.11.1995	Transformed into Macro	A-1a	26.78	7.68	3.58	Transformed back to Macro bar by accretion
	Meso	A-1	34.61	21.30	3.46	Merge A-1b & A-1c to be one Meso-bar
	Transformed into Meso	A 2	26.17	19.44	2.955	Expanded as a Meso-bar through sediment accretion
	Transformed into Macro	A-3	67.63	13.80	5.20	Transformed back to Macro-bar by merging A4, A5, A6, A7 and A8 through accretion
25.10.1999	Transformed into Micro	A-1a	11.98	4.733	1.37	1998 monsoon flood washed away much of bar. Remnants are visible as indistinct micro-bar complex
	Meso	A-1	22.88	6.80	6.12	Bar diminished but still meso in size
	Micro	A-1b	1.61	2.06	1.28	New bar created by dissection of A1a
	Micro	A-2	14.63	8.52	4.00	Transformed into a Micro-bar by 1998 flood. Remnant stable and vegetated
	Macro	A-3	74.53	35.33	4.42	Transformed into a macro-bar by accretion. Stabilised and vegetated
17.10.2002	Micro	A-1a	0.82	1.85	0.55	Transformed into remnant Micro-bar
	Meso	A-1	19.98	6.70	6.78	Still a Meso-bar
	Transformed into Micro-bar cluster	A-1b	1.42	3.09	1.05	A cluster of new micro-bars formed by dissection and accretion
	Micro	A-1c	4.56	4.95	1.42	New cluster of micro-bars created by dissection of A-
	Micro	A-1d	0.67	1.20	0.92	

	Micro	A-1e	0.89	1.70	0.56	1a & widespread, local accretion
	Micro	A-1f	0.82	1.46	0.78	
	Meso	A-2	25.09	11.50	3.97	Transformed into a meso bar by accretion. Stable bar with vegetation
	Macro	A-3	51.99	23.34	3.57	Transformed into a Macro-bar. Stable, with vegetation
21.11.2009	Micro	A-1a	6.95	7.45	2.83	Remained Micro-bar
	Meso	A-1	23.98	12.27	8.11	Still Meso-bar
	Meso	A-2	22.16	11.28	3.83	Macro-bar. Stable, with vegetation
	Macro	A-3	57.79	26.93	6.35	Stable Macro-bar with vegetation
13.10.2015	Meso	A-1a	15.36	5.58	3.81	Transformed into Meso-bar
	Meso	A-1	17.13	8.70	3.16	Meso-bar, size some what reduced
	Macro	A-3	39.08	24.63	2.64	Became a stable bar with vegetation cover. Transformed into a macro bar.
	Micro	A-2	12.86	6.51	2.74	Transformed into a Micro-bar stable bar with vegetation when about 50% of bar joined Majuli Island

Any change in the BDI value will demonstrate the transformation in the fluvial landform feature depicting the extent and behaviour of channel instability processes. During the flood, the capacity of the channel to transport sediments becomes high while on the falling of flood it becomes weak and started depositing sediment in a haphazard manner. This resulted in creating mid-channel bar, elongated bar and anabranches in the channel. When the size of the bar increases braiding intensity increases. This is because the channel becomes shallower and narrower due to the falling of flood which makes the channel hydraulically less efficient and starts depositing on the edge of the existing braided bar.

In 1987, A-1 (Dabar Chapori), was a single, macro-bar (68.1 km^2). The record of changes in this bar is described in Table 3.4 (above) and BDI values are graphed in Figure 2.21. In 1993 this bar was dissected by sub-channel to be fragmented into two meso-bars and one micro-bar. The BDI, based on the change between 1987 and 1993, was 28%. In 1995 several of the micro-bars rejoined and A-1 turned back into a macro-bar, with the BDI rising to 50%. During the major monsoon flood of 1998, this macro-bar was washed away, leaving a number of micro-bars, which are visible in the image for 1999. The BDI in 1999 increased again, to 53%. The BDI of A-1 was calculated because this is the most transient of all the sandbar present in the study reach. In 2002, A-1 the size of the bar decreases, the BDI declined to 43% and a cluster of new micro-bars formed by dissection and accretion nearby. In 2009, A-1 sandbar the BDI increased slightly to 45% but the cluster of new sandbars were completely washed away by the high discharge flow. Finally, in 2015 A-1 was transformed back into a meso-bar, with a further reduction in BDI to 22%.

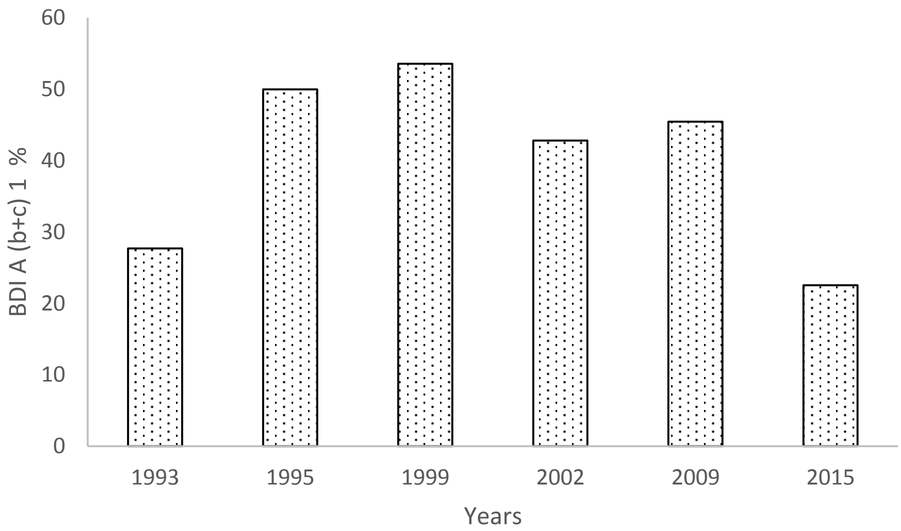

Figure 2.21. Record of Bar Deformation Index values for braid bar A-1.

In 1987, braid bar A-2 (Burha Chapori), was a meso-bar (18.25) km^2. In 1993 the BDI decreased to 84%. In 1995 the BDI value increased to105%. After the high monsoon flood in 1998, the bar was reduced in size by erosion and dissection, becoming a micro-bar (14. 62 km^2) with the BDI decreasing again, to 58%. In 2002 the size of the bar recovered to again become a meso-bar (25.09 km^2) and the BDI increased to 100%, which indicates that the bar had returned the size it had in 1987. In 2009, the bar shrank slightly and the BDI decreased to 88%. Finally, in 2015 A-2 transformed into a micro-bar (12.86 km^2). It became a stable bar with vegetation cover and a BDI of 51%, indicating the bar was half its original size (Figure 2.22).

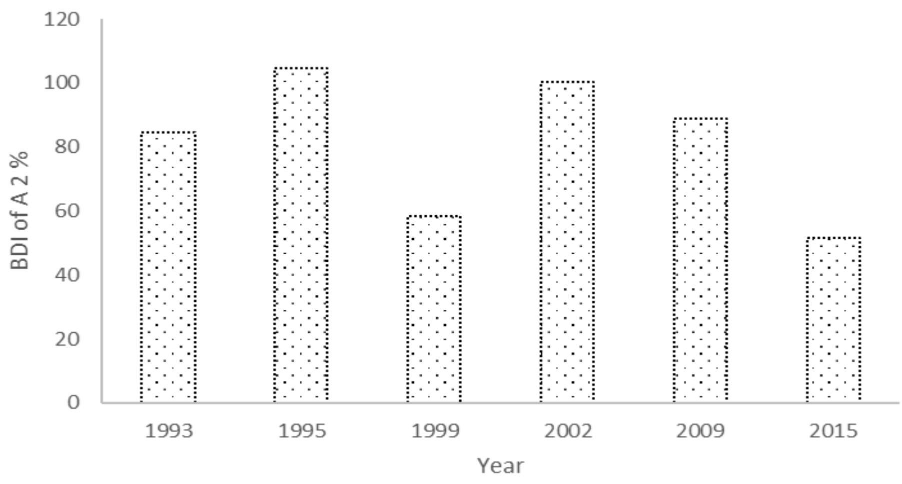

Figure 2.22. Record of Bar Deformation Index values for braid bar A-2.

Bar A-3 (Natun Kartik Chapori), was a meso-bar (18.25 km^2) in 1987. It grew into a macro bar (43.71 km^2) in 1993, with a BDI of 240%. This was due to the amalgamation of adjacent bars with A-3 through accretion (Table 2.23). The bar grew again through further accretion, with the BDI rising to 340%. In 1999, continued accretion had increased the BDI again, to 408%. That is, the bar was four times larger than when first observed Erosion between 1999 and 2002 reduced the size of braid bar A-3, although it still met the criterion for classification as a macro-bar. In 2002, the BDI value of A-3 was reduced to 285%. In 2015 the area of the bar was again reduced, with BDI decreasing to 214% BDI (Figure 2.23).

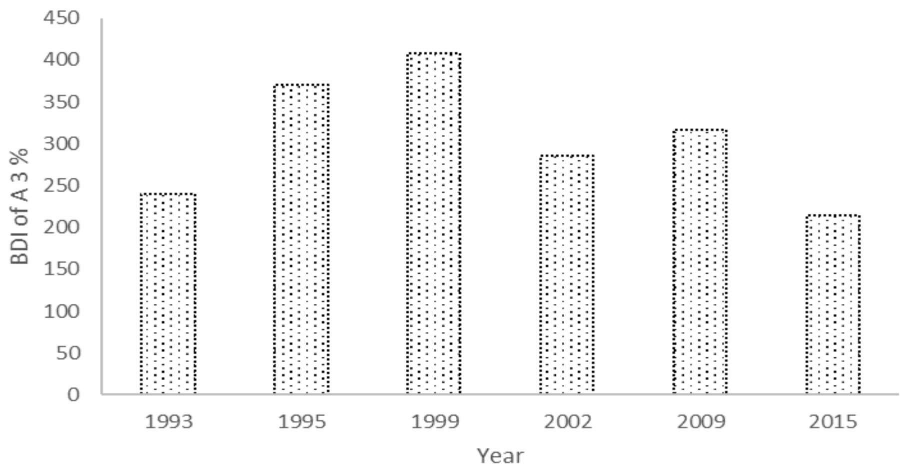

Figure 2.23. Record of Bar Deformation Index values for braid bar A-3.

3.8 Conclusion

This chapter outlined the development of new braiding indices and their application in measuring the braiding intensity of the river Brahmaputra. These newly developed braiding indices were used for validating the medium-term landscape evolution model for the river Brahmaputra in subsequent chapters. Based on the research reported in this chapter, it may be concluded that the southern part of Majuli Island is increasingly exposed to the threat of bank erosion due to river widening, intensified braiding and northward migration of the thalweg channel. These morphological trends are liable to result in serious loss of land and damage to the lives and livelihoods of people living and working close to the southern edge of the island.

Quantitative analysis of river channel changes and process-response relationships in the Brahmaputra suggest that sub-reach 2, alongside the southern part of Majuli Island's southern bank, is particularly volatile morphologically. Therefore, chronicling and explaining the history of channel evolution in this complex, braided river and developing a model capable of forecasting future channel changes in the medium-term are necessary not only to better understand river system dynamics and process-response relationships responsible for channel evolution, but also to inform river training and bank stabilisation measures designed to protect Majuli Island from erosion by the great River Brahmaputra.

Chapter 4. Modelling morphological evolution and change in braided rivers

4.1 Introduction

The study and forecasting of channel adjustments and morphological changes play an important role in river science, management and conservation. Time and space scales of interest for river management and restoration are decades and tens of kilometres, respectively, which are typically larger than those commonly adopted in model-based studies intended to improve understanding geomorphological processes (Church, 2007). Large, braided rivers are modelled far less frequently than single-thread streams, whether using conceptual models (Surian, 2015), empirical models (Rhoads, 1992; Alchouri et al., 2015) or numerical models (Ferguson and Church, 2009; Vide, 2010) and, to date, no Computational Fluid Dynamics (CFD) model has been applied and fully evaluated at the mesoscale (10-100 km, 10 -100 years) in a braided river system (Bertoldi, 2005; Ferguson, 2007; Kleinhas et al., 2010).

Limited use of physics-based, deterministic models to simulate braided rivers is partially explained by the fact that such systems are highly complex and exhibit unpredictable behaviours (Paola and Georgiou, 2001). Autonomous evolution and responses to changes in the variables that control process and form in braided systems are highly sensitive to their initial state (Lane and Richards, 1997) and, no matter how sophisticated a deterministic model may be, it is highly unlikely that any physical-based, river model could reproduce the exact time-dependent evolution of a braided stream like the Brahmaputra (Thorne et al., 1993). This is due to:

(i) uncertainties in initial model and boundary conditions (e.g., inflow distribution of water and sediments, the spatial distribution of grain size),

(ii) upscaling problems in bank erosion and non-uniform sediment transport modelling approaches (Mosselman, 2012), and

(iii) partially understood, multiple, nonlinear feedback loops in the coupled flow – morphology – sediment transport system (Haff, 1996).

The fact is that the evolution of a braided system is deterministically-predictable only at very short timescales. The possibility for quantitative, deterministic prediction quickly breaks down over medium to long timescales (Paola, 2001).

4.2 Modelling braided rivers

According to Mosselman (1995), different mathematical models of river planform change were developed, which helps in understanding the underlying processes, yet they are considered valid and easy to use software packages. Schuurman et al., (2013) used the 2D depth average morphodynamic model which produce many morphological characteristics and dynamics of a braided river with a chosen set of boundary conditions yet insufficient for long-term modelling. With a few notable exceptions, limited attention has been paid to morphological behaviour and change in very large, braided river systems like the Brahmaputra over management-relevant time and space scales (Thorne et al., 1993; Richardson and Thorne, 1998; Mount et al., 2012; Sarker et al., 2014). This is due, in part, to the high cost and difficulty of research on very large rivers, limited data availability (especially for politically-sensitive rivers, for which data are classified) and the inherently unpredictable and risky behaviour of very large, braided river systems.

Hindcasting using models provides insight regarding historical process-form linkages and past evolution of rivers, which provides the basis for understanding and explaining morphological responses to past events. Modelling also allows investigators to study how environmental process drivers, such as climate, geology and vegetation act through processes of erosion, sediment transport and deposition to effect channel adjustments that can, through time, transform channel morphology. Popular models used to simulate fluvial hydraulics at the reach scale level and over short to medium timescales include MIKE 11, ISIS, ONDA, FLUCOMP, Flood Modeller pro, TUFLOW and HEC-RAS. Some of these are one dimensional (1D) models, and some are mixed 1D and two dimensional (2D) models.

With respect to modelling the Brahmaputra, 1D (i.e. long-stream flow field) models are insufficient to simulate hydraulics and morphology in braided streams due to lack of information simulating the transverse flow field. For adequate simulation of the flow field, 2D or, ideally, three dimensional (3D) numerical models are required. That said, at present, 3D models (which include the vertical flow field) are too numerically expensive for use at medium to macro space and time scales, in large rivers.

A reduced complexity model (RCM) is an alternative approach to simulating braided rivers numerically. These models run much faster than fully, physics-based models because they represent process-form relations in complex geomorphological systems in a simplified manner. While this allows the models to simulate longer reaches over longer timespans, the simplifications involved in RCM approaches can reduce their capacity to make detailed forecasts of future channel morphologies as, for example, the exact locations of future anabranches and bars in the braided pattern. Notwithstanding this, RCMs have been shown to be able to simulate evolution and change in overall stream morphology (e.g. channel width and braiding intensity), evolutionary trajectory (e.g. narrowing/widening or incision/aggradation), and sediment dynamics (e.g. net sediment budget) (Ziliani et al., 2013).

Past studies have evaluated the capacity of RCMs to reproduce laboratory experiments (Doeschl-Wilson, 2005), topographic detail in short river reaches (Nicholas and Quine, 2007), and processes that operate over geological timescales (Coulthard et al., 2002). However, little attention has so far been paid to the capacity of RCMs to simulate channel behaviour in very large braided river systems at time and space scales useful for river management.

To address this research gap, this study evaluated the capacity of an RCM to model selected morphological features, based on comparisons between:

i. modelled channel bed elevations and those observed through cross-sectional surveys,

ii. simulated thalweg channel migration rates and directions and those observed from available satellite images, over relatively short periods (e.g. 1 to 2 years, or a single flood event).

For changes over longer periods, it was accepted that it would be more appropriate to compare the statistical characteristics of simulated and observed braided characteristics (e.g. braiding intensity, average channel width) as suggested by Nicholas (2005).

To generate data useful for braided river model validation, some system-scale generalisation of braided river features and behaviour is required. There is a rich literature on braiding indices, mostly focused on planform parameters (Bridge, 1993; Egozi, 2008; Mosley, 1983) and topographic aspects (Wilson, 2005); as well as methods designed to characterise the planform pattern of a braided river (Murray and Paola, 1996; Sapozhnikov et al., 1998). Most of the research using RCMs to date has been performed in the context of hindcasting and forecasting sediment yields at catchments and/or reach scales (Coulthard et al., 2002; Ziliani et al., 2013; Meadows, 2014). A negligible amount of research has been conducted on the utility of RCMs to hindcast and forecast morphological evolution in very large rivers that exhibit profound morphological change, intensively braided patterns and complex evolutionary trajectories. Therefore, in this study, an attempt was made to evaluate the capacity of an RCM to simulate the morphological behaviour and planform change in the River Brahmaputra near Majuli Island, Assam.

4.3 Landscape evolution models

Landscape evolution models (LEMs) are a category of reduced complexity models. They are cellular models that simulate long-term landscape development and they are at the opposite end of the model spectrum to CFD-based models (Table 4.1). LEMs simulate hydrological, fluvial and slope processes in 2D, using a cellular grid and reduce the complications involved in setting up boundary conditions, and slope-channel coupling. These models route multiple flow routing which enables landforms such as slopes and rivers to migrate and change their morphology over time (Coulthard, 2002).

Murray and Paolo (1994) wrote the first cellular model LEM for braided rivers. This model routes water discharge through grid cells representing the channels within the braid plain, depending on their relative elevations and the overall bed slope. Their model was able to reproduce the dynamic behaviour of a braided river such as lateral migration of channel and bars (Coulthard, 2007). There are various LEMs such as SIBERIA, GOLEM, CASCADE, CHILD and CAESAR

Lisflood. Details of these models are presented in Table 4.2. From the Table, it emerges that CAESAR Lisflood is appropriate for simulating medium-term landscape evolution of the River Brahmaputra. However, it does not meet the criteria to include tectonic effects on the river within the model.

Table 4.1. Salient features of LEM and CFD models for simulating channel morphology.

Model Type	Time-scale	Space-scale	Capacity to simulate fluvial process-response mechanisms
Landscape evolution model (LEM)	Designed to model river and catchment evolution over medium to very long time periods (10 – 10,000+ years)	Designed to the model river and catchment evolution over large areas (10 - 100 km^2)	Designed to model long-term landscape development such as hydrology, fluvial erosion, slope processes, tectonic changes, climate and lithology combine drainage density and the shape characteristic of the drainage basin.
Computational fluid dynamics (CDF)	Designed to model a small part of the river for relatively short time periods (1 to a few years) Usually applied to specific flood periods or short periods of high fluvial change	Designed to model small features or single cross-sections of river, or at most, short reaches.	Designed to investigate hydraulic flow properties over unchanging topography and model flood propagation and inundation extent. Unsuitable to simulate river evolution as the river morphology does not change in a CDF model.

Table 4.2. Salient features of various LEM models for simulating channel morphology.

Attributes	SIBERIA	GOLEM	CASCADE	CHILD	CAESAR Lisflood
Study associations	Between hydrology, tectonics and catchment from geomorphic time scale.	Landscape evolution linkages between erosion and tectonics.	Landscape evolution linkages between erosion and tectonics.	Landscape evolution linkages between erosion and tectonics.	Between hydrology, catchment or reach from geomorphic time scale.
Type of Mesh or grid	grid cell representation of the river channel.	grid cell representation of the river channel.	Irregular grid (the area where there is repeated action near river channel have more nodes).	Irregular grid (the area where there is repeated action near river channel nodes).	Small square grid cells (from 1 m ... 50 m ... 100 m etc.) to represent the landscape.
Surface Erosion	Diffusive slope process	Diffusive slope process	Diffusive slope process	Diffusive slope process	Diffusive slope process
Landsliding	No clear representation	Slope failure threshold	No clear representation	No clear representation	Slope failure threshold
Erosion/ deposition Process	By channel flow	By channel flow	By channel flow	By channel flow	By channel flow
Flow routing process	The steepest line of descent	The steepest line of descent	CASCADE flow model	The steepest line of descent	LISFLOOD-FP flow model
Sediment transport equation	Universal sediment transport function	Universal sediment transport function	Universal sediment transport function	Einstein (1950)	Einstein (1950) and Wilcock & Crowe (2003)
Number of grain size	One	One	One	Two (sand and gravel)	Nine (based on grain size distribution)
Suspended sediment	No	No	No	No	Yes
Catchment or reach scale size and time step		Large scale catchment (square grid cells 1 km × 1 km) and from 100,000 to 10,000,000 years.			Small to bigger catchment or reach and from 10 to 10,000 years.
Insertion of meandering channel and braiding channel	No	No	No	Meander	Meander and Braiding channel both
Representation of discharge regime	Runoff constant	Runoff constant	Runoff constant	Sequence of discrete storm events	Hourly or daily discharge or rainfall time series
Validation	Experimental and field geomorphological data				Field data from flood records and alluvial stratigraphies

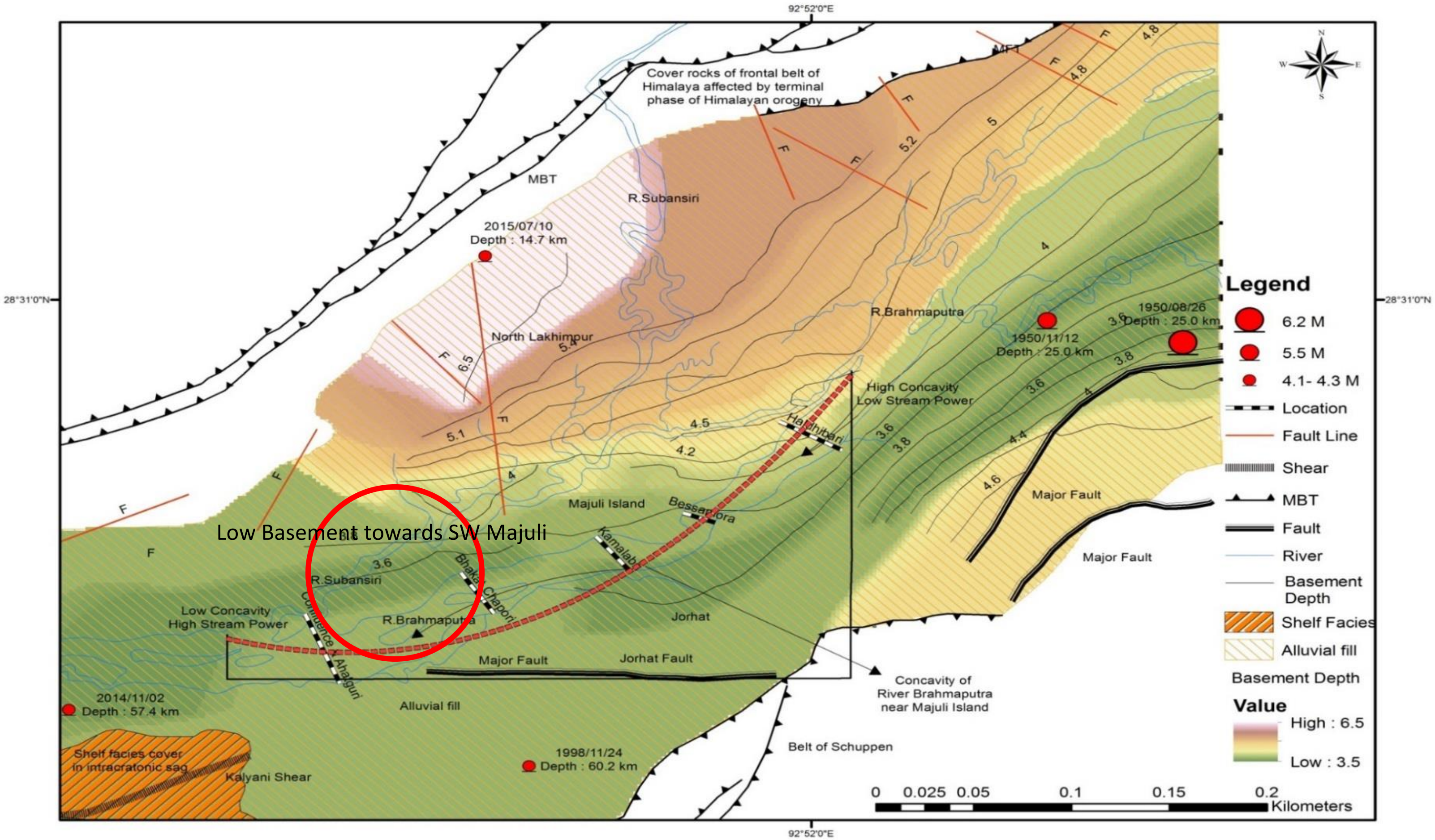

Figure 3.1. Fluvio-Seismic tectonic disposition showing profile concavity, faults, epicentres and geological structure. Source, Seismotectonic map of Assam, Seismotectonic Atlas of India.

The tectonic setting of the Majuli Island is shown in Figure 3.1. The island is situated between the Bouguer gravity anomaly (contours 220–240 mGal) and first-order basement depth contours 3.6 to 5.0 km (Narula et al., 2000). The tectonic map clearly shows a prominent ‘low’ in the SW part of the island. Th remainder of Majuli Island falls into the lower part of the ‘central uplift’ zone. Seismological evidence suggests that the Himalaya mountains to the west of the Majuli Island, and the Indo-Burma thrust areas to the east, both experienced significant large earthquakes (greater than magnitude 4) between 1950 and 1993 (Narula et al., 2000). However, the area of the Brahmaputra valley where the Majuli Island is located is an aseismic zone. This observation is in line with the study of the Coda waves (Hazarika et al., 2009) generated by smaller earthquakes (magnitudes varying from 1.2 to 3.9). Consequently, the CAESAR-Lisflood (C-L) model is appropriate for simulating the morphological change in this large, complex braided river because the influence of tectonic activity is of limited significance to the morphological evolution of the Brahmaputra near Majuli Island. The C-L model operates through hydrological, hydraulic, fluvial and slope erosion sub-models and can also represent the hydrological effects of different types and densities of catchment vegetation cover. The C-L model can indicate inundation extent by exporting simulated water levels to a DEM or it can be linked to an existing, 2D or 3D hydraulic model to support physics-based routing of water across a landscape.

The structure of the C-L model is shown in Figure 3.2. The name of the model is derived from ‘CAESAR’, which is an acronym, standing for ‘Cellular Automaton Evolutionary Slope and River’, and LISFLOOD, which is just a name that refers to a GIS-based, distributed model for river basin-scale water balance and flood simulation. The combined, C-L model represents the river basin landscape using a grid of uniformly-sized cells, within which development of the landscape is determined by the interactions between cells that have fluxes of water and sediment as inputs and outputs. Water and sediment routing, and hence landscape changes, are simulated using rules (i.e. each cell is an automaton whose behaviour is governed by simple cause and effect rules) based on simplifications of the physics of water flow and sediment movement

(Nicholas, 2005). The model uses square grids to represent the dynamics. The cellular grid is user-defined and the maximum number of cells in the DEM is limited only by the computer power and memory available. CAESAR has been run with up to 2 million grid cells but is best suited to applications with 250,000 to 500,000 cells. Generally, C-L can simulate periods of 10 – 100 years with these numbers of grid cells, but smaller numbers of grid cells are necessary for very long simulations, which may range from thousands to tens of thousands of years (Figure 3.3)

A good example of the application of the C-L model was its use in the River Waitaki, New Zealand for exploring interactions between vegetation and morphological dynamics of a braided, gravel-bed, reach. The reach length was 20 km and the braid plain was 4 km wide, and simulations were run for 20 years duration (Coulthard, 2007). The C-L model's outputs suggested how changes in vegetation cover interact with flow and sediment transport patterns to drive morphological responses. The findings were used to inform sustainable management of the river. Like the Waitaki, the Brahmaputra has a braided planform that tends to change its channel morphology very rapidly, with serious implications for sustainable management of the impacts of those changes on the lives and livelihoods of people living in and close to the river. In that respect, the success of C-L in its application to the River Waitaki, New Zealand, is encouraging. Hence, based on both the underpinning theory of reduced complexity, cellular automata models, and CAESAR-LISFLOOD's success in modelling the history of landscape evolution of a complex, braided river (albeit a much smaller one than the River Brahmaputra near Majuli Island), there was reasonable optimism that a C-L model would be (a) possible and (b) informative. Consequently, in this research, a 40 km study-reach near the south part of Majuli Island was modelled for a duration of 20-years to help understand river system dynamics and forecast future channel changes in the River Brahmaputra (Figure 4.4).

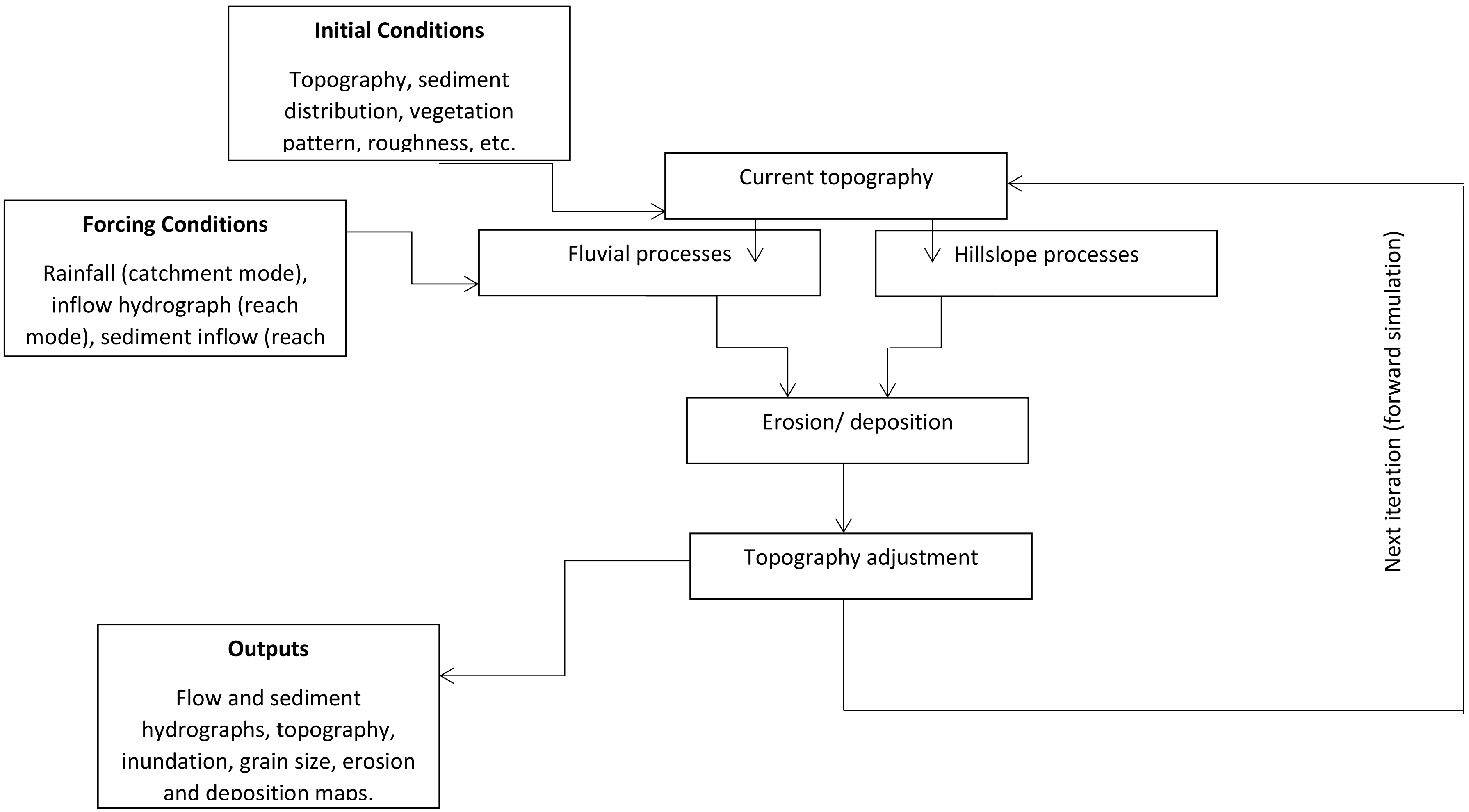

Figure 3.2. Conceptual structure of the CAESAR model. Source: Coulthard and De Wiel Van (2007)

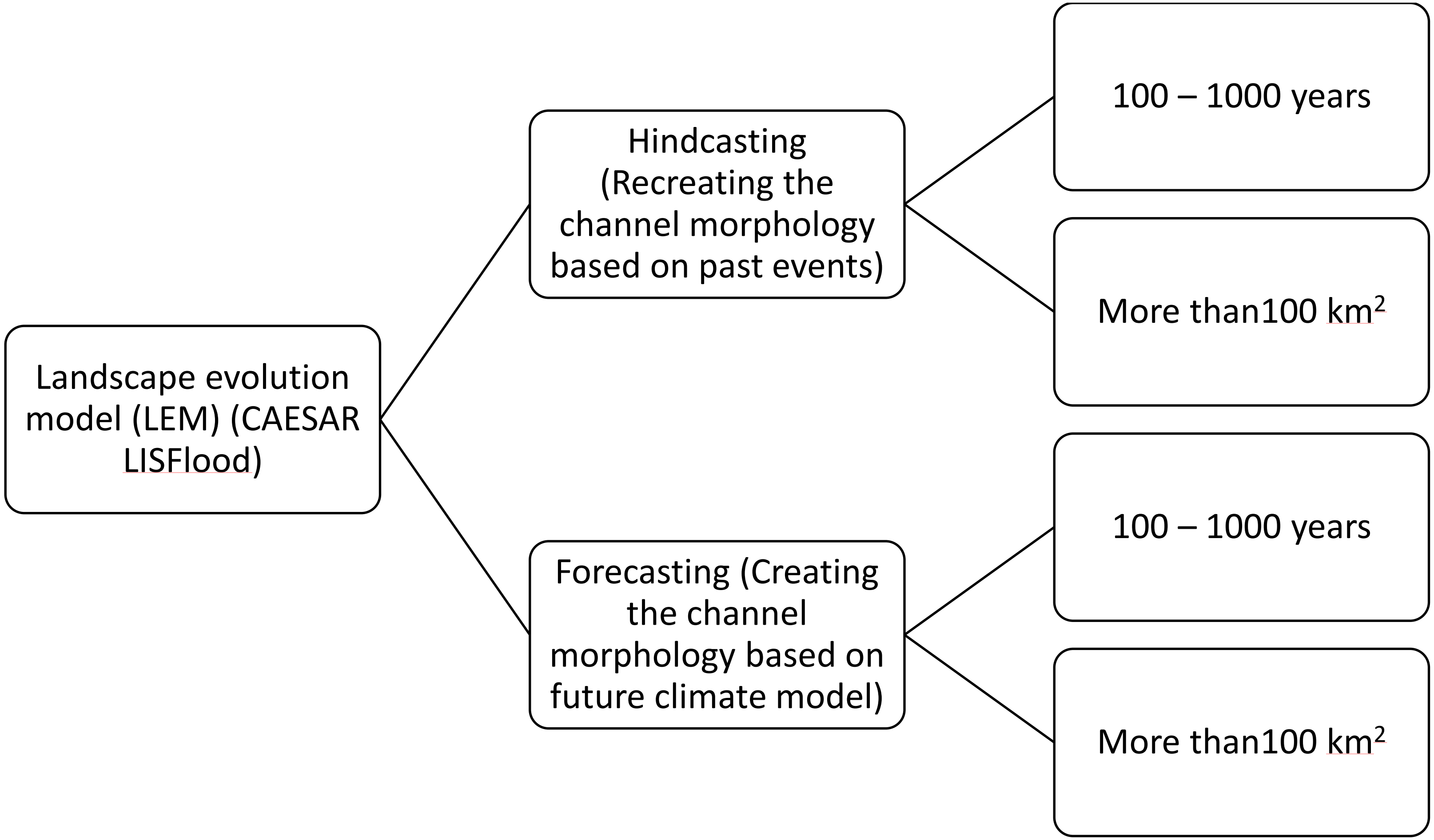

Figure 3.3. Structure of the CAESAR-LISFLOOD model.

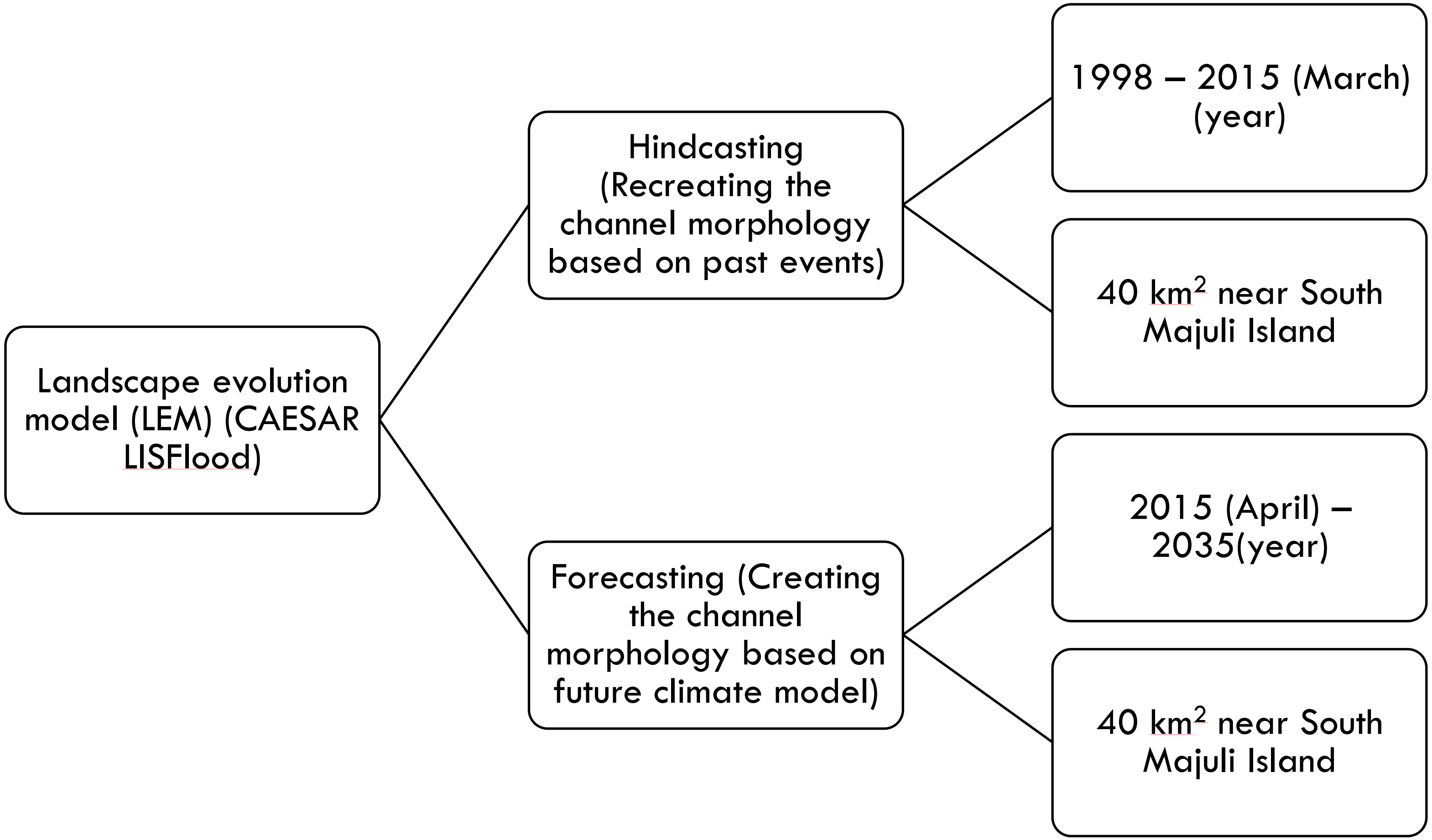

Figure 3.4. Structure of the CAESAR-LISFLOOD model built to simulate the River Brahmaputra in the study reach.

Chapter 5. CAESAR-LISFLOOD: operation, parameter selection, data requirements and model set up

5.1 Introduction

This chapter address operation, parameter selection, data required and model set up required to use C-L as a medium term, landscape evolution model for the River Brahmaputra near Majuli Island. The chapter also discusses data preparation, including bathymetry, discharge and suspended sediment loads needed to run the C-L model. C-L can be run in three different modes:

(i) catchment,
(ii) reach,
(iii) tidal.

In this research, the ‘reach’ mode was selected. There is no requirement for rainfall data to run a C-L model in reach mode. Setting up a reach mode model requires that the initial topography and bathymetry of the modelled reach be defined in a DEM and that initial boundary conditions be specified for discharge, sediment input (both amount and particle size distribution), and vegetation pattern (which affects surface roughness).

5.2 Topography and Bathymetry

It is challenging to survey cross-sections in a very large, braided river like the Brahmaputra, and to do so was well beyond the scope and resources available to this project. In fact, there only 65 monumented cross-sections within the 918 km length of the Brahmaputra in India (see Figure 1.14), even given all of the resources available to the States of Arunachal Pradesh and Assam. Hence, in this study, reliance was placed on data available for these cross-sections.

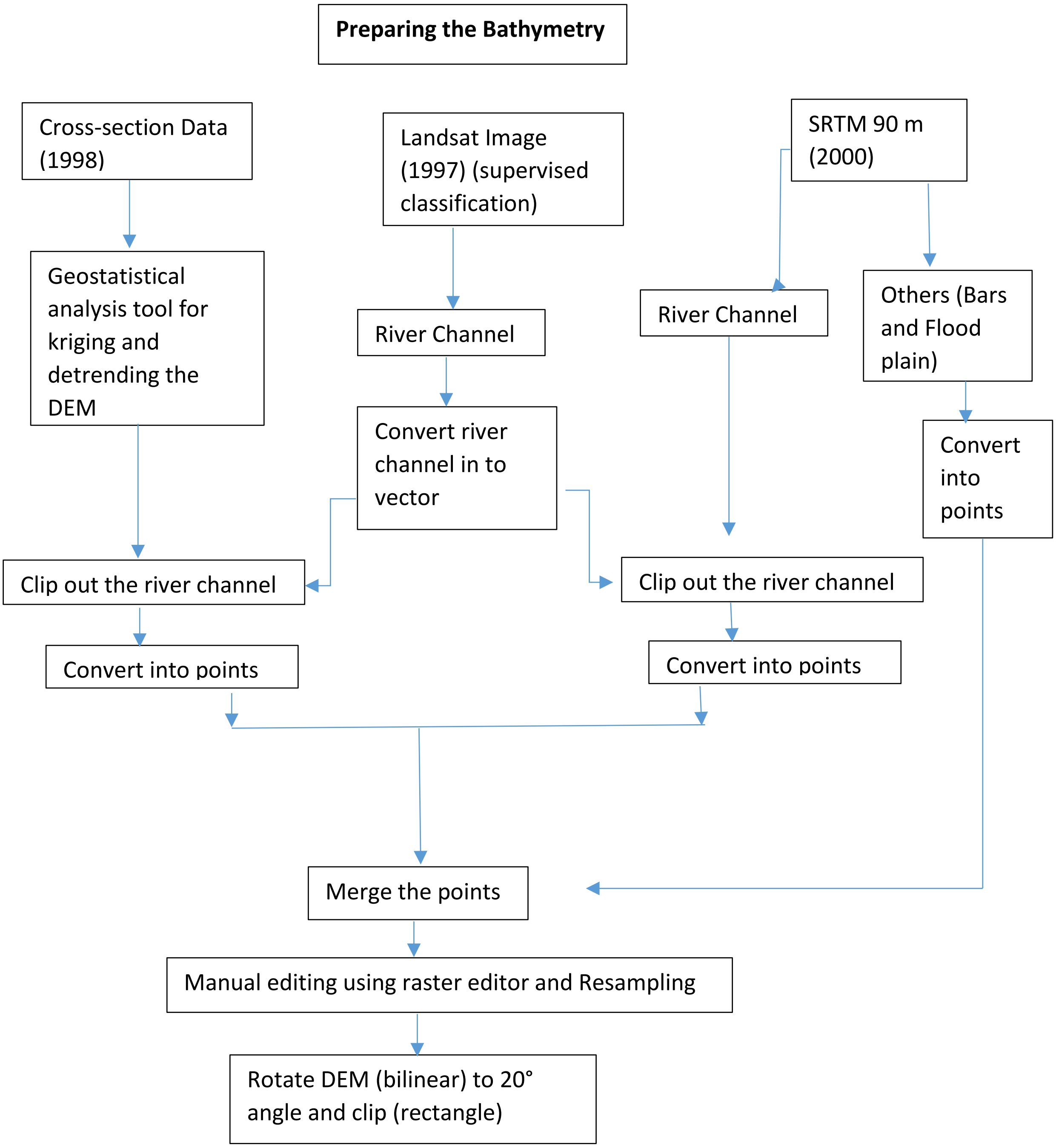

Figure 4.1. Flowchart showing steps followed in preparing the river bathymetry.

5.3. Preparing the cross-sectional data

Data from cross-sections CS 44 to CS 59 (see Figure 1.14) in 1998 were used as the initial topographic and bathymetric data representing the Brahmaputra in the study reach. However, these cross-sections are too unevenly spaced and too widely spaced to support the application of triangulation methods to create a DEM. Instead, the geostatistical wizard in ArcGIS was used to perform exponential ordinary kriging. The justification for using the ordinary kriging was to keep the model as simple as possible (Table 5.1).

Table 5.1. Advantages and disadvantages of Triangulation and Ordinary Kriging methods for application in this research. Source Carter and Shankar (1997).

Grid Interpolation Method	Description	Advantages/Disadvantages
Triangulation	Creates triangles by joining lines between data points in such a way that no triangle edges intersect.	Very good at preserving abrupt changes in topography. Triangulation works best when there is an even distribution of data, as it uses only three values in the interpolation. Cannot be used for extrapolation.
Ordinary Kriging	Associated with the acronym Best Linear Unbiased Estimator (BLUE).	Considered the best as it minimises the residual variance of the grid and allows confidence intervals to be calculated. The variogram model allows the spatial structure to be accounted for. Kriging can use any number of points, with 12- 15 being recommended.

Exponential ordinary kriging was applied to generate river bathymetry because it provides a better representation of the bed, bars and floodplains than circular, linear, spherical and gaussian ordinary kriging methods. The governing equation is:

$$\text{Exponential ordinary kriging} = \gamma(h) = C_{\circ} + C[1 - \bar{e}^{\left(\frac{h}{a}\right)}]$$

where, $C_{\circ}$ = nugget effect, C = scale, a = range, h = horizontal distance, and $C_{\circ}$, C and a = the three parameters in the model variogram equation (Carter and Shankar, 1997).

The geostatistical wizard in ArcGIS produced three different semi-variogram values for the ordinary kriging model of the river Brahmaputra. These values were used to fit the model to the available, cross-sectional data. In Figure 4.2, Red Dots are the binned values (which show local variation in the semi-variogram) and Blue Crosses are the average values (which show smooth changes in the semi-variogram. The best model is the one which has a root mean square standardized error near to unity (Figure 4.3).

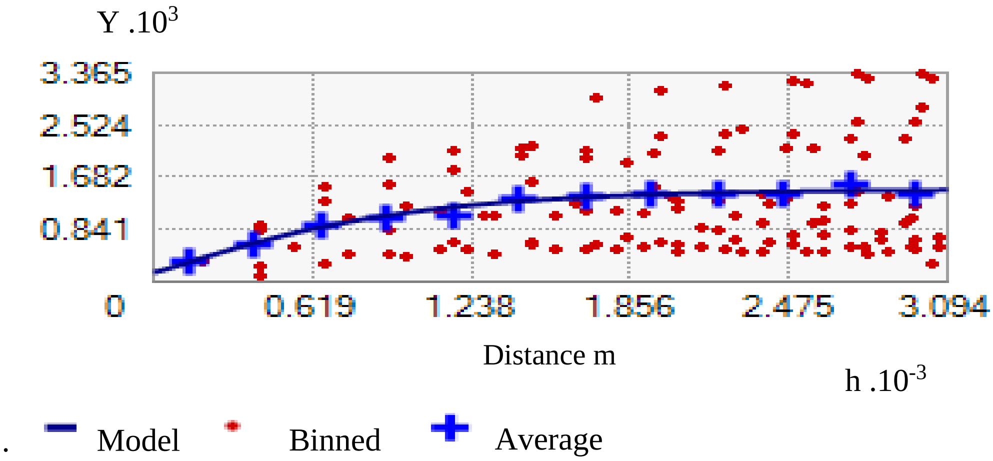

Figure 4.2. Semi-variogram model of the ordinary kriging model.

With the nugget effect = 0, number of lags = 12, and the partial sill = 0.0013, the root mean square standardised error = 0.92

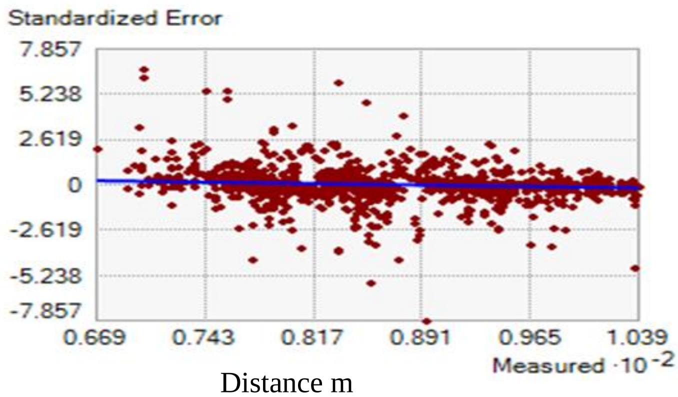

Figure 4.3. Standard error of the ordinary Kriging model.

The kriging method calculated grid node values in the reach using the nearest surveyed neighbour points, which could be some distance away. Hence, this approach may smooth out important local features like sub-channels, braid bars and floodplain hollows and hills.

To counterbalance the risk of important features being missed, additional information on the bathymetry of the river was obtained from the available ground, oblique and orthogonal aerial photographs used in remote sensing techniques.

Also, a Shuttle Radar Topography Mission (SRTM) derived, 90 m resolution DEM for the year 2000 and a Landsat image acquired on 27 October 1997 were used to identify sub-channels, bars and important floodplain features.

The SRTM collected radar interferometry data over 80% of Earth's landmass from latitude 60° N to 56° S in February 2000. C-band (λ= 5.6 cm) data acquired during the mission, that are currently being processed by the Jet Propulsion Laboratory (JPL), have horizontal and vertical accuracies near 20 m and 16 m, respectively, with a linear error at 9% confidence (Jordan et al., 1996).

Due to non-availability of satellite images for 1998, a Landsat image taken during the 1997 low flow period was used to mask the river channel from the kriging DEM. It was, therefore, implicitly assumed that there were no dramatic changes in the landscape depicted between the low flow condition in October 1997 and the start of the model runs, in January 1998.

Based on this assumption, the krigged river channel bathymetry was clipped using the river channel observed in the 1997 Landsat image. The clipped DEM and SRTM DEM were then converted into points using the conversion tool in the Arc toolbox in ArcGIS. Following this, the krigged, channel points were merged with the SRTM DEM floodplain and sandbar data points to create a 2D bathymetry for the landscape in study reach.

Subsequently, some manual editing was conducted within the river channel through the application of the raster editor tool. Successively, bathymetry was resampled to 100 m ×100 m (cellular grid) resolution from 90 m × 90 m (cellular grid) resolution. A cellular grid resolution of 240 m was found to be sufficient to represent representative components of the river's bathymetry, because the dimensions of sub-channels, bars and islands in the River Brahmaputra that are significant to reach-scale morphology have been found to be equal to, or larger than, several hundred metres (Sarker et al., 2014).

Next, the new 100 m × 100 m DEM was rotated through a 20° angle using a bilinear method using the rotate tool in Arc map (Figure 4.4). This was necessary so that the direction of flow in the C-L model was from right to left. Finally, the bathymetric DEM was converted from a raster file into an asci file, so that it could be used to support simulations in the C-L model.

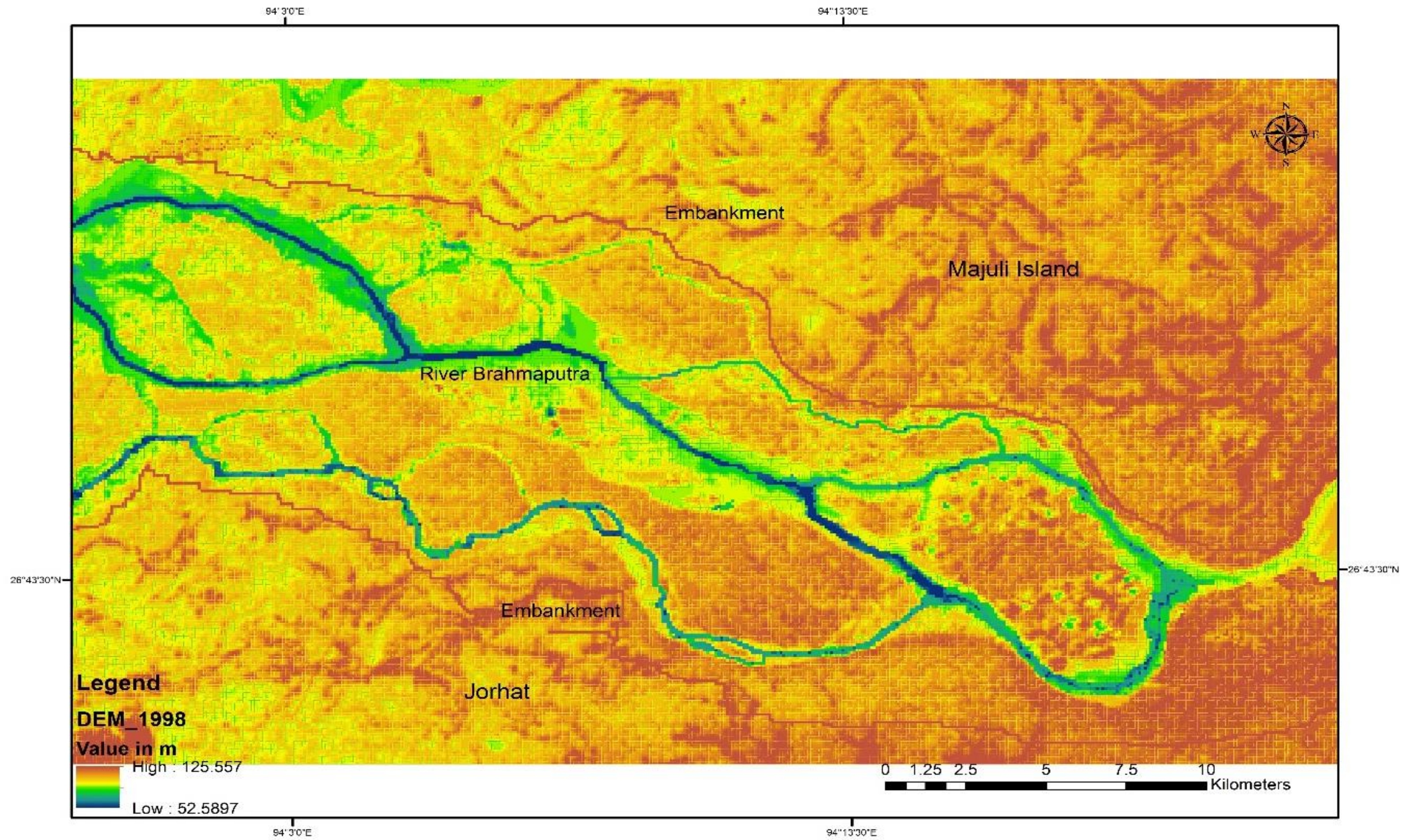

Figure 4.4. 1998 cellular bathymetry of the River Brahmaputra and its floodplains near Majuli Island.

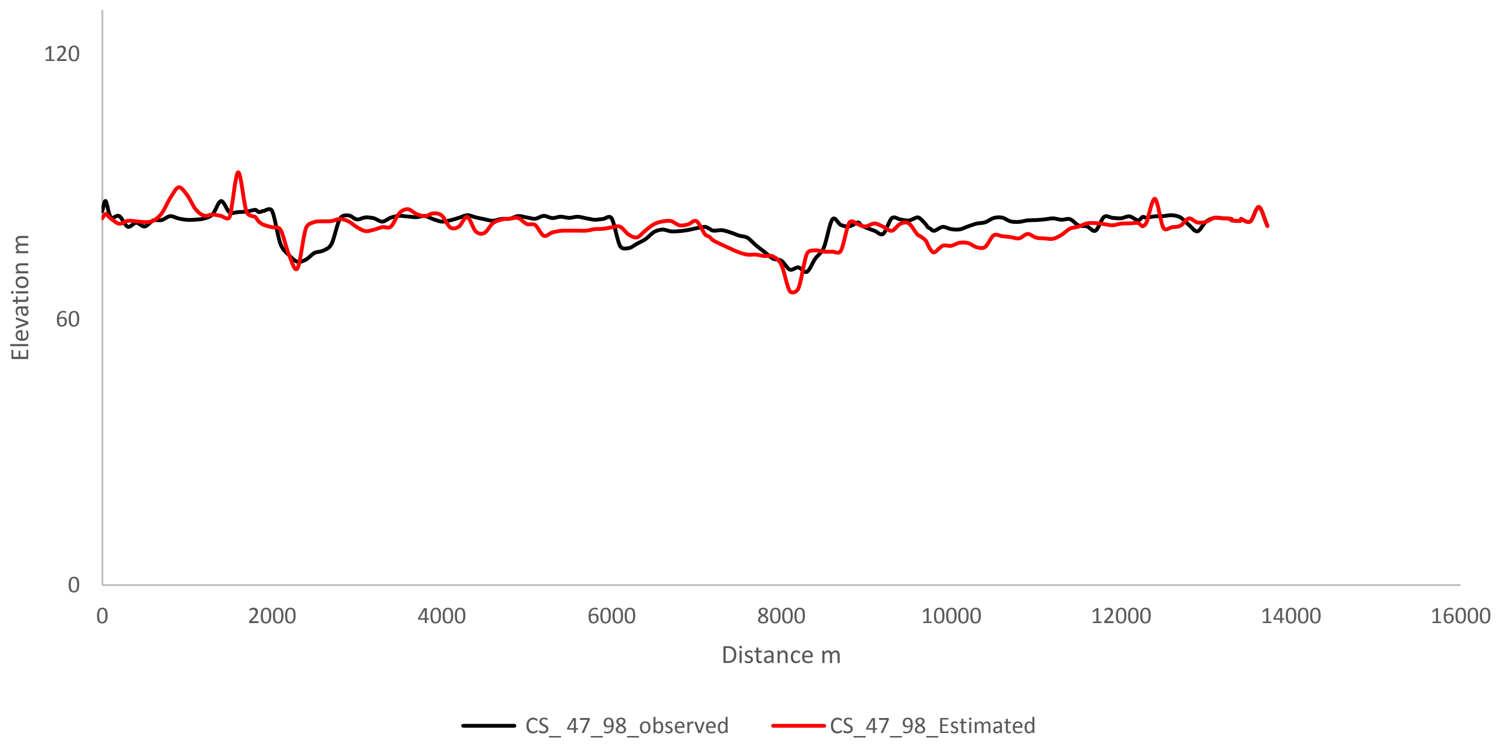

Figure 4.5. Cross-section CS 47 (1998) observed and the estimated.

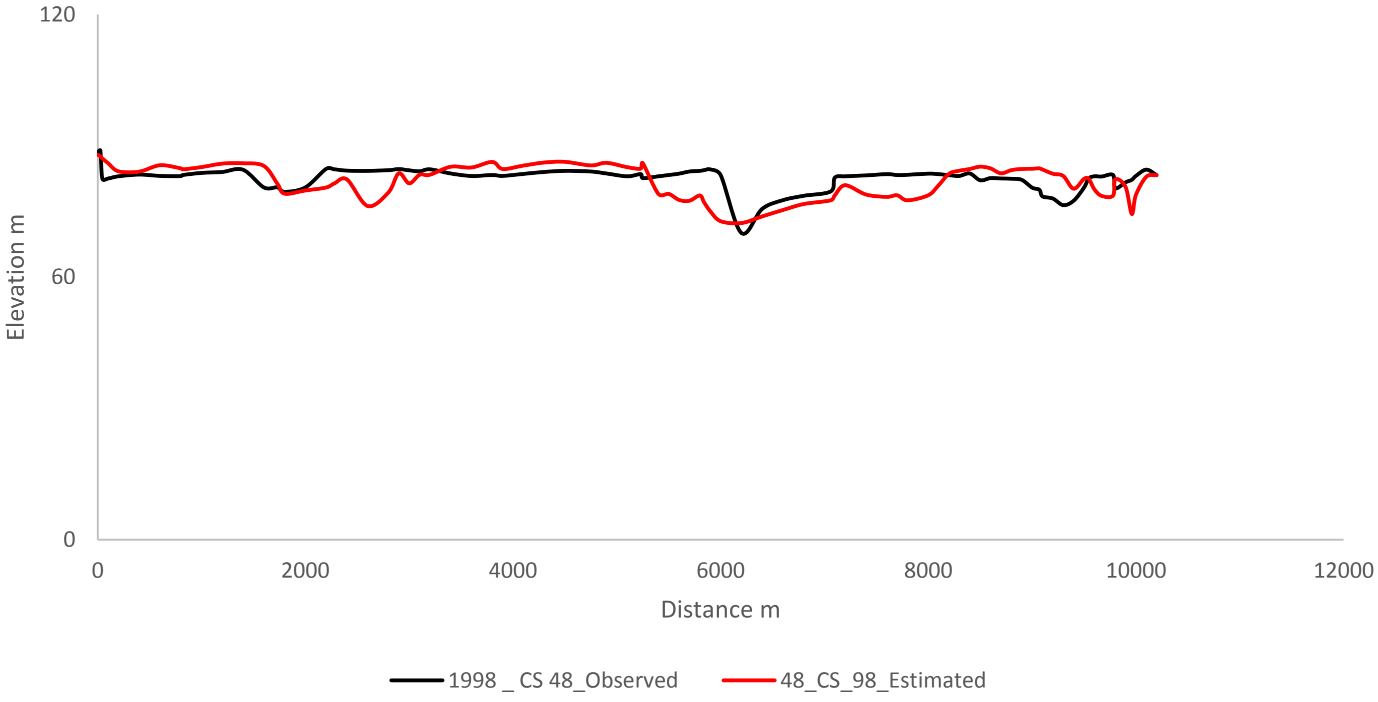

Figure 4.6: Cross-section 48 (1998) observed and the estimated.

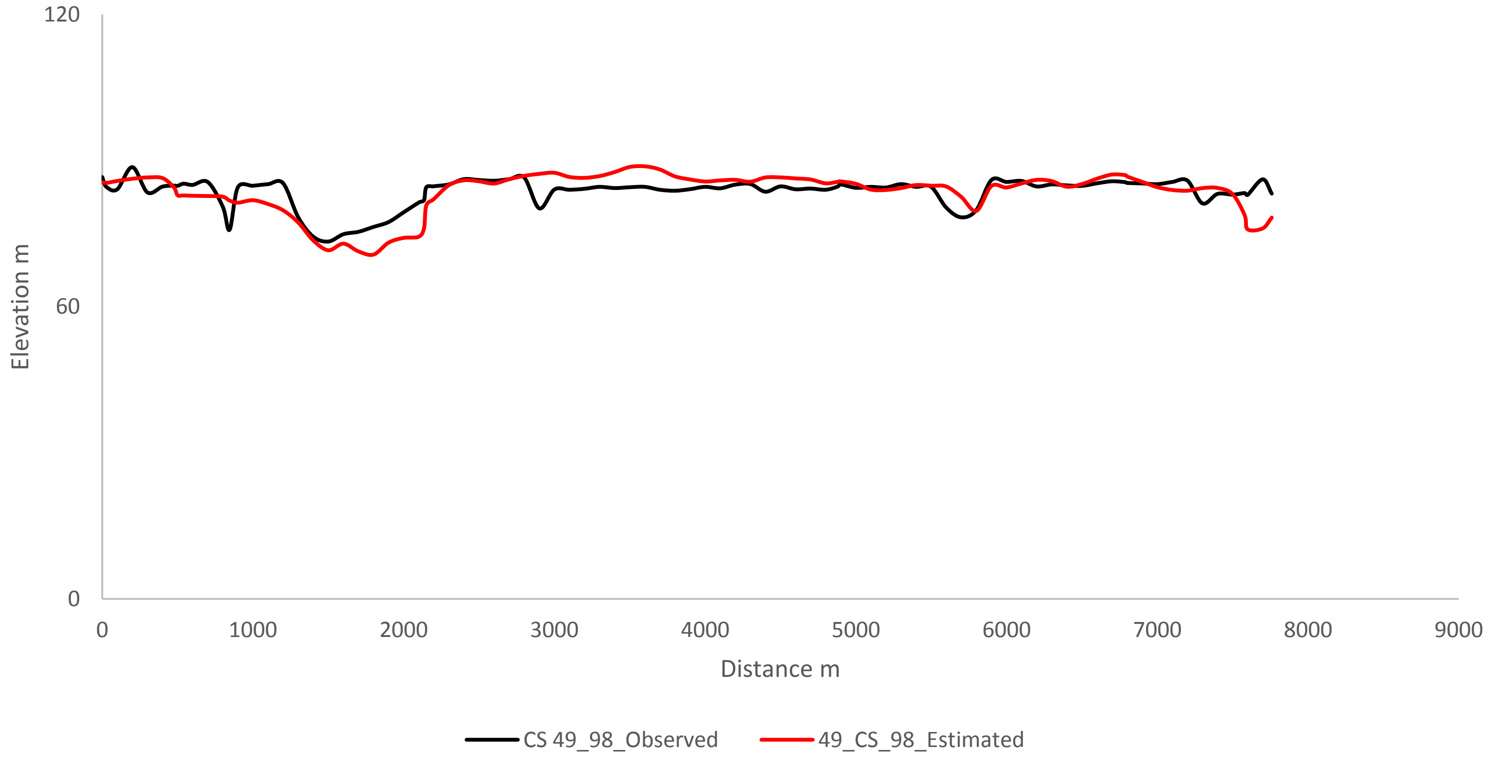

Figure 4.7: Cross-section 49 (1998) observed and the estimated.

New versions of the three available cross-sections were generated from the DEM 100 × 100 m resolution grid size and these estimated cross-sections are compared to the surveyed (observed) cross-sections in Figures (4.5 to 4.7). It is clear that noticeable differences exist between the observed and estimated cross-sections. This is because some of the original information gathered in the surveys has been lost in the process of creating the DEM and due to the relatively coarse resolution of the 100 × 100 m DEM used in the modelling. Discrepancies were smaller in the finer-gridded DEM, but it was necessary to use a coarser grid in the DEM that was used in the C-L modelling to keep model run times manageable.

5.4 Preparing the catchment and flow parameters

The only discharge gauging station on the Brahmaputra in Assam is at Pandu, which is 200 km downstream from Majuli Island (Figure 4.8). Data records from this station include daily mean discharge and suspended sediment load. These data were used to estimate daily mean discharges in the river near Majuli Island based on a comparison of the catchment drainage areas at Pandu and Bessamora (Figure 4.9), calculated in ArcGIS using the hydrology tool. The catchment area at the Pandu GDS site near Guwahati is 417,100 km^2. The catchment area at Beesamora on Majuli Island is 13, 5351 km^2. Discharges at Beesamora were estimated by scaling those measured at Pandu, using the ratio of these drainage areas:

Mean daily discharge of Beesamora =

$$\frac{Daily\ mean\ discharge\ of\ Pandu}{Pandu\ catchment\ area} \times Beesamora\ catchment\ area$$

Daily mean discharges were estimated for the 17 year period between 1998 and 2015 (Figure 4.10) and these daily mean discharges were used to run the C-L models in the hindcasting study. Table 5.2 describes the different flow parameters used in the model, flow model operation, flow parameter selection and justifications for selection of these parameters.

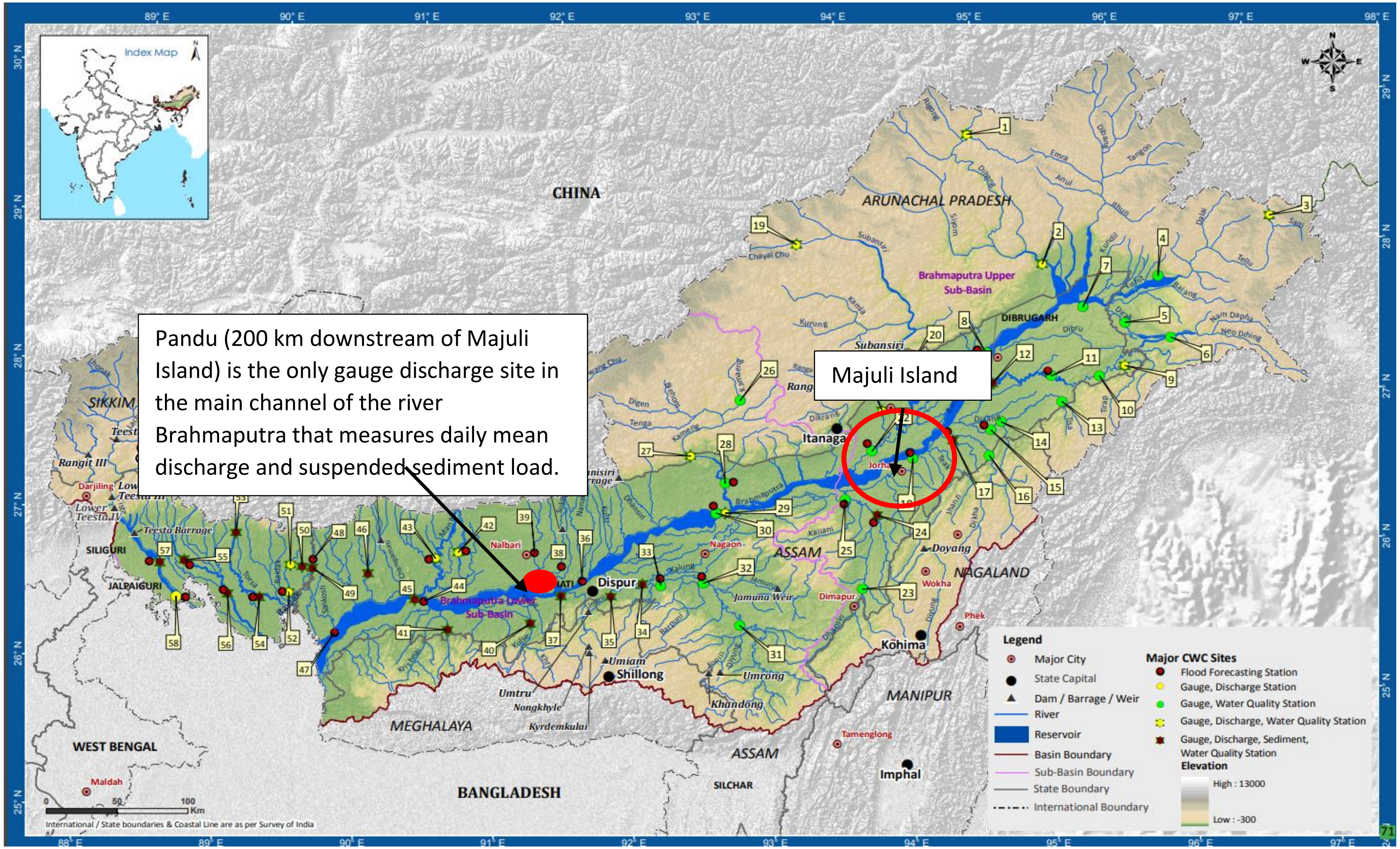

Figure 4.8. Brahmaputra basin showing Pandu gauging station and Majuli Island study reach. Source: http://india-wris.nrsc.gov.in.

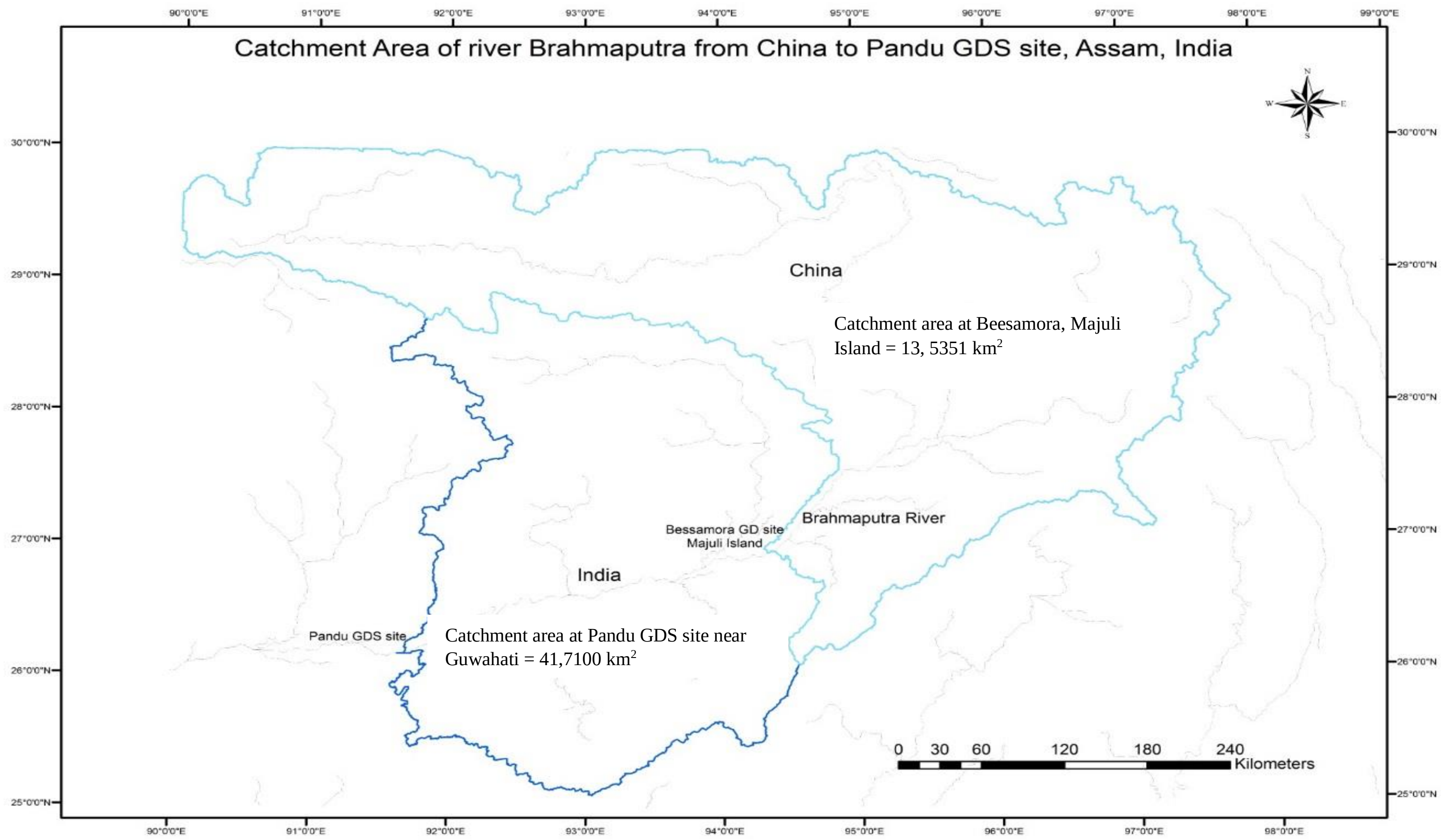

Figure 4.9. Catchment drainage areas at Pandu GDS site and Beesamora, Assam, India.

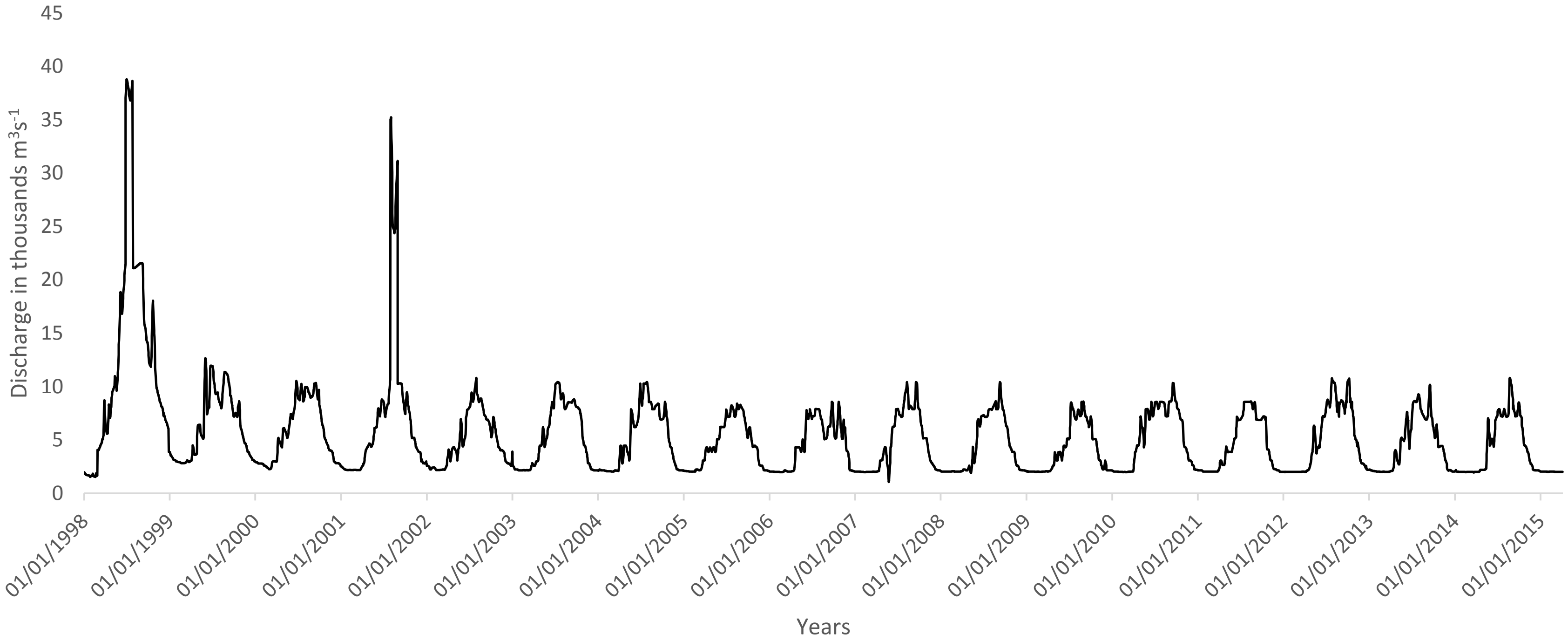

Figure 4.10. Daily mean discharge hydrograph for the Brahmaputra near Majuli Island from 1998 to 2015. Source: Water Resource Department, Govt. of Assam, India).

Table 5.2. Preparing discharge and flow parameters used in the C-L model.

Parameters	Units	Suggested values	Selected values	Justification	Model operation
input/output difference (Q_{diff})	m^3s^{-1}	0-1	0 – 500 Unsteady, uniform flow 0 m^3s^{-1},Unsteady, non-uniform flow 500 m^3s^{-1}	The value based on the daily mean discharge flow during low flow condition, which is 1500 m^3s^{-1} according to the hydrograph. A value less than 500 will compromise the runtime. Setting the value below 1500 m^3s^{-1} will minimise discrepancies between input and output discharges.	The input-output difference is used to speed up the C-L model. This permits the model time step to increase from c.10 seconds to up to 30 min. during low flow periods. The value of the input-output difference (m^3s^{-1}) between input and output discharges that is acceptable to allow the model to run in this faster mode. Generally, it can be set to be close to a low flow value or the mean annual flow.
Min. Q for flow depth calc. (d_{min})	m	10 m cell size 0.1, and a 50 m cell size of 0.5.	100 m cell size d_{min} used was 1.	In this research, the grid cell size is 100 m, therefore 0.1 m is the suitable value for running the C-L model.	This is a threshold value above which C-L will calculate a flow depth that will cause erosion or deposition. This variable dependent upon grid cell size.
Max. Q for flow depth calc. (d_{max})	m	1000 (default)	1000 (default)	The default value was used, as no proper explanation is given in C-L guidance to justify any adjustment to this parameter.	The water added from every cell must be greater than Min Q , but less than the limit set in the C-L model. If the value is reduced it will add more water to the headwaters rather than gradually flowing down the catchment.
Water depth threshold for erosion	m	0.01 (default)	0.01(default)	The default value was used, as no proper explanation is given in C-L guidance to justify any adjustment to this parameter.	Flow depth at which C-L starts to calculate erosion. This is normally set to 0.01. In higher resolution, DEMs a smaller value is generally used and *vice-versa* in a very lower resolution DEM, such as greater than 50 m.
Slope of edge cells (S_{edge})	m	-	0.01	Braided river systems generate deposition within the channel. In this research, a value of 0.01 m was able to generate deposition in models, which resulted in creating braided sub-channels in the river.	If the value is set too low the C-L model will create more deposition or if set too high it will create scour heading back upstream.

Evaporation rate	m day^{-1}	-	0.06	The average evaporation rate in Assam is 0.06 m day^{-1} (Source: Central Water Commission, Govt. of India.).	--
Courant number (α)	-	0.7	0.7	Values are 0.5 for 50 m DEM, 0.2 for 10 m etc. For cells equal to or above 50 m the recommended value is 0.7 (Bates et al., 2010).	This controls numerical stability and speeds up the flow model. Numerical instability creates chequerboard results and slows the model.
flow threshold (h_{flow} threshold)	m	0.00001	0.00001	The default value was used, as no explanation is given in C-L documents to justify an adjustment to this parameter.	This is the water elevation surface difference between two cells. This value is used to prevent the flow model from trying to move water when the gradients between two cells are too small.
Froude number flow limit (F*r*)	-	0.8 (default)	0.8- 1	In this research values, 0.8 – 1 were used to run the C-L model, which is appropriate for the Brahmaputra (Woldemichael et al., 2010).	A value 0.8 creates sub-critical flow in the C-L model. A value of 1 creates supercritical flow. Froude number affects the speed of the flood wave. This can cause increases in water depth and reduces erosion rates in the reach.
Manning's n	-	0.04-0.05	0.04	A value of 0.04 is appropriate for the River Brahmaputra (Woldemichael et al., 2010)	Manning's n controls flow resistance and flow depth. Higher values result in lower flood peaks due to wave attenuation.

5.5 Preparing suspended sediment load parameters

Suspended sediment loads were estimated using estimated daily mean discharges at Beesamora and the suspended sediment load rating curves made available for coarse, medium-fine and fine sand at the Pandu gauging station, between 1998 and 2015 (Figures 4.11 to 4.13). These are essential empirical correlations between sediment discharge (y-variable) and water discharge (x-variable), for the River Brahmaputra at that location. The form of the curve is a power function with the form:

$$S = aQ^b$$

where, S = sediment discharge (m^3s^{-1}), Q = discharge (m^3s^{-1}), a = an empirically-derived constant and b = an empirically-derived exponent.

The sediment rating curve for coarse sediment load is,

$$SSL\_C = 0.00000001x^{2.84}$$

the curve for medium-fine sediment load is,

$$SSL\_M = 0.00000673x^{2.25}$$

and the curve for fine sediment load is,

$$SSL\_F = 0.0002x^{2.05}$$

where, SSL = sediment discharge (m^3s^{-1}), x = discharge (m^3s^{-1}), a = a constant and b = an exponent. These estimated daily suspended sediment loads were used to run the C-L models (Figure 4.14).

In CAESAR Lisflood sediment load units are in m^3s^{-1}/ model time steps. The input discharge data is in m^3s^{-1} and input suspended sediment grain size data are in m^3s^{-1} as the output file will have a similar structure.

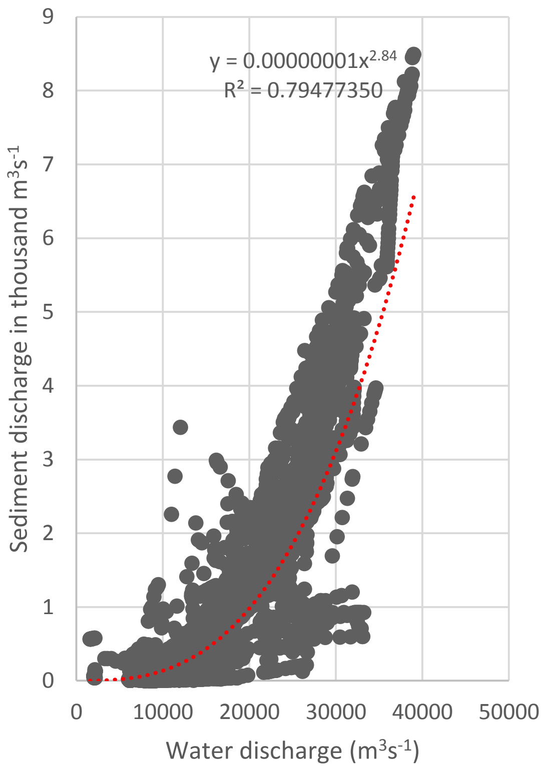

Fig 4.11. Sediment rating curve for coarse sediment in the River Brahmaputra at Pandu GDS (1998-2015).

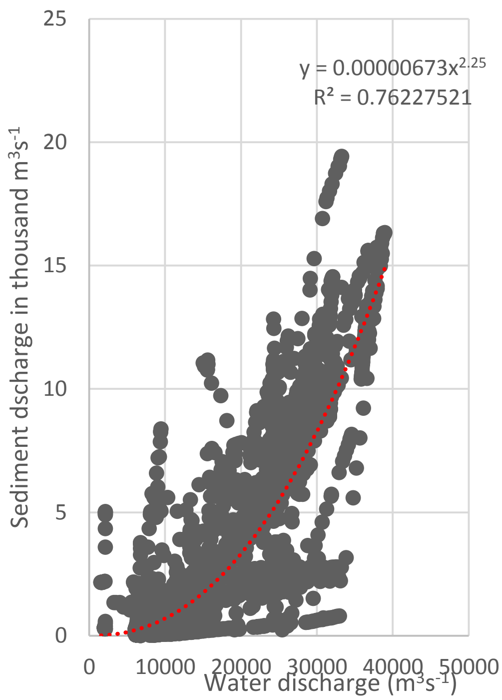

Fig 4.12. Sediment rating curve for medium fine sediment in the River Brahmaputra at Pandu GDS (1998 -2015).

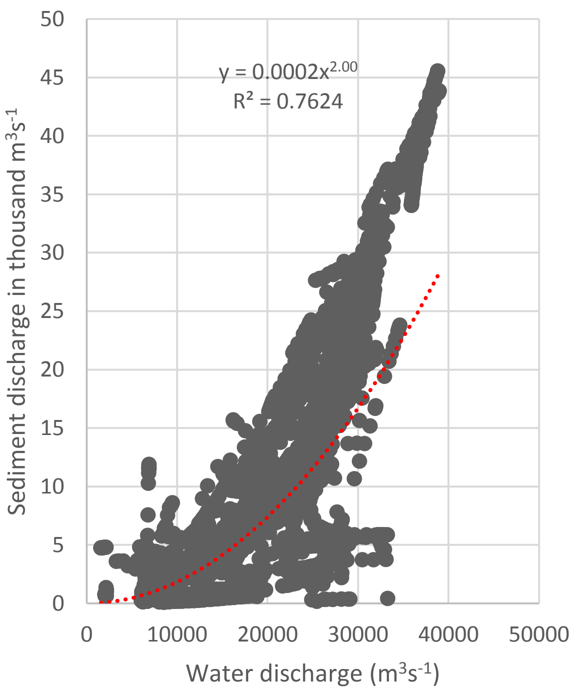

Fig 4.13. Sediment rating curve for fine sediment in the River Brahmaputra at Pandu GDS (1998 - 2015).

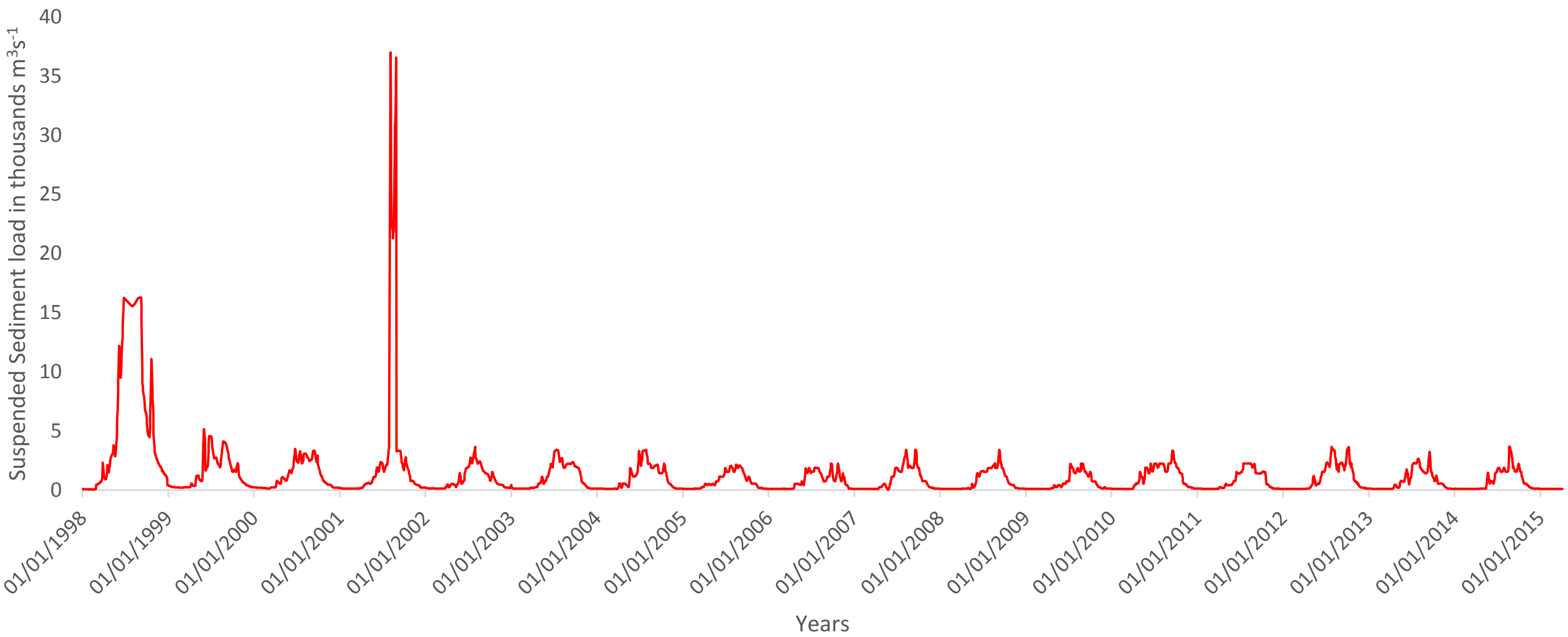

Figure 4.14: Synthetic daily mean suspended sediment load hydrograph 1998- 2015 for the River Brahmaputra near Majuli Island. Source: Water Resource Department Govt. of Assam, India.

5.6 Preparing sediment transport parameters

Discharge is the main driver of landscape evolution in the C-L model, but, geomorphological changes result from erosion, sediment transport and deposition. Sediment transport is calculated for multiple size fractions in the C-L model, with coarser material transported in the form of bedload and finer, more mobile sediment fractions moving as suspended load. For heterogeneous mixtures, the C-L model employs up to 9, user-defined grain size classes and, depending on the sediment transport relationship selected, lateral erosion parameters are distributed spatially (Van De Wiel et al., 2007).

As reported earlier, no bedload data are available for River Brahmaputra in Assam. As the vast variety of sediment carried by this great river moves in suspension (bedload probably makes up no more than 5 or 10% of the total load), it was accepted that suspended sediment load were sufficient to run the model.

In a reach mode C-L model, the bed consists of one active layer and one bedrock layer. The active layer represents the erodible, alluvial deposit in the bed of the river. The bedrock layer is fixed and cannot be eroded (Van De Wiel et al., 2007). In the model, sediment incoming from upstream plus or minus that exchanged with the active layer and any derived from bank erosion is routed downstream using Rubey's law, which provides the basis on which to calculate the velocity of suspended sediment load (Van De Wiel et al., 2007).

The C-L model offers a choice of two sediment transport relations, namely that of Peter Wilcock and Joanne Crowe (2003) and that of Hans Albert Einstein (1950). In reach mode, if the re-circulation tab is checked, the output of sediment from the downstream boundary (as calculated using the selected sediment transport equation) is fed back into the reach model through its upstream boundary at the beginning of each iteration.

For interior cells, suspended sediment is distributed from the current cell to neighbouring cells with lower elevations. If the sediment transport capacity is less than the input from cells upstream, the excess suspended sediment load is kept in the cell until next iteration. (Van De Wiel et al., 2007).

Table 5.3. Preparing parameters used in the sediment transport module of the reach mode C-L model.

Parameters	Units	Suggested values	Selected values	Justification	Model operation
1. Transport relation: Wilcock-Crowe or Einstein	-	-	Both were tested.	In the Brahmaputra, grain size varies from silt to sand. Either formula could be used and both were tested. Wilcock and Crowe work very well in the braided river system.	Einstein (1950) is predominantly used in sand bed streams that include grains ranging between 0.785 and 28.65 mm (Gomez and Church, 1989). Wilcock and Crowe's formula (2003) was developed from flume experiments using five different sand-gravel mixtures, with sizes ranging between 0.5 and .64 mm.
2. Max erode limit (ΔZ_{max})	m	0.01	0.02	Based on experiments 0.02 m was selected as this did not create check-pattern erosion and deposition and it allowed the model to run faster. Setting it to 0.03 and 0.04 m created checkbox-patterns and slowed down the model run time.	This parameter regulates the maximum amount of material that can be eroded or deposited within the cell. It prevents the numerical instability caused by too large amounts of material being moved from cell to cell in a single timestep. When the value is set high then this will result in some numerical instability – blocky or check pattern erosion and deposition patterns. On the other hand, if the value is set too small the model will run too slowly. This factor also depends on the grid cell size. For a 10 m DEM recommended value is 0.01 m.
3. Fall velocity (ν_f)	m s^{-1}		0.584	Calculated for the fine sand (0.2 mm). Rubey's law is appropriate for rivers which have heavily turbulent flow. This includes River Brahmaputra. Hence, this law is applicable (expert advice from Prof. Nayan Sharma, IIT R, India, 2015).	Rubey's law: $R=\frac{\sqrt{W^2V^2p^2fluid+32Z(Pparticle-Pfluid)\mu Vg}+WV^2Pfluid}{\frac{8}{3}(Pparticle-Pfluid)g}$ where V = fall velocity, cm/sec; p = mass density, g/cm^2 ; R = particle radius, cm; μ = dynamic viscosity, dyne-sec/cm^2 ; g = gravitational acceleration cm/s^2; W = pressure drag coefficient, dimensionless = 0.5305; Z = viscous drag coefficient, dimensionless = 0.622; ϕ' = phi size. Source: Watson (1969).
4. Active layer thickness (L_h)	m	0.1	0.1	This value is greater than four times of maximum erode limit. The default value was used, with no explanation given to justify an adjustment to this parameter.	The thickness of a single active layer which represents bedload, surface layers and subsurface layers. The default normal range for this parameter is 0.1- 0.2 and it must be 4 times the maximum eroded thickness. This defines the thickness of the active, alluvial layer in the bed.

5. Proportion to be recirculated		1	1	A reach mode C-L model was used in this research. The re-circulate checkbox was ticked. This function is only applied when sediment input and output from a reach is set to zero in the simulation in C-L.	When the re-circulate checkbox is ticked during runtime, sediment that departs from the right-hand side of the DEM is fed back in via the upstream boundary. This is only used in reach mode and prevents the model from unrealistically degrading or aggrading the reach during the simulation.
6. In channel lateral erosion rate (Λ)	-		20-50	Higher values were used as the river Brahmaputra is a wide and a shallow river.	This regulates the in-channel lateral transport of suspended sediments. Higher values result in shallow, wide channels whereas lower values result in deep, narrow channels.
7. Lateral Erosion (λ)	m	(0.01-0.001)	(0.0001)	Lateral erosion rate 0.0001m was used for the River Brahmaputra, because of the presence of sinuous, anastomosed reaches which are identical to meandering rivers. This also speeded up model runs.	According to Prof. Tom Coulthard, based on his wide experience with using the C-L model the lateral erosion rate for a braided river should be 0.01m to 0.001m and 0.0001m for a meandering river. Though the study reach is predominantly braided it has sub-reaches that are anastomosing and some braided channels which are dissecting the sandbars.
8. Number of passes for edge smoothing filter (N_{smooth})	-	100 (default)	10-30	Values10-30 were considered as the Brahmaputra has highly sinuous meanders and anabranches as well as braided reaches. More details are discussed in Chapter 6 (Table 6.3).	Low values are recommended for high sinuosity, meandering or braided channels, whereas high values are recommended for meandering or straight channels. This specifies the number of passes made by the edge-smoothing filter and is used to calculate local bend radius of curvature and lateral erosion rate.
9. Number of cells to shift lateral erosion downstream (N_{shift})	-	(1-5)	2-5	One-tenth of the N_{smooth}. More details are discussed in Chapter 6 (Table 6.3).	This determines the number of cells required for downstream migration of meandering bends. This value must be an integer which should be one-tenth of the N_{smooth}.
10. Maximum difference	-	0.0001 (default)	(0.0001-0.0002)	The width of the river Brahmaputra ranges from 9 km to 18 km near	This calculates the cross-channel gradient from the radius of curvature, which regulates the lateral distribution of sediments

allowed in cross-channel smoothing of edge values. ($\Delta\nabla_{max}$)				Majuli Island. Therefore a lower value is most appropriate. More details are discussed in Chapter 6 (Table 6.3).	eroded from the outer bank and delivered to the point bar in a meander bend. A lower value is recommended if the channel is wide.
11. Grain size	(mm)	-	Three-grain sizes: 2mm, 0.212mm and 0.075mm	These three-grain sizes represent the three, available daily mean suspended sediment rating curves for the River Brahmaputra.	Up to 9-grain size fractions are available in the C-L model. However, only three-grain sizes were used to run the C-L model for river Brahmaputra based on data available from Pandu.

5.7 Preparing slope processes parameters

One of the strong points of the C-L model is that it simulates lateral as well as downstream morphological changes, including situations where the river widens or migrates not only by eroding the stream bank separating the channel from the floodplain, but also coupled hillslope-channel processes responsible for the erosion and mass failures (landslides, shallow slides, slope creep) in the much taller terraces and the valley sides.

Slope model parameters include: slope failure threshold, creep rate and soil erosion rate. These parameters are user-defined. In the slope sub-model, sediments are moved from high elevation cells (the active layer) to one or more of the adjacent, lower cells (receiving layer) until the slope angle is lower than the threshold angle for failure (Coulthard, 2002, Meadows, 2014).

In the slope sub-model, an iterative process is applied to check for failures in adjacent cells by comparing the slope angle to the threshold angle until the slope becomes stable. C-L then routes failed slope sediments from the active layer in unstable areas to cells in the receiving layer. This allows freshly-derived sediment from slope failures under gravity to be transferred from failing slopes into the river channel(s) (Coulthard, 2002, Hancock et al., 2015).

Due to lack of higher resolution data, to describe the slope failure threshold in the present study slope angles were derived from the 100 m grid cell DEM using the ‘slope’ tool in the ArcMap spatial analyst toolbox. This tool calculates the maximum rate of change in elevation between a cell and its neighbours and produces a raster file with the maximum slope value for each cell. The output raster file backed up the observation made by the candidate during fieldwork that in Majuli Island slopes steeper than about 10° (Figure 4.15) are rare and are usually unstable (Figure 4.16), while slopes gentler than about 10° are usually stable (Figure 4.17) Slope near Burha chapori (A 2) (figure 4.18) is comparatively higher than 10° and therefore these region experience higher lateral erosion and channel migration.

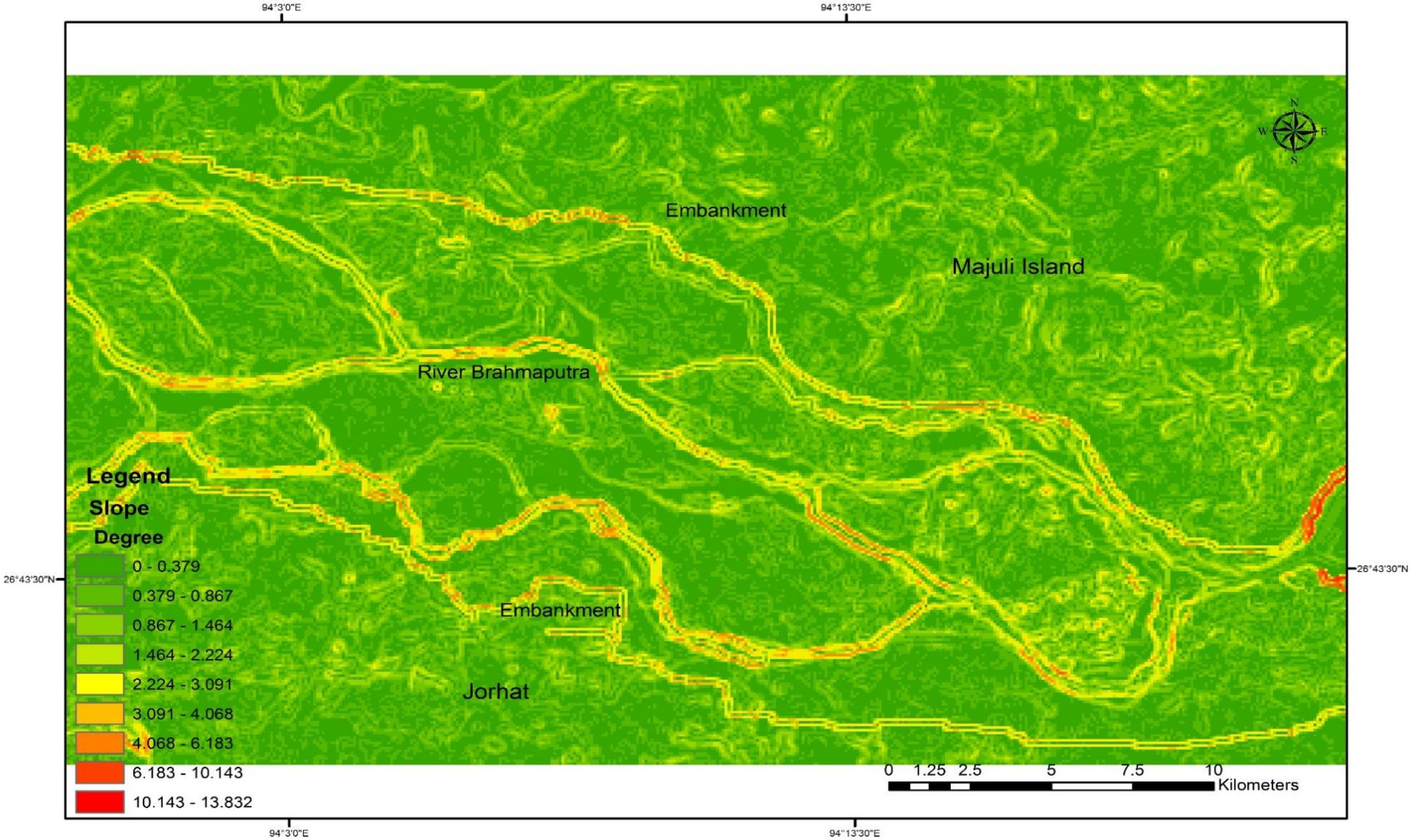

Figure 4.15. Slope model of the river Brahmaputra near Majuli Island.

Based on field observation backed up by slope analysis using the DEM, a threshold slope of 10° was selected as being the most appropriate for use in the reach-scale model.

Soil erosion rate is also a user-defined parameter. This parameter controls the rate of soil removal by surface erosion of the hillslope depending on soil type and land management practise. This parameter was not used in the current research as this parameter, E_r is still under development and has not yet been extensively tested (Coulthard et al., 2013, Meadows, 2014).

The value of C_{rate} was set at 0.0025, which is a default value (Table 5.5).

Figure 4.16: Bank of the river Brahmaputra near Majuli Island where the slope is higher than 10° angle (near A 1 sandbar) where to protect the bank temporary structure were laid.

Figure 4.17: Bank of the river Brahmaputra (anabranch) near Majuli Island (Kamalabari) where the slope is less than 10° angle.

Figure 4.18: Bank of the river Brahmaputra (the thalweg channel) near Majuli Island (Buhra chapori) where the slope is more than 10° angle submerged in flood water during 2016 flood. (Temporary erosion protection structure were laid to protect the bank from erosion).

Table 5.4. Preparation of parameters of slope failures in the C-L model

Parameter	Units	Suggested value	Selected values	Justification
Slope	Degrees	-	10-13	Based on the field observations, slope analysis using the DEM and experimental test runs of the C-L model for the study reach.
C_{rate}	myr^{-1}	0.0025	0.0025 (default value)	The default value was used as there is an absence of steeper slopes in the low-amplitude terrain of Majuli island, apart from steep river cliffs that form and collapse very quickly in bars and banks subjected to lateral, fluvial erosion.
E_r	myr^{-1}	-	-	This parameter was not in use in this research as this is still under development.

5.8. Preparing the vegetation parameters

C-L simulates the influence of in-channel and riparian vegetation on fluvial processes using a vegetation growth model that allows a vegetation layer to develop above the active layer. This vegetation layer shields the underlying sediment from fluvial entrainment, limiting the volume of material that can be removed from a cell during a model step. Vegetation parameters in C-L are vegetation shear stress, grass maturity and the proportion of erosion that can occur when vegetation is fully grown. All these parameters are user-defined. They act as a governor to regulate the influence of vegetation on bed scour and lateral channel erosion. C-L also recognises that vegetation can be destroyed during a flood and, therefore, the vegetation's critical shear stress (τ_{crveg}) was used in this study to simulate the degree to which the shielding effect of vegetation on fluvial erosion is lost during flood events.

To evaluate the effect of vegetation on river channels under measured conditions researchers have used laboratory-based flume experiments (Gran and Paola, 2001; Tal and Paola, 2010; Tal et al., 2004). These innovative experiments have shown that, in perennial streams, increased vegetation densities growing on unsubmerged bars and floodplains can stabilise the banks, reduce lateral erosion, increase mean channel depths to significantly reduce width-depth ratios and braiding indices. Importantly, studies like those listed above are starting to explore the effects of vegetation not only on linear bank erosion but also on planform channel patterns. Essentially, as vegetation density and resistance increase the river is forced to occupy a larger number of smaller channels, decreasing the braiding index and promoting an anastomiosed pattern.

According to Prosser (1996), the τ_{crveg} values range from:

1. around 70 Pa for heavily degraded aquatic plants or tussock and sedge,
2. >105 Pa for undisturbed aquatic plants,
3. >180 Pa for lightly degraded tussock and sedge, and,
4. > 240 Pa for undisturbed tussock and sedge.

In this research, and based on observations during fieldwork (Figures 4.19 and 4.20), the value of τ_{crveg} selected was 180 Pa, which is also is a default

τ_{crveg} value in the C-L model. 180 Pa is suitable for the River Brahmaputra as vegetation there can be put in the category of 'lightly degraded tussock and sedge' because of its presence of vegetated meta-stable sandbars, but also its relatively low density. Preparation of vegetation parameters is described in Table 5.3.

Figure 4.19: Vegetation cover on the sandbar of the river Brahmaputra near Majuli Island.

Figure 4.20: Vegetation cover and a newly formed deposition adjacent to the sandbar of the river Brahmaputra near Majuli Island.

Table 5.3. Preparation of parameters of vegetation growth model in the C-L model

Vegetation parameters are largely based on restricting erosion occurrences. In CAESAR Lisflood vegetation is not a specified plant, bush, grass or tree but it is more concerned with how vegetation will impact on erosion and deposition within the channel.

Parameter	Units	Suggested value	Selected value	Justification	Model Operations
τ_{veg}	Year	—	0-1	The growth rate is set to 1 then after 1 year the vegetation maturity will be 1.	This is the speed at which vegetation reaches its full maturity in years.
τ_{crveg}	Pa	—	180	The Brahmaputra has three types of braid bar. They are (i) unstable sandbar with no vegetation cover, which should ideally have a 70 Pa τ_{crveg} value; (ii) semi-stable braid bar with human habitation, which should ideally have a 180 Pa τ_{crveg} value, and; (iii) stable braid bar with thick vegetation cover, for which 240 Pa would be ideal (Prosser, 1996). However, a constant τ_{crveg} = 180 Pa or Nm^2 was used because in the C-L model there is no option to assign different τ_{crveg} values to these three categories of braid bar.	This parameter controls the gradient of the relationship between maturity and time i.e. maturity reset to zero. The value of the bed shear stress above which vegetation will be removed by fluvial erosion by fluvial erosion. If the value is set low vegetation will be easily cleared away or if the value is set high vegetation will act as a resistance.
The proportion of erosion that can occur when the vegetation is fully grown.	-	0-1	0.1	If it is set to 1, then vegetation will have no influence and erosion will occur, however, if it is set to 0 when fully grown there can be no scour or lateral erosion. In this C-L model, it was set to 0.1 which means the amount 1 x normal erosion with vegetation maturity of 0, and 0.1 x normal erosion with vegetation maturity of 1.	This parameter determines how vegetation maturity impact on the inchannel lateral erosion rate and the lateral bank erosion.

Vegetation on the floodplain and banks also contributes to hydrological changes and riparian vegetation increases hydraulic resistance (Baptist, 2003; Gurnell and Petts, 2006; Bennett et al., 2008) increases bank resistance due to root systems (Thorne, 1990, Pollen and Simon, 2005, Eaton, 2006), decreases the effective boundary shear stress (Abernethy and Rutherford, 2001) and enhances bar sedimentation (Gurnell et al., 2001). The growth of vegetation leads to sediment trapping (Gurnell and Petts, 2006, Baptist, 2003; Braudrick et al., 2009).

Weaker banks lead to channel widening so that mid-channel bars can develop. In this study, a constant value of τ_{crveg} was used, equal to 180 Pa. In the C-L model, the vegetation maturity parameter affects the channel lateral erosion rate. If it is set to 1, then vegetation has no influence and erosion will occur unfettered. However, if it is set to 0 then when the vegetation is fully grown there can be no erosion. The maturity parameter for newly deposited sandbars should be 1, which means that 100% of expected erosion occurs. Similarly it should be 0.1 for vegetation on bars with a maturity of 1 year (meaning that 10% of normal erosion occurs). It should be set to 0 for densely vegetated bars, meaning that no erosion was allowed. But in this research, a constant value 0.1 was used as C-L doesn't have provision for applying separate value for different sandbars.

Vegetation also has a complex association with river dynamics and morphology due to its effects on bank erodibility and stability. It can significantly change near bank flow velocities, as well as increasing the cohesion and physical resistance to erosion of bank material. According to Thorne (1990), vegetation can reduce river bank erosion and increase bank stability with respect to mass failure. It can (1) slow near bank velocities, reducing boundary shear stress and thus flow erosivity, (2) reduce soil erodability, (3) increase bank shear strength through soil reinforcement and by improving bank drainage and (4) lead to accretion at the base of the bank, by damping turbulence. Transforming these flow and bank properties can influence channel shape (Mackin, 1956; Nanson and Knighton, 1996; Millar, 2000). In summary, vegetation reduces bank erosion rates and the supply of bank erosion-derived sediment to the river, which hinders braiding and promotes development of a meandering or anabranching/anastomosed planform in what might otherwise be a braided reach. This could not be simulated using C-L, but it is worth noting in the context of sub-reach scale changes in the character of the channel of the Brahmaputra within the study reach and with respect to options for managing bank erosion and land loss on the southern margin of Majuli Island.

Chapter 6: Hindcasting of landscape evolution of the river Brahmaputra

6.1. Introduction

The study of channel adjustments and the prediction of morphological change play important roles in river management and conservation policies. Nevertheless, the time and space scales of interest for river management, (i.e., scales of decades and tens of kilometres) are typically larger than those most frequently adopted in studies intended to improve understanding geomorphological processes through modelling (Church, 2007). Large-, braided rivers have been modelled less commonly, frequently than single-thread streams whether using conceptual (Simon, 1989; Surian, 2015), empirical (Rhoads, 1992) or numerical approaches (Ferguson, 2009, Martin-Vide, 2010) and no Computational Fluid Dynamics (CFD) model has been applied and fully evaluated at the mesoscale (10-100 km, 10 -100 years) in a braided river system (Bertoldi, 2005; Ferguson, 2007).

As discussed in Chapter 4, with a few notable exceptions, little attention has been paid to braided stream behaviour of large braided river systems like the Brahmaputra over management-relevant time and space scales (Thorne et al., 1993; Richardson and Thorne, 1998; Mount et al., 2012; Sarker et al., 2014). This is due, in part, to the high cost and difficulty of research on large rivers, limited data availability and the inherently unpredictable behaviour of braided river systems.

For changes over longer periods, it was accepted that it would be more appropriate to compare the statistical characteristics of simulated and observed braided characteristics (e.g. braiding intensity, average channel width) (Nicholas, 2005).

To generate data useful for braided river model validation, some system-scale generalization of braided river features and behaviour is required. There is a rich literature on braiding indices, mostly focused on planform parameters (Bridge, 1993; Egozi, 2008; Mosley, 1983) and topographic aspects; as well as methods designed to characterize the planform pattern of a braided river (Murray and Paola, 1996; Sapozhnikov, 1998). Most of the research using RCMs to date has performed in the context hindcasting and forecasting sediment yields in catchments or reaches (Coulthard et al., 2002; Ziliani et al., 2013; Meadows, 2014). A negligible amount of research being conducted on using RCMs to hindcast and forecast river evolution in streams that exhibit profound morphological changes, braiding patterns and complex evolutionary trajectories. Therefore in this study, an attempt was made to evaluate the channel behaviour and planform change of the river Brahmaputra near Majuli Island, using the CAESAR-LisFlood (C-L) RCM.

6.2. Calibration and sensitivity analysis

This section describes calibration and sensitivity analysis of all the C-L models built in this research to hindcast morphological changes observed over a 17 year period (1998 – 2014), in a 40 km reach of the river Brahmaputra to the south of Majuli Island. The bed level in 1998 was used as the initial boundary condition and, initially, 15 C-L models were run to test the sensitivity of model outputs defining channel evolution, for the calibrated model settings, with a 1-year spin-up period.

A CL model was run for a meandering river Teifi for a 4.2 km reach near Lampeter, Wales with a 10 m resolution DEM. The simulations were carried out for short period of 171 days with high and low flows (20 – 200 m^3s^{-1}) which took 42 hours to complete on a desktop PC (Van De Wiel et al., 2007). As described in Chapter 4, the river Brahmaputra near Majuli Island has huge and variable daily mean water discharge (1,000 – 45,000 m^3s^{-1}) and a heavy suspended sediment load (1000 – 20,000 m^3s^{-1}). The initial bathymetry had a spatial resolution of 90 x 90 m, but it was reclassified to 100 x 100 m resolution to allow the model to run faster (as described in Chapter 4). With those inputs of discharge and suspended sediment, and the C-L model running in unsteady and non-uniform flow mode, it took 24 hours to complete each year of the hindcasting simulations. For comparison, it took 35 hours to complete each year of a simulation with the model running in unsteady, uniform flow mode (Table 6.1). Due to these long run times, it was only possible to run a limited number of C-L models. Hence, 15 models were calibrated and run. Out of 15 calibrations, only 10 C-L models were able to generate the morphological changes occurring in the river Brahmaputra. Therefore 5 models were eliminated as they were producing deep gorges which are not the characteristic of the river Brahmaputra. These models fail to activate the secondary channels both in peak flow or low flow season. This results in unable to reproduce planform change in the river channel.

Table 6.1.Simulation set up			
Model flow mode	Simulation	Duration (hours)	Input-output difference of flow Q (m^3s^{-1})
Unsteady, uniform flow	1 year	35	0
Unsteady, non-uniform flow	1 year	24	500

Of the 10 C-L models, 6 used the Wilcock and Crowe (2003) sediment transport model and other 4 used the Einstein (1950) sediment transport model. Runs using Wilcock and Crowe were able to produce similar channel planform patterns and changes to those observed in the available Landsat images. In contrast, runs made using Einstein's sediment transport equation produced planforms featuring a deep, wide thalweg channel and the river activate the secondary channels, during the monsoonal, high flow season which otherwise remain dry during low flow season. Details of the relative performance of models using the two sediment transport methods are discussed later in this Chapter.

Uncertainty analysis is the study of how variations in the output of a model can be distributed, qualitatively or quantitatively to different sources of variation and how the response of the model depends upon the information fed into it (Salttelli et al., 2000). Good modelling practice requires that the modeller proceeds with an assessment of the confidence that can be placed on model outcomes, based on using uncertainty analysis to estimate the importance of each factor and, specifically, to identify those factors that are most relevant to calibrating the model (Ziliani et al, 2013). The analysis addresses the sensitivity of outcomes to (1) variation in model parameters such as the thickness of sediment layer in the sediment transport scheme, or the dimensions of the grid cells, and (2) uncertainty in model input data for topography, discharge, grain size distribution etc. There are two types of uncertainties in modelling: uncertainty of model parameters and uncertainty of time.

The Generalised Likelihood Uncertainty Estimation (GLUE) (Beven and Binley, 1992) is a method in which uncertain observed data can be used to calibrate a none error-free model and allow the uncertainty in model parameters to be assessed without making restrictive assumptions about the error in the observed data. It is based on rejecting the idea that there is a unique, optimum parameter set in a model calibration, and instead identifying the many different combinations of parameter values that may equally be acceptable in simulating the system under study (Hunter et al., 2005).

The range of parameter values used to run the C-L models built in this research (e.g. discharge, sediment input, vegetation and slope) were derived from:

1. the relevant published literature citing values used in previous applications of C-L,
2. expert advice from the actual originator of the model, Prof. Coulthard,
3. exploratory runs of the C-L models prior to the formal calibration and validation programme,

However, limitations were imposed by difficulties in accessing the data required to fully represent conditions in the modelled reach of the Brahmaputra at Majuli Island.

Consequently, the GLUE method could not be applied in calibrating the C-L models because it was computationally intensive. Instead, a method called ‘blind testing’ (Ewen and Parkin, 1996) was used in the selection of model parameters and the number of models to be used in the hindcasting programme. In the blind testing method, the modeller can set the output uncertainty bounds from a much smaller number of simulations (Bathurst et al., 2004). In this method the final bounds of the parameter values are set based on expert judgement, literature review or field measurement but not on the basis of extensive calibration. Therefore, in this study, 10 sets of parameters were used to run the C-L models which were based on the sensitivity of parameters and model run time.

6.2.1. Sensitivity to discharge

In an unsteady, uniform flow model, the input discharge varies through time but is always equal to output discharge. C-L models 4 and 7 used unsteady, uniform flow with the discharge input-output difference = 0 m^3s^{-1} at all times (details were given in Chapter 4, in the section of flow parameters). In the unsteady, non-uniform flow models (1, 2, 3, 5, 6, 8 and 9) the difference between discharge input and output was set at 500 m^3s^{-1} (again, for details see Chapter 4). The channel planforms and changes simulated by models using (a) unsteady, non-uniform flow with an input-output difference of 500 m^3s^{-1} and (b) the Wilcock and Crowe sediment transport model provided the best match to those observed in the available Landsat images (1999- 2014).

6.2.2. Sensitivity to bed roughness

The morphology of a river is known to be sensitive to small changes in flow resistance. The Manning roughness coefficient, n, was used to represent flow resistance in all the C-L models built in this research project. In a braided river, surface roughness differs significantly between the bed, bars and floodplains **(**Schummer et al., 2018**).** This is especially the case where the bars and floodplain are relatively stable and mostly covered by vegetation. Hence, ideally, when modelling a braided river, different Manning's n values should be used for the channels, bar surfaces and floodplains. However, the C-L model does not make provision for separate Manning's n values to be used for the channels, bar surfaces and floodplains. Consequently, in this research, a uniform Manning roughness coefficient of n = 0.04 was used. Although this resulted in more sediment being deposited on bars and floodplains than would be expected in nature, the planform pattern of bars simulated by the C-L models with a constant n-value of 0.4 provided the best fit with bar patterns observed in the available Landsat images (1999- 2014).

6.2.3. Sensitivity to lateral erosion coefficient

Lateral migration of the thalweg was evident in all ten C-L models, with rates and patterns being highly sensitive to the value selected for the lateral erosion coefficient. According to Prof. Coulthard, and based on his long experience with the C-L model, lateral erosion coefficients of 0.01 to 0.001 m are typical for braided rivers, which 0.0001 m is typical for meandering rivers. In this study, it was found that setting the lateral erosion coefficient to 0.001 m resulted in very long run times (as described in Chapter 4, the section on sediment and flow parameters). For example, setting the lateral erosion coefficient used in C-L models 5, 6 and 7 to 0.001 m not only resulted in these models running very slowly but also created a 'checkbox effect' depicting instabilities in flow routing through the river channel. The other models used a value of 0.0001m. This reduced run times and eliminated the 'checkbox effect'. Though the Brahmaputra is classed as a braided river, the study area features some reaches that are anastomosed in character (i.e. multiple anabranches that operate semi-independently) and some reaches that are braided (i.e. a single large channel with flow divided around mid-channel bars). Therefore, running C-L with a lateral erosion coefficient of 0.0001 m seems suitable for the Brahmaputra, because of the presence of anastomosing anabranches which behave in a manner similar to meandering rivers. Also, thalweg channel migration rates and patterns simulated by models using a lateral erosion coefficient = 0.0001 m produced the best fit to thalweg channel migration rates and patterns observed the Landsat images (1999- 2014).

6.2.4. Sensitivity to grain size

C-L allows a spatially variable sediment size distribution (with up to nine size classes) to be modelled and it simulates selective erosion, sediment transport as bedload and suspended load, and deposition of different size fractions (with deposition of bedload and suspended load being managed separately) (Coulthard and Van De Wiel, 2006).

As described in Chapter 2, no bedload data are available for the Brahmaputra in Assam. Available daily mean suspended sediment load data for the

Brahmaputra, specify grain sizes as very coarse (2.00 mm), medium sand (less than 2 mm – greater than 75 μm) and very fine sand (75 μm) (further more details are given in Chapter 4). Therefore, this research available suspended sediment data were used to run the simulations. As discussed in Chapter 2, during the field survey campaign, sediment samples were collected from selected locations in the Brahmaputra near Majuli Island and subject to particle size analysis in the geotechnical laboratory at Tezpur University (Figure 5.1).

Figure 5.1. Drying and sieving the sediment samples collected during fieldwork.

Sediment samples were dried and sieved using a 9-sieve stack. It was found that, on average, 65% of the sediment was silt and clay (<64 μm), 32% = very fine sand (<75 μm), 1.26% = fine sand (150 – 212 μm), 0.84% = medium sand (300 – 600 μm) and 0.155% = coarse sand (1 – 2 mm). It is notable that the percentage of coarse sediment (medium and coarse sand) in the Brahmaputra is tiny compared to the percentage of fine sediment (silt and clay). Given the low availability of grain size data, it was decided to use just three-grain sizes in the C-L models. As silt and clay constitute wash load in the Brahmaputra (for which the load is controlled by supply rather than transport capacity), it was not attempted to simulate the dynamics of this very fine sediment in the C-L models. As a result, the models were unable to simulate the exact numbers of bars observed in the Landsat images (1999- 2015), although the models were able to simulate broad morphological changes in the study reach of the river.

6.3. Model evaluation criteria

Quantifying medium to long-term evolution and change in the morphology of a braided river requires the use of statistically-derived indices that characterise the channel form and pattern, such as braiding intensity and average channel width (Nicholas, 2005; Sharma and Akhtar 2012). Hence, when assessing the capacity of the C-L model to simulate morphological evolution and change in study reach, it is necessary to identify indices suitable for testing goodness of fit between simulated and observed morphologies and morphological changes. For this purpose, three aspects of channel morphology and change were selected:

1. The behaviour of the main branch: Thalweg Migration Index (TMI).
2. Planform pattern and change at the reach scale:
    a. Modified Plan Form Index (MPFI),
    b. Modified Flow Geometry Index (MFGI),
    c. Bar Deformation Index (BDI).
3. Cross-sectional and long-profile forms and changes:
    a. Cross-section modelled,
    b. Long-profile modelled,
    c. Wetted perimeter

The ways in which these representations of morphology and morphological change were evaluated are illustrated in Figure 5.2.

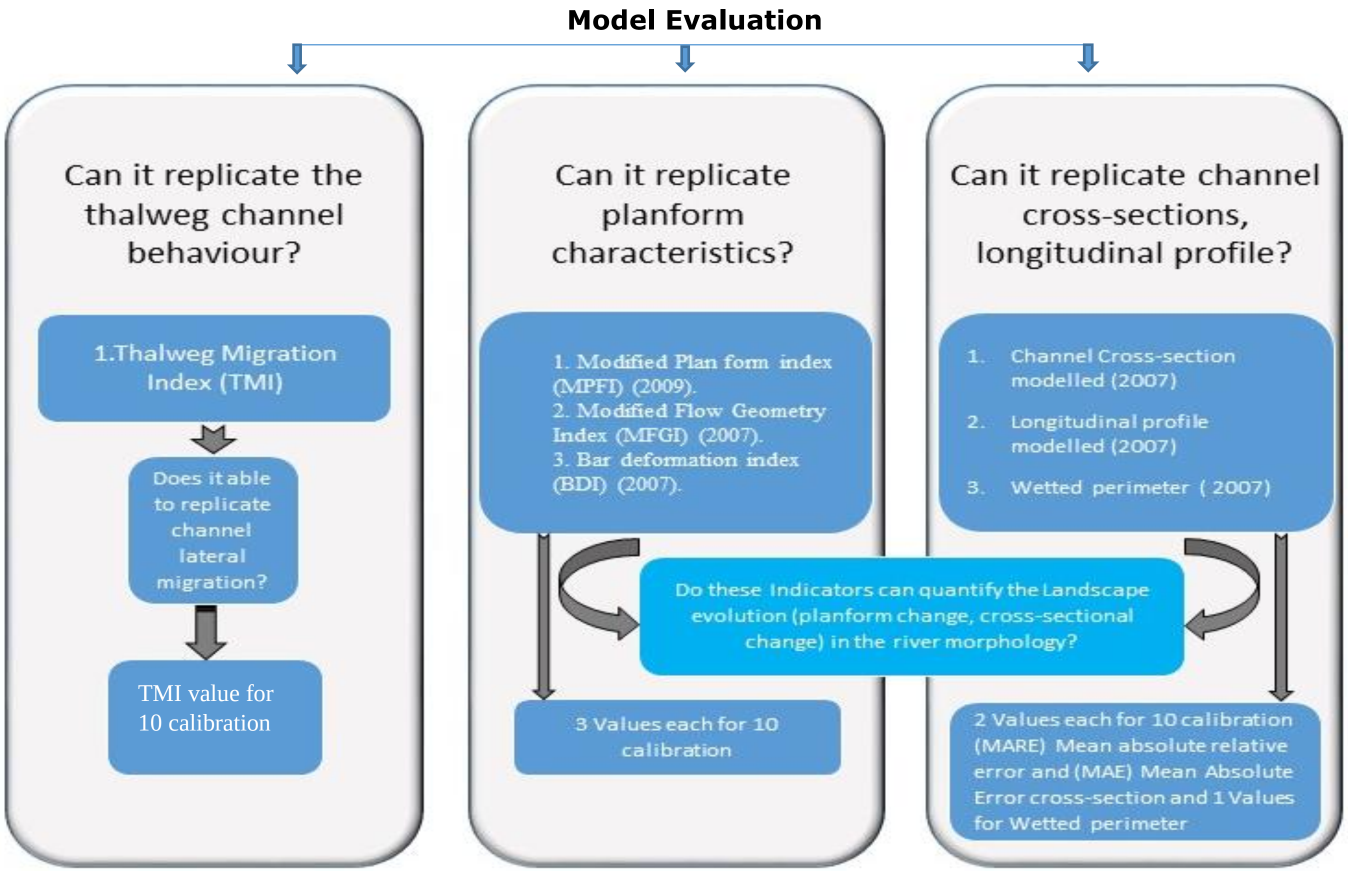

Figure 5.2. Model evaluation criteria used in testing the hindcasting models.

6.3.1. The behaviour of the thalweg channel

As discussed in Chapter 3, the initial bathymetry data was produced using available cross-sectional data collected by the Water Ressource Department (an Indian Government Agency authorised to collect river data) in March 1998 together with 90 m resolution SRTM data collected in 2000. These are the closest matched planform and bathymetry data available to define the three-dimensional morphology of the Brahmaputra near Majuli Island.

Cross-section data were used to characterise channel bathymetry and the initial position of the thalweg channel. SRTM data were used to derive the elevation of the floodplain. In a braided/anastomosed river like the Brahmaputra, it is sometimes difficult to identify the main anabranch. Hence in this study, the deepest channel (i.e. the one containing the thalweg) was considered to be the main anabranch. In the contexts of short-medium to long-term channel evolution (that is the time-scales of most interest to river management and engineering), lateral migration of the thalweg channel is one of the most important characteristics to be modelled in this research. Hence, it was essential to establish the degree to which the C-L model could reproduce the behaviour of the thalweg channel observed between 1998 and 2015. This involves investigating not only how the thalweg channel changes and shifts in response to flood events and high sediment influxes that influence its behaviour directly, but also how head-cutting processes in secondary channels can lead to the creation of a new thalweg channel due to the diversion of flow away from the existing thalweg channel.

6.3.2. Planform pattern and change at the reach scale

Validating the spatial and temporal distributions of flow depths and inundation areas in a cellular model is straightforward where field data are available and channel patterns are simple (Coulthard et al., 2007). However, validation in great, braided rivers like the Brahmaputra is more challenging. Validation options rest on parameters for planform change and/or topological metrics such as the braiding index, which can be used to compare modelled to observed channel characteristics (Coulthard et al., 2007; Nicholas et al., 2006) using sequences of aerial photographs or historical maps to show braiding development.

Paola (2001) suggested that for models designed to simulate high-level system characteristic (e.g. channel planform) it may be inappropriate to compare predictions of lower level properties (e.g. flow patterns, anabranching, sandbar size and shape, etc.). According to Coulthard (2007), the use of planform data can be limited by the frequency of aerial photographs or map updates. Also, each photograph or map only represents a single moment in time, which may be unsuitable for rapidly changing systems such as braided rivers. Repeat topographic surveys (using LiDAR etc.) or satellite images (Landsat images etc.) provide a better basis for evaluating morphological changes over time, but these accessing satellite images or LiDAR equipment is expensive and performing conventional field surveys both expensive and highly labour intensive. Therefore in this study Landsat images were used to evaluate the planform changes, which are freely available.

The planform characteristics of the braided channel simulated by C-L should reliably reproduce the planform characteristics observed in nature. To provide a quantitative assessment of the similarity between modelled and observed planforms a number of indices of channel morphology can be used (Nicholas et al., 2006). In this study, Modified Planform Index (MPFI), Modified Flow Geometry Index (MFGI) and Bar Deformation Index (BDI) were used to quantify the resemblance between modelled and observed planforms and to compute and compare simulated and observed trends of planform change.

6.3.3. Cross-sectional and long-profile forms changes

The capacity of C-L to reproduce cross-sectional and long-profile changes observed due to process-response mechanisms of channel adjustment in the River Brahmaputra near Majuli Island was also tested. Specifically, changes in cross-section, thalweg long-profile and wetted perimeter were quantified from repeat cross-sectional surveys available for various locations in the study reach. As described in Chapter 2, the Water Resource Department of the Government of India, Assam has in the past surveyed 65 cross-sections on the Brahmaputra within the territory of Assam. Data are available for surveys conducted in 1988, 1998 and 2007. No further no cross-sectional surveys have been undertaken since 2007.

The data sources used in evaluating the capability of the10 C-L models to hindcast changes the study reach are listed in Table 6.2.

Table 6.2: Evaluation criteria and source data.

Evaluation criteria	Observed	Modelled
Thalweg channel behaviour	TMI of Landsat images (1999, 2002, 2009 and 2014) low flow season. (exact date of acquiring tabulated in chapter 2)	TMI of 10 C-L models (1999, 2002, 2009 and 2014) low flow season.
Planform change	MPFI of Landsat images (1999, 2002, 2009 and 2014) low flow season. (exact date of acquiring tabulated in Chapter 2)	MPFI of 10 C-L models (1999, 2002, 2009 and 2014) low flow season.
Channel Geometry	MFGI of observed CS 47, 48, 49 (2007) low flow seasons.	MFGI of 10 C-L models CS 47, 48, 49 (2007) low flow seasons.
Channel adjustments	Observed cross-section CS 47, 48, 49 (2007) low flow seasons.	10 C-L model cross-sections CS 47, 48, 49 (2007) low flow seasons.

6.4. Thalweg migration index (TMI)

Though the River Brahmaputra is considered to be a braiding river, three types of the channel are observed in the study reach:

1. the main or thalweg channel,
2. anabranches, which dissect sandbars and form the braided pattern,
3. anastomosing channels, which are long, narrow channels generally 3 to 5 km in length that bifurcate from the main, thalweg channel but re-join it further downstream.

As C-L is a Reduced Complexity Model (RCM), it cannot be expected to simulate the precise number or configuration of every anabranch or secondary channel in braided and anastomosed sub-reaches. However, the behaviour of the main channel is particularly important and, recognising this, the capacity of C-L to reproduce observed migration of the main or thalweg channel was investigated. That behaviour, in simulated and observed records, was quantified using a newly developed parameter termed the Thalweg Migration Index (TMI).

As described in Chapter 3 TMI represents the direction of movement of the thalweg channel. If the TMI value of the thalweg channel is distance = or > +1.5 from the river centreline (0) then the thalweg channel is migrating north (i.e. towards Majuli Island). A TMI value that is = or < -1.5 from the centreline (0) indicates that the thalweg channel is migrating south (away from Majuli Island). For a northward migrating case, TMI_Observed is the observed TMI value and TMI _Modelled is the modelled TMI value.

$$1.5 \longleftarrow 0 \longrightarrow -1.5$$

Migrating towards North Bank	Centreline	Migrating towards South Bank

Table 6.3: Sediment transport parameters used in the hindcasting C-L models.

Model	Sediment transport flow	Lateral erosion rate (m)	Number of passes	Number of cell shift lateral erosion downstream	Maximum difference allowed in cross-channel smoothing (m)	Note & observation thalweg channel migration
1,2,3 & 4	Wilcock & Crowe	0.0001	20 - 10	4 - 5	0.0002	Thalweg channel flowing along the similar route as observed in the Landsat images near the Neemati ghat. The thalweg channel became wider and shallower (Table 6.5) (Figure 5.3)
5 & 6	Wilcock & Crowe	0.001	30	2 - 3	0.0001	Thalweg channel flowing along the north bank near Kamalabari instead of flowing near Neemati ghat. The thalweg channel became wider and shallower.
7	Einstein	0.001	10	3	0.0001	Thalweg channel flowing in the similar route like the observed thalweg channel. The thalweg channel became wider and deeper. (Figure 5.4)
8, 9 & 10	Einstein	0.0001	20	2 - 4	0.0002	Thalweg channel flowing in the similar route like the observed thalweg channel. The thalweg channel became wider and deeper.

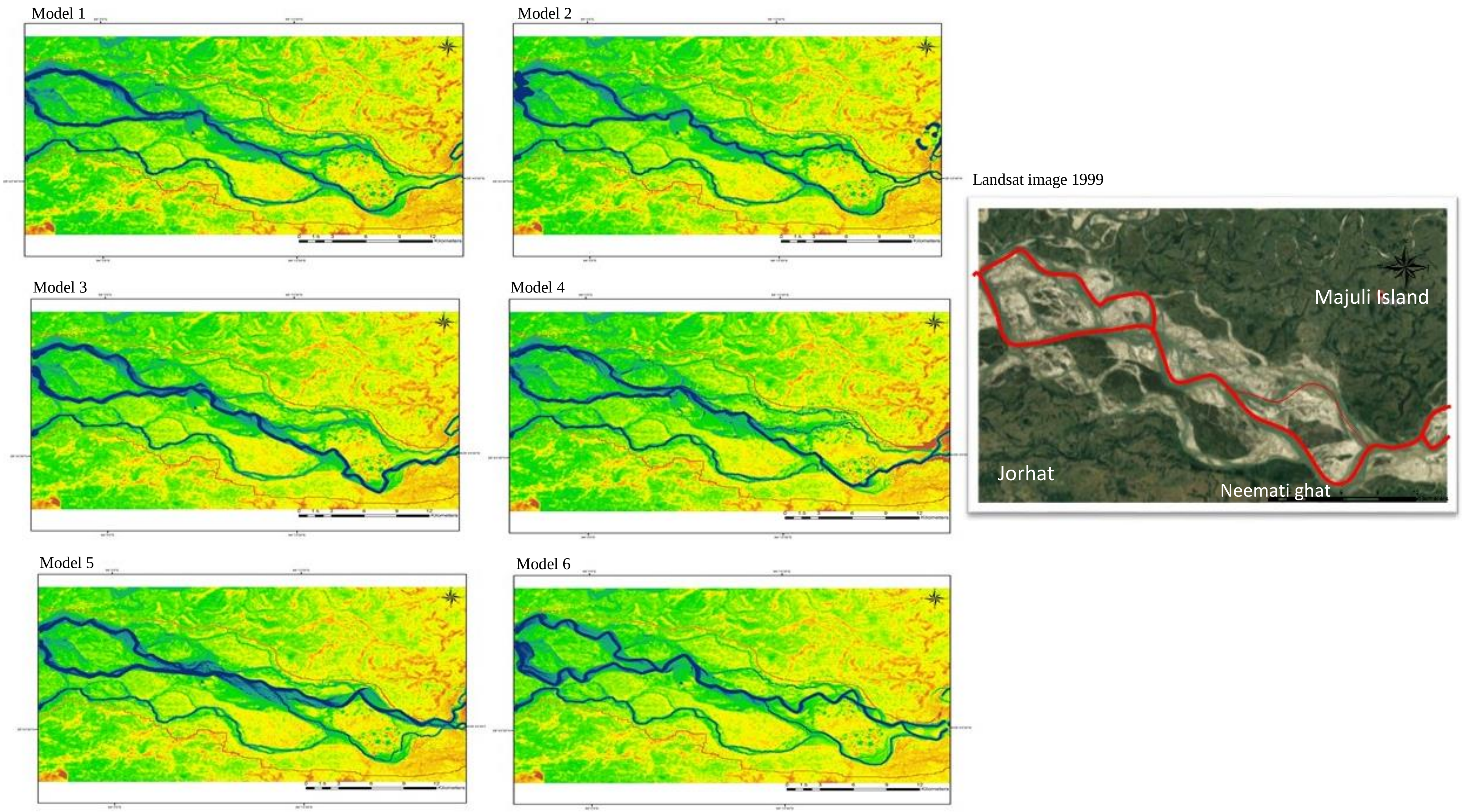

Figure 5.3: Movement of thalweg channel in the six CL model and the Landsat Image of the river Brahmaputra (1999).

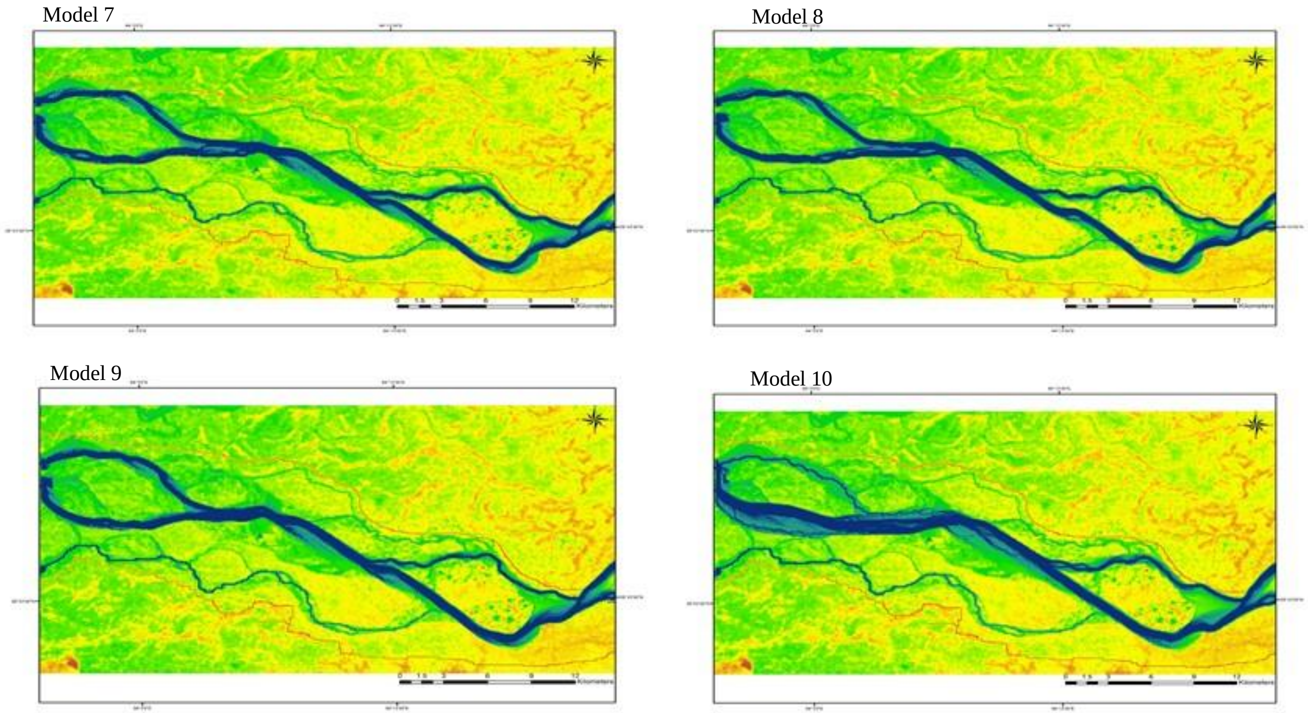

Figure 5.4: Movement of thalweg channel in the four CL model and the Landsat Image of the river Brahmaputra (1999).

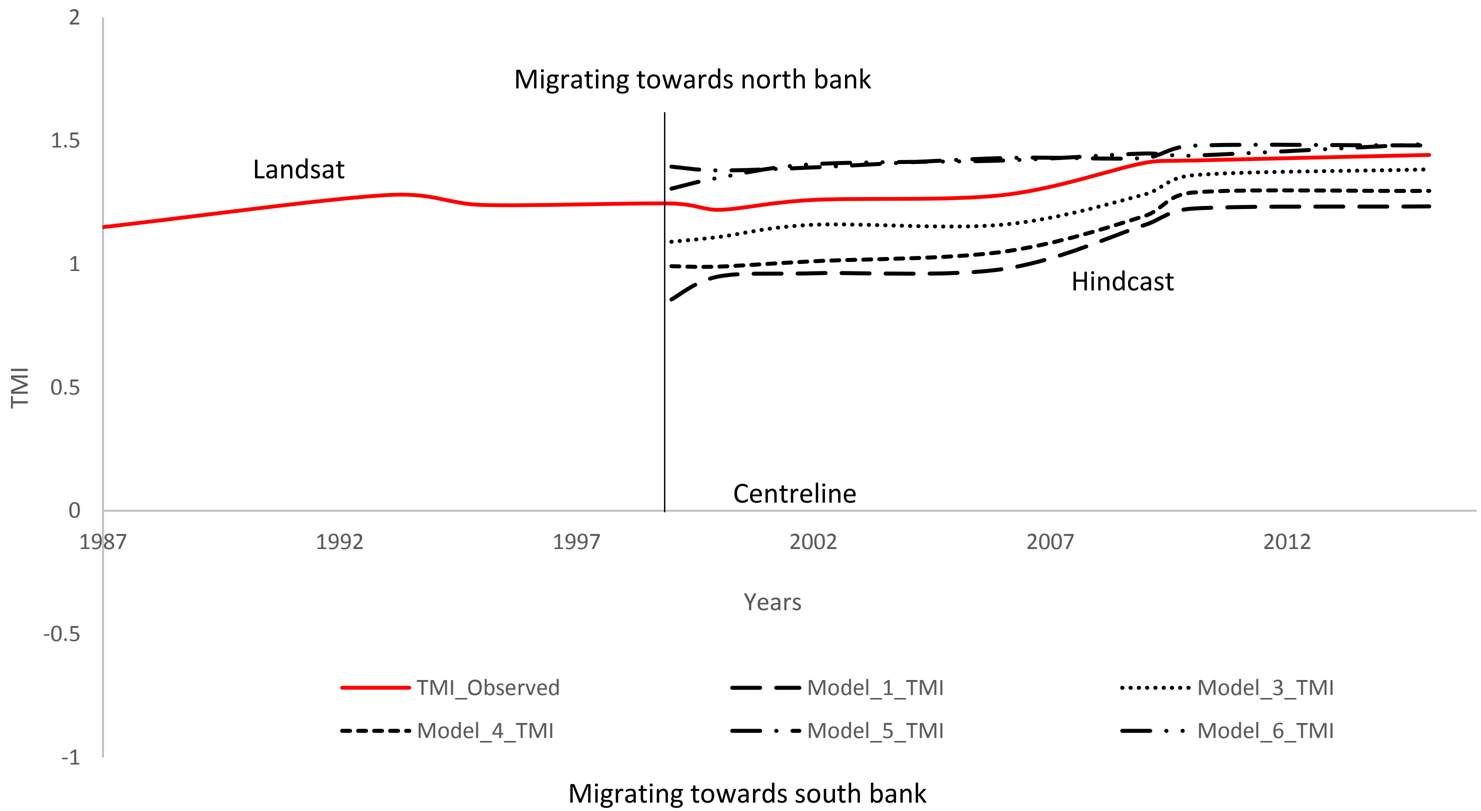

Figure 5.5: Comparison of the observed TMI with the five modelled TMI of the river Brahmaputra near Majuli Island.

In this chapter, the TMI values of the five models were displayed in the graphs (Figure 5.5) to quantify the thalweg channel migration (TMI of rest of the models are displayed in the appendix 1). They were compared with the TMI value of observed thalweg channel from Landsat images of 1999, 2002, 2009 and 2015. These four years have been selected for comparison (i) availability of Landsat images without cloud coverage (ii) they were the subsequent years of major flood events in the River Brahmaputra. All the 10 models performed differently (Figure 5.3, 5.4). The (Table 6.3) depict how changes in different parameter were able to produce different flow pattern of thalweg channel.

Models 1 and 2 were able to represent the similar route of the observed thalweg channel but they have don’t exhibit the TMI value closed to the observed ones. On the other hand Model, no 3 and 4 were able to represent the similar route of the thalweg channel. They were also able to exhibit the TMI value closed to the observed ones. All the four models were depicting the thalweg channel migration towards the north bank near Majuli Island. Wilcock and Crowe sediment transport model was used to hindcast the CL model in these four models. In the river Brahmaputra during the dry season the thalweg channel and other subsidiary channels became narrow and shallow, this is due to low discharge flow. This was clearly visible in the four models described here.

In models 5 and 6 (Table 6.3) the thalweg channel took a different route. Instead of flowing along the south bank, near Neemati ghat, it flowed along the north bank. Therefore these two models cannot be considered as a suitable representation of thalweg channel movement in the study reach. They were exhibiting higher TMI value than the observed TMI value (Figure 5.5). In these above mentioned 6 models the rate of sediment supply was higher than the capacity of the channel to move it. In this process, the surplus sediments were deposited in the channel bottom or deposited in the floodplains allowing the thalweg channel to migrate.

Models 7, 8, 9 and 10 used the Einstein sediment transport equation and they performed differently from the rest of the CL models. The TMI value of these four models are shown in the appendix 1. In models C-L 7 - 10, the thalweg channel became wider and deeper. This was because the channel has washed the sediment without leaving any trace of sediment input along with eroding the banks. This phenomenon is called wash load. Due to this reason the subsidiary channel remain dry during low flow as the main channel attains the capacity to flow the discharge and suspended sediment load.

6.5. Modified plan form index

Modified Plan Form Index (MPFI) is one of the indicators used in this research that quantifies the braiding planform pattern. During low flows condition, the river becomes shallow and braiding intensity is high. The low flow season was used in this research to calculate MPFI values as the Landsat data used to compute the observed MPFI values were acquired during low flow conditions. As discussed in chapter 3, MPFI values calculated from the Landsat images for both the sub-reaches have increased since 2009.

The width of the channel, number of braiding channel and number of sandbars were the main component used in computing MPFI. C-L models 1 to 6 used the Wilcock and Crowe sediment transport model, and these models were able to reproduce intense braiding. This is due to the thalweg channel becoming shallower and wider, activating the dry, secondary channels and dissecting sandbars to create new anabranches (Figure 5.9, 5.10). In this section MPFI values of the model, no 1- 6 were displayed for both the sub reach (Figure 5.6). Model no 3 exhibiting the MPFI value close to the observed Landsat image MPFI (O) values (Figure 5.7, 5.8).

C-L models 7 to 10 used the Einstein sediment transport equation, which were unable to generate braiding. In this case, the thalweg channel became deeper and wider, was unable to activate the dry channels to create new anabranches during low flow. The MPFI values of these four models are shown in the appendix 2.

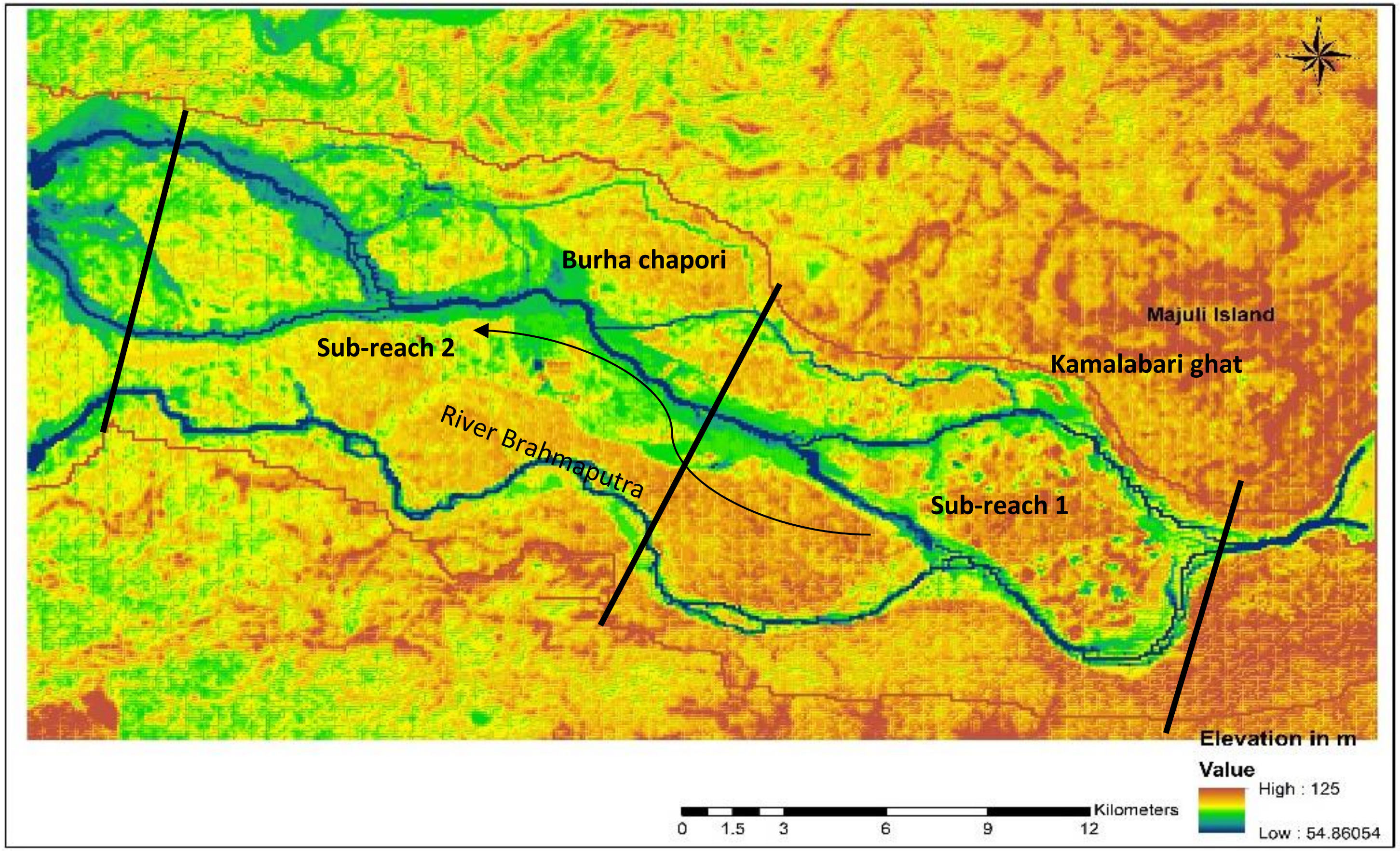

Figure 5.6. Sub-reaches used to calculate MPFI for each model and observation.

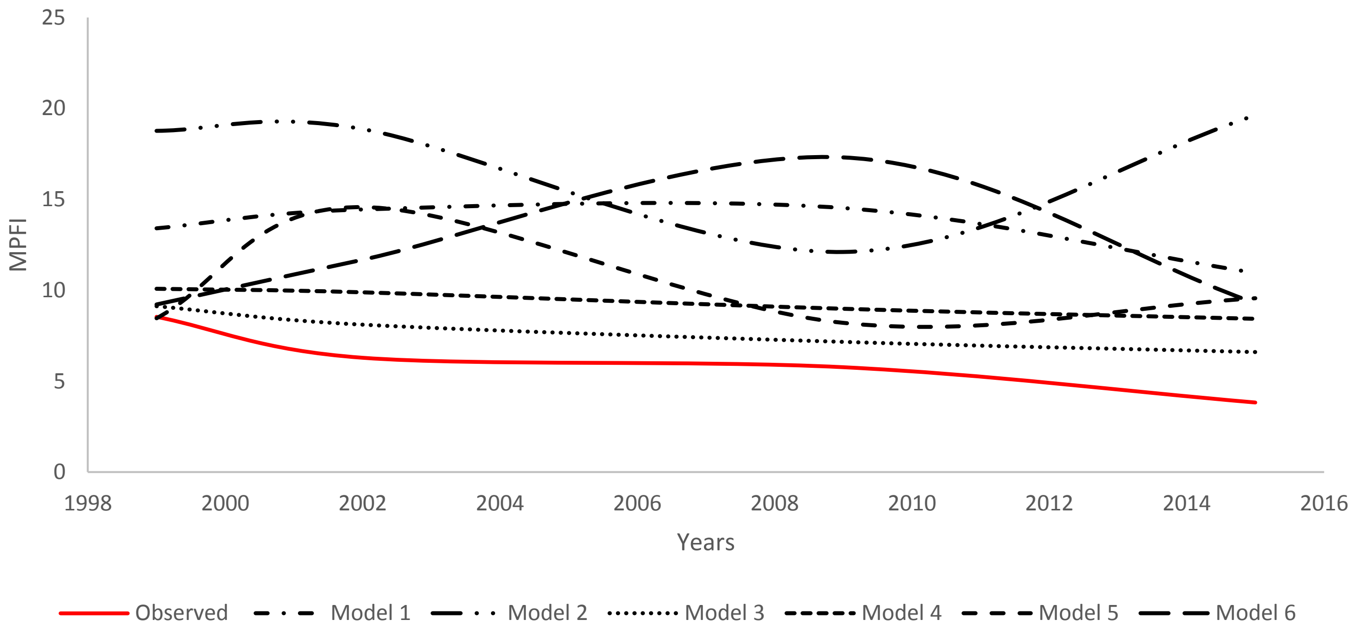

MPFI Thresholds
MPFI < 6 – High braiding
6 > MPFI < 18- Moderate braiding
MPFI > 18 - less braiding

Figure 5.7: MPFI value of the six C-L model of the sub-reach 1.

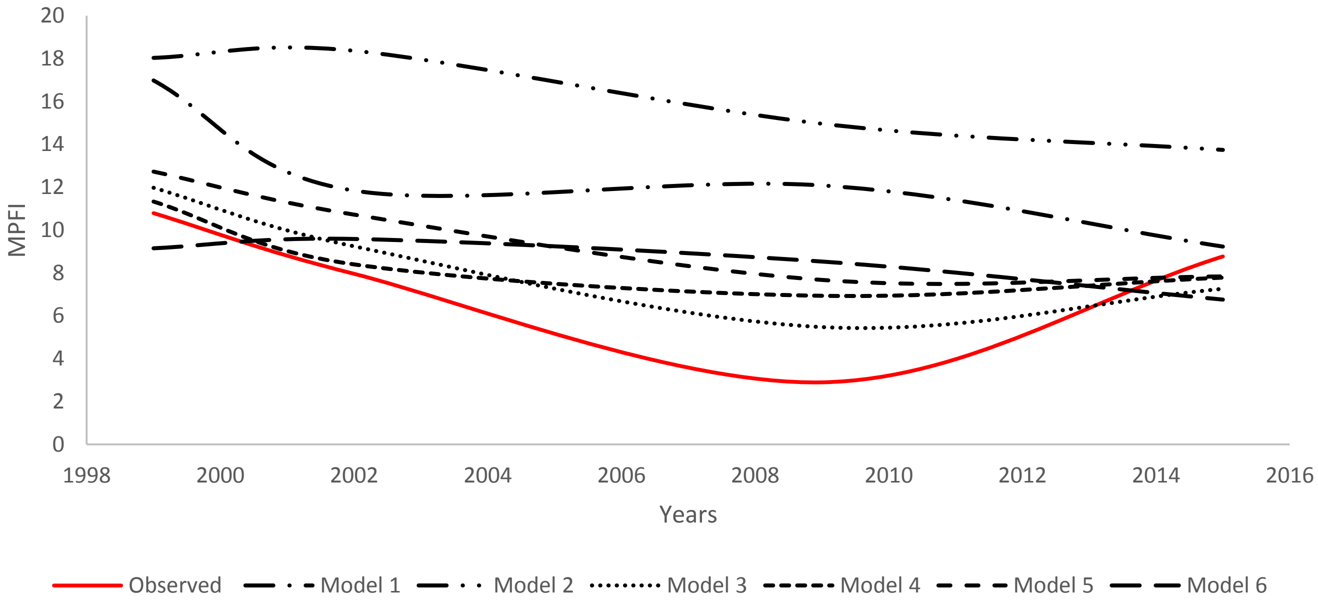

MPFI Thresholds
MPFI < 6 – High braiding
6 > MPFI < 18 - Moderate braiding
MPFI > 18 - less braiding

Figure 5.8: MPFI value of the six C-L model of the sub-reach 2.

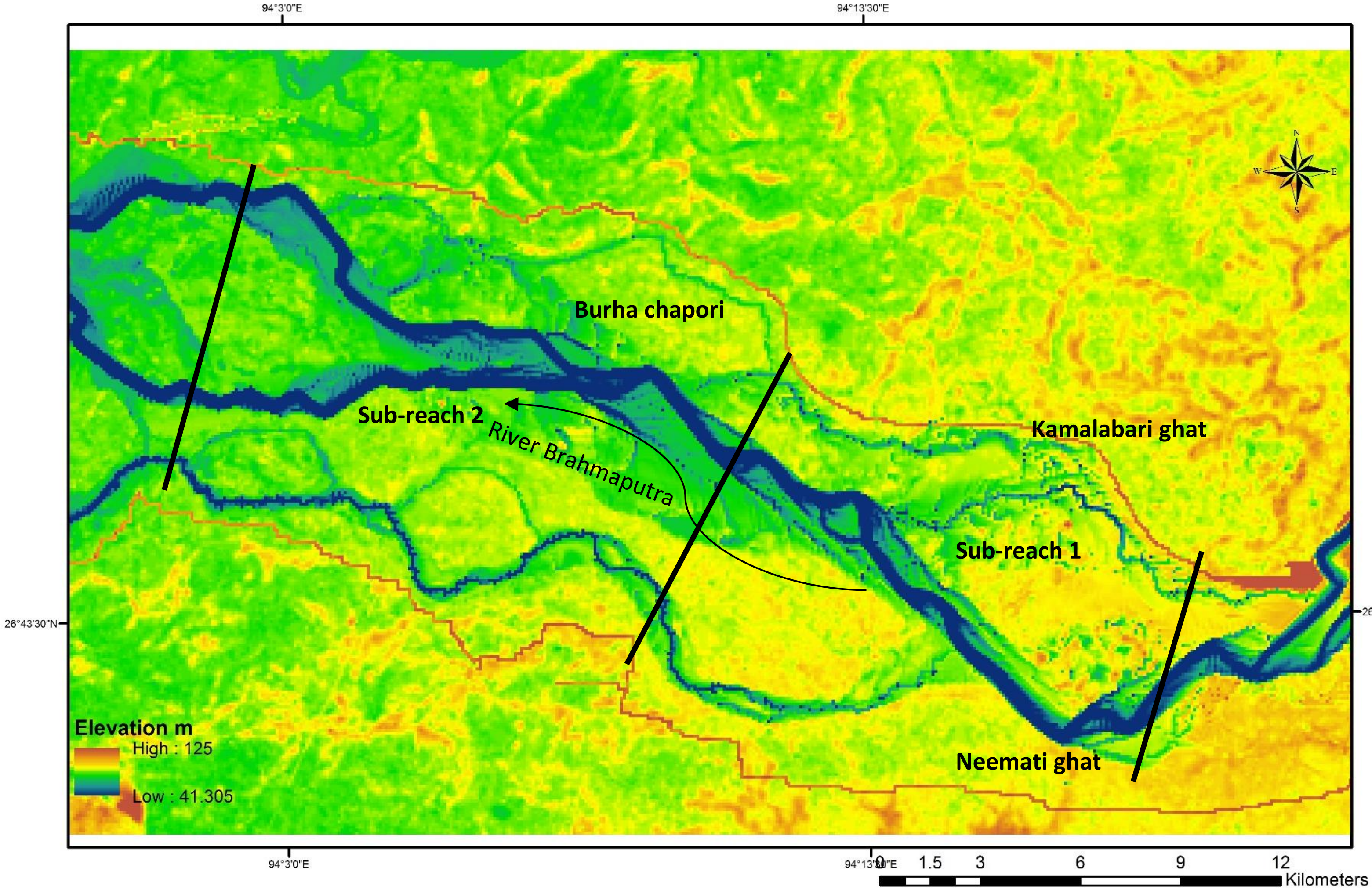

Figure 5.9: C-L model no 3 (2009) during low flow season showing the formation of braiding channel.

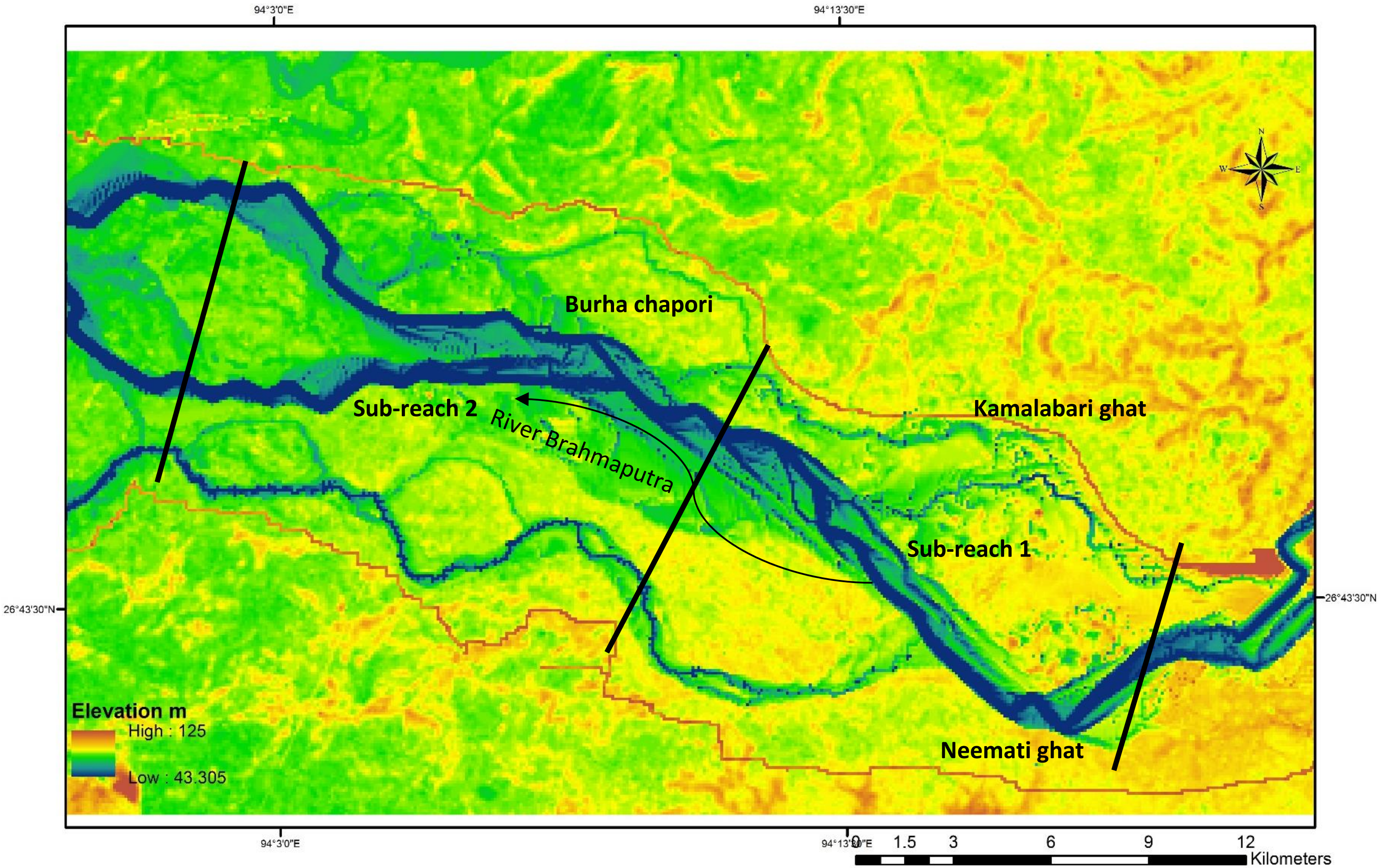

Figure 5.10: C-L model no 3 (2015) during low flow season showing the formation of braiding channel.

Sharma and Akhtar (2012) computed values of Sharma's (2004) Plan Form Index (PFI) for 120 cross-sections of the Brahmaputra in Assam (Figure 5.11). They then divided the river into 12 sections based on their morphological patterns (Figure 5.11). Among these, Majuli Island falls into Section 9. In Figure 5.12, Section, 9 is shown as being moderately braided prior to 2008 but it became highly braided in 2008, which coincides with the outcome of the hindcast C-L models.

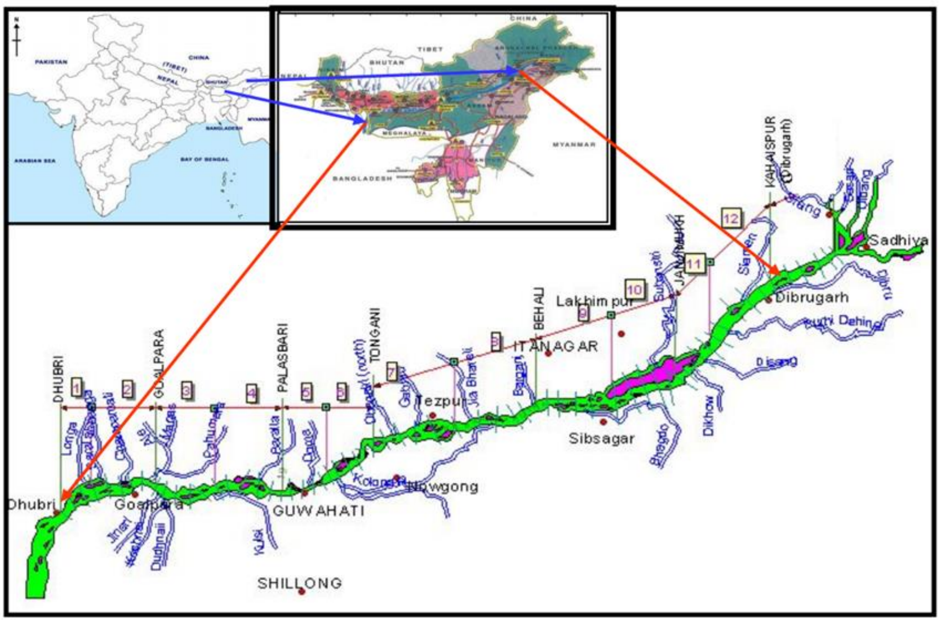

Figure 5.11. Cross-sections of river Brahmaputra used in PFI computations by Sharma and Akhtar (2017).

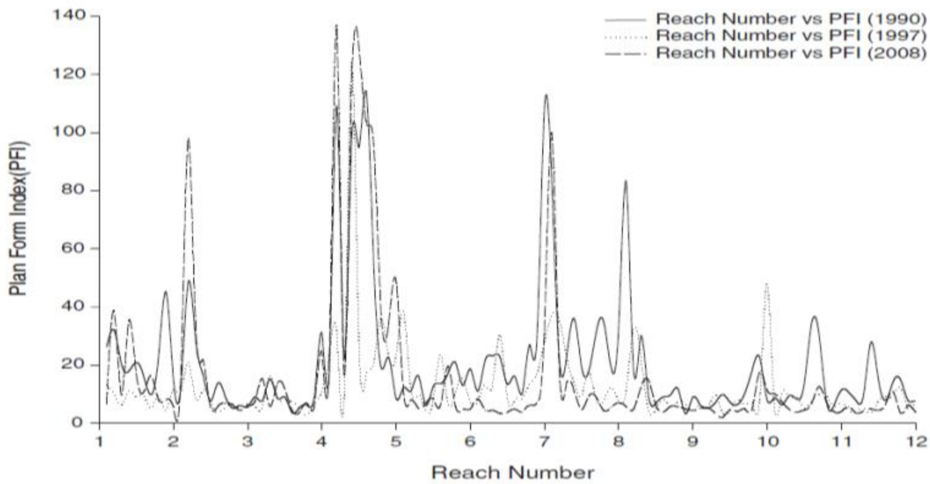

Figure 5.12. PFI values in the 12 sections of river Brahmaputra, Source: Sharma and Akhtar (2017). Note: Majuli Island is in section 9.

6.6. Modified flow geometry index

As discussed in Chapter 3, higher values of MFGI signify higher braiding intensity, with commensurately reduced hydraulic efficiency due to increased energy dissipation caused by surface roughness and form drag. Modelled values of MFGI for the three cross-sections generated by the C-L models have plotted along with the observed MFGI values for cross-sections 49, 48 and 47. For C.S. 48 in 2007, the MFGI value generated using C-L model 3 has the best fit compared with the observed MFGI value. Both the observed and modelled MFGI values depict moderate braiding in 2007 (Figure 5.14).

MFGI Thresholds
MFGI > 5 - Low Braided

5 > MFGI < 15 - Moderate Braiding

MFGI > 15 - High Braiding

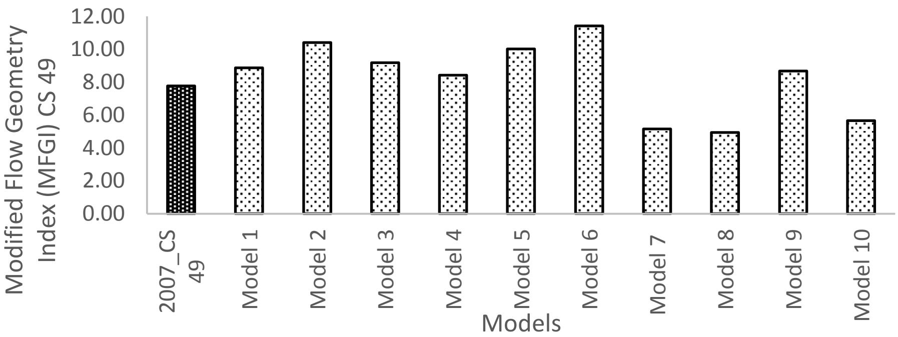

Figure 5.13: MFGI of CS 49 (2007) of all the CL model and observed CS 49 (2007).

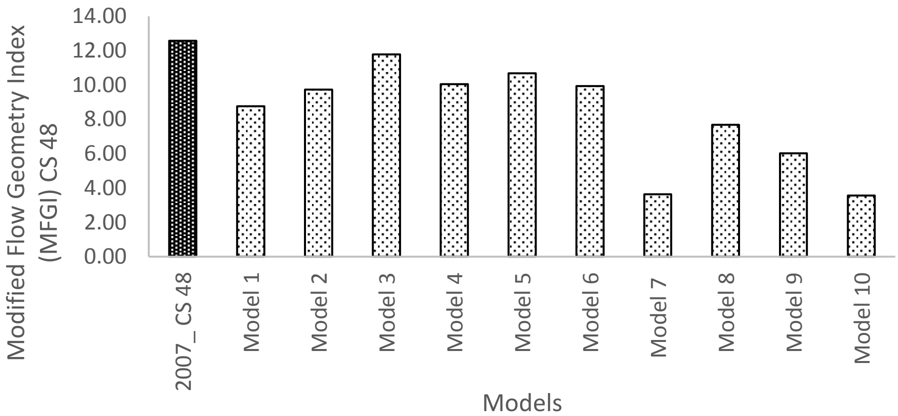

Figure 5.14: MFGI of CS 48 (2007) of all the CL model and observed CS 48 (2007).

Results for C.S. 49 in 2007 are plotted in Figure 5.13. The MFGI value generated by C-L model 4 has the best fit compared with the observed MFGI value. The modelled and observed value both indicate moderate braiding in 2007.

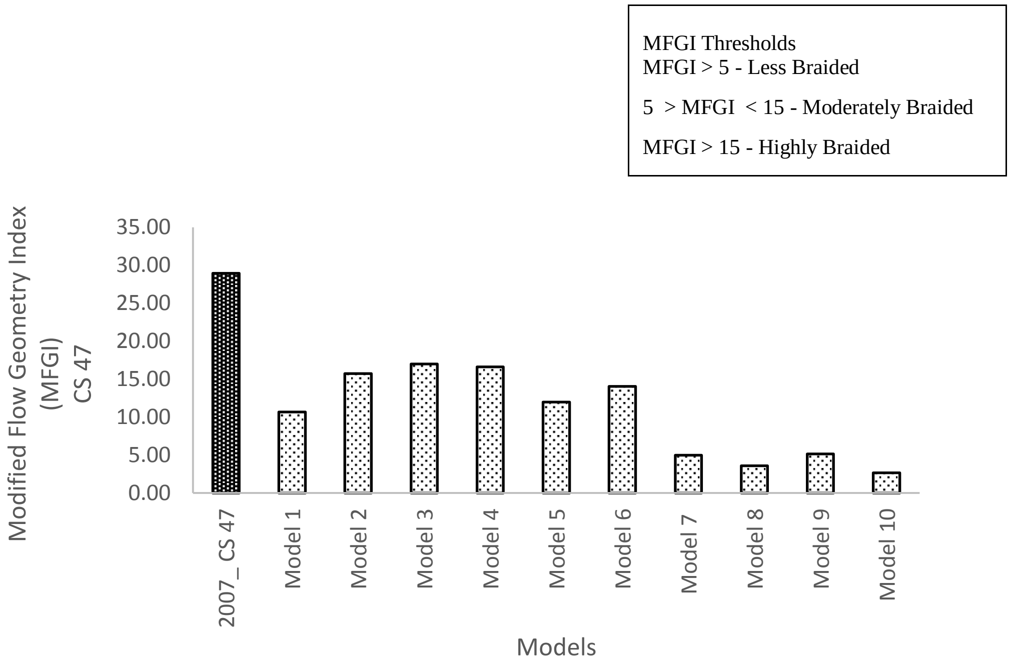

Figure 5.15: MFGI of CS 47 (2007) of all the CL model and observed CS 47 (2007).

For C.S. 47 (Figure 5.15) C-L models 3 and 4 do about equally as well as each other, although neither is a very good fit.

Table 6.5: Average width (km) and depth (m) of the thalweg channel of River Brahmaputra near Majuli Island

Cross-section	Observed CS 2007		Model 3 CS 2007		Model 4 CS 2007	
	average width (km)	average depth (m)	average width (km)	average depth (m)	average width (km)	average depth (m)
CS 49	4.4	12.41	3.9	13.3	3.65	10
CS 48	3.67	7.78	3.92	11.9	3.86	10.75
CS 47	4.34	7.05	4.55	10.69	4.4	9.79

Channel width and average depth are key indicators of channel size and shape. In both C-L models 3 and 4, the width of the river channel changes (Table 6.6). The widths and depths of the thalweg channel and secondary channels also change in both the models (Table 6.5). Therefore from the table, it can be inferred that the C-L models were capable to change the width of the large braided river like the Brahmaputra and able to change the river morphology such as thalweg channel migration, cross-sectional change, width and depth of the thalweg channel and minor channels. It was observed from the C-L models of that anabranches and anastomosing channel, act as an agent of erosion like the thalweg channel and widens the river channel. A 3 sandbar was a stable sandbar with vegetation cover, therefore, it acts as a resistance to the thalweg channel and allowing the thalweg channel to move towards north bank instead of south bank; eroding A 2 and the adjacent sandbars. The anastomosing channel which was flowing along A 3 sandbar was not powerful enough to erode the south bank and the A 3 sandbar. However the thalweg channel has eroded the river banks near Neematighat in the south bank (Figure 5.15, 5.16).

Table 6.6: Average width (km) of the River Brahmaputra near Majuli Island

Year	Observed (Landsat)	Model 4	Model 3
1999	12.00	10.15	11.12
2002	12.00	10.15	11.12
2009	11.38	11.10	11.18
2014	13.21	11.13	11.18

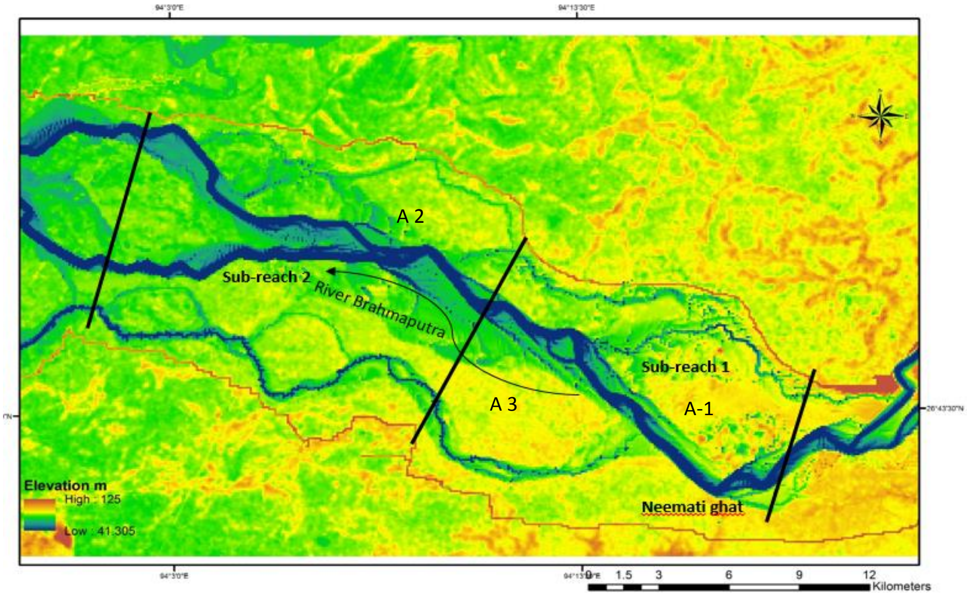

Figure 5.15: Thalweg channel eroding the river bank near Neemati ghat (2009) model no 3.

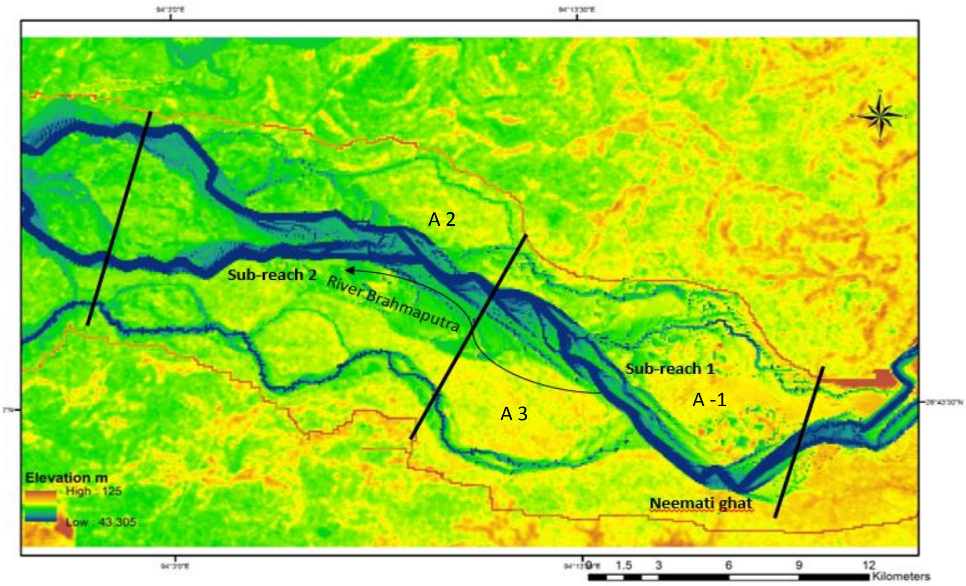

Figure 5.16: Thalweg channel eroding the river bank near Neemati ghat (2015) model no 3.

6.7. Wetted perimeter

Wetted perimeters generated using the 10 C-L models are plotted together with observed values for cross-sections C.S. 49, 48 and 47 in 2007 (Figures 5.17 – 5.19). The results illustrate that wetted perimeters generated using models 3 and 4 provide the best fits with the observed wetted perimeters.

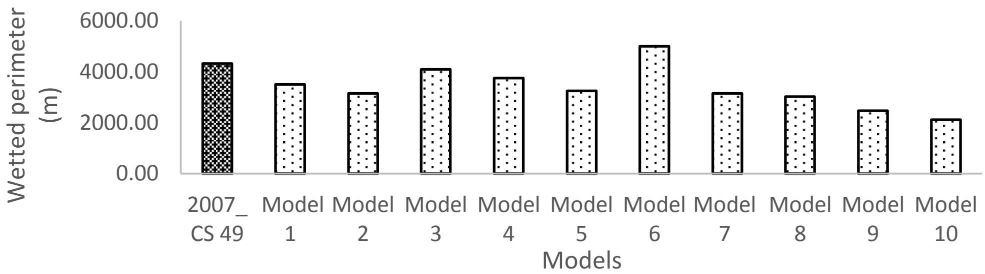

Figure 5.17: Wetted perimeter observed for cross-section C.S. 49 in 2007 and generated using the ten C-L models.

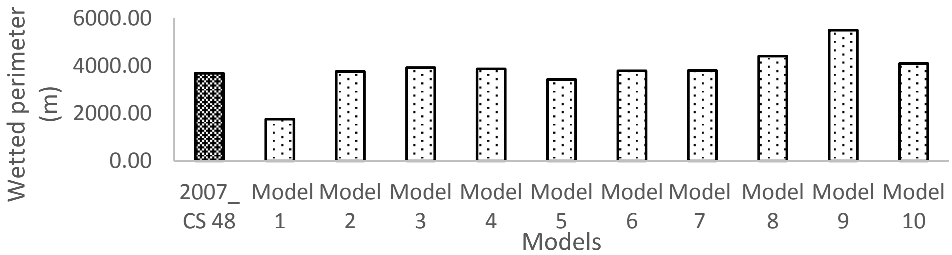

Figure 5.18: Wetted perimeter observed for cross-section C.S. 48 in 2007 and generated using the ten C-L models.

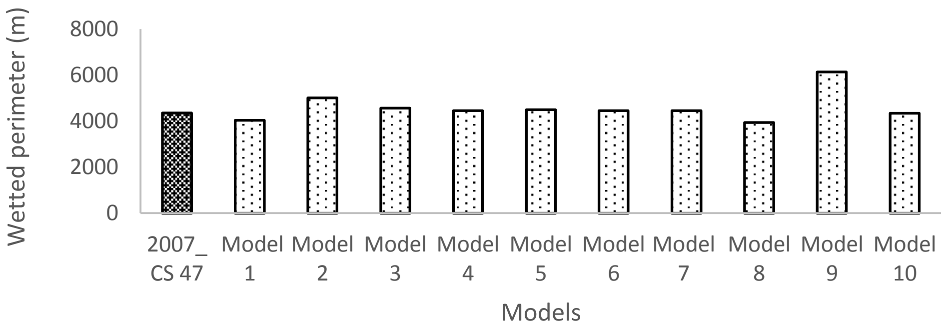

Figure 5.19: Wetted perimeter observed for cross-section C.S. 47 in 2007 and generated using the ten C-L models.

6.8. Bar deformation index (BDI)

In C-L, water and sediment are routed from cell to cell in a computational grid using simple concepts representing the governing conservation equations for mass and momentum (Sapozhnikov et al., 1998). The C-L model appears to reproduce the main dynamic behaviour of the thalweg channel and formation of braiding channels separated by sand bars within which the flow shifts continuously from the path to path, reforming and deforming sandbars. C-L helps in comparing measures of spatial pattern and temporal dynamics of sandbars and braided channels. In the C-L model, flow divergences tend to produce convergence in the sediment flux and therefore create local deposition. Further, this local deposition enhancing flow divergence leads to bar formation; conversely, flow convergence creates instabilities and leads to deformation of sandbars.

Table 6.7. Bed roughness and vegetation parameters of C-L model 3 and 4.

Model	Manning Roughness (-)	Vegetation crit shear (Pa)	Grass maturity	The proportion of erosion that can occur when vegetation is fully grown (0-1)
Model 3	0.04	180	0	0.1
Model 4	0.04	180	1	0.1

The bed roughness should be different for river bed, bar and floodplain surfaces. In this research n = 0.04 is applied to all of the wetted surface. Similarly, vegetation shear stress (τ_{crveg}) should be different for floodplain, stable bars and mobile bars. In case of A 1 (Figure 6.20) which is an unstable sandbar with no vegetation cover should ideally have 70 Pa (τ_{crveg}) which is a heavily degrading sandbar (Prosser, 1996). On the other hand, A 2 is a stable sandbar with human habitation, hence 180 Pa is suitable for this sandbar, which is a lightly degraded sandbar. Conversely, A 3 sandbar (Figure 5.20) is a long stable sandbar with thick vegetation cover, therefore 240 Pa is ideal. But in this research, a constant τ_{crveg} 180 Pa (Table 6.7) was used as C-L doesn't have provision for applying separate τ_{crveg} value for different sandbars. With 0 and 1 yrs, grass maturity and 0.1 proportion of erosion that can occur when vegetation is fully grown as a default value (detail discussed in chapter 4) were used to run the C-L models.

Under such condition, the C-L models should generate more sediment deposition on the floodplains and sandbars and result in increased size and shape of the sandbars. However, the C-L models performed differently. Though the models have produced more deposition than erosion they fail to exhibit a similar trend of increase or decrease in the size of the sandbars like the Landsat images. This is because of the non-availability of cohesive grain size in the model which resulted in less deposition or erosion or vice versa than the actual one (Figure 5.21). This was proved from the bar deformation index. The BDI quantifies the change in the size of the sandbars in percentage. Taking the size of A 1, A 2 and A 3 for the year 1987 as 100% (i.e.) the reference size of the sandbars (Table 3.4), BDI values were calculated from the hindcasted models. The figure 5.21 compares the observed BDI of sandbars A 1 O, A 2 O and A 3 O with the model BDI of model 3 and 4. From the figure 5.21, it can be demonstrated that BDI of model No 3 (M_3) and 4 (M_4) exhibits a similar pattern in sandbar reshaping; correspondingly other models demonstrating the similar pattern in sandbar formation. However, the C-L models were not able to reproduce appropriate shape and size of a sandbar in a coarse resolution of 100 m when compared with sandbars of Landsat images. The BDI of other C-L models are attached in the appendix 3.

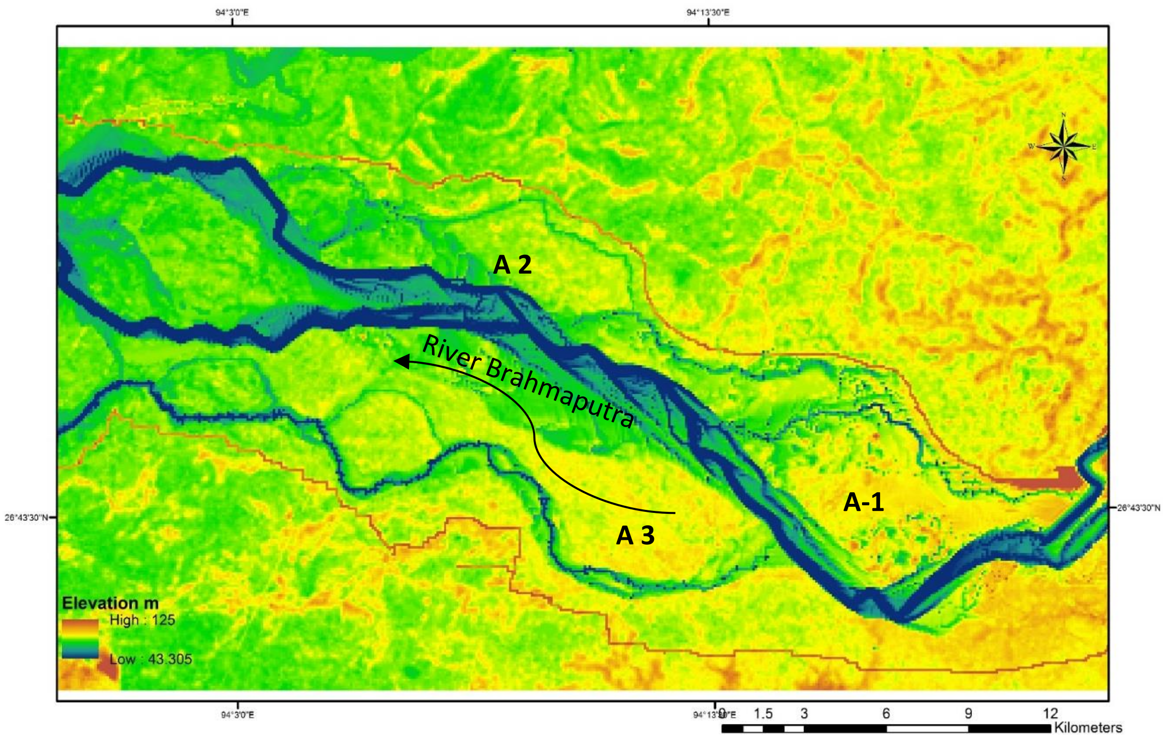

Figure 5.20: Braid bars A1, A 2 and A 3 model no 3, 2015.

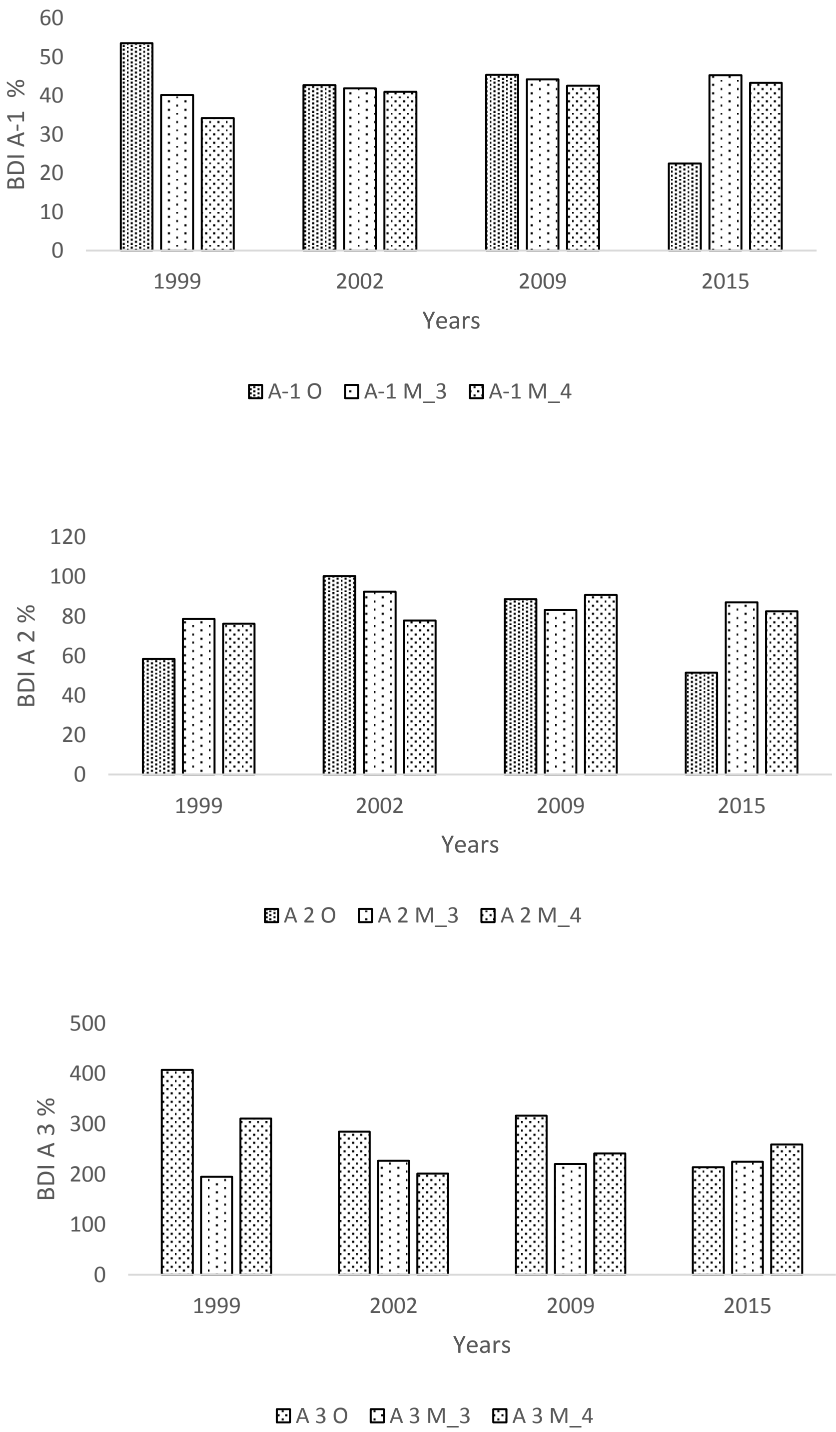

Figure 5.21: Bar Deformation of A 1, A 2 and A 3**.**

6.9. Cross-section and longitudinal profile evaluation

As described in chapter 2 the Water Resource Department (Govt. of Assam, India) has surveyed 65 cross-sections (see Figure 1.14) on the River Brahmaputra in Assam. Cross-sections within the study reach are C.S. 45 to C.S. 58, which were surveyed during 1988, 1992, 1998 and 2007. At C.S. 49, 48 and 47 the main channel was narrow and shallow in 1988 and 1998, while in 2007 C.S. 48 and 47 the main channel was split into two large, second-order channels, one adjacent to the north bank and the other one in the middle along with a number of small channels that sprang up in the area (detail in Chapter 2). One of the small channel adjacent to the south bank emerged as an anastomosing river which remains the same in the C.S 48, 47, 46 and 45 in the year 1998 and 2007. Since 2007 no cross-sectional surveys have been conducted by the Water Resource Department, Government of Assam. Due to non-availability of cross-section data after 2007, the C-L models cannot be validated for the subsequent years. Hence, in this research, the 1998 cross-section data were used as the base year to assess how the channel cross-section changed up to 2007. In this process, all the model cross-section data (C.S. 49, 48 and 47) of 2007 were compared with the 2007 observed data for the same cross-sections. These are the only cross-sections which fall within the 40 km study reach.

As described in Chapter 4 there is lack of availability of high-resolution DEM for the river. Hence, in this research, SRTM, 90 m resolution and cross-section data were used to derive the bathymetry using the geo-statistical wizard in ArcGIS. It is difficult to develop detailed cross-sections from a ~100 m resolution DEM. However, in comparing observed and modelled cross-sections, if the model was able to reproduce a similar shape of cross-section and pattern of change, it was taken to be a reasonably good fit. Evaluation of the C-L models for the C.S. data was undertaken using Mean Absolute Error (MAE) and Mean Absolute Relative Error (MARE).

6.9.1. Mean absolute error (MAE)

Mean Absolute Error (MAE) is an absolute error. This metric records in real units between the observed and modelled datasets. It is a non-negative metric that has no upper bound. For a perfect model, the value of MAE is zero. MAE provides no information about under-estimation or over-estimation.

MAE is equivalent to the Total Sum of Absolute Residuals (TSAR) (Stephenson, 1979) that was suggested for the comparison of single event models in a major review of evaluation criteria that was conducted by Green and Stephenson (1986) and thereafter endorsed by ASCE (1993). It is not weighted towards higher magnitude or lower magnitude events but instead evaluates all deviations from the observed values, in both an equal manner and regardless of sign.

$$\text{MAE}=\frac{1}{n}\sum_{i=1}^{n}\left|Qi-\hat{Q}i\right|$$

where, Qi = observed (i.e. expected) value, $\widehat{Qi}$ = modelled (i.e. forecast) value where i = 1 to n data points.

6.9.2. Mean absolute relative error (MARE)

Mean Absolute Relative Error (MARE) is a relative error. This metric encompasses the mean of the absolute error made relative to the observed record. It has also been termed ‘‘Relative Mean Error’’ (RME) (Khalil et al., 2001), ‘‘Mean Relative Error’’ (Karunanithi et al., 1994; Elshorbagy et al., 2000; Teegavarapu and Elshorbagy, 2005). It is a non-negative metric that has no upper bound. For a perfect model, the MARE value is zero. This metric records as a ratio between the observed and modelled datasets.

MARE is a relative metric which is sensitive to the forecasting errors that occur in the lower magnitudes of each dataset. Here the errors are not squared, the evaluation metric is less sensitive to the larger errors that usually occur at higher magnitudes.

The principal difference between RAE and MARE is that the later measurement is expressed in units that are relative to the observed record, as opposed to units that are relative to variation about the mean of the observed record. This could be challenging to understand in an operating or decision-making context (Makridakis, 1993).

$$\text{MARE}=\frac{1}{n}\sum_{i=1}^{n}\frac{|Qi-\widehat{Qi}|}{Qi}$$

where Qi = observed (i.e. expected) value, $\widehat{Qi}$ = modelled (i.e. forecast) value where i = 1 to n data points.

These absolute and relative error terms were used to measure the discrepancies in elevation between the observed and the modelled cross-sections (Table 6.8). In figure (5.22...5.24) observed C.S. 49, 48 and 47 (1998, 2007) are plotted against modelled cross-sections generated by C-L models 3 and 4. C-L model 3 is the best fit for the three cross-sections, followed by model 4, which was also able to represent the three cross-sections with fewer inconsistencies than those in the other C-L models. The cross-sections of rest of the C-L models are exhibited in appendix 4.

The fit of long-profiles through the study reach are plotted in figure 5.25. The observed longitudinal profiles for 1998 and 2007 are plotted and compared with the modelled longitudinal profile of C-L models 3 and 4. The observed long-profiles illustrate that initially, the reach was more degrading than aggrading although, in 2007 the river in the study reach started to aggrade. Both C-L models 3 and 4 were able to replicate the aggrading behaviour of the river Brahmaputra in the study reach that began in 2007. The process of aggradation led to the reach becoming moderately to highly braided.

Table 6.8: Performance Metrics of cross-sections (change in elevation) C.S. 49, 48 and 47 in 2007.

		Model 1	Model 2	Model 3	Model 4	Model 5	Model 6	Model 7	Model 8	Model 9	Model 10
CS_49	MARE in m	0.036592	0.060501	0.026162	0.030039	0.045843	0.049264	0.087409	0.083802	0.083024	0.088807
	MAE in m	2.879789	4.815654	2.087678	2.366433	3.547782	3.938417	7.104106	6.853093	6.64742	7.181731

		Model 1	Model 2	Model 3	Model 4	Model 5	Model 6	Model 7	Model 8	Model 9	Model 10
CS_48	MARE in m	0.049346	0.049554	0.039246	0.038884	0.049125	0.054363	0.06353	0.062226	0.061522	0.064218
	MAE in m	3.989765	3.977406	3.180654	3.132951	3.947035	4.340896	5.04999	4.951467	4.89166	5.095994

		Model 1	Model 2	Model 3	Model 4	Model 5	Model 6	Model 7	Model 8	Model 9	Model 10
CS_47	MARE in m	0.038333	0.051786	0.03011	0.033356	0.073656	0.044787	0.068199	0.065253	0.054826	0.076626
	MAE in m	3.135555	4.273163	2.47315	2.740029	6.061858	3.688042	5.616669	5.368662	4.429968	6.336175

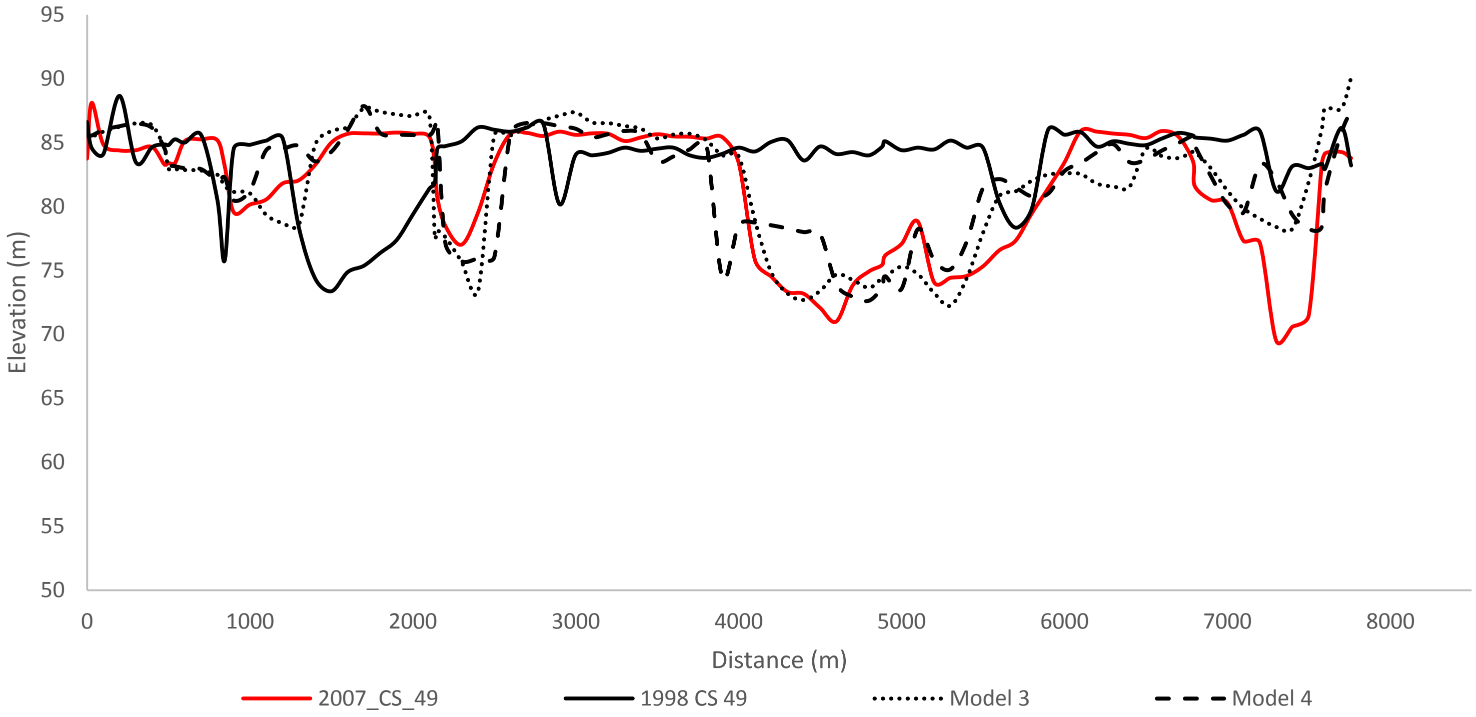

Figure 5.22: Modelled and Observed cross-section 49 (1998 and 2007).

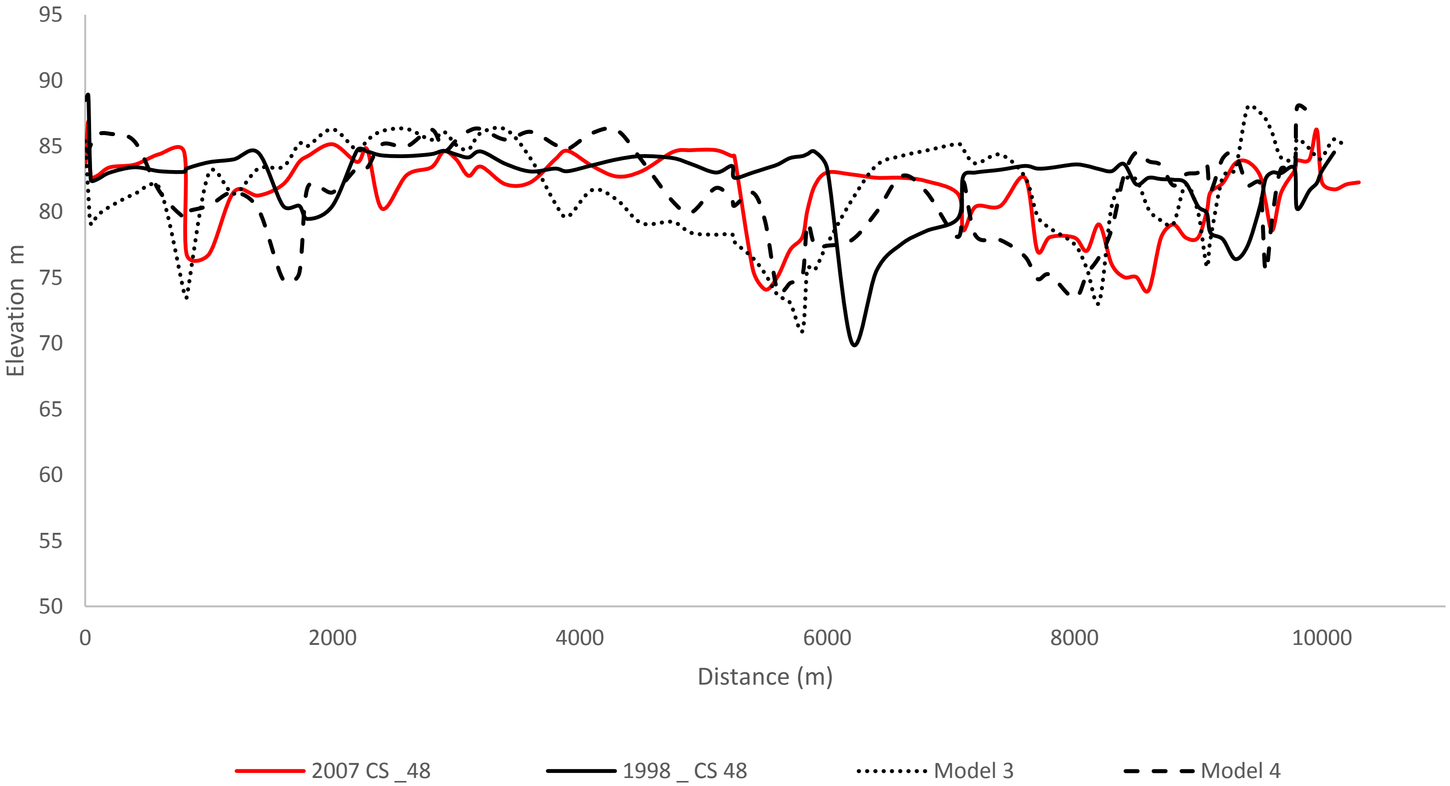

Figure 5.23: Modelled and Observed cross-section 48 (1998 and 2007).

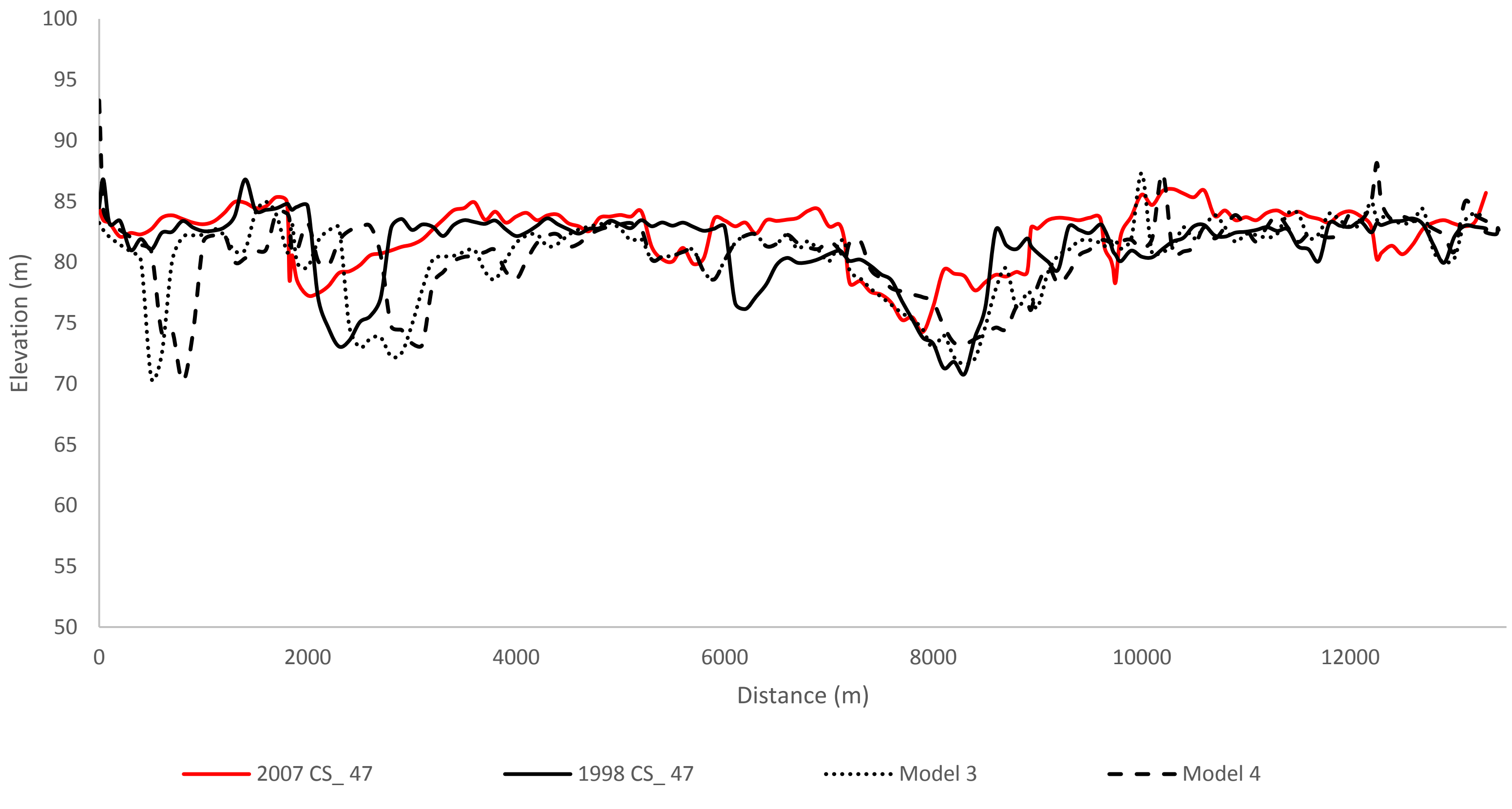

Figure 5.24: Modelled and Observed cross-section 47 (1998 and 2007).

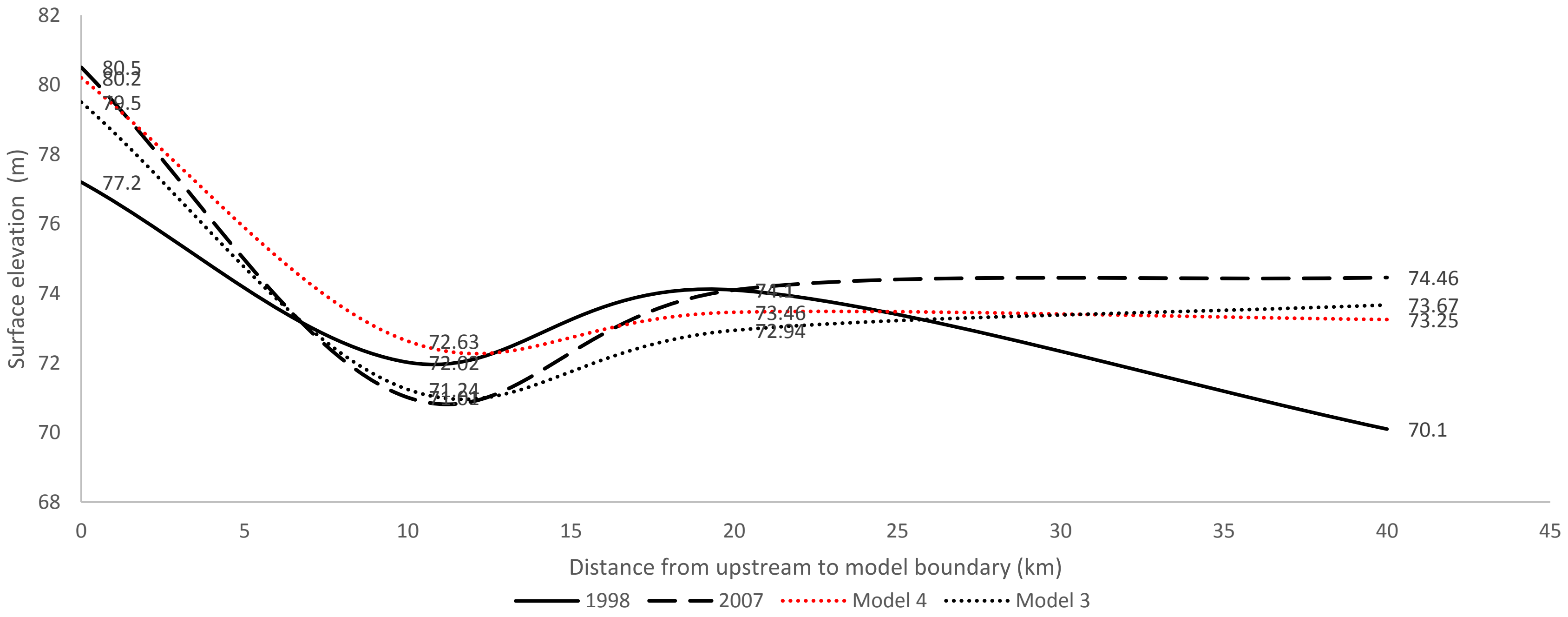

Figure 5.25: Thalweg channel longitudinal profile of river Brahmaputra near Majuli Island, 1998 (observed) 2007 and Model No 3 (2007) and Model No 4 (2007).

6.10. C-L model ranking process and selection of the best fit

The six braiding indices and two statistical measures were used to evaluate the performance of the 10 C-L hindcasting models, provide the basis to identify the best fit C-L model which will be used to forecast medium-term channel evolution in the study reach of the river Brahmaputra near Majuli Island. To achieve this, an Analytic Hierarchy Process (AHP) model was used to rank the 10 C-L models (Figure 5.26). AHP is a method of measurement using a ratio scale. It is used to develop ratio scales from both discrete and continuous, paired comparisons. These comparisons may be taken from actual measurements or from a fundamental scale (Table 6.9) which reflects the relative strength of preferences and feelings (Satty, 1987, Akhtar et al.,2011).

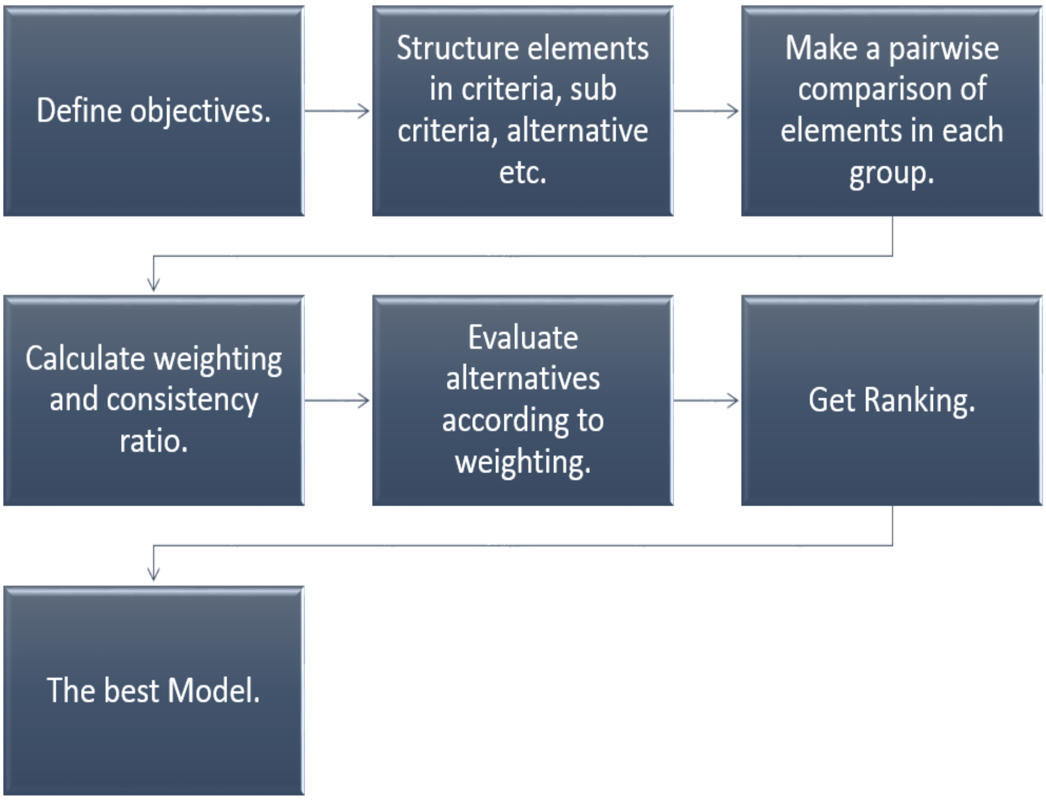

Figure 5.26: Analytic Hierarchy Process (AHP) model structure

Figure 5.27 Analytical Hierarchy Process

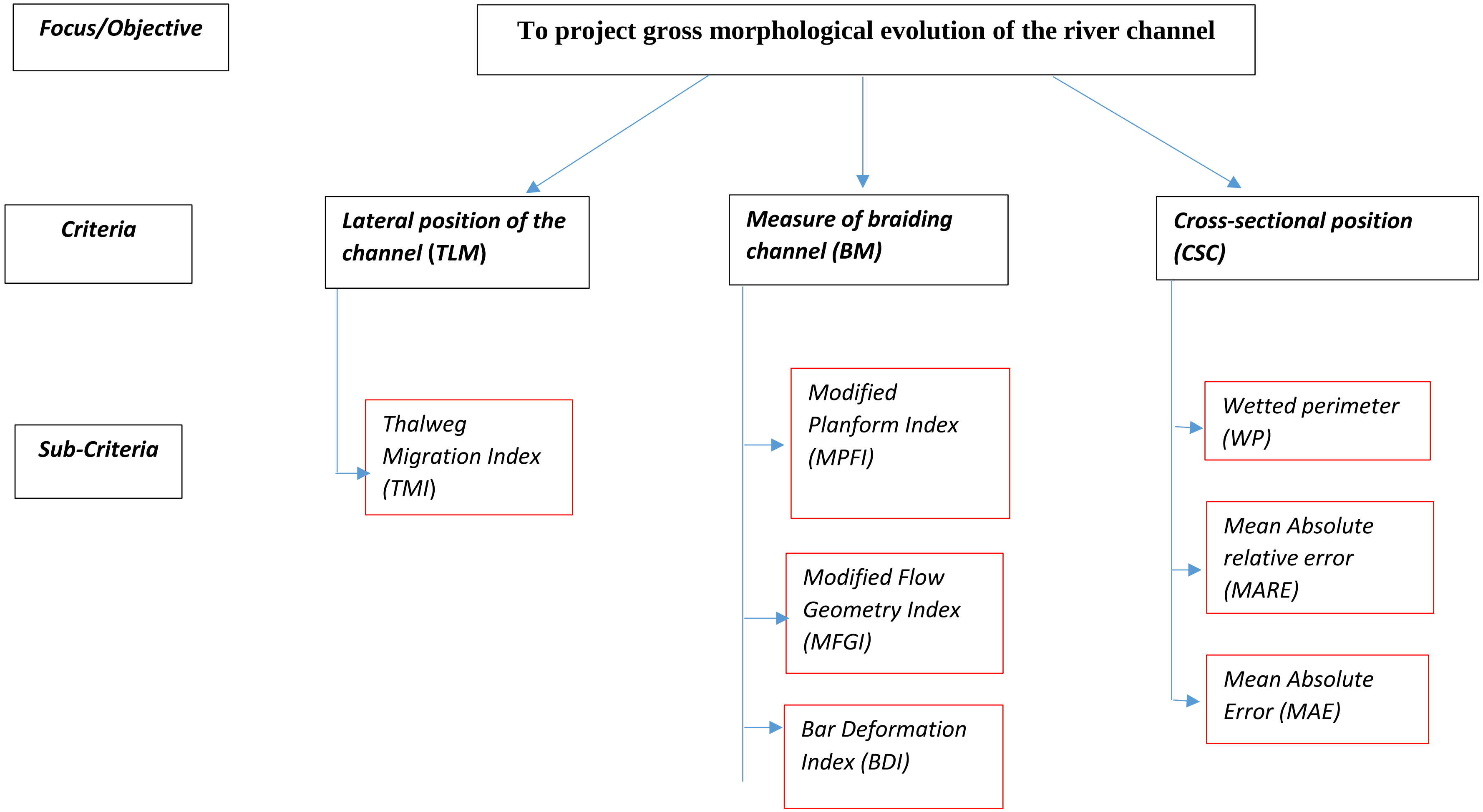

Table 6.9: The intensity of importance on an absolute scale. Source: (Saaty, 1994.)

The intensity of importance on an absolute scale	**Definition**	**Explanation**
1	Equal importance	Two activities contribute equally to the objectives
3	Moderate importance of one over another	Experience and judgment strongly favour one activity over another
5	Essential or strong importance	Experience and judgment strongly favour one activity over another
7	Very strong importance	An activity is strongly favoured and its dominance demonstrated in practice
9	Extreme importance	The evidence favouring one activity over another is of the highest possible order of affirmation
2, 4, 6, 8	Intermediate values between the two adjacent judgements	When compromise is needed
Reciprocals	If activity *i* has one of the above numbers assigned to it when compared with activity *j*, then *j* has the reciprocal value when compared with *i*	
Rationals	Ratios arising from the scale	If consistency were to be forced by obtaining n numerical values to span the matrix

Table 6.8: Random consistency index (RI).

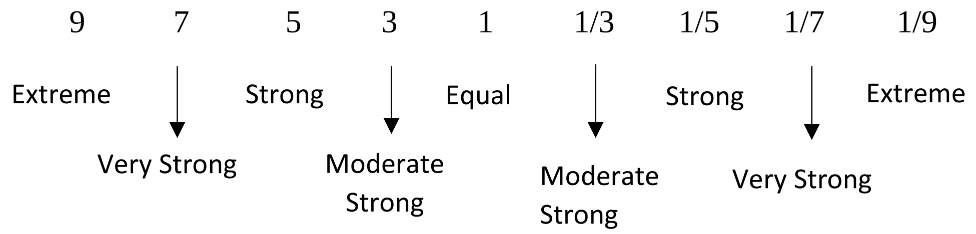

n	**1**	**2**	**3**	**4**	**5**	**6**	**7**	**8**	**9**	**10**
Random Consistency index (R.I.)	0	0	0.58	0.9	1.12	1.24	1.32	1.41	1.45	1.49

The comparison is made of simple pair-wise judgement between two elements or criteria, to define how many times more important one element is compared with another (Saaty, 1996, Vargas, 1990). The judgment is made in a square matrix (Saaty, 1994).

To model a problem using the AHP, a hierarchic or a network structure is needed to represent the problem and pairwise comparisons to establish relations with the structure. In the AHP model one has to have an objective or focus and or the problem. To identify the best-fit one has to divide the elements into criteria, sub-criteria and alternatives based on their priorities (Figure 5.27).

The aim of this research was to hindcast and forecast the overall, morphological evolution of the river Brahmaputra at Majuli Island. The AHP model for this research was therefore based on three criteria and 7 sub-criteria matrices. The criteria for this exercise were:

1. the lateral migration of the thalweg channel (TLM),
2. the braiding intensity (BM) and,
3. the cross-sectional position (CSC).

The sub-criteria were:

a. thalweg migration index (TMI),
b. Modified Plan Form Index (MPFI),
c. Modified Flow Geometry Index (MFGI),
d. Bar Deformation Index (BDI),
e. Wetted perimeter (WP),
f. Mean Absolute Relative Error (MARE) and,
g. Mean Absolute Error (MAE)

Justification of weight or preference

Criteria: (Table 6.11)

A. Thalweg Migration (or the lateral channel stability plays a major role in reach-scale planform change. Weight = 7 (very strong importance).

B. Braiding Indices were able to demonstrate the level of braiding in the study reach, which indicates within channel morphology. Weight = 5 (high importance).

C. Cross-section change affects local geometry and dimensions of main and secondary channels. Weight = 3 (moderate importance).

A is equally important to A – 1

B is important but moderately important than A.

C is the less important than A & B

A has been demonstrated to be more important than B and C.

Sub Criteria:

Thalweg Migration Index (TMI):

1. TMI is the most important criteria in this AHP model. This is because in planform change as it is able to showcase the behavioural change of the thalweg channel. TMI is included in this ranking process as it indirectly plays a significant role in planform change.

Local Scale Planform Change:

1. Modified Planform Index (MPFI): MPFI is important as it is able to demonstrate the planform change occurred in the sub reach.

2. Modified Flow Geometry Index (MFGI): MFGI is moderately important as it is able to demonstrate the cross-sectional change in terms of a threshold value. MFGI also consider the sub-channels changes occurred in the cross-section.

3. Bar Deformation Index (BDI): BDI is least important as it focuses on the change in the size of the sandbar in the sub reach which also represents the planform change in the respective of sub –reach.

Cross-sectional Change:

1. Wetted Perimeter (WP): The most important as it is able to demonstrate the cross-sectional area.

2. Mean absolute relative error (MARE): Moderately important as it involves the mean of the error made relative to the observed record (TIM Meadow, 2014).

3. Mean Absolute Error (MAE): Less important (It is not weighted towards higher magnitude or lower magnitude events, but instead assesses all deviations from the observed values, regardless of sign).

Table 6.11: Pairwise comparison matrix and calculated weights for each criterion and sub-criteria.

Criteria

	TLM	BM	CSC		Consistency Vector	CI	RI	Consistent
TLM	1	5	7		3.13	0.027311	0.58	**Yes**
B M	0.2	1	3		3.02			**As it is less than 1**
CSC	0.14	0.33	1		3.00		**If CI is closer to RI then less trustworthy the preferences are**	
Sum	1.34	6.33	11		9.16			
				Av. Consistency	3.05			

Normalised Criteria

	TLM	BM	CSC	Total	Average (W)	Score	Rank
TLM	0.74	0.78	0.63	2.17	0.72	72%	**1**
B M	0.14	0.15	0.27	0.57	0.19	19%	**2**
CSC	0.10	0.05	0.09	0.24	0.08	8%	**3**
sum	**1**	**1**	**1**		1		

Normalised sub-criteria

Thalweg Lateral Migration		
	TMI	Total
TMI	1	1
Sum	1	

Braiding Index			
	MPFI	MFGI	BDI
MPFI	0.65	0.77	0.50
MFGI	0.13	0.15	0.33
BDI	0.22	0.08	0.17
Sum	1	1	1

Cross-section			
	W.P	MARE	MAE
W.P	0.55	0.69	0.33
MARE	0.18	0.23	0.50
MAE	0.27	0.08	0.17
Sum	1	1	1

Score of sub-criteria

TMI	72%
MPFI	12.16%
MFGI	3.99%
BDI	2.85%
WP	0.80%
MARE	0.48%
MAE	0.24%

Table 6.12: Evaluations values of all the evaluations sub-criteria.

	TMI	MPFI 1	MPFI 2	MFGI 49	MFGI 48	MFGI 47	BDI A 1	BDI A 3	BDI A 2	WP 49	WP 48	WP 47	MARE 49	MARE 48	MARE 47	MAE 49	MAE 48	MAE 47
MODEL 1	1.4426	10.95	14.23	8.09	10.19	18.85	50.12	230.45	77.36	3751.98	3863.73	4650.76	0.036	0.049	0.038	2.879	3.98	3.13
MODEL 2	1.2341	19.62	13.73	8.53	12	16.59	42.19	234.25	91.39	4101.76	3925.31	4571.38	0.06	0.049	0.051	4.81	3.97	4.27
MODEL 3	1.1747	7.6	7.26	8.87	9.29	10.77	45.37	224.76	87.06	3509.37	1752.84	4043.54	0.026	0.039	0.03	2.08	3.18	2.47
MODEL 4	1.3842	8.43	7.78	9.4	9.99	10.84	43.32	259.14	82.63	3045.73	1854.12	3910.91	0.03	0.038	0.033	2.36	3.13	2.74
MODEL 5	1.2969	9.56	7.83	11.02	10.9	12.11	51.25	248.57	94.35	3654.03	3626.41	5003.14	0.045	0.049	0.073	3.54	3.94	6.06
MODEL 6	1.4812	9.29	6.75	11.41	10.31	14.19	52.38	259.22	96.27	5008.41	3792.53	4462.17	0.049	0.054	0.044	3.93	4.34	3.68
MODEL 7	1.4876	19.33	13.67	5.15	3.64	5.00	47.55	271.78	87.83	3147.74	3805.03	4462.17	0.087	0.063	0.068	7.104	5.04	5.61
MODEL 8	0.95	19.42	16.18	5.65	3.56	2.65	46.46	271.86	96	3030.18	4103.01	4344.6	0.0838	0.062	0.065	6.853	4.95	5.36
MODEL 9	0.88	29.08	34.79	8.68	7.67	5.13	45.48	262.9	85.69	2475.54	4409.33	3945.25	0.083	0.061	0.054	6.64	4.89	4.42
MODEL 10	0.9	27.45	29.11	4.94	9.53	13.59	34.8	226.85	75.17	2112.14	5500.41	6145.977	0.0888	0.064	0.076	7.18	5.09	6.33
	12.231	160.73	151.33	81.74	87.08	109.72	458.92	2489.78	873.75	33836.9	36632.72	45539.9	0.5886	0.528	0.532	47.376	42.51	44.07

Table 6.13: Normalised evaluations values of all the evaluations sub-criteria.

	TMI	MPFI 1	MPFI 2	MFGI 49	MFGI 48	MFGI 47	BDI A1	BDI A 3	BDI A 2	WP 49	WP 48	WP 47	MARE 49	MARE 48	MARE 47	MAE 49	MAE 48	MAE 47
MODEL 1	0.12	0.25	0.35	0.10	0.12	0.16	0.06	0.27	0.09	0.11	0.10	0.10	0.06	0.09	0.07	0.06	0.09	0.07
MODEL 2	0.10	0.44	0.34	0.10	0.14	0.14	0.05	0.27	0.11	0.12	0.10	0.10	0.10	0.09	0.10	0.10	0.09	0.10
MODEL 3	0.13	0.17	0.18	0.11	0.11	0.09	0.05	0.26	0.10	0.10	0.05	0.09	0.04	0.07	0.06	0.04	0.07	0.06
MODEL 4	0.15	0.19	0.19	0.11	0.11	0.09	0.05	0.30	0.10	0.09	0.05	0.09	0.05	0.07	0.06	0.05	0.07	0.06
MODEL 5	0.14	0.22	0.19	0.13	0.13	0.11	0.06	0.29	0.11	0.11	0.09	0.11	0.08	0.09	0.14	0.07	0.09	0.14
MODEL 6	0.16	0.21	0.17	0.14	0.12	0.12	0.06	0.30	0.11	0.15	0.10	0.10	0.08	0.10	0.08	0.08	0.10	0.08
MODEL 7	0.16	0.44	0.34	0.06	0.04	0.04	0.05	0.32	0.10	0.09	0.10	0.10	0.15	0.12	0.13	0.15	0.12	0.13
MODEL 8	0.11	0.44	0.40	0.07	0.04	0.02	0.05	0.32	0.11	0.09	0.11	0.09	0.14	0.12	0.12	0.14	0.12	0.12
MODEL 9	0.10	0.66	0.85	0.11	0.09	0.04	0.05	0.31	0.10	0.07	0.12	0.09	0.14	0.12	0.10	0.14	0.12	0.10
MODEL 10	0.10	0.62	0.71	0.06	0.11	0.12	0.04	0.27	0.09	0.06	0.14	0.13	0.15	0.12	0.14	0.15	0.12	0.14

Table 6.14: Ranking of 10 calibrated models using AHP model.

	TMI	MPFI 1	MPFI 2	MFGI 49	MFGI 48	MFGI 47	BDI A 1	BDI A 3	BDI A 2	WP 49	WP 48	WP 47	MARE 49	MARE 48	MARE 47	MAE 49	MAE 48	MAE 47	Total	Rank
MODEL 1	8.49	3.02	4.24	0.39	0.47	0.66	0.16	0.77	0.26	0.09	0.29	0.08	0.03	0.04	0.03	0.01	0.02	0.02	19.08	4
MODEL 2	7.26	5.41	4.09	0.42	0.55	0.58	0.13	0.78	0.31	0.10	0.29	0.08	0.05	0.04	0.05	0.02	0.02	0.02	20.21	6
MODEL 3	9.36	2.09	2.16	0.43	0.43	0.37	0.14	0.75	0.29	0.08	0.13	0.07	0.02	0.04	0.03	0.01	0.02	0.01	**16.44**	**1**
MODEL 4	11.02	2.32	2.32	0.46	0.46	0.38	0.14	0.86	0.28	0.07	0.14	0.07	0.02	0.03	0.03	0.01	0.02	0.01	**18.65**	**2**
MODEL 5	10.33	2.63	2.33	0.54	0.50	0.42	0.16	0.83	0.32	0.09	0.27	0.09	0.04	0.04	0.07	0.02	0.02	0.03	18.73	3
MODEL 6	11.80	2.56	2.01	0.56	0.47	0.49	0.17	0.86	0.32	0.12	0.28	0.08	0.04	0.05	0.04	0.02	0.02	0.02	19.92	5
MODEL 7	11.85	5.33	4.07	0.25	0.17	0.17	0.15	0.91	0.30	0.08	0.28	0.08	0.07	0.06	0.06	0.04	0.03	0.03	23.92	8
MODEL 8	7.57	5.35	4.82	0.28	0.16	0.09	0.15	0.91	0.32	0.07	0.31	0.08	0.07	0.06	0.06	0.03	0.03	0.03	20.38	7
MODEL 9	7.01	8.01	10.37	0.42	0.35	0.18	0.14	0.88	0.29	0.06	0.33	0.07	0.07	0.06	0.05	0.03	0.03	0.02	28.37	10
MODEL 10	7.17	7.57	8.68	0.24	0.44	0.47	0.11	0.76	0.25	0.05	0.41	0.11	0.07	0.06	0.07	0.04	0.03	0.03	26.55	9

Subsequently comparing all the elements of criteria and sub-criteria pairwise with respect to the objectives or opinion. Then arrange the elements into the matrix and compute the normalised principle Eigenvector of the matrix (Table 6.11).

The matrix N for 3 criteria.

$$N = \begin{matrix} 1 & a_{12} & a_{13} \\ a_{12}^{-1} & 1 & a_{23} \\ a_{13}^{-1} & a_{23}^{-1} & 1 \end{matrix}$$

Sum of columns Sc_1, Sc_2, and Sc3.

Normalised and calculated first normalised principle Eigen Vector (X).

$$X = \begin{matrix} \frac{1}{S_{c1}} & \frac{a_{12}}{S_{c2}} & \frac{a_{13}}{S_{c3}} \\ \frac{a_{12}^{-1}}{S_{c1}} & \frac{1}{S_{c2}} & \frac{a_{23}}{S_{c3}} \\ \frac{a_{13}^{-1}}{S_{c1}} & \frac{a_{23}^{-1}}{S_{c2}} & \frac{1}{S_{c3}} \end{matrix} \quad X_i = \begin{matrix} \sum \frac{row_1}{n} \\ \sum \frac{row_2}{n} \\ \sum \frac{row_3}{n} \end{matrix}$$

Consequently, calculate the largest Eigen Vector (λ) of the matrix and Consistency Vector of the matrix. Consistency Vector is required to calculate the Consistency Index (C.I). Consistency Index is verified using Random Index. If C.I is closer to R.I then the less trustworthy are the preferences.

$$\lambda = S_{c1}X_1 + S_{c2}X_2 + S_{c3}X_3$$

$$C.I = \frac{\lambda - n}{n-1}$$

In this AHP model C.I is 0.027 and R.I is 0.58, which indicates the preferences selected were consistent and trustworthy (Table 6.10). The value of the evaluation criteria were normalised and were multiplied by the score of the sub-criteria (Table 6.12. 6.13). Subsequently the models were ranked based on the outcome of AHP model. From the outcome of the AHP, C-L models 3 and 4 achieved the best and second best performances (Table 6.14). Model 3 was an unsteady, non-uniform flow model. Model 4 was an unsteady, uniform flow model. On the basis of these findings, it was decided to use C-L models 3 to forecast the morphological evolution of the channel in the study reach of the River Brahmaputra near Majuli Island for next 20 years.

Conclusion:

This chapter summaries C-L models operation and their outputs in modelling the landscape evolution of the river Brahmaputra near Majuli Island. The method knows as blind testing was used in this research to calibrate 10 C-L models to hindcast the channel morphological change of the river Brahmaputra. In this method, a small number of calibrations are applied to final bounds of parameter values based on expert judgment, values known from the relevant literature and field measurements (Bathurst et al., 2004).

For validating the C-L models newly developed braiding indices were used. The Analytic Hierarchy Process was used in this research to quantify and rank the performance of each model in producing outcomes that matched observed parameters of morphological change. The AHP established that C-L models 3 and 4 performed the best, according to the blind testing approach to calibration adopted in this study, with C-L model 3 slightly performed better than model 4.

This chapter demonstrates that the model C-L model no 3 parameter combination was best able to hindcast the morphological behaviour of the River Brahmaputra in the study reach. This model combination was able to generate the major morphological changes in the channel such as lateral shifting of the thalweg channel and planform changes which was observed in the Landsat images.

Chapter 7: Morphological Forecasting

7.1. Introduction

This chapter concerns forecasting future evolution and change in the study reach. Using model no 3 as the best fit model hydrological models were used to model medium term channel evolution of the river Brahmaputra near Majuli Island. The primary inputs needed to run the models in forecasting mode are estimates of the discharges of water and sediment that will enter the study reach from upstream. Hence, the first step in setting up the models was to obtain future water and sediment hydrographs from the global hydrological models. The global hydrological models were part of ISIMIP Fast track data. Applying these data a medium term (20 years) channel evolution C-L model were run for the river Brahmaputra near south Majuli Island. This chapter also describes about the forecasting trends of planform change and the thalweg migration by the application of the newly developed braided indices.

7.2. Forecasting programme design

One-dimensional (1D) flow models are insufficient to tackle problems of braided streams due to lack of information with regard to transverse flow field. Hence, for better and more realistic flow field assessment, two-dimensional (2D) or three dimensional (3D) numerical models are to be used. 3D models are too numerically expensive for macro scale river reaches. Hence 2D enhanced model should be used for such macro-scale reach for a realistic hydrological modelling. There is an increasing demand for understanding, predicting and controlling large braided rivers (Schuurman et al., 2018).

From ISIMIP Fast track data one LSM and one GHM models were selected. In a 100×100 m grid cell size eight 2D hydrological models were forecasted using the same parameters of hindcasted from the best-fit models (Model No 3). The daily discharge data have been taken from the one LSM (H08, JULES) and GHM (LPJmL, MacPDM) models (Table 7.2) for the year 2015 till 2035 and daily sediments discharge have been estimated using the same sediment rating curve used to estimate daily sediment discharge for hindcasting models (Chapter 4). The reason for using a matrix of 4 LSM/GHM x 1 C-L models was that the morphology of the Brahmaputra is transient and highly responsive to changes in the flow and sediment regimes – which are the drivers of morphological change. Using these four models in combination will provide a spectrum of forecasts for the future behaviour of the volatile river channel in the study reach, from which it should be possible to synthesise a reasonable range of possible morphological futures.

Morphological channel geometry is, by its very nature, a three-dimensional phenomenon and consideration of channel morphology and evolution in this study has considered changes in the planform, cross-sectional and long-profile planes. Nevertheless, it is changes in the bank lines of the Brahmaputra that pose the most immediate and serious risks to land, people and infrastructure on Majuli Island and at other locations adjacent to the great river.

At the reach-scale, bank retreat and advance in very large, braided rivers like the Brahmaputra are driven by the long-term development of island and nodal reaches, medium-term development and migration of bends in the near-bank anabranches, and growth, migration and destruction of braid bars; which involves processes which operate at relatively small spatial scales of 3 to 6 km and over shorter temporal scales 2 to 5 years (Colemen, 1969; Thorne et al., 1993; Mount et al., 2013).

Until recently, the poor availability and expense of high definition, remotely-sensed images needed to investigate rates and patterns of bank line migration along large rivers meant that bank line migration was poorly understood and almost impossible to forecast (Best and Bristow, 1993; Richardson, 1997). However, Mount et al., (2013) noted that, "At the present time due to the development and availability of remotely sensed technologies, coupled with widening accessibility to GIS, have led to the emergence of the remote sensing of rivers as a sub-discipline of fluvial geomorphology,".

Focusing on channel changes that generate bank line migration in the study reach, a time series of DEMs of the river during the low flow season (February - March) were extracted from the C-L forecasting model runs to investigate medium-term planform change, channel behaviour, bank retreat and bed incision. During low flow, channel morphology features are generally visible distinctly. DEMs were the C-L model outputs that demonstrate the change in channel during four intermediate periods: 2015-2020, 2020-2025, 2025-2030 and 2030-2035 at a 100 × 100m resolution (Table 7.1). These DEMs were used for calculating forecasting trends of the river Brahmaputra using braiding indices.

Table 7.1: Modelled images used to drive forecasted planform change, channel behaviour and sandbar formation and deformations.

Hydrological Models	Modell Image date acquired	Discharge Q in Bessamora $m3s^{-1}$
H08	15/03/2020 15/03/2025 15/02/2030 15/03/2035	965.763 1061.903 920.25 1040.837
JULES	15/03/2020 15/03/2025 15/03/2030 15/02/2035	1610.5 1680.188 2313.749 1036.686
LPJmL	15/03/2020 15/03/2025 15/03/2030 15/03/2035	1227.63 1065.17 1246.44 1067.72
MacPDM	01/03/2020 15/03/2025 16/03/2030 15/03/2035	5743.671 5555.087 5987.272 4778.421

Having forecast future trends of geomorphic change, the newly developed versions of the morphological indices that can be used to quantify complex fluvial and morpho-dynamic changes in braided rivers were applied to the model outputs. These indices (Chapter 3) represent key aspects of river channel change including thalweg channel migration, river planform pattern, flow geometry, and deformation of braid bars. Differencing of dems for the forecast channel at different times between 2015 and 2035 also allowed calculation of the net sediment balance, indicating whether morphological adjustments will in future be dominated by processes of deposition or scour. Assessment of values and trends of change in these indices, together with consideration of the balance between deposition and scour, will support evalaualtion of the degree to which the forecasts based on different models generate consistent or inconsistent forecast morphological patterns.

7.3. Selection of Global hydrological models (GHM) and Land surface models (LSM) for medium term forecasting.

Chapter 6 reported how ten C-L models were built and tested by hindcasting morphological behaviours and changes in a study reach of the River Brahmaputra near Majuli Island, Assam for a 17-year period (1998- 2014). This chapter reports how the best two C-L models (identified in Chapter 6) were used to forecast the morphological behaviour of the channel during a 20-year period (2015 – 2035). The intent is to forecast the broad morphological evolution of the River Brahmaputra near Majuli Island, and identify possible responses to the impacts of climate change on flow and sediment regimes of this very large, braided river. .

To represent future flow and sediment regimes, two Global Hydrological Models (GHMs) and two Land Surface Models (LSMs) were selected from those included in the Inter-Sectoral Impact Model Inter-comparison Project (ISI-MIP) Fast Track phase. These models were used to generate possible future hydrological and sediment inputs to the study reach during a 20-year period starting in 2015 and ending in 2035.

ISI-MIP has been developed by a coordination team at the Potsdam Institute for Climate Impact Research, working closely with modelling teams from water, biomass, agriculture, infrastructure and human impacts/health sectors. The principal objectives of the ISI-MIP Fast Track project relate to application of global climate models to predict the socio-economic impacts of climate change, by comparison to a future with a steady climate. The ISI-MIP fast-track also aims to quantify the uncertainty in the impacts of climate change, both across climate impact models and sectors, and for different levels of global warming.

ISIMIP input data are available on a 0.5^{o}x0.5^{o} lat-long grid. The ISI-MIP coordination team provides bias-corrected climate data from the GCMs participating in the CMIP5. These data cover the time period from 1950 to 2099 and future projections for all RCPs (RCP 2.63, RCP 4.5, RCP 6.0, RCP 8.5).

Climate change impact data for input to forecasting C-L models were acquired from ISI-MIP Fast Track data were acquired for the area around 26.92^{o} N latitude and 94.33° E longitude. The data are from future climate scenario HadGEM2_ES/RCP 8.5.

“RCP 8.5 combines assumptions about high population and relatively slow income growth with modest rates of technological change and energy demand and GHG emissions in absence of climate change policies” (Riahi et al., 2011). The scenario links to the pathway which comprises of highest greenhouse gas emission when compared with other RCPs (Fisher et al., 2007; IPCC, 2008). RCP 8.5 is the upper bound of the RCPs with a CO^2 concentration continuing to swiftly increase, reaching 940 ppm by 2100 (Figure 6.1).

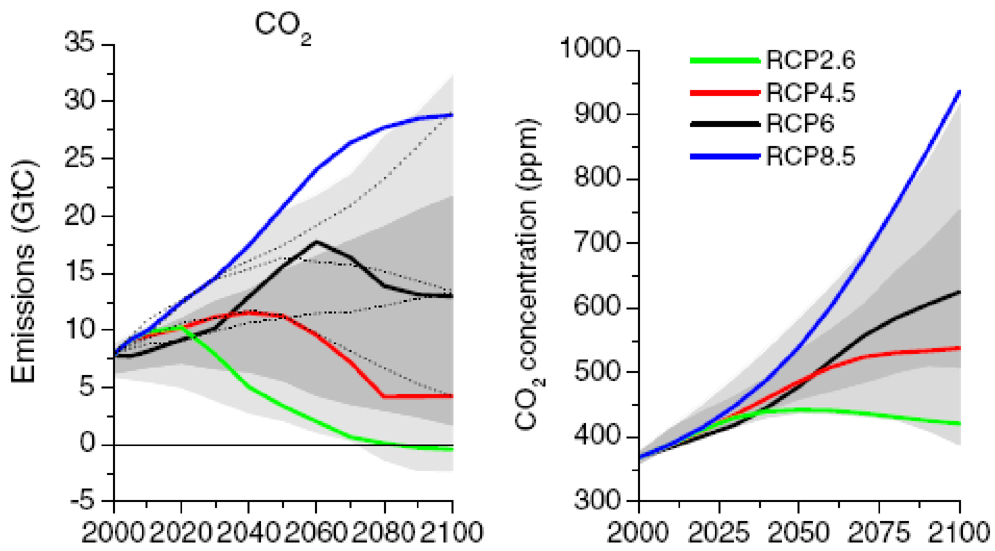

Fig 6.1. Emissions of CO_2 across the RCPs (left), and trends in concentrations of carbon dioxide (right). Grey area indicates the 98th and 90th percentiles (light/dark grey). SOURCE: Van Vuuren et. al. (2011)

“RCP 8.5 is a so-called ‘baseline’ scenario that does not include any specific climate mitigation target. The greenhouse gas emission and concentrations in this scenario increase considerably overtime, leading to a radiative forcing of 8.5 W/m^2 at the end of the century” (Riahi et al., 2011).

Under this scenario, the world would be 4^0C warmer by the end of the 21^{st}-century, and the probability of flooding is increased for 37% of the global land area. According to this scenario, there is expected to be a 24.5% increase in the magnitude of extreme high flows in rivers like the Brahmaputra (Asadisch and Krakauer, 2017).

34 models participated in ISI-MIP Fast Track. From them, models appropriate for providing hydrological inputs to the forecasting C-L+ models were selected for use in this research. The selected models are H08, JULES, which are Land Surface Models (LSMs), and LPJmL and MacPDM, which are Global Hydrological Models (GHMs) (Table 7.2) (Haddeland et al., 2011). The models are compared under naturalised conditions: i.e. human impacts such as storage in artificial reservoirs and agricultural water withdrawals are not included in the model runs. LSMs have been developed within the climate community and GHMs have been developed within the hydrologic community.

H08 and JULES use snow schemes based on a physically-based energy balance approach while LPJmL and MacPDM models are based on the conceptual degree-day approach. The models also use different snow energy balance approaches: for example number of snow layers, snow albedo values and how much liquid water can be retained within the snowpack. In the Himalayan region, snow accumulates over the years in several models, which contributes to the model differences. The model simulating the lowest Snow Water Equivalent (SWE) numbers is H08, which uses a relatively simple, one-layer snow scheme and fairly low snow albedo values. In H08, snow albedo varies between 0.6 and 0.45, whereas several other models use snow albedo values up to 0.8. This leads to increased net radiation at the snow surface compared to many other models (Haddeland et al., 2011).

The understanding of how the models perform differently for naturalised conditions and how current climate provides important information to understand why some models might respond differently in future runs using climate projections is very important in hydrological research. The four models used in this research to forecast medium-term landscape evolution of river Brahmaputra have different flow regime. MacPDM forecasted for relatively higher runoff compared to other models (Figure 6.3 b). Similarly, LPJmL forecasted high runoff during peak flow season (May- September) but during the dry season the flow is relatively low (900- 1200 m^3s^{-1}) (figure 6.2 b). On the other hand, H08 forecasted relatively high runoff value during the fall season (Sep- Nov) but during the dry season the flow is low (400- 1400 m^3s^{-1}) (figure

6.2 a). JULES is another model which forecasted higher runoff during the dry season (1650 – 2500 m^3s^{-1}) (Figure 6.3 a) (Haddeland et al., 2011).

In the Brahmaputra Basin, cloudiness during the Indian monsoon reduces incoming solar radiation and generates high humidity. The effect is to limit terrestrial water loss to evapotranspiration. Models using the Thornthwaite evaporation equation are unable to simulate these effects because that method relies solely on air temperature only to calculate potential evapotranspiration, therefore, actual evapotranspiration can be substantially lower than that predicted using the Thornthwaite method. Models using the Penman-Monteith or Priestly-Taylor methods are therefore better for the Brahmaputra Basin because in these models it is the incoming shortwave radiation or humidity that limits evapotranspiration (Haddeland et al., 2010).

As all the simulations were based on naturalised conditions, the effects of dams and water withdrawals are not taken into consideration. Consequently, these models tend to overestimate runoff in basins with large or multiple dams and extensive irrigation. However, in the Brahmaputra Basin, there are (at least as yet) no mega-dams (Figure 6.4) and agriculture in the region is not heavily dependent on water withdrawal from the River Brahmaputra. In fact, Assam is rich in abundant rainfall there is little pressure on the water resources provided by the River Brahmaputra. Hence, using LSMs and GHMs models that ignore anthropogenic water use will not overestimate runoff from the upper basin that inputs discharge to the study reach in Assam. This research attempts to apply these flow and sediment models to generate the inputs of water and sediment needed to run the C-L model and then use the best C-L models identified in Chapter 6 to forecast trends and patterns of evolution and change in channel morphology in the study reach.

Table 7.2. LMS and GHM Models including their main characteristics. (Source: Haddeland et al., 2010).

Model name	**Model Time Step**	**Meteorological forcing variable**	**Energy Balance**	**ET Scheme**	**Runoff Scheme**	**Snow Scheme**	**Reference**
H08	6 hrs	*R, S, T, W, Q, LW, SW, SP*	No	Bulk formula	Saturation excess/ beta function	Energy Balance	Hanasaki et al. 2008a
JULES	1 hr	*R, S, T, W, Q, LW, SW, SP*	Yes	Penman-Monteith	Infiltration excess/ Darcy	Energy Balance	Cox et al. 1999
LPJmL	Daily	P, T, LW_{net}, SW	No	Priestley Taylor	Saturation excess	Degree Day	Bondeau et al. 2007; Rost et al. 2008
MacPDM	Daily	P, T, W, Q, $\mathrm{LW_{net}}$, SW	No	Penman-Monteith	Saturation excess/ beta function	Degree Day	Arnell 1999; Gosling and Arnell 2010

The bold letters models are Land Surface Models (LSMs) and the other two are Global Hydrological Models (GHMs). R = rainfall rates; S= snowfall rate; P = precipitation (rain or snow distinguished in the model); T = air temperature; W= wind speed; Q = specific humidity; LW = longwave radiation flux (downward); $\mathrm{LW_{net}}$ = longwave radiation flux (net); SW = shortwave radiation flux (downward); and SP = surface pressure.

Bulk formula: Bulk transfer coefficient is used when calculating the turbulent heat fluxes.

Beta function: Runoff is a nonlinear function of soil moisture

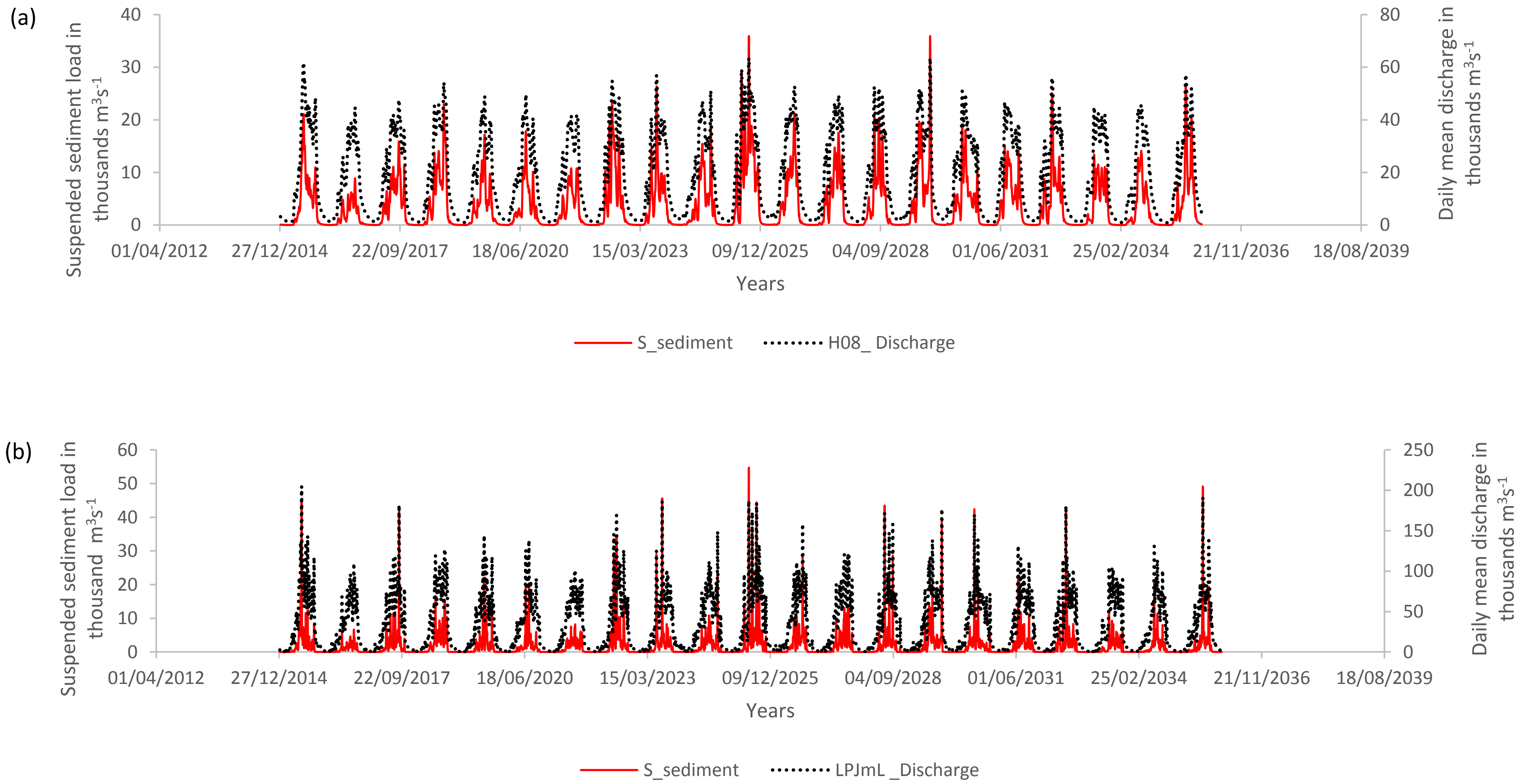

Figure 6.2: Daily mean discharge and suspended sediment load H08 (1) and LPJmL (2).

(a)

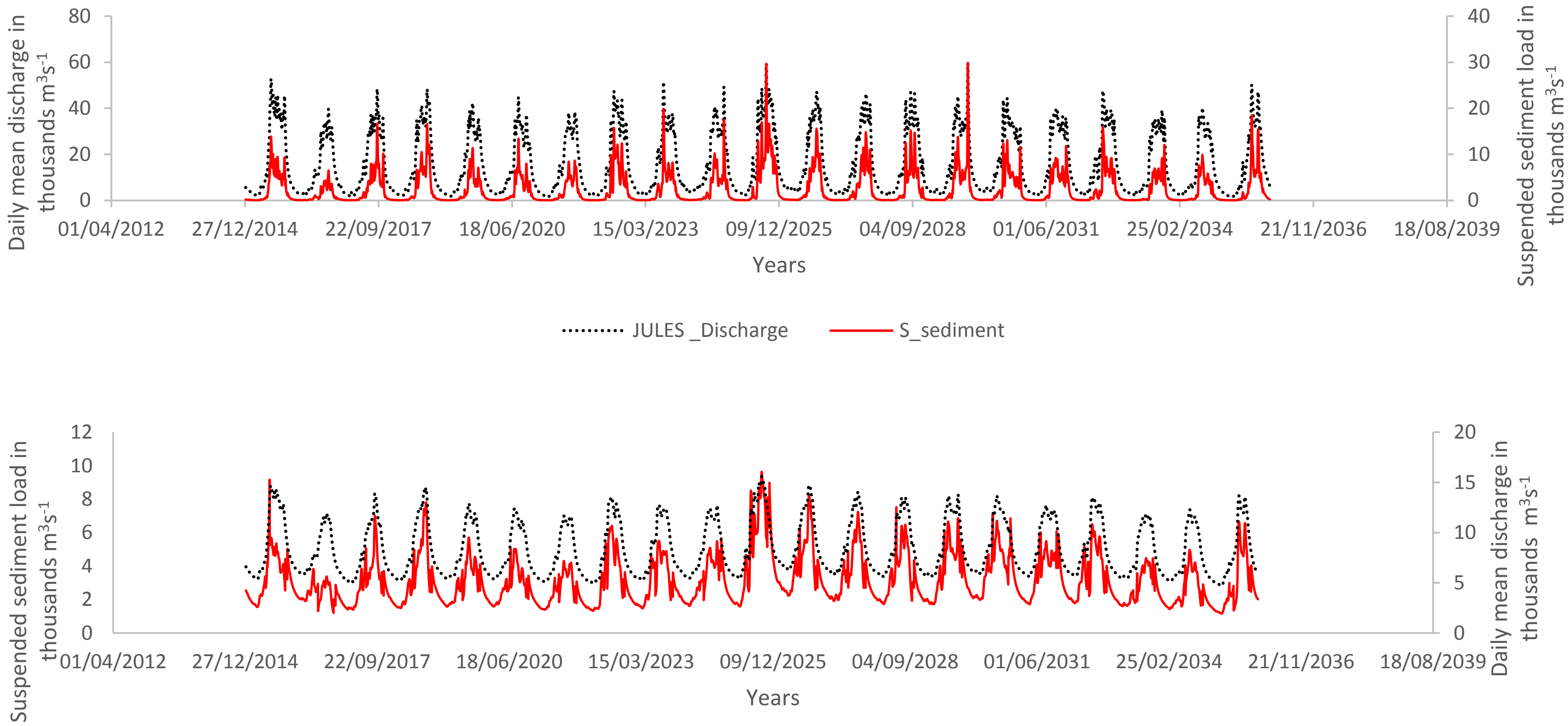

(b)

Figure 6.3: Daily mean discharge and suspended sediment load JULES (3) and MacPDM (4).

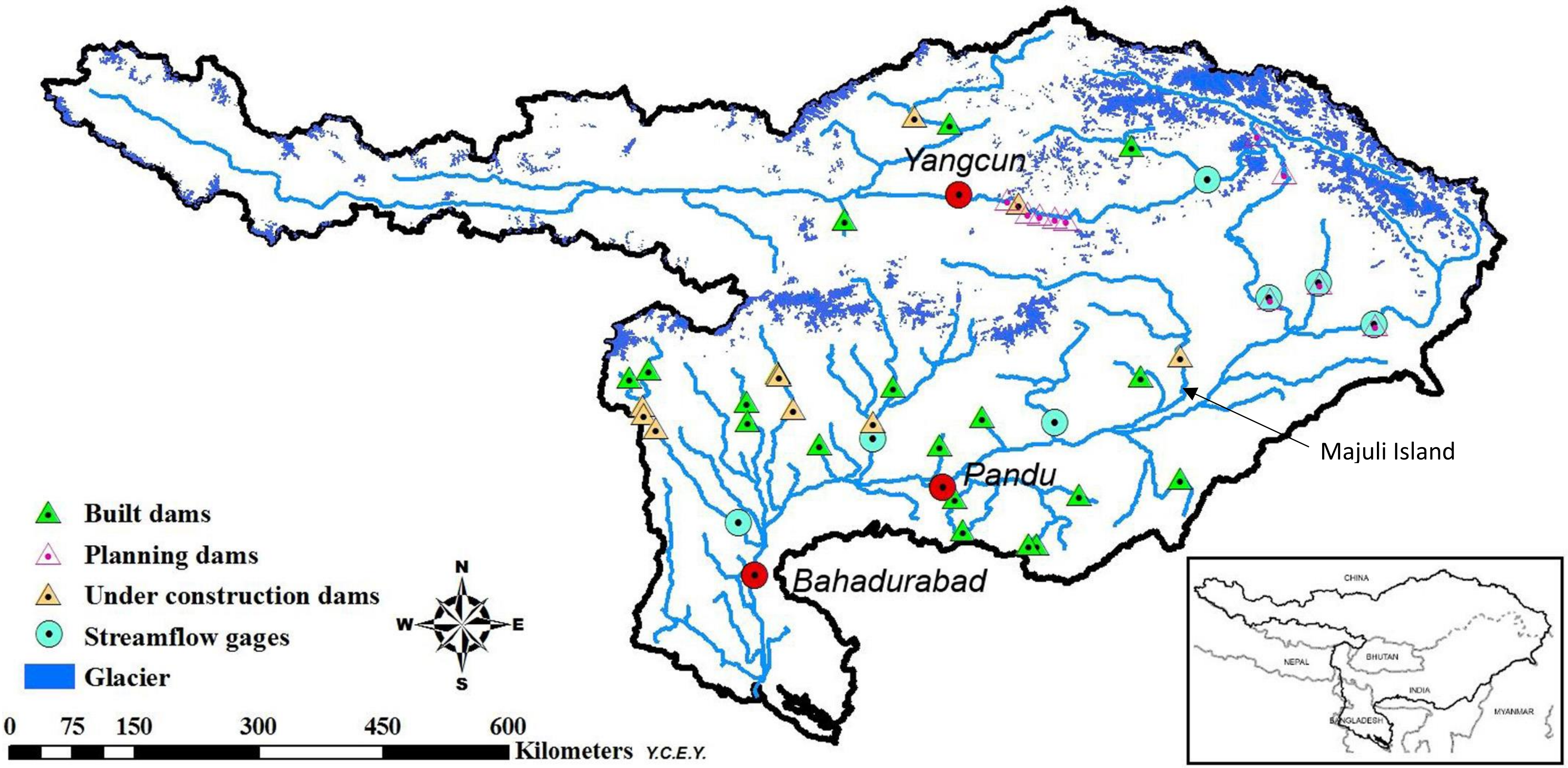

Fig.6.4. Glaciers, dams and publicly-accessible stream gages of the Brahmaputra basin (data from the Randolph Glacier Inventory, version 3.2) (Ray et al. 2015).

The objective is to investigate the capacity of C-L to forecast morphological futures that are consistent and realistic and to understand how likely it is that climate change will drive problematic morphological modifications of the river that may threaten the livelihoods or even the lives of people living on Majuli Island and along the Brahmaputra River. The models which were able to generate an appropriate representation of the morphological pattern of the river Brahmaputra were H08 and LPJmL C-L+ models. The output of these two models will be discussed and displayed in this chapter. The other two models are attached in the appendix.

7.4.Thalweg migration index

As described in chapter 3, thalweg migration index (TMI) checks the limit and extent of channel migration in a braided stream. This quantifies the thalweg channel instability and the direction of its movement. As described in the chapter 3, if the TMI is below or (+) 1.5 from the centreline (0) then it is moving towards the north bank and if the TMI is above or (-) 1.5 from the centreline (0) then the thalweg channel is migrating towards the south bank. In both the H08 (Figure 6.6) and LPJmL C-L+ models TMI values were calculated for 20 years and were plotted in the graph at 5 years interval. The results of both the models exhibit similar migration pattern i.e. the thalweg channel moving towards the north bank, towards Majuli Island (Figure 6.5). (The TMI of MacPDM and JULES are attached in appendix 5). In H08 and LPJmL models in C-L+ model the chute channels started headcutting and eventually it joins the thalweg channel (Figure 6.7, 6.8). Later in 10 to 15 years the chute channel capture the thalweg channel and divert the flow of thalweg channel towards the north bank. This resulted in erosion near Burha Chapori (A 37) and nearby sandbar (discussed in more detail in BDI section). The average width of the thalweg channel (Table 7.3) depict that the channel is becoming wider in succeeding years.

Model	Table 7.3: Average width of the thalweg channel in study reach (km)	
Year	H08	LPJmL
2020	2.94	2.9
2025	3.24	3.35
2030	3.06	2.91
2035	3.42	2.91

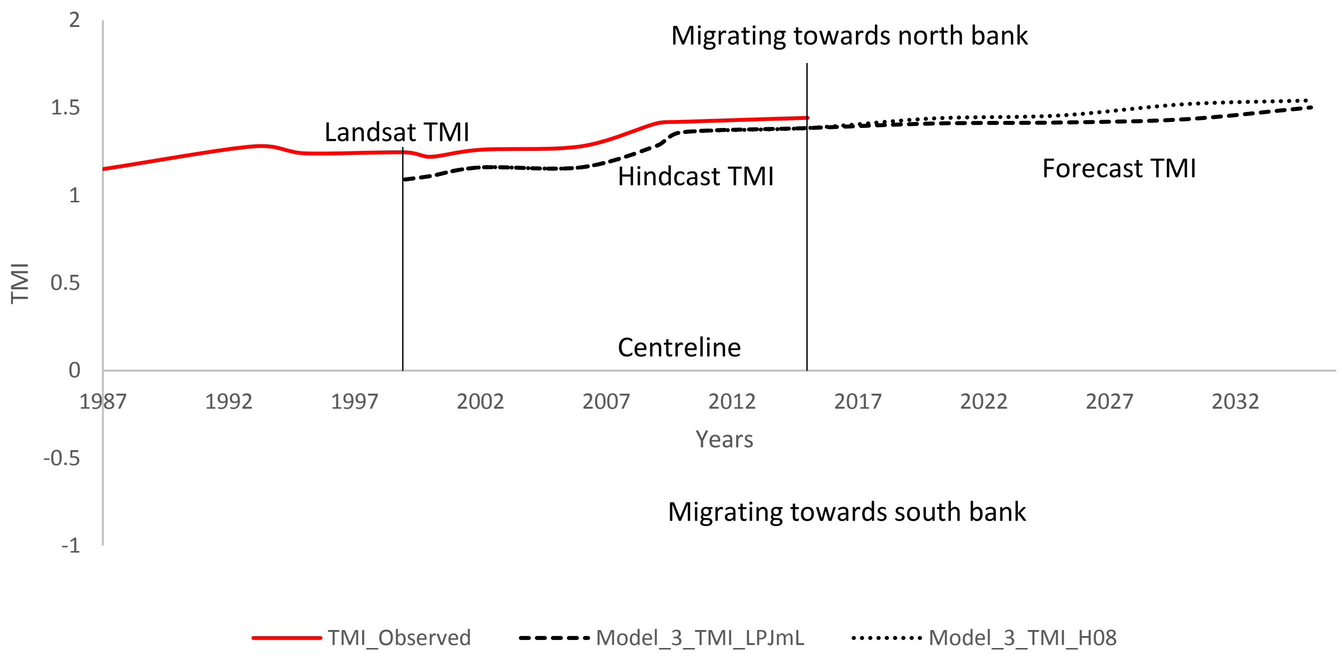

Figure 6.5: TMI of all the two models of C-L+.

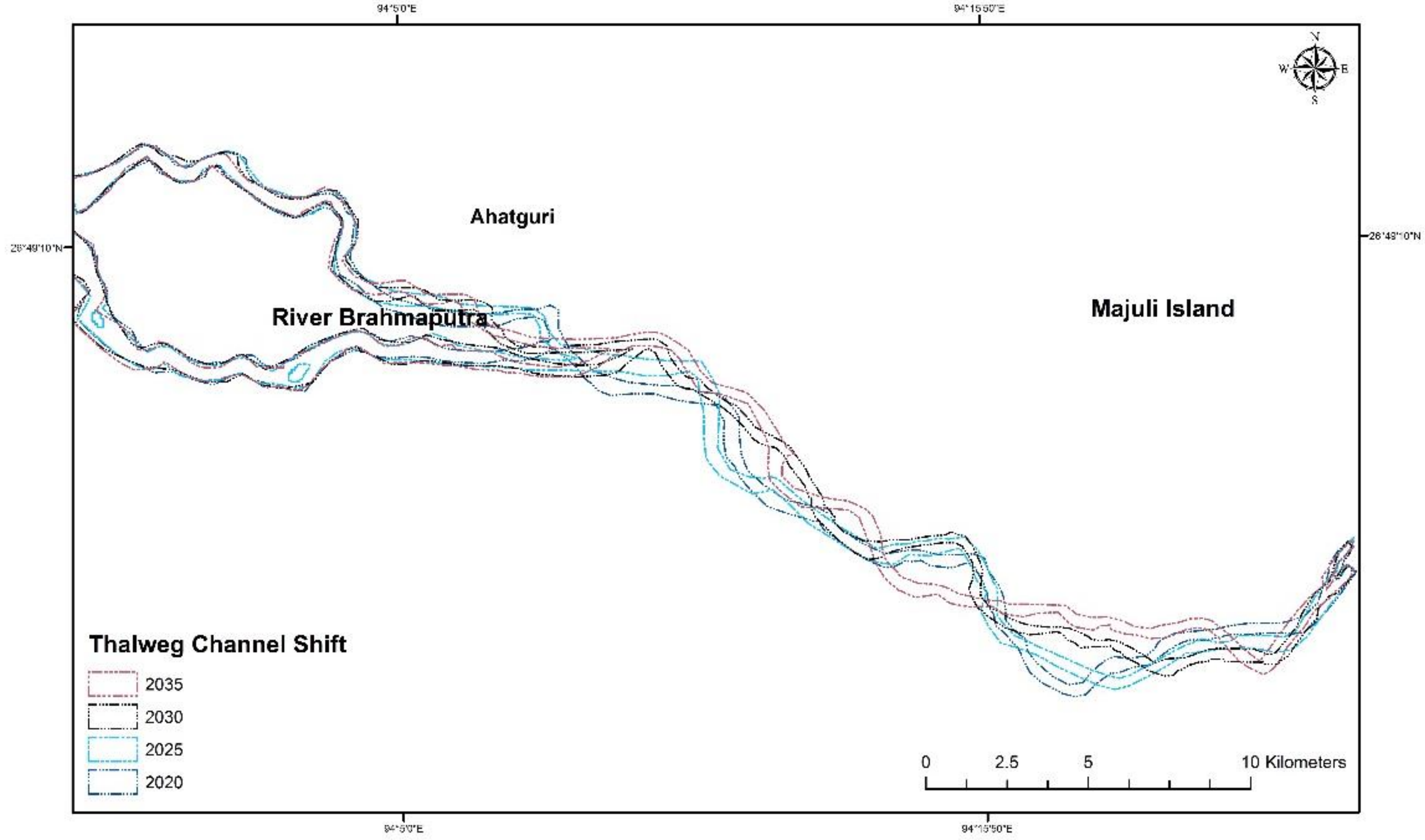

Figure 6.6: Showing Thalweg channel migration of H08 model of CL+ model no 3 among all the models.

The width of the channel and braiding process are strongly affected by the higher amount of discharge. In H08 and LPJmL C-L+ models, widening of channel width was observed (Table 7.4), similarly significant change was observed in the thalweg channel. The thalweg channel was becoming wider and shallow and is lateral shifting towards north i.e. towards Majuli Island. Anabranching is another type of phenomenon observed in H08 and LPJmL C-L+ the models. Head-cutting channels incise the sandbars to form multiple braiding channels. After 10 to 15 years these channels become connected and have formed chute channels and eventually, some of these chute channels become dominant channel branches (Schuurman et al., 2018). These new chute channels subsequently capture the thalweg channel and divert the flow of the river to a different path, causing a major lateral shift of the channel branches, sandbar formation, and deformations, migrations of sandbars and bifurcation of the main channel. All these processes were observed in the H08 and LPJmL C-L+ models for 20 years forecasting of the landscape evolution of river Brahmaputra near Majuli island (Figure 6.7, 6.8).

Model 3	Table 7.4:Average width of the River Brahmaputra near Majuli Island in km	
Year	H08	LPJmL
2020	11.18	11.18
2025	11.18	11.18
2030	12.11	11.73
2035	12.11	12.73

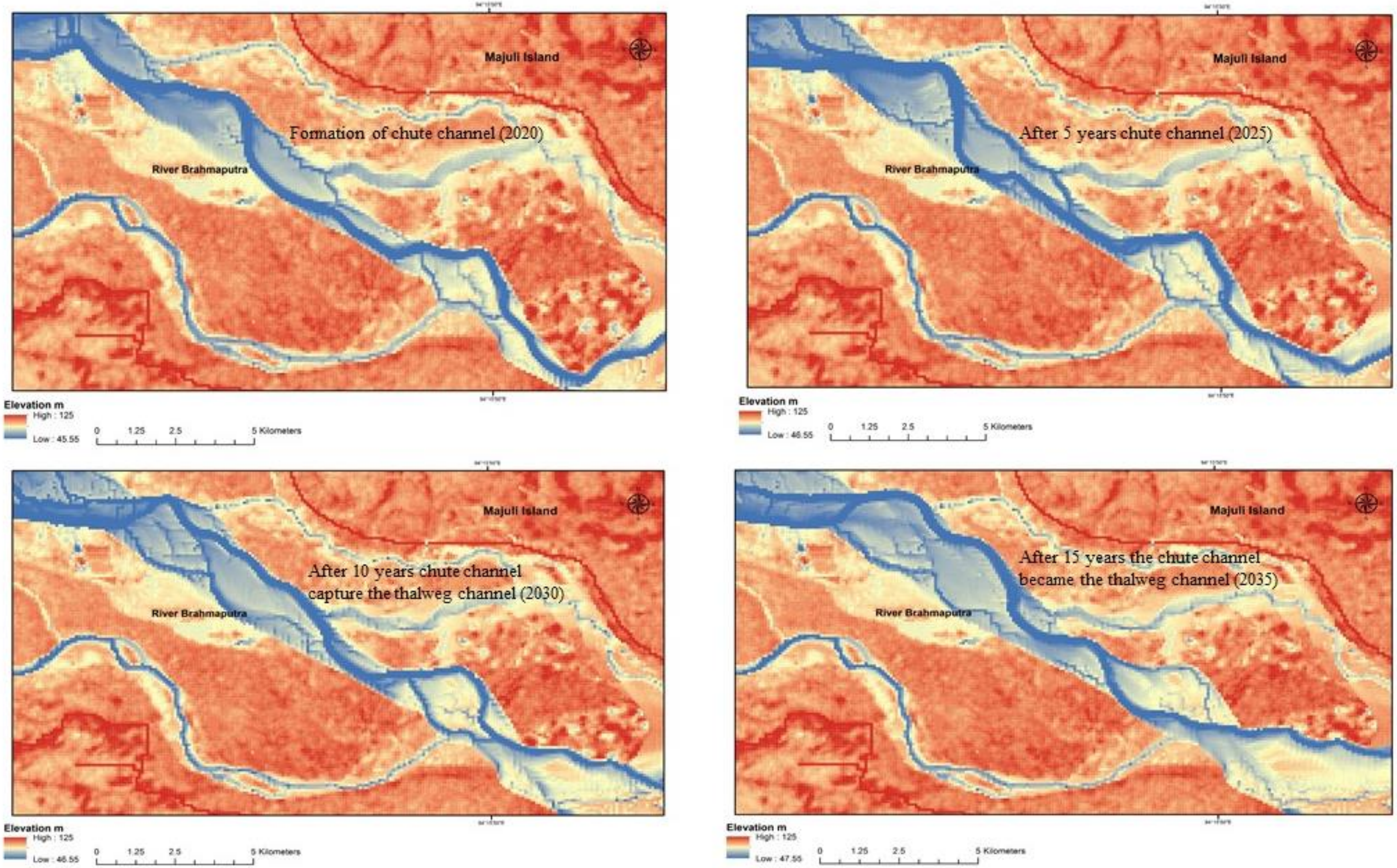

Figure 6.7: Thalweg channel capture by chute channel in H08 C-L+ model.

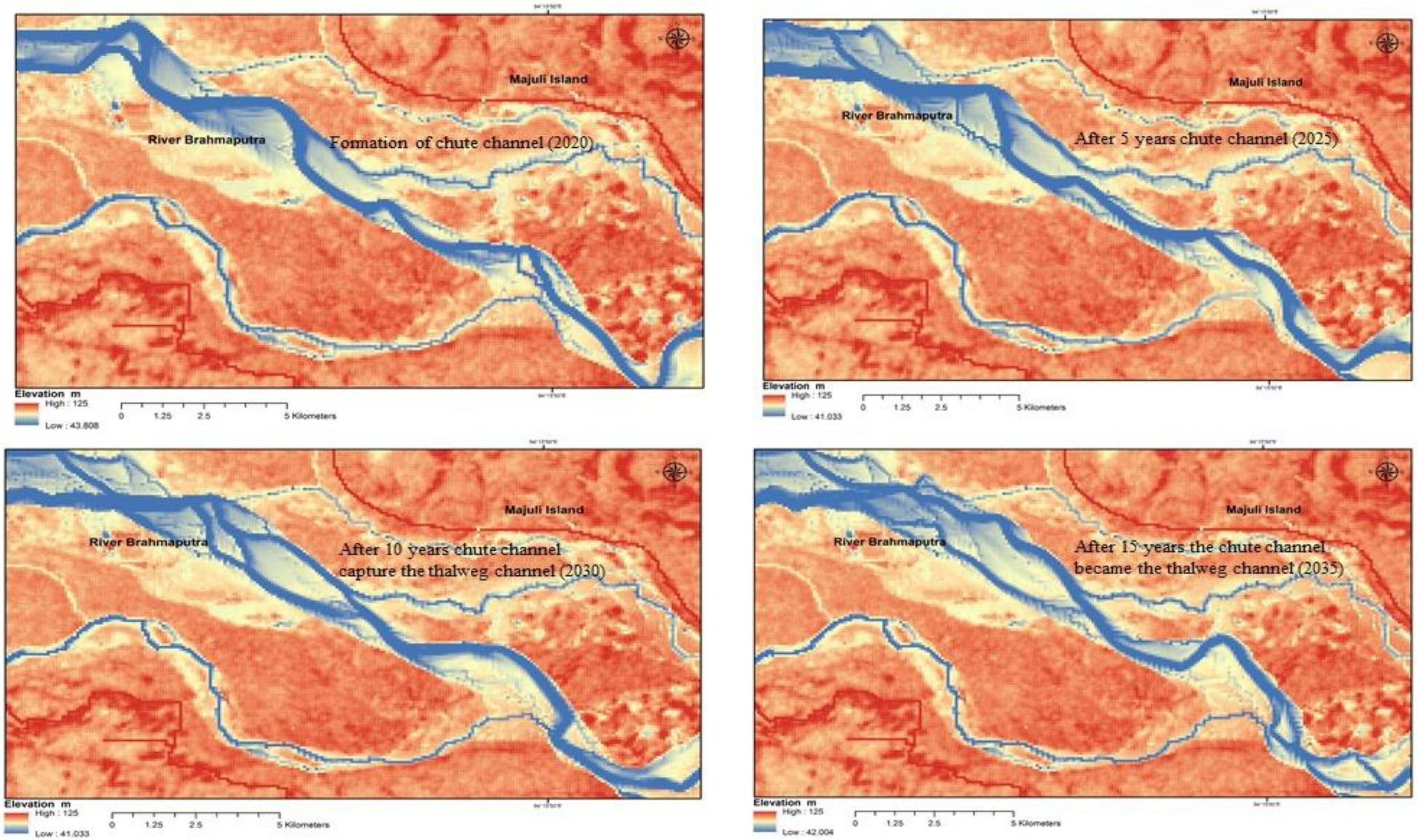

Figure 6.8: Thalweg channel capture by chute channel in LPJmL C-L+ model.

7.5. Modified plan form index

Forecasted Modified Plan Form Index (MPFI) for the H08 and LPJmL C-L+ models were computed and were plotted against 5-year intervals (2020, 2025, 2030 and 2035) (Figure 6.10, 6.11) for 20 continuous years. The low flow season was used in this research to calculate the MPFI values. This is because the Landsat data used to compute the MPFI value in chapter 3 were acquired during low flow condition. In both the sub-reaches (Figure 6.9), in the H08 and LPJmL C-L+ models it can be observed that the models were able to produce a comparable hydrological pattern in forecasted scenarios when associated with the Landsat images of past events described in chapter 3. As described in chapter 3 the MPFI values for both the sub-reaches increases since 2009 and it intensify after the flood event of 2012, and remain highly braided in subsequent years, especially in the sub-reach 2. After 2009 more new braided channels, sandbars were created and activate the dry channels during high peak flow which creates erosion in the river bank. In sub-reach 1 (Figure 6.10), H08 and LPJmL C-L+ model were generating moderately braiding intensity according to the set threshold level discussed in chapter 3. From the C-L+ models, this can be determined that during a discharge flow range of 920 – 1200 m^3s^{-1}, the thalweg channel became wider and shallower and the river was unable to transport the suspended sediment load. This was clearly observed in both H08 and LPJmL models and therefore generating more braiding channels in future. In sub-reach 2 in both H08 and LPJmL C-L+ models, were displaying a similar trend i.e. highly braiding (towards 2035) (Figure 6.11). MPFI of other two models were attached in the appendix 6.

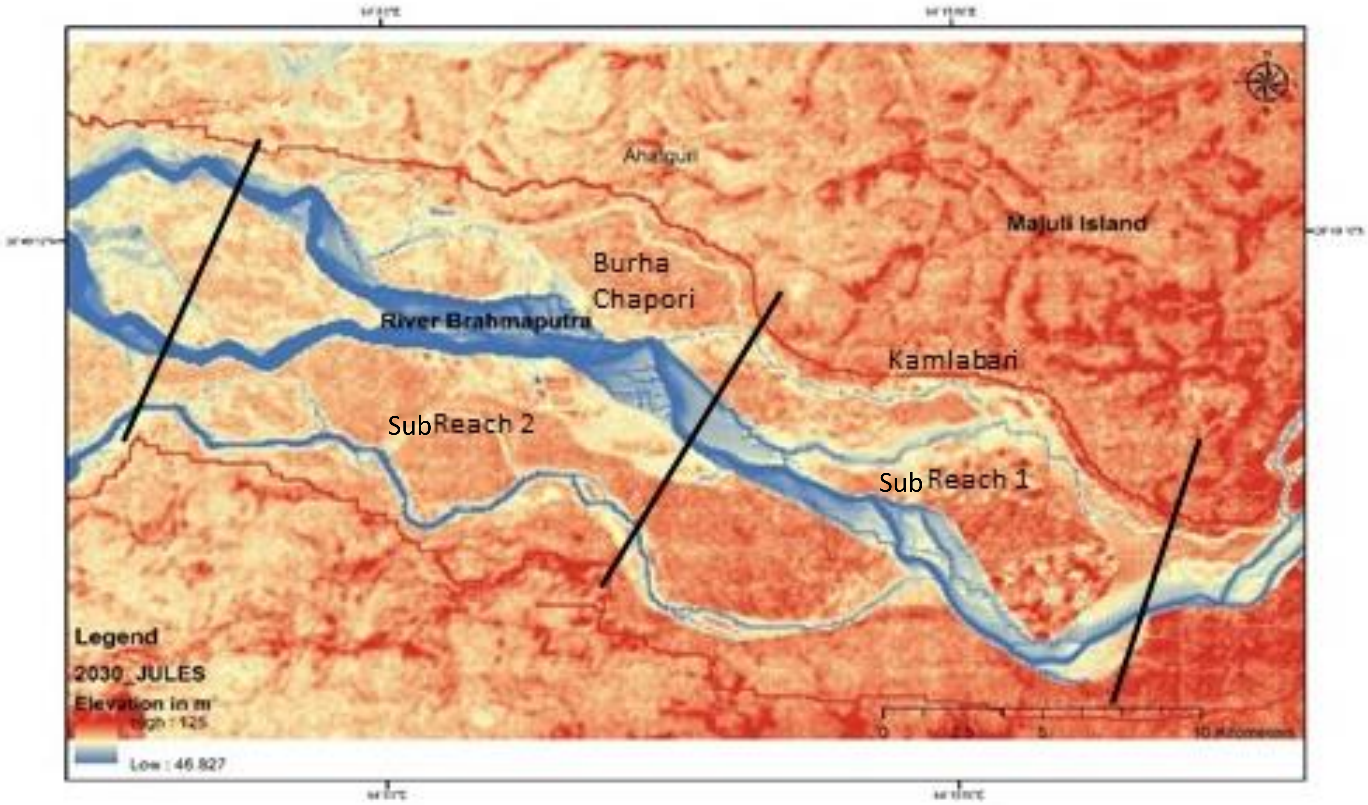

Figure 6.9: Sub reaches No 1 and 2 used to calculate MPFI of all the models, in the figure H08 (2025).

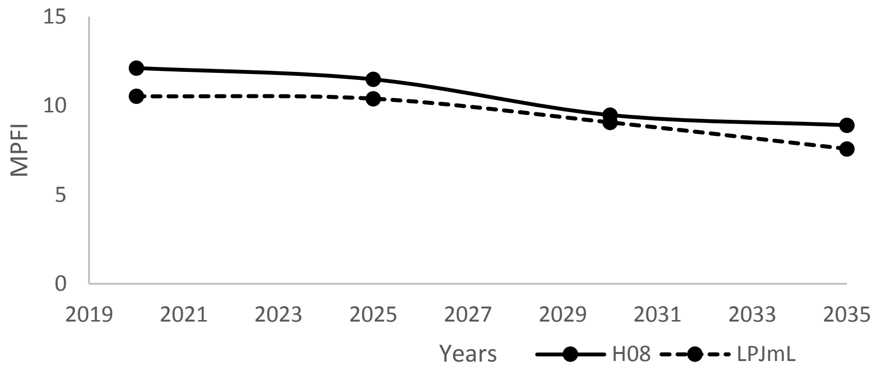

Figure 6.10: MPFI of sub reach 1 of H08 and LPJmL C-L+ models.

MPFI Thresholds
MPFI < 6 – High braiding
6 > MPFI < 18 - Moderate braiding
MPFI > 18 - less braiding

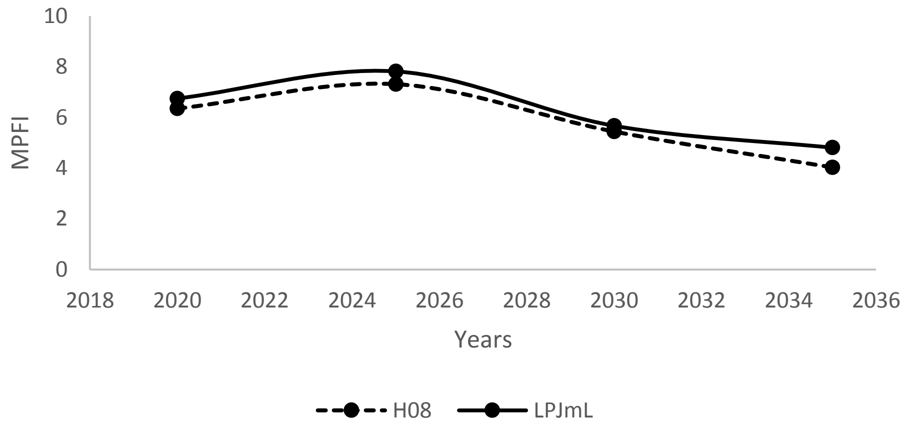

Figure 6.11: MPFI of sub reach 2 of H08 and LPJmL C-L+ models.

7.6. Modified flow geometry index

As discussed in chapter 3 cross-sections and water depth perform a significant role in computing MFGI value to determine the level of braiding in the river channel or reach. H08 and LPJmL both the C-L+ models, cross-sections were derived using the conversion tool to convert the line into points. Later these points were used to extract the elevation values by using extract point tool in Arc Gis. Using these process three cross-sections were derived for 20 years in 5 years interval (2020, 2025, 2030 and 2035) for the CS 47, 48 and 49 (Figure 6.12).

From the cross-sections, it can be discerned that at CS 47 (Figure 6.15) the two C-L models retains the two existing bifurcated channels and generated multiple small channels. In CS 48 and 49 (Figure 6.13 and 6.14) the main channel became wider, shallower and more braided in 20 years. These two hydrological C-L+ model were generating higher MFGI value in CS 47 (Figure 6.18) exhibiting highly braiding. In this region, the river bed became shallow and the average slope became 0.86^{o}, therefore the suspended sediment carrying capacity of the river became low, making the river hydraulically less efficient and resulting in more braiding. In CS 48 (Figure 6.17) and 49 (Figure 6.16) the MFGI value for the next 20 years in both the models H08 and LPJmL C-L+ model was also exhibiting highly braiding with higher MFGI value. (MFGI of other two C-L+ models are displayed in appendix 7).

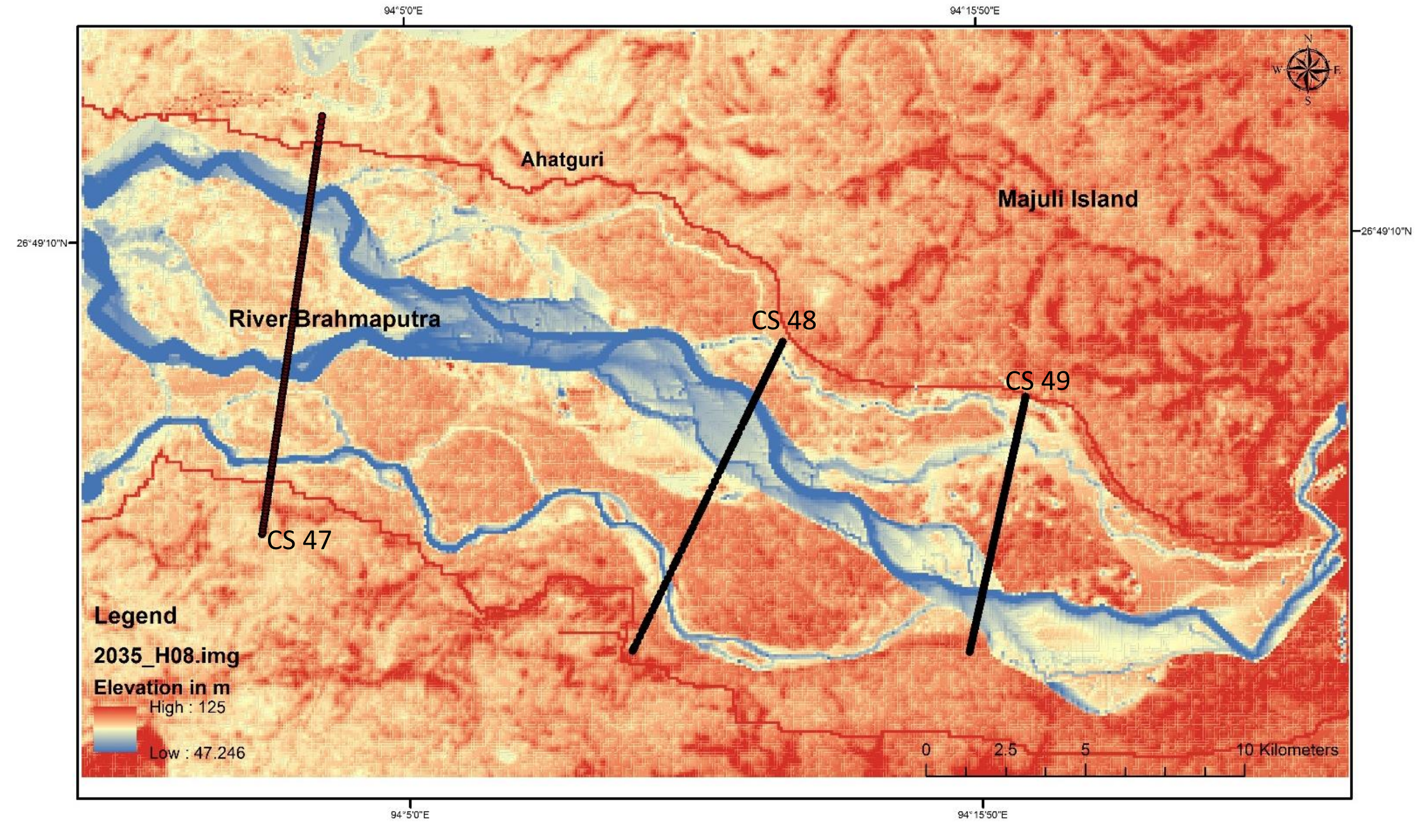

Figure 6.12: Cross-section 47, 48 and 49 used to calculate MFGI of all the C-L+ models, H08 (2035) is displayed in this figure.

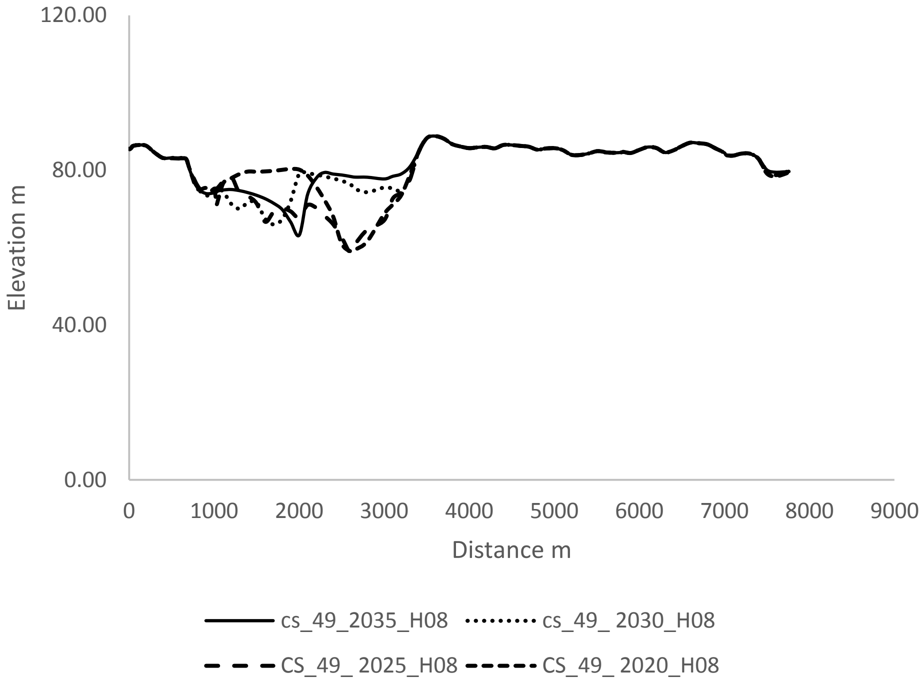

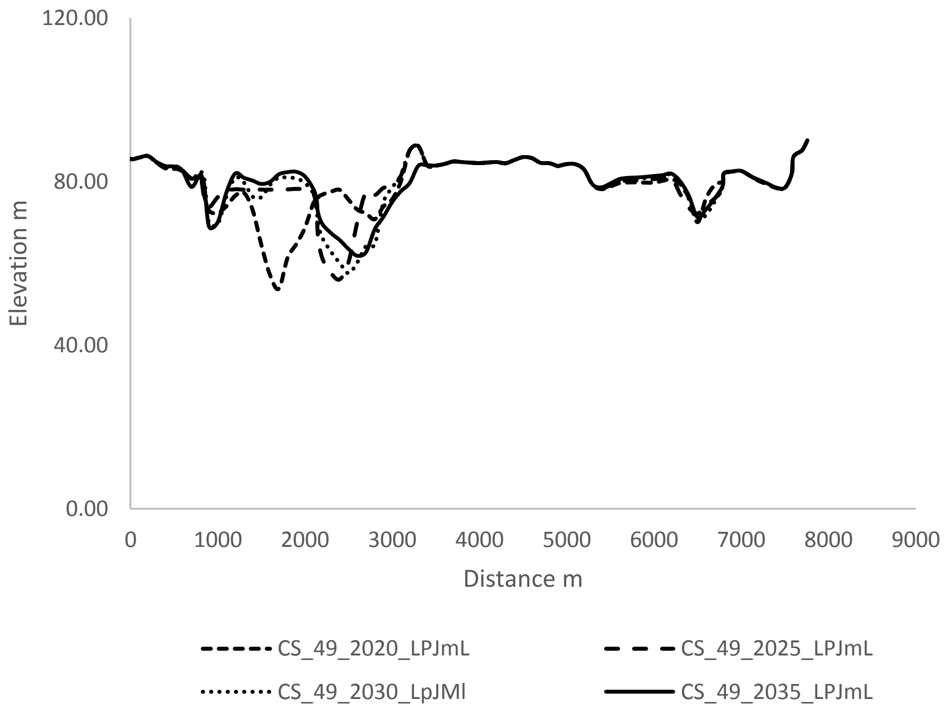

Figure 6.13: Forecasted cross-section 49 of the river Brahmaputra near Majuli Island.

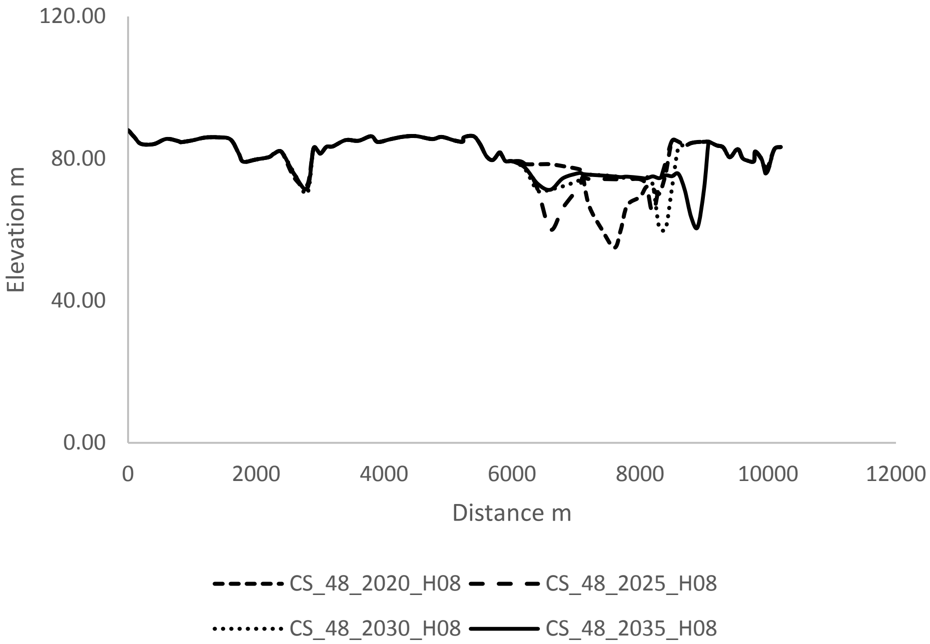

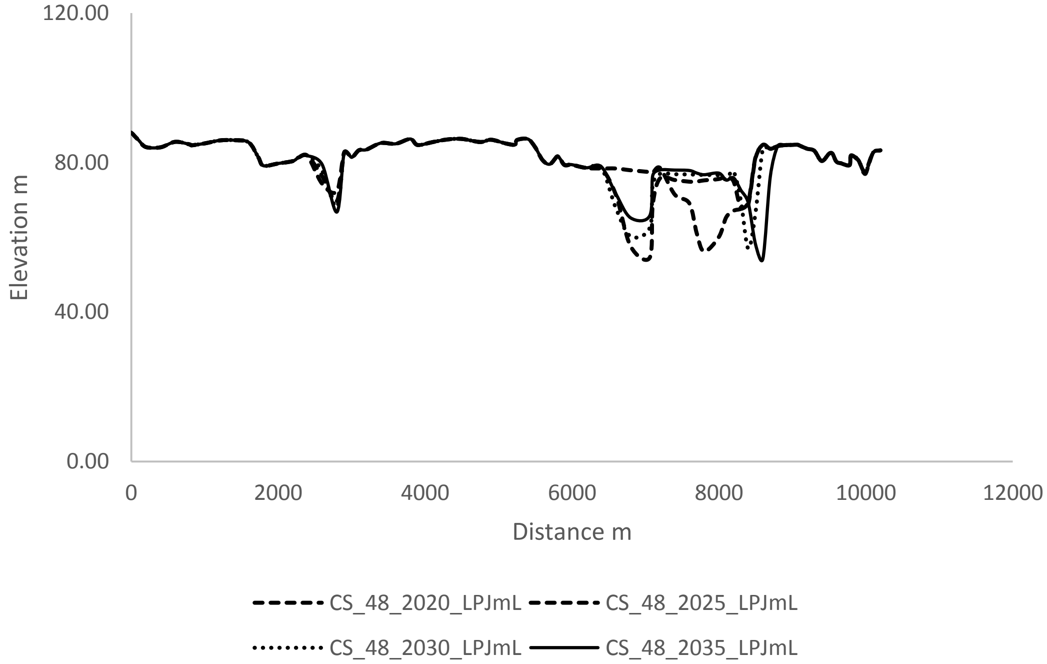

Figure 6.14: Forecasted cross-section 48 of the river Brahmaputra near Majuli Island.

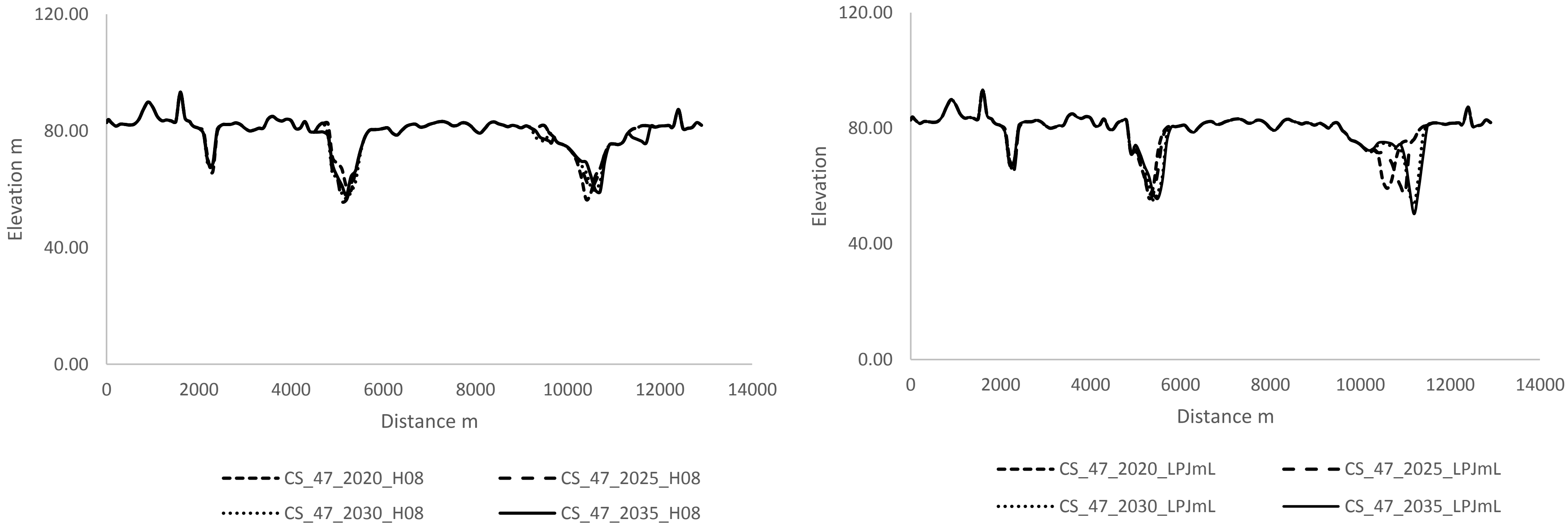

Figure 6.15: Forecasted cross-section 47 of the river Brahmaputra near Majuli Island.

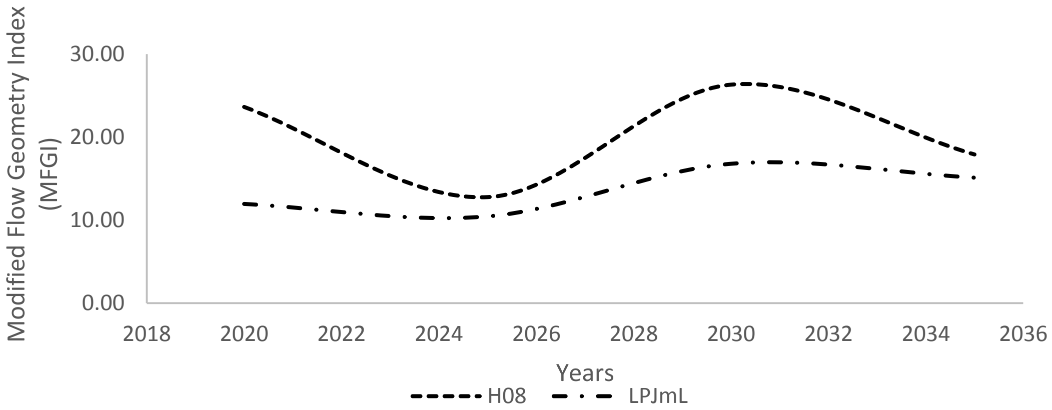

Figure 6.16: MFGI of CS 49 of H08 and LPJmL C-L+ model.

MFGI Thresholds
MFGI > 5 - Less Braided

5 > MFGI < 15 - Moderately Braided

MFGI > 15 - Highly Braided

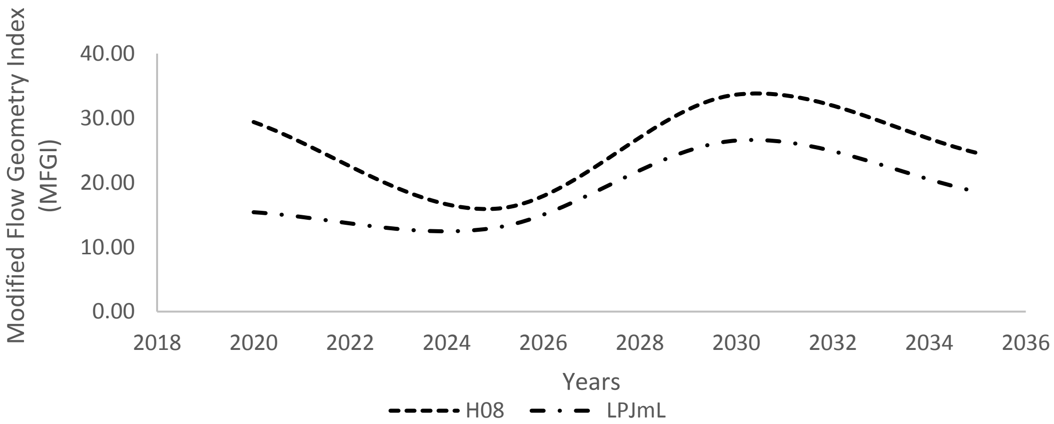

Figure 6.17: MFGI of CS 48 of H08 and LPJmL C-L+ model.

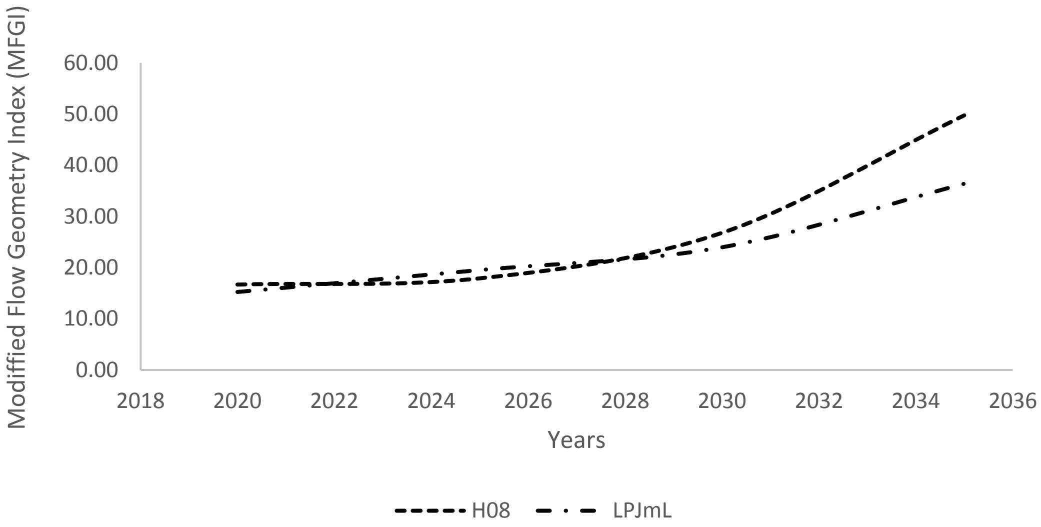

MFGI Thresholds
MFGI > 5 - Less Braided

5 > MFGI < 15 - Moderately Braided

MFGI > 15 - Highly Braided

Figure 6.18: MFGI of CS 47 H08 and LPJmL CL+ model.

7.7. Bar deformation index (BDI)

Braid bars in river Brahmaputra can be classified into two categories (i) stable braid bars, which are covered by vegetation and (ii) unstable braid bars which are transient in nature. An unstable braid bar changes its shape and size based on the amount of flow of water discharge and suspended sediment load. The Manning roughness plays an important role in bar formation and deformation. The Manning roughness coefficient used in both the C-L+ models is 0.04 m for river Brahmaputra. This Manning roughness coefficient was used for both the river channel and floodplains; however, the bed roughness on the floodplains and sandbars should be higher than in the channel due to vegetation, human-induced obstructions and other irregularities (Schuurman et al., 2018). Uniform bed roughness resulted in more sediment on the sandbars and floodplain. The process of deposition was observed in the all hydrological model of C-L+ model no 3. Using the forecasted scenarios of the C-L+ models no 3 bar deformation Index (BDI) were calculated for three selected sandbars and they were represented as a percentage. They are labelled A-1, A 2 and A 3 (Figure 6.20).

A-1 was the most transient, unstable bar, A 2 was a small, stable bar with vegetation cover and human habitation. A 3 was the longest stable bar with vegetation cover. As described in chapter 3, BDI exhibits the transient nature of fluvial landforms (sandbars) features. Taking the size of A-1, A 2 and A 3 for the year 1987 as 100% i.e. the reference size (Table 3.4) of the sandbar, forecasted BDI values were computed for 20 years. In the H08 and LPJmL models of C-L+ model minor difference in the percentage size of the sandbars were observed (Figure 6.19). These C-L+ model in 100×100 m resolution dem and limited grain size data, were not able to produce detail change in the shape and size of the braid bars but it was able to depict a broad picture of the percentage change in their sizes. This minor difference in BDI was due to the difference in discharge flow in each model. The BDI of other two models are attached in the appendix 8.

(a)

(b)

(c)

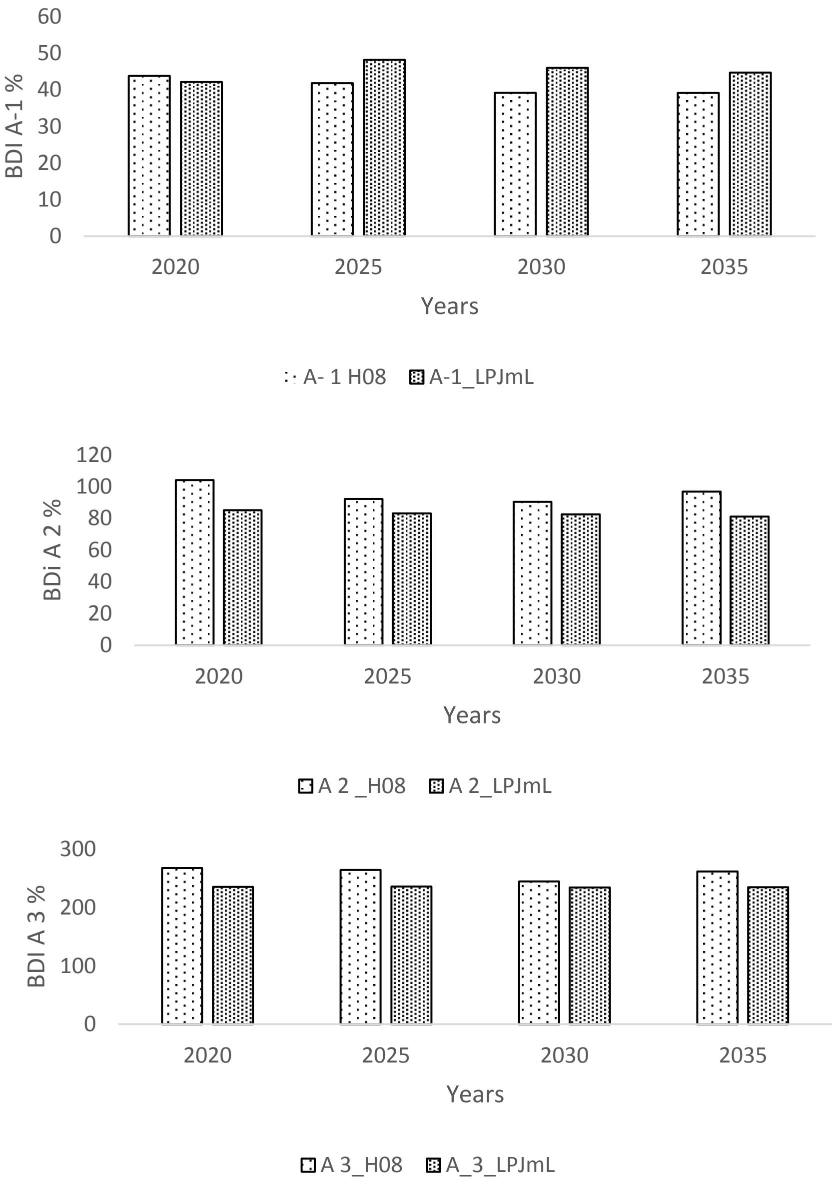

Figure 6.19: BDI of A 1 (a), A 2 (b), A 3 (c) of C-L+ model

From the figure 6.19 it can be inferred that the A-1 in LPJmL C-L+ is increasing in size while in H08 C-L+ model it is reducing in size this is due to variable discharge flow. On the other hand A 2 in both the models is reducing it size. This is due to the thalweg channel is adjacent to this sandbar which accelerate erosion during peak discharge period. In the case of multi-channel rivers, the braided form is known to be related to a high-energy flow environment, mobile bed sediments providing a heavy bed material load, and easily eroded bank materials. This results in creating flow division and channel bifurcation (Figure 6.21).

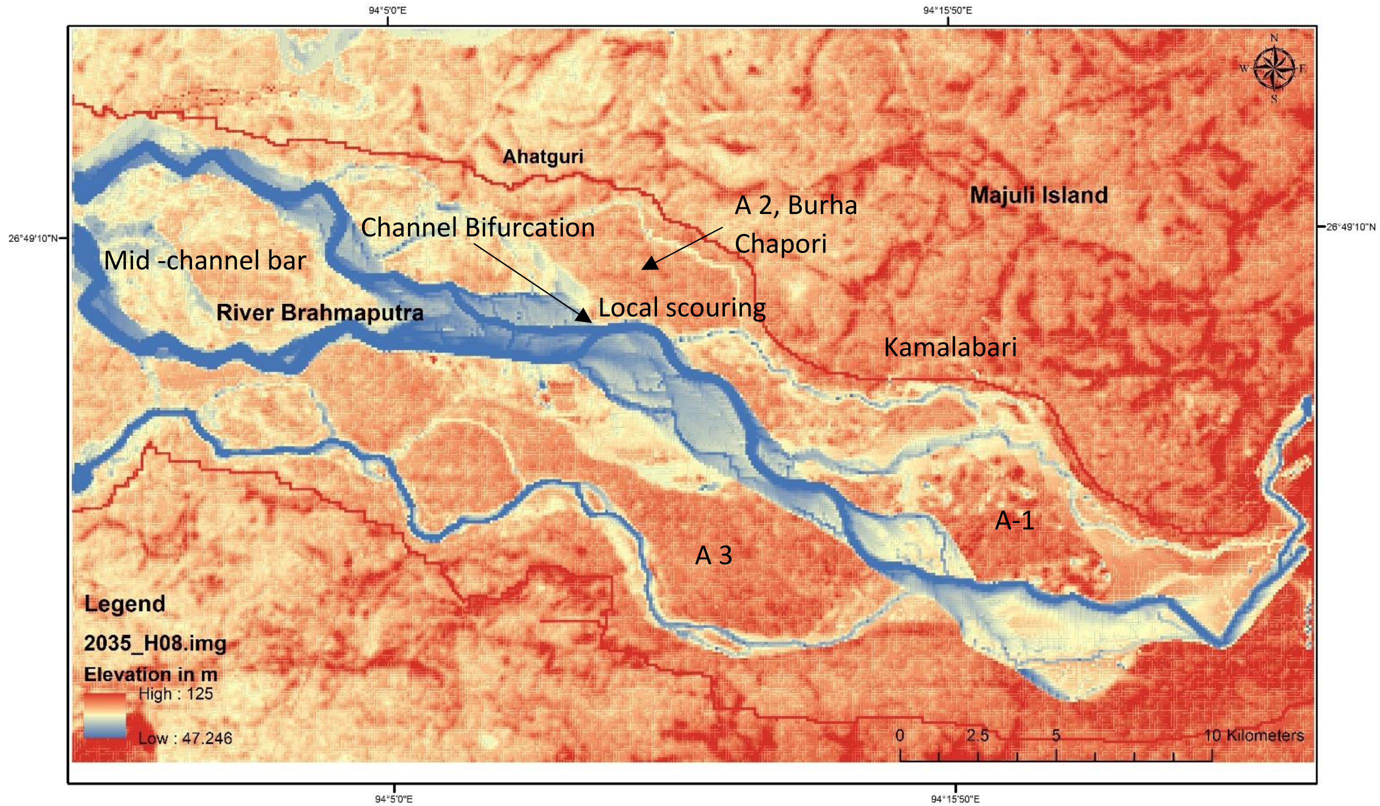

Figure 6.20: Three braid bars used to calculate BDI in all the C-L+ models.

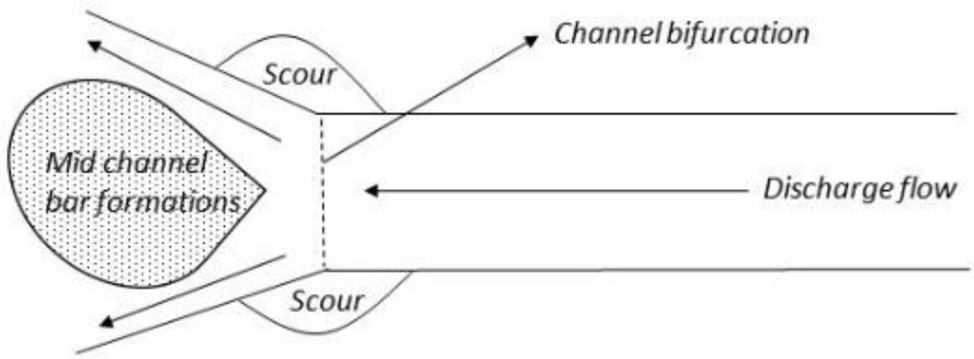

Figure 6.21: Flow patterns in a river model bifurcation.

The depth-to-width ratio of an alluvial stream decreases due to bank erosion and widening, possibly coupled with bed accretion due to deposition of bank-derived sediment, a threshold is reached where, for a given level of specific energy, the single-thread velocity field breaks up into two, or more, separate flow threads. This hydraulic division of the flow field generates one or more zones of relatively low energy flow, where sediment deposition is favoured. Local scour below the high-velocity filaments, coupled with accretion in low energy areas, drives hydraulic division of the flow and may lead to the morphological bifurcation of the channel (Richardson and Thorne, 2001). This phenomenon was observed in all the four forecasted C-L+ model no 3. Due to the channel bifurcation near bar A 2, forming a mid-channel bar and occurring local scouring near Burha Chapori. Hence the local bank erosion in this region and shifting of thalweg channel will likely to create more erosion near Burha Chapori (Figure 6.20) in future. The size of the A 3 bar remain persistent as it is a stable bar covered by vegetation.

7.8. *C-L+ produces forecasts that are both plausible and consistent with the results of recent morphometric investigations.*

Mahanta and Saikia (2017) calculated the sediment deposition and scour in six reaches of the Brahmaputra in Assam during the four periods: 1957 - 1971, 1971 -1977, 1977 - 1981 and 1981 - 1989 (Figure 6.22 *a*, *b*). In this study, Majuli Island falls in the fifth reach (CS 41 - 51) in their study area. According to Mahanta and Saikia (2017), there was more deposition than erosion during three of the four periods of observation, the exception being 1971 - 1977.

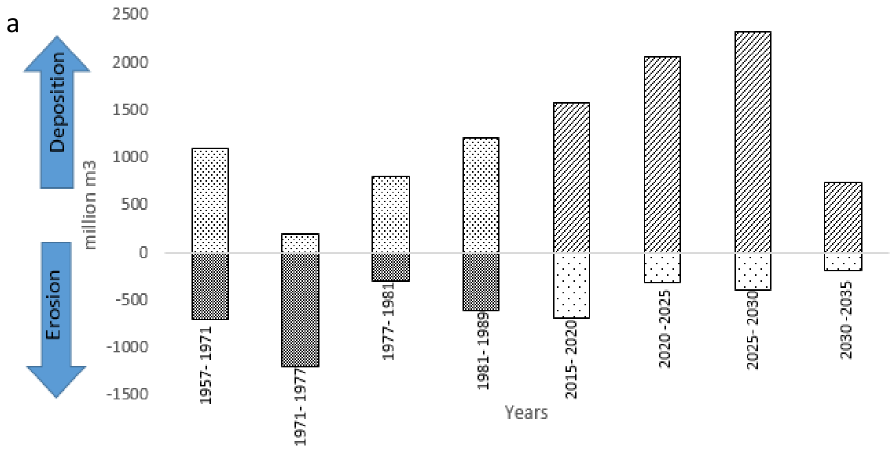

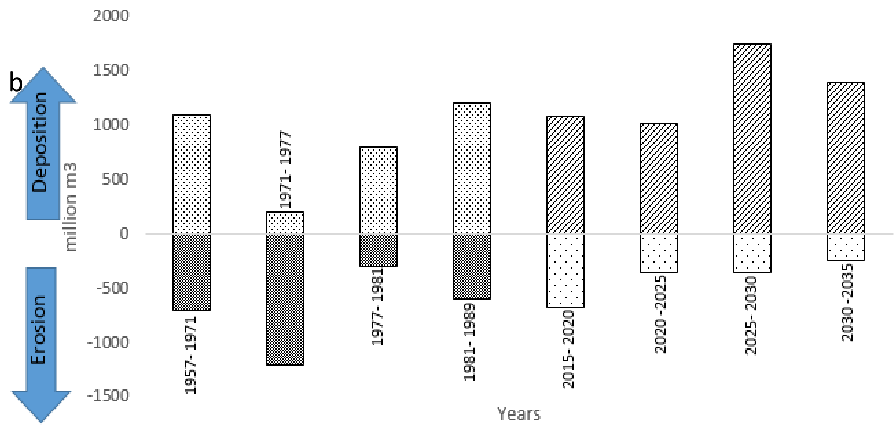

Figure 6.22. Deposition and erosion in the Brahmaputra near Majuli Island. Calculated erosion and deposition quantities for four periods between 1957 and 1989 are reproduced from Mahanta and Saikia (2017). deposition and erosion quantities forecast for four periods between 2015 and 2035 using C-L+, with hydrology models H08 and LPJmL, are shown in graphs a. and b, respectively.

In this study, the amounts of deposition and erosion forecast using the C-L+ model with hydrological models H08 and LPJmL have been added to the results of the study by Mahanta and Saikia (2017), to extrapolate the deposition/erosion graph into the future, by adding histogram bars for the periods 2015 - 2020, 2020 - 2025, 2025 - 2030, and 2030- 2035, in figures 6.22 a and b, respectively. The graphs show that amounts and inter-period variability of erosion and deposition forecast by C-L+ are similar in magnitude to those calculated for the previous periods. Hence, it may be concluded that these forecasts are entirely plausible. Forecasts generated by both C-L+ models suggest that the amount by which deposition exceeds erosion is likely to increase in future, which is consistent with higher discharges and increasing sediment inputs to the study reach associated with climate change predicted by the hydrology models. The trend for increasing dominance of deposition over erosion forecast using C-L+ is stronger for the H08 climate model (Figure 6.22a) than for the LPJmL landscape model (Figure 6.22b). This is as expected, as H08 predicts a great increase in runoff than does LPJmL. In either case, increased deposition is consistent with the formation of more braid bars and sub-channels, channel widening, increased braiding intensity and retreat of the river banks, especially on the southern edge of Majuli Island (see Figures 6.7 and 6.8).

Conclusion:

This chapter demonstrates that the model C-L + H08 combination was best able to forecast the morphological behaviour of the River Brahmaputra in the study reach. This model combination was able to generate chute cut-off channels that developed across large bars and other minor sub-channels that subsequently enlarged to become dominant sub-channels or anabranches over periods of 10 to 15-years. Some of these growing sub-channels grew large enough to become the thalweg channel, others captured so much flow from the thalweg channel that they replaced it. In either case, the effect of thalweg channel switching or capture was to move the primary flow route northwards, towards Majuli Island.

Additionally, the C-L + H08 combination of models created sub-channels (including thalweg channels) that were shallow and wide, with greater propensity for dissecting sand bars to create more sub-channels and, hence, more intense braiding, which is consistent with the established relationships between channel width, bar dissection and MPFI.

Based on C-L + H08 forecasts, it seems likely that the Brahmaputra in the study reach will remain highly braided and that the main flow routes will continue to move northwards through thalweg channel switching and capture. This will, in turn, instigate more bank erosion along the southern edge of Majuli Island.

Chapter 8. Discussion and key contributions to knowledge

8.1 Context

To date, limited attention has been paid to simulating the morphological behaviour of large, braided river systems at time and space scales relevant to river management, due to difficulties with data collection and the inability of physics-based models to handle the complexities and unpredictabilities inherent to rivers of this type (Kasper et al., 2018). To address this research gap, this study has performed original research on the River Brahmaputra near Majuli Island that has: identified a practicable modelling approach; developed a reduced complexity model to hindcast and forecast morphological evolution; developed novel indices of braiding morphology and change; used those indices to evaluate the performance of that model, and; interpreted model outcomes to make recommendations for sustainable bank stabilisation and river training works that could protect lives, livelihoods and property in vulnerable communities living close to the river on Majuli Island.

8.2 First contribution to knowledge: identifying an appropriate modelling approach for simulating channel evolution at a reach-scale and over the medium-term in large, braided rivers like the Brahmaputra near Majuli Island

Numerical models are useful tools for investigating channel evolution processes in space and time scale. However, there is a dearth of morphodynamic models suitable for modelling the morphology of braided rivers (Kasprak et al., 2018). Examination of the literature confirms that, historically, large, braided rivers have been modelled far less frequently than single-thread rivers. Recently, however, there have been significant successes in modelling the morphodynamics of bars in fine-grained, braided rivers over mesoscale time (Nicholas, 2013; Schuurman et al., 2013, 2015). Similarly, in coarse-grained, braided rivers, Kaspark et al., 2018 have developed a morphodynamic model for bar movement in gravel-bed, braided rivers, by coupling CFD with a rules-based sediment transport algorithm to route bedload and simulate the evolution of the bed topography.

These, ‘physics-based’ approaches to simulating fine- and coarse-bedded braided rivers have very high computational demands that can only be met using high-performance computing resources, which limits their practicality for use in applied, investigative and management-related applications. Also, in large, complex, braided rivers cannot be calibrated or applied in politically-sensitive locations, where access to the detailed hydrological, hydraulic, topographic and sediment data required to run them (see, for example, Zilani et al., 2013; Nicholas et al., 2013, Kasprak et al., 2018) is severely limited.

Simulating the geomorphic functioning of very large, braided rivers, therefore, remains research challenge (Ashworth and Lewin, 2012). In the case of the Brahmaputra, the width of the channel varies from 9 km to 23 km, in places the depth of the river exceeds 10 m, and the planform varies between braided, anabranching and anastomosing. However, even in a huge, complex braided river with limited data like this, modelling is possible, using a type of simplified morphological model known as a reduced complexity model or RCM (Murray and Paola, 1994; Coulthard et al., 2002; Thomas and Nicholas, 2002).

RCMs have advantages for modelling braided rivers because of they:

1. can model real landscapes and simulate their geomorphic responses to climate change, neotectonics and land use impacts.

2. can model all parts of the catchment using continuous simulation.

3. assimilate hydrological, fluvial and slope process and reduce many of the complications associated with boundary conditions, slope/channel coupling etc. that are problematic in other types of models.

4. allow the drainage network to change and migrate over long timescales.

5. are suitable for investigating how geomorphic processes interact.

6. can reproduce typical behaviours including meandering, braiding and lateral erosion.

RCMs have disadvantages for modelling braided rivers because:

1. some fluvial forms, such as ripples, dunes, pools and riffles, are lacking in models of this type, though it is unclear, whether the omission of these small-

scale morphological features significantly affects the results at larger, reach and riverine landscape-system scales.

2. RCMs have proved difficult to validate quantitatively and they are, therefore, believed to be unsuitable for detail morphological simulations needed for engineering applications, such as predicting local bank instability, or identification of stable locations for the construction of a bridge. However, this weakness is irrelevant when a RCM is used to forecast broader-scale evolution in a reach or riverine landscape.

Some RCMs are cellular automaton models capable of simulating morphodynamics at large spatial scales and over long time scales, albeit at the expense of some physical explanation and morphological reliability (Nicholas and Quine, 2007; Thomas et al., 2007; Zilani et al., 2013). That is why, in this research, a reduced complexity model was selected to model medium-term landscape evolution in the Brahmaputra, near Majuli Island.

8.3 Second contribution to knowledge: development of a medium-term, hindcasting/forecasting model for riverine landscape-evolution in the Brahmaputra near Majuli Island

Most research using RCMs in the context of braided rivers concerns hindcasting and forecasting sediment yields at the reach or catchment scales (Coulthard et al., 2002; Zilani et al., 2013; Meadows, 2014). Less research has been conducted on using RCMs to hindcast and forecast river channel evolution and practically none has been done on hindcasting and forecasting riverine landscape-evolution in a very large, braided river reach that exhibits profound morphological changes and shifts in planform location and patterns while following a complex evolutionary trajectory. Simulating braid bar creation, modification and destruction and island morphodynamics is a challenge, but one that must be addressed if braided river evolution is to be understood and explained (Amsler et al., 2005).

As described in Chapter 5, gaining access to hydrological data for the Brahmaputra presented another, different kind of challenge. Data for classified rivers are restricted in India, and only through special efforts could initial bathymetry for the study reach be generated, based on access gained to cross-section data and an SRTM, 90 m resolution, DEM.

Gupta (1995) stated that there is a need for more research on channel planform change in tropical rivers. Gilvear (2000) noted that there are a limited number of studies conducted on the morphological evolution of very large, tropical rivers (e.g. Rutherford and Bishop (1996) on the Mekong, Speight (1965) on the Auranga, Salo et al. (1986) on the Amazon and Ucayili, Gilvear et al. (1999) on the Lungwa), but none of these is comparable in morphological complexity to the Brahmaputra. There is also need to develop a predictive capability with respect to planform change in highly mobile rivers, for geomorphic, management and engineering reasons (Gilvear, 2000).

Large braided rivers are especially mobile in character. Hence, it is particularly difficult, but also important, to be able to forecast future changes in the positions of the bank lines of these type of rivers, which have implications for people and property located close to the channel. To address this issue, this research has developed a technique to forecast anabranch channel changes and banking shifting in a mobile, braided river despite the absence of fine-resolution bathymetric data needed to develop a fine-mesh grid in a DEM. According to Sarker et al. (2014), a resolution of 240 m is sufficient to define the characteristic components of the river bed as the width of the major anabranch channels and islands in the River Brahmaputra exceed several hundred metres.

It was recognised early in the research that modelling a very large braided river with discharges greater than 10,000 m^3s^{-1} and sediment loads greater than 5,000 m^3s^{-1} over two decades would result in long run times, even in a reduced complexity, cellular automata model like C-L. For that reason, initial work centred on setting up the model to make run times achievable (Table 8.1).

Table 8.1. Simulation run-time estimation.

Plan	DEM resolution (m)	Time (years)	Simulation run-time estimation with the Core-i7 processor and unsteady state, non-uniform flow (hours)	Run-time (days)
A	90	20	960 (1-year simulation takes 48 hrs)	40
B	100	20	480 (1-year simulation takes 24 hrs)	20
C	240	20	360 (1-year simulation takes 15 hrs)	15

C-L Model	DEM resolution (m)	Time (years)	Simulation run-time estimation with the Core-i7 processor and unsteady state, non-uniform flow (hours)	Run-time (days)
A	100	20	700 (1-year simulation takes 35 hrs in unsteady state, uniform flow model as the model is slow)	30
B	100	20	480 (1-year simulation takes 24 hr unsteady state, non-uniform flow to speed-up model)	20

Three experiments were run to establish the run-time required for the C-L model with different DEM resolutions and model modes (Table 8.1). Based on these experiments, DEM resolution was set at 100 m x100 m, with flow and sediment transport parameters adjusted to speed up the simulation runtime to the point that 20-year duration, hindcasting and forecasting simulations were possible for the Brahmaputra. Daily time steps were selected because of the availability of daily mean discharge and suspended sediment data from the Water Resource Department, Govt. of Assam, India.

Run times also depended on the discharge. Smaller discharges ran quicker than large floods, and *vice-versa*. For example, the period 1998 to 2001 took a long time to run due to the occurrence of a monsoon extreme flood event in 1998 (see Figure 4.10). Appropriate DEM resolutions were used to reduce run-times while still outputting acceptable results. During these experiments, the model was tested using DEMs with 90, 100 and 240 m grid cell resolutions. A dedicated, Core i7 processor computer was used, so that simulation run faster. The values selected for flow and sediment transport parameters also affected the simulation run-times. For example, the experiments revealed that, if the minimum value of the lateral erosion coefficient is selected (0.0001), the run-time increases while if higher values are selected, run time decrease (see Table 5.3).

Once the experimental runs were complete, 10 C-L models were run for the river Brahmaputra in two flow modes (i. unsteady, uniform flow and ii. unsteady, non-uniform flow) using a 100 m x 100 m DEM and appropriate flow and sediment parameters. C-L models in the two different modes were found to perform quite differently. In unsteady, uniform flow mode, the C-L model took 35 hours to run just 1-year of simulation. However, in unsteady, non-uniform flow mode, the C-L model took only 24 hours to complete 1-year of simulation.

The suggested range of coefficients for lateral migration in braided rivers is 0.01- 0.001 m, and for meandering rivers it is 0.0001 m. As explained in Chapter 5, in this study C-L models were run with a lateral erosion coefficient of 0.0001 m which is suitable for the river Brahmaputra, because of the presence of anastomosing anabranches, which behave in a manner similar to that of meandering rivers. Just three-grain sizes (coarse, medium-fine and fine) were used to run the C-L models because no data were available to define the silt and clay fractions of the suspended load sampled in the Brahmaputra at Pandu. The only suspended load was modelled because no measurements of bedload are made in the Brahmaputra.

Initial runs established that the C-L models failed to produce a number of sub-channels and braid bars comparable to those present in satellite images (Figure 7.1). Despite this, the C-L models were able to simulate the main morphological features, including stable and deformable sandbars and islands, switching and migration of the thalweg channel, and lateral migration in anastomosing anabranches. Figure 7.1 compares morphological changes output by the C-L hindcasting model (*Hi*) for 1998 and 2009, and the C-L forecasting model (*Fo*) for 2020 and 2030 *(Note: both forecasting models use the H08 model for future hydrology)* to satellite images *(St)* taken in 1998, 2009, 2015 and 2018.

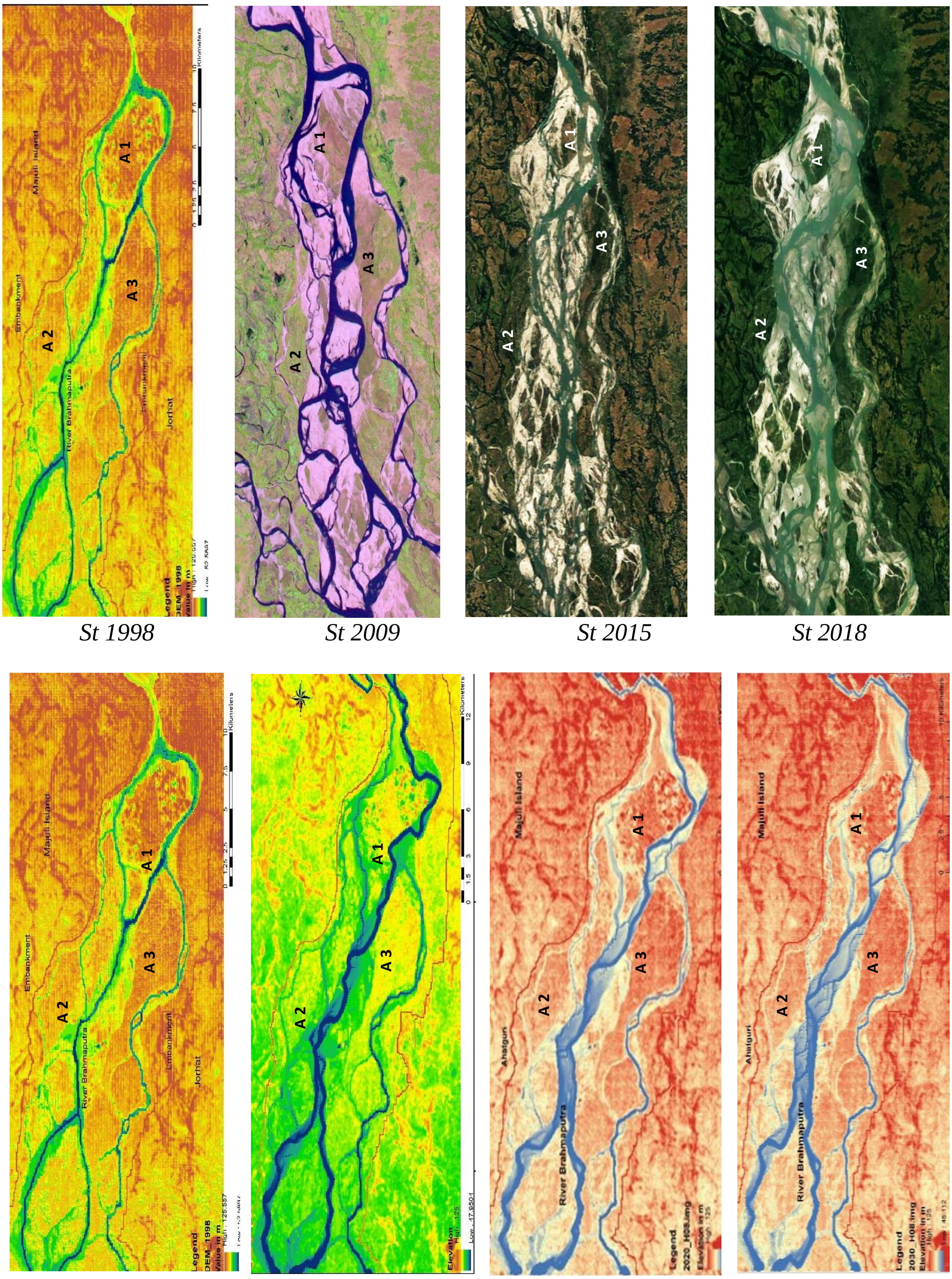

St 1998 *St 2009* *St 2015* *St 2018*

Hi 1998 *Hi 2009* *Fo 2020* *Fo 2030*

Figure 7.1. Comparison of C-L model outputs with satellite images. Compare Hi 1998 with St 1998, Hi 2009 with St 2009; Fo 2020 (H08) with St 2015, and; Fo 2030 (H08) with St 2018. St = Satellite imagery, Hi = hindcasting model, Fo = forecasting model.

The greatest agreement between observed and forecasted C-L model results are the northward lateral migration of thalweg channel and highly braided channel in the study reach as outlined in chapter 7. Although the magnitude of lateral migration of the thalweg channel and number of the braided channel were not similar. Similarly, the size of the sandbars was not precisely same as seen in the satellite imageries (Figure 7.1). This was due to inadequate suspended sediment data used to model the C-L models. As discussed in chapter 2 nearly 50% of suspended sediment load was measured from the river banks and sandbars of the river Brahmaputra during the fieldwork. There was no continuous daily silt data available to model the landscape evolution of the river Brahmaputra. Besides this, the coefficient of vegetation shear stress was same for different types of the sandbar in the C-L model (discussed in chapter 5). Hence there was a least agreement on the rate of sandbar formation and deformation due to inadequate data and uncertainty of vegetation shear stress (τ_{crveg}) parameter.

A short-term morphological study was conducted by Karmakar et al., (2016) for the river Brahmaputra further downstream of Majuli Island near Guwahati. A 2D CFD model Mike 21C was used to model channel morphological change for 12 km reach for two consecutive pre and post-flood season in 2007 and 2008. Acoustic Doppler current profiler (ADCP) was used to generate bathymetry data and hydrological data. The study predicted the alignment of the thalweg channel for navigation purpose and also determined the best groyne field based on scouring, deposition and channel alignment and dredging volume. The channel alignment was validate using satellite images (Figure 7.2). Their results show that they were able to capture the shape of the channel, therefore, there was a strong agreement in the channel alignment.

On the contrary due to the paucity of hydrological data a simplified reduced complexity model was used in this research to model 40 k reach and for 20 years. The rcm model was simulated using estimated hydrological and bathymetric data. Nonetheless, the use of ADCP for a PhD project will be expensive therefore bathymetry data were generated using surveyed cross-section data of Water Resource Department and SRTM data. However, this study was able to achieve to forecast the medium-term channel evolution of the river which encompasses lateral thalweg migration, braiding intensity of the channel and bar formation and deformation. The hindcasted models were validated by the application of planform indices using satellite images due to the absence of bedload data or results from the previous studies. This is the first research undertaken to hindcast and forecast medium-term landscape evolution of the river Brahmaputra. This kind of reduced complexity landscape evolution model which was performed in the river Brahmaputra near Majuli Island can be replicated in other parts of the river Brahmaputra to model the long-term morphological changes occurring in the channel.

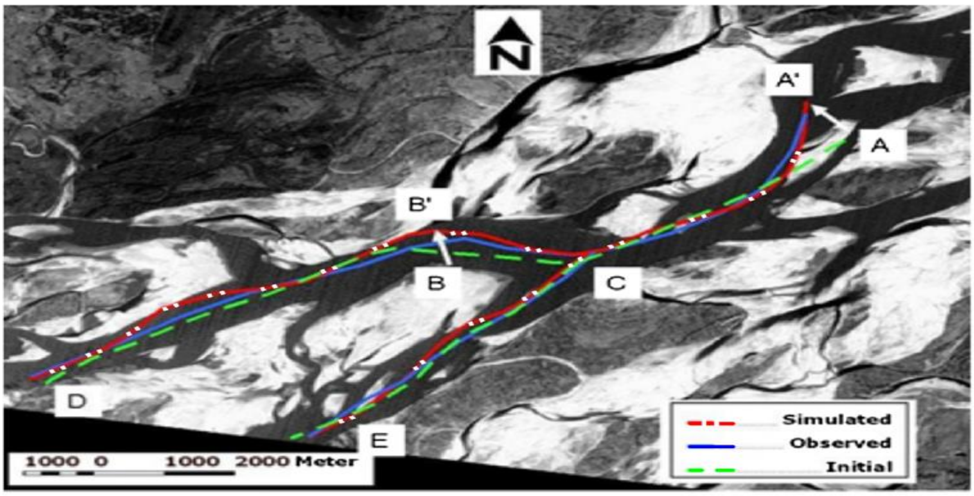

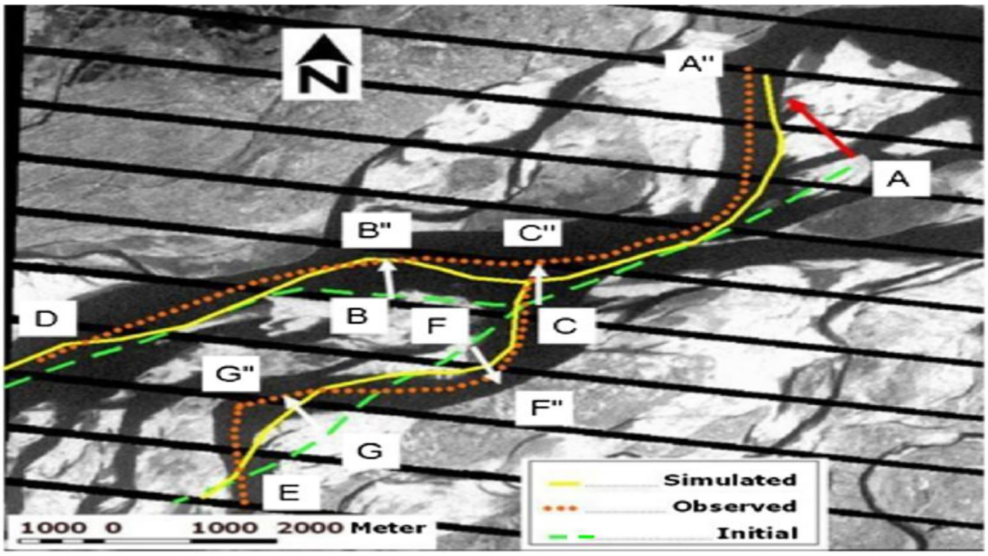

Figure 7.2: Morphological changes in thalweg: (a) 2007 post flood season (base map data from Indian Remote Sensing); (b) 2008 post flood season (base map data from ETM+ USGS). Source: (Karmakar et al., 2016).

8.4 Third contribution to knowledge: Development of novel braiding indices to quantify planform changes and validate model outcomes in braided rivers, including classified rivers where access to data is restricted.

Braided rivers are characterised by a multiplicity of laterally-mobile and intersecting sub-channels (Leopold and Wolman, 1957). According to Egozi and Ashmore, (2008), there has been a negligible amount of quantitative analysis on ways to quantify the degree of braiding and its response to changes in the variables that control morphology and drive channel evolution. Generally, indices of braiding pattern and intensity have been based on (i) bar dimensions and frequencies (Brice, 1960, 1964; Rust, 1978; Germanoski and Schumm, 1993); (ii) the number of channels in the network (Howard et al., 1970); and (iii) the total channel length within a given river length (Hong and Davies, 1979; Mosley, 1982; Friend and Sinha, 1993).

Germanoski and Schumm (1993) modified the Brice index by adding a total number of bars (N_b) per reach length (L_r) (Figure 7.3A). Rust (1987), on the other hand, measured braids and channel wavelengths using the mid-line of the channel surrounding each bar, in order to minimise sensitivity to stage variation. Howard et al. (1970) proposed two braiding indices, which are known as 'channel count indices'.

These channel count indices are:

(i) the mean number of links intersected by cross-sections of the river in successive river length (Figure 7.3D),

(ii) the total number of links in the measured reach (Figure 7.3E).

On the other hand, Hong and Davies (1979) proposed a total sinuosity index by computing the total length of channels per unit length of the river. Mosley (1982) has modified the total sinuosity index by substituting the straight-line reach length with the length of the main channel. Other studies (Ashmore, 1991; Chew and Ashmore, 2001) have also applied a 'channel count index'. In 2004, Sharma first proposed a new braiding index known as Plan Form Index (PFI), which measures mean flow intersecting the cross-section, mean width of the channel and number of braided channels. As part of this research, the PFI was reconsidered and improved to produce the new Modified Plan Form Index (MPFI) (Figure 7.4), which provides a better parameter with which to quantify

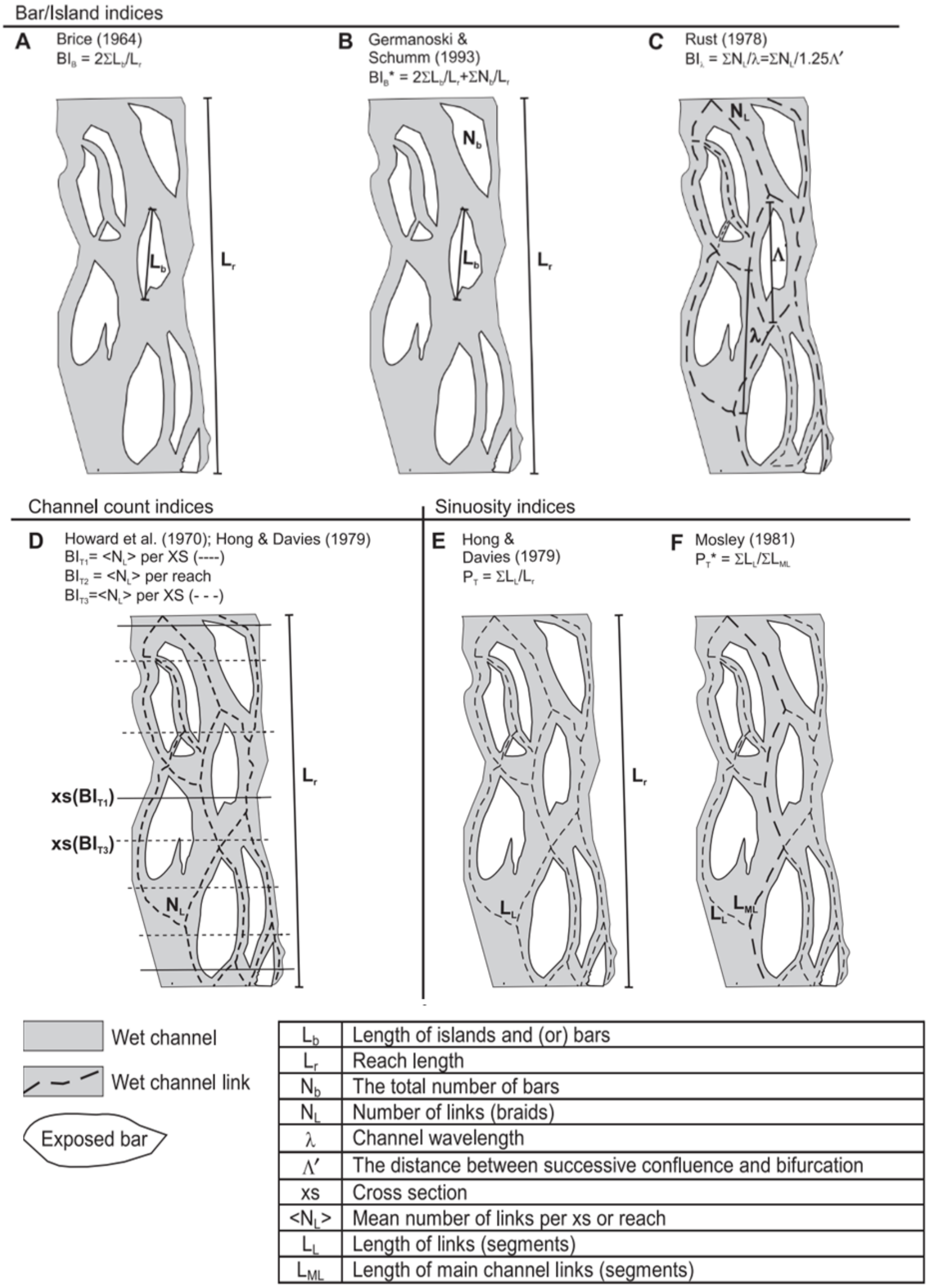

Figure 7.3. A selection of braiding intensity indices and the parameters measured to calculate the value of each index. In diagram C, the thickest line denotes the first-order channel (Williams and Rust, 1969). Source: Egozi and Ashmore (2008).

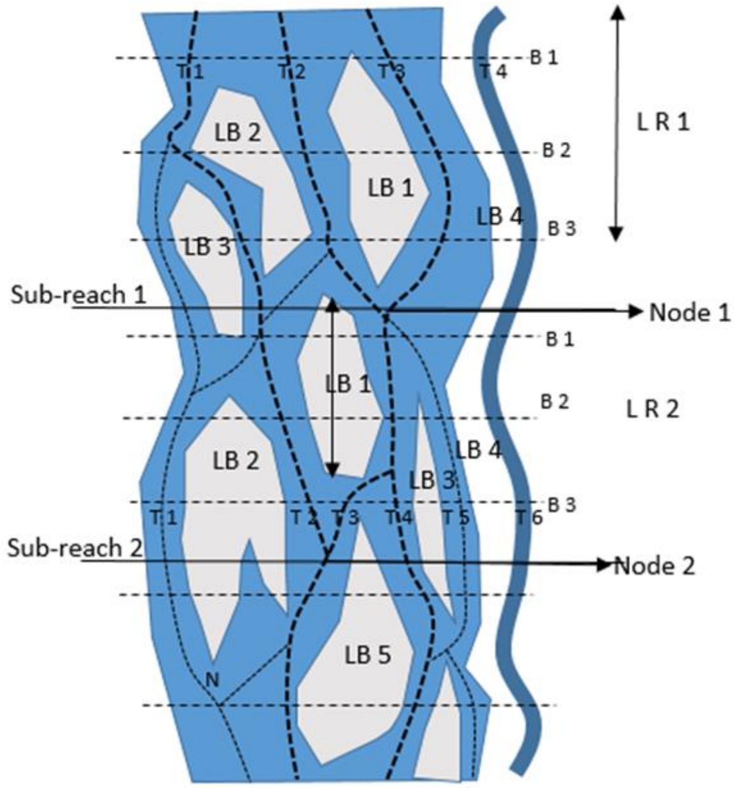

Figure 7.4. Modified Plan Form Index and its parameters, where, LB = length of the bar, LR = length of a node or reach, T = flow top width, B = channel width, N = number of sub-channels or anabranches.

changes in the braiding intensity in a reach that occur as the river morphology evolves or responds to changes in the controlling variable. The MPFI measures the lengths of braided bars, mean width of the channel, mean channel flow intersecting the cross-section and number of braiding channels in a reach.

Like the Germanoski and Schumm (1993) index, MPFI reliably represents braiding intensity because it decreases the probability that a reach with a single, large braid bar can have an equivalent or larger MPFI value than a reach with several, smaller bars. In a braided river, braiding intensity is positively correlated with the channel width. MPFI reflects this because it takes the mean width of the channel into account. Again, this strengthens the utility of MPFI as a measure of braiding intensity. Additionally, the node used as the basis for measuring MPFI is a user-specified reach. Therefore, MPFI is able to capture features of the local morphology and morphological changes in the reach. This makes MPFI suitable

Figure 7.5: Causes and effects of braiding mechanism.

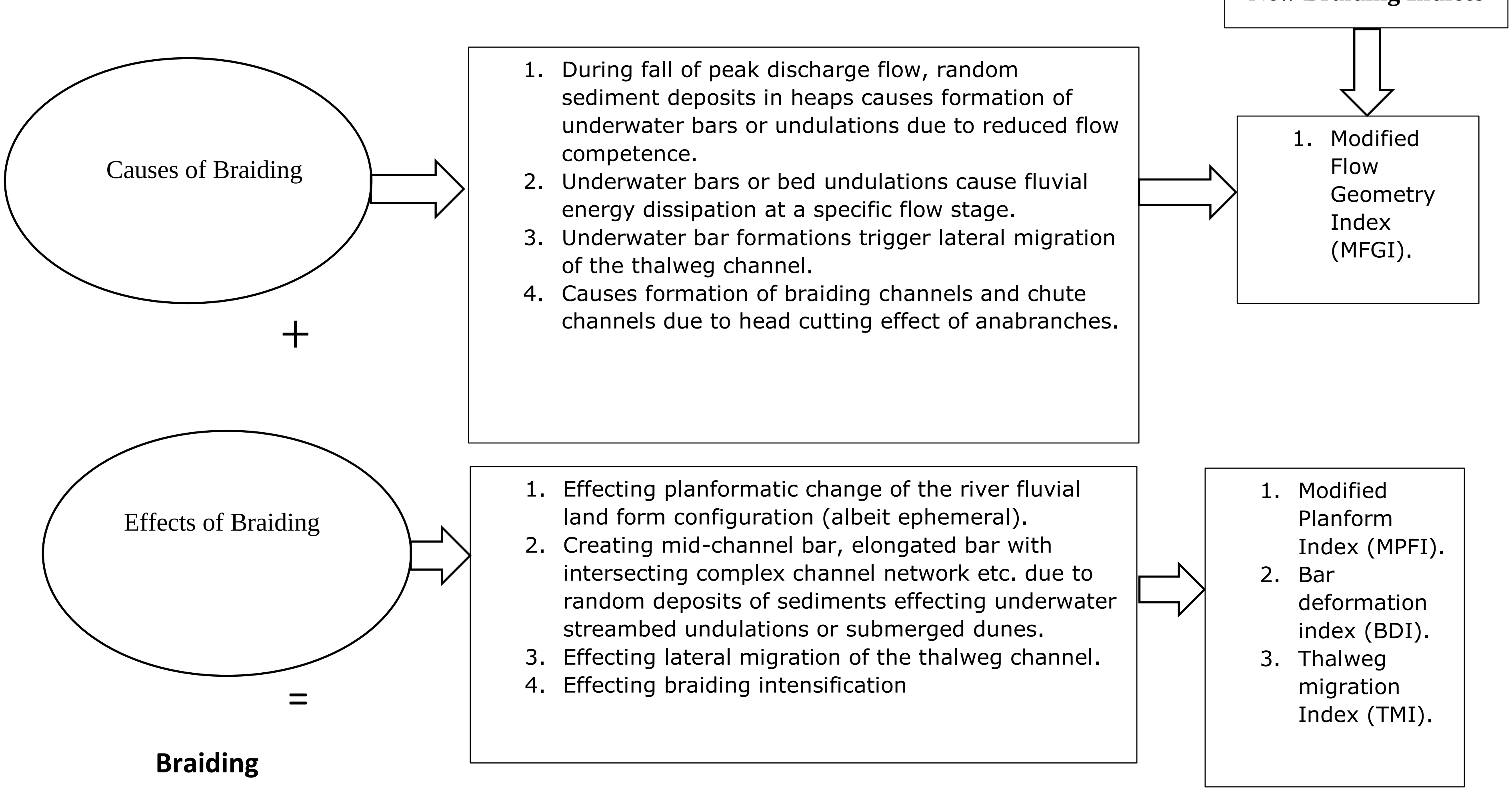

for representing braiding intensity in complex, braided rivers which have elements of anastomosing, anabranching and meandering patterns, because it takes into account the mean flow which intersects the cross-section (the emergent bar) at a specified stage. The stage is associated with the mean annual discharge. This removes the stage dependency that limits the utility of earlier braiding indices.

In the previous braided river morphological studies, the quantification of the cause of braiding was not addressed. The braiding indices such as Brice (1964), Chew and Ashmore, (2001) etc. were able to quantify the effect of the braiding mechanism where their end product is to quantify the braiding intensity of the river channel using satellite imageries. These studies have not taken into account the underwater undulations in energy dissipation in creating braiding in there braiding indices. These undulations regulate the physics of braiding mechanism where they control the energy loss or energy conservation in the river channel based on a specified stage flow. The underwater undulation causes turbulence in the boundary, these turbulence cause energy dissipation in the channel. During flood, the capacity of the channel to transport sediments becomes high while on the falling of flood it becomes weak and started depositing sediment in a random manner. This resulted in creating mid-channel bar, elongated bar and anabranches in the channel. All these braiding mechanism results in lateral shifting of thalweg channel or channel capture of the thalweg channel by chute channels. In this research, MFGI quantifies the cause of braiding by quantifying the underwater undulation at a specified flow stage (see Figure 2.15). The higher MFGI value will result in more loss of energy and becomes hydraulically incompetent to transport the sediments. However, the MPFI, TMI and BDI indices are offshoots of MFGI. The end product of these three braiding indices is to quantify the effect of braiding intensity in terms of planform change (MPFI), the lateral shift of the thalweg channel (TMI) and bar formation and deformation (BDI). The lateral shift of the thalweg channel is the effect of underwater bar disposition. TMI measure this lateral shift of the thalweg channel at a specified flow stage. Whereas BDI quantifies the reshaping of the sandbars also at specified flow stage. The above stated newly developed braiding indices are suitable for studying spatiotemporal changes occurring in a braided river.

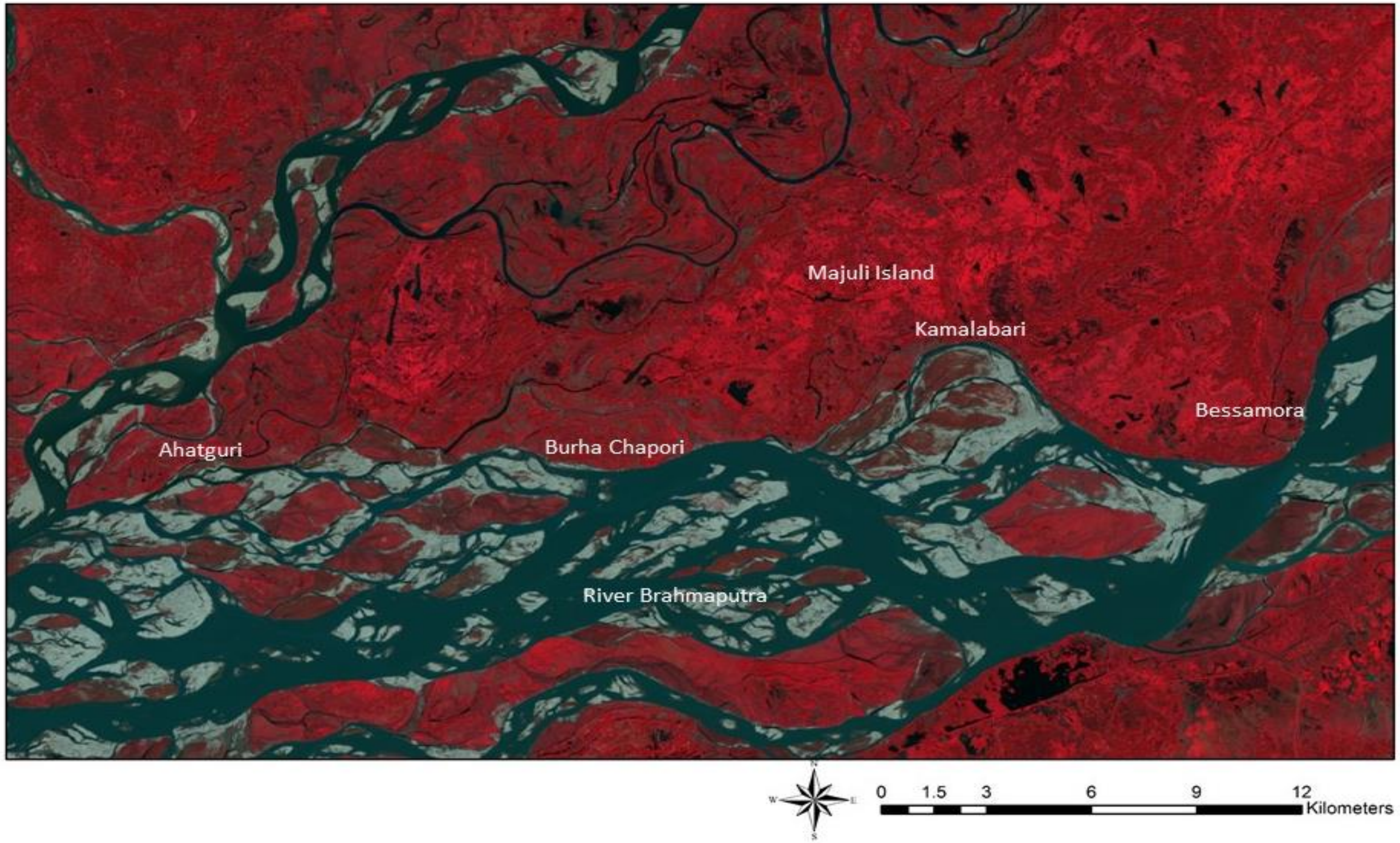

Figure 7.6: Selected locations used to calculate MPFI, MFGI and TMI near South Majuli Island using Landsat images (2015).

Table 8.2: Summary of MPFI, and MFGI, TMI at selected locations near South Majuli Island using Landsat images.

Location	MPFI (2007)	MPFI (2015)	MPFI (2018)	MFGI (2007)	TMI (2007)	TMI (2015)	TMI (2018)
Bessamora	7.54	7.32	7.35	6.46	0.94	0.98	0.98
Kamalabari	5.77	5.45	5.40	12.56	1.2	0.99	0.99
Burha Chapori	2.90	2.67	2.65	26.21	1.38	1.44	1.44
Ahataguri, Brahmaputra Subansiri confluence	2.26	2.22	2.20	56.66	1.38	1.46	1.46

From the table, it can be discerned that with the increase in the value of MFGI, the MPFI value decreases (i.e. more braiding). Therefore this justifies the fact that the higher is the MFGI value higher is the braiding intensity and lateral shifting of the thalweg channel. MFGI value is based on the measured cross-sections collected from Water Resource Department. There was no recent cross-section survey undertaken for the river Brahmaputra hence MFGI cannot be calculated for recent years. BDI was calculated for individual bars which are discussed in chapter 3, 6 and 7. When the size of the bar increases braiding intensity increases. This is because the channel becomes shallower and narrower due to the falling of flood which makes the channel hydraulically less efficient and starts depositing in the edge of the existing braided bar. The table exhibits that the river channel near Bessamora and Kamlabari (Figure 7.6) was relatively moderately braided than Burha chapori and Ahataguri where the channel appears to be highly braided. The lateral movement of the thalweg channel also depends on the pattern of the sediment deposition. Higher is the braiding intensity due to random sediment deposition resulting in pushing the channel towards northward near Majuli Island.

An important application of the novel braiding indices is in validating morphological models, including RCMs and cellular automata, like the C-L models used in this research. The significance of this approach is explained below.

Morphological river models may be validated using any of various techniques, including comparing model outputs to measured discharges, flow depths and inundation areas, to monitored sediment yields, or to surveyed bathymetries (Murray and Paola, 2003; Thomas and Nicholas, 2002; Coulthard et al., 2007; Meadows, 2014). For example, in a study of the River Waitaiki, New Zealand the morphological model was validated by comparing modelled bedload yield to measured bedload yield. But bedload cannot be measured in the huge river like the Brahmaputra. Suspended load is measured in the Brahmaputra, but it is 80% or more ‘wash load’ – that is sediment that is passing through the reach, but which is finer than the bed material and which does not play a significant role in forming its morphology. Hence, it is difficult to validate a morphological model using measured sediment data in a river like the Brahmaputra, where only suspended sediment load data is available.

Recognising this problem, a viable, alternative approach to validating the braided river models developed in this reach had to be identified. The solution found was to develop and apply novel, planform-based braiding indices that could be calculated using only the available, sequential satellite images and channel morphology maps output by the C-L models (Hooke, 1984, Nicholas, 2005). This is consistent with the proposal by Nicholas (2005) that model evaluation should be carried out by (i) comparison of specific, morphological features identified using satellite images with model prediction, and (ii) use of statistical characteristics of braided river systems (braiding intensity, average channel width) over sufficiently long timescales for changes to be significant.

While the papers cited above are relevant, the idea for the new approach developed here actually stems from the observation by Coulthard et al., (2007) that modelled planform changes could potentially be compared to observed planform changes using the braiding indices.

It was recognised that opportunities for validation using the new approach are limited by the frequency at which cloud-free satellite images of the study reach are available. Nevertheless, in the case of classified or remotely-located and inaccessible rivers, there may be no practical alternative to validating morphological models using planform indices. It may therefore be concluded that the universal availability of remotely sensed aerial images and the reliability of the new, non-stage dependent braiding indices does provide a practical method for validating reduced complexity models of large braided rivers where hydrological, hydraulic and sediment data are non-existent or restricted and the river bathymetry or cross-sections are either lacking or classified.

To generate indices suitable for braided river model validation, some reach-scale generalisation of braided river features and behaviours is required (Bridge, 1993; Egozi, 2008; Mosley, 1983; Murray and Paola, 1996; Sapozhnikov, 1998). However, when available indices were considered, it was determined that they did not provide a suitable basis for the reach-scale generalisation necessary to support model validation due to the limitations detailed in Chapter 3 and summarised above (for example, stage-dependency). This is why modified indices were developed. Hence in this research new braiding indices were developed and used to measure and validate planform change in a complex large river, for which there are no alternative approaches to model validation.

As outlined in Chapter 3 the newly developed braiding indices are

(i) thalweg migration index (TMI), which measures the lateral movement of the thalweg sub-channel;

(ii) modified planform index (MPFI), which measures braiding intensity and changes therein;

(iii) modified flow geometry index (MFGI), which measures variations in the morphology of the submerged parts of the river channel, and;

(iv) bar deformation index (BDI), which quantifies relative changes in the sizes of islands and/or braid bars.

In summary, development of these four indices has contributed to knowledge by facilitating quantification of changes observed during the morphological history of Majuli Island, as well as providing the basis for model validation through hindcasting, and for quantitative forecasting of the future possible morphological evolution using appropriate models. Finally, the indices also offer a platform on which to assess the impact of physical processes of erosion and sedimentation on the people and property within and along the river corridor.

8.5. Recommendations that could help inform policymakers, water resource planners, and river engineers seeking solutions for sustainable bank stabilisation and river training works needed to protect lives, livelihoods and property in vulnerable communities on Majuli Island.

8.5.1 Context

Contributions to knowledge resulting from the basic research performed in this project and reported above have the potential to help inform policymakers, water resource planners and river engineers responsible for managing river-related risks to people (including their livelihoods and their property), and key infrastructure (especially, flood banks) on Majuli Island. In this section, risks associated with flooding, large-scale lateral erosion, local-scale bank and bar erosion and lateral migration of the channel are dealt with in turn.

8.5.2 Identifying and assessing current and future erosion hazards and risks due to lateral migration of the Brahmaputra's thalweg sub-channel

Forecasts of future channel evolution produced by this research can be used to identify areas particularly liable to erosion caused by lateral migration of the thalweg sub-channel. An example is study braid bar A2 (*Burha chapori*), where there are risks associated with the lateral erosion hazard because, although the bar is sparsely vegetated, it is inhabited.

According to both the C-L forecasting models, study bar A2 (*Burha chapori*) and adjacent sandbars might be significantly eroded within the next twenty years due to continued (or accelerated) northward migration of the thalweg sub-channel towards Majuli Island. Additionally, it is forecast that the thalweg sub-channel may bifurcate in the vicinity of A2, which would be likely to result in local widening of the channel and further erosion of this sandbar (Figure 7.7).

Study bar A1 (Figure 7.8) is another unvegetated bar that is deformable and highly transient in nature. However, unlike A2, it is not inhabited. Both historical satellite images and hindcasting models establish that the position, size and shape of this sandbar fluctuate frequently depending on the magnitude of the monsoon flood, and forecasts produced by both C-L models indicate that study bar A1 will continue to deform and shift in the future. However, at A1 the erosion hazard poses little or no risk to people or property because the land is undeveloped and uninhabited. This will also be the case in future provided that the bar remains uninhabited.

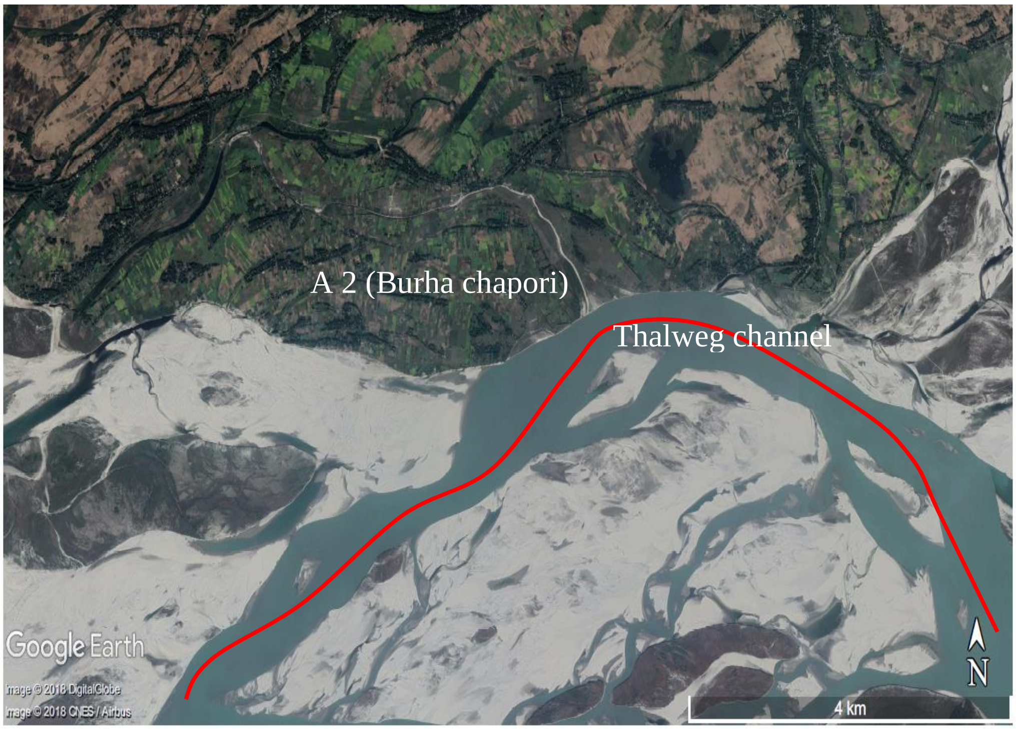

Figure 7.7. Image showing the A2 braid bar in 2018. The bar is located adjacent to the thalweg sub-channel, and prone to future erosion if the thalweg continues to migrate northwards.

The information that could be useful for local authorities and river engineers which emerges from monitoring of past bar deformation and forecasting of future dynamics of the sub-channel-sediment-sandbar system is that it may be wise in the coming years and decades to relocate the current inhabitants of braid bar A2. This can be executed by attempting to stabilise this sandbar means fighting one of the main characteristics of morphological evolution in the mighty Brahmaputra, which is northward migration of the thalweg channel. Model forecasts also indicate that the future security and safety of any population that might develop on this study bar A1 could not be guaranteed, for the same reason. Hence, it would be wise for development or the establishment of any permanent settlements on this island to be discouraged or, if possible, prevented for the foreseeable future.

In contrast to study bars A1 and A2, the future for A3 that is forecast by C-L modelling is that historical trends of vegetation colonisation and stabilisation of the land are likely to continue (Figure 7.9).

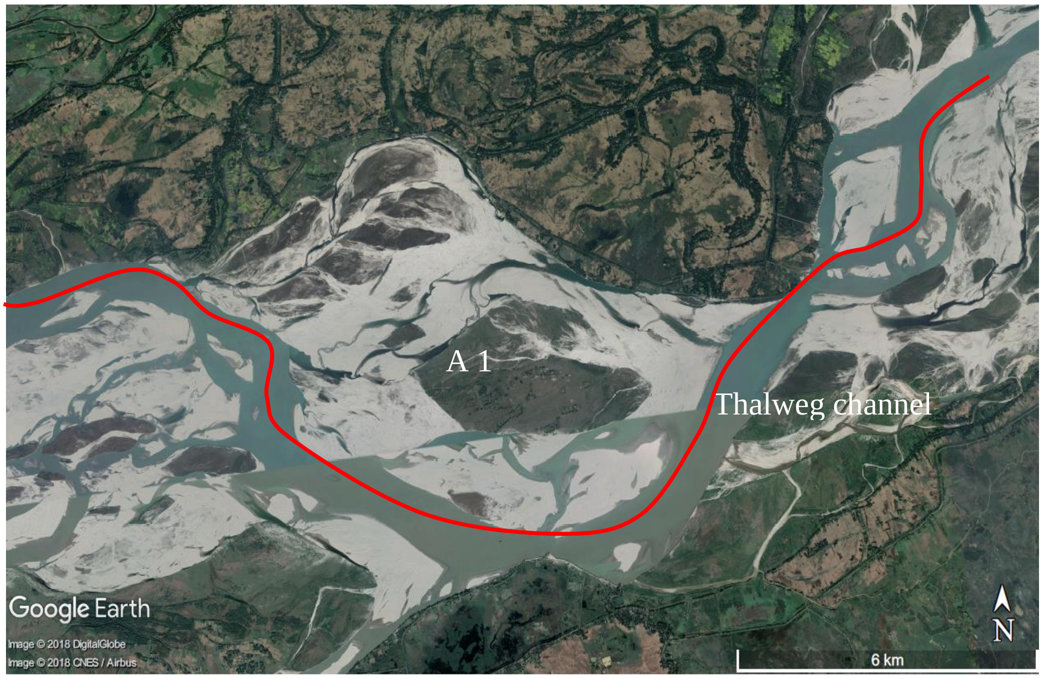

Figure 7.8: 2018 image showing the A 1 sandbar, which is the most transient of the three bars studied in detail in this project.

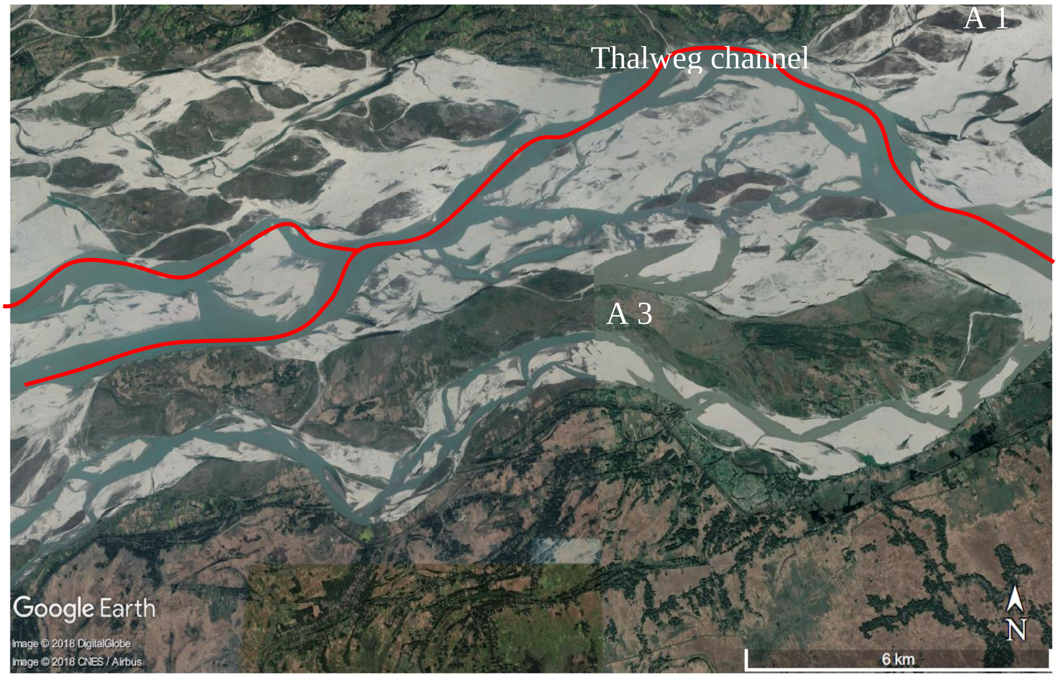

Figure 7.9: 2018 Image showing A 3 sandbar, which has elongated and stabilised due to colonisation by dense vegetation.

This is understandable because, unlike study bars A1 and A2, this braid bar now lies to the south of the thalweg sub-channel, which is therefore migrating away from it. While nearby sub-channels in the braided river will in future continue to pose local erosion hazards to this macro-bar, it is likely that its evolution will be dominated by growth due to sediment accretion that dominates scour locally, as well as at the reach-scale. The message to local authorities and river engineers is that erosion hazards associated with small sub-channels may be manageable using conventional engineering methods, and that limited development and some habitation of this bar may be sustainable, provided that not too much of the dense, natural vegetation that is key to its stability cleared for settlements or, particularly, agriculture. That is easy to say, but it could be difficult to manage in practice. In that context, it would be very useful for the authorities, engineers and village leaders to be able to access and understand the outputs of reliable forecasting models that demonstrate the potentially catastrophic consequences for these communities should future clearance of natural vegetation allow renewed erosion and deformation of their land on a scale that engineers simply could not prevent.

8.5.3 Flood prevention and management of hazards to key infrastructure

Flooding is a major hazard threatening communities on Majuli Island and flood prevention relies primarily on the protection provided by 12 embankments (Figure 7.10).

With respect to future flood risk management, it must be borne in mind that eight of these twelve embankments have already exceeded their engineering design lives (Table 8.3) and these embankments are known to have lost some of their capability to withstand floods due to their age and condition (Society for Socioeconomic Development, 2013).

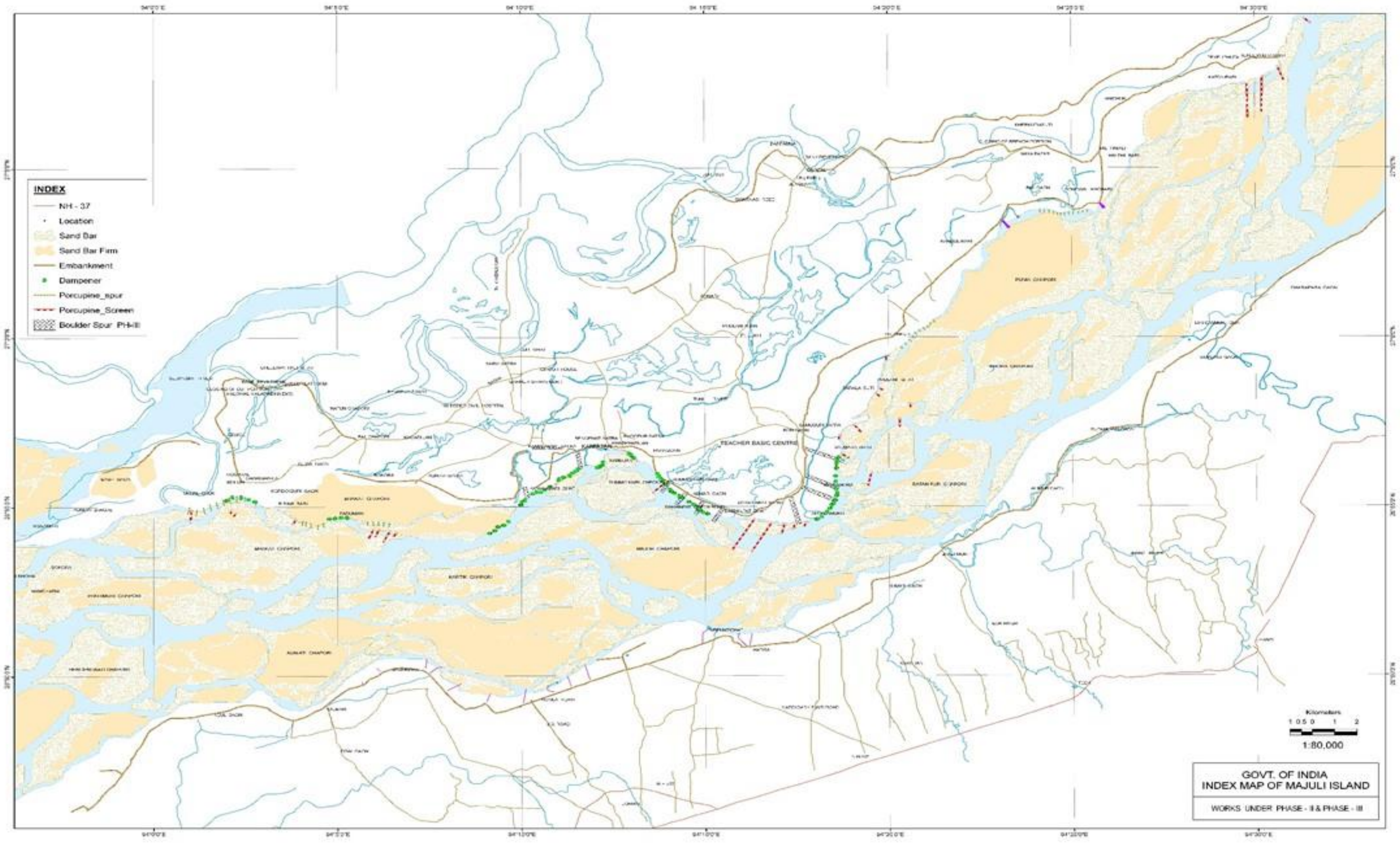

Figure 7.10. Flood embankments and river training structures intended to protect them at critical locations on Majuli Island.
Source: Brahmaputra Board, Guwahati

Table 8 3: List of embankments and their expiry dates.

Embankment	Date of expiry of design life
Subansiri (mile 10 to 21)	1995
Kherkhuti	1991
Budhakalita – Kakorikota	1987
Tekelifuta – Haldibadi, Kherkhuti	1981
Haldibadi – Bessamera	1978
Kamalabari – Budha Kalita	1980

These embankments are aptly described as the lifeline of Majuli Island, which is worrying in a future which, according to the H08 hydrology model, is likely to feature larger and more frequent monsoon floods. In this research, the study reach includes the Kamalabari - Budha Kalita embankment, which is over 35 years old.

Management of flooding and threats to flood defence infrastructure on Majuli Island are being tackled by the Government of India on a long-term as well as a short-term basis. To identify short-term measures, the Brahmaputra Board has constituted a Committee of Experts comprising senior officers from the Water Resources Department, Central Water Commission, Central Water and Power Research Station and the Brahmaputra Board itself to identify and suggest immediate anti-erosion measures to be taken up for protection of key infrastructure on Majuli Island. Such is the magnitude and wide extent of the problems identified by the Committee of Experts that the Brahmaputra Board has, acting on their recommendation, formulated a scheme to spend the equivalent of over US$ 92 million just to achieve short-term reductions in the risks associated with river flooding and erosion.

These short-term measures are not regarded as adequate to solve the problems faced by residents of Majuli Island. Hence, with regard to long-term measures, the Brahmaputra Board prepared detail project report (DPR) amounting to nearly US$ 13 million for protection of Majuli Island from flooding and erosion. This scheme is being implemented in three phases. Phase-I work (costing US$

6 million) was approved by the Government of India in January, 2004 and work began immediately. The work had three components:

(a) Closing of breaches in the embankments.

(b) Raising and strengthening of the embankments.

(c) Casting and laying on permeable reinforced cement concrete (RCC) porcupine screens, spurs and dampeners to protect embankments from erosion at critical locations indicated in Figure 7.10.

To investigate the effect of the river training measures listed in component (c) on braiding forms and processes in the Brahmaputra, the new braiding indices developed in Chapter 3 were applied to the study reach for the periods prior to and after 2004. From the braiding analysis of Landsat images and C-L models, it was established the river channel braid was less intense and the river was relatively stable prior to 2004.

The results (reported in detail in Chapter 3) demonstrate that, following construction of bank protection and river training works, braiding intensity increased sharply and the channel widened. Also, the thalweg channel started to migrate northwards after flood event of 1993. There was deficit of rainfall during 1991 and 1992 (Dar et al., 2000) and during these two years due to low discharge flow made the river incapable to transport the sediment load and unevenly depositing the sediment and joining the small sandbars near A 3 sandbars (Table 3.4) into one elongated and a stable sandbar (see Figure 2.19). This made the thalweg channel shift northward and through time it has become deeply entrenched along the bank of Majuli Island. As discussed in chapter 3 the reach was moderately braided before 2004 river training measures were executed this is because the river was flowing following the natural depression (cause due to northward tilting of the riverbed) present near the southern tip of the Majuli island i.e. near the confluence of the river Brahmaputra and river Subansiri (see Figure 3.1). During this process, the river started eroding the river banks and sandbars which are adjacent to the thalweg channel. Therefore to protect these vulnerable areas Govt. of India in January 2004 installed RCC porcupines, spurs and dampeners (Figure 7.10) in this area as a measure to protect the banks from erosions. However, this resulted in more damage to the riverbed as the river becomes uncontrollable and started eroding those areas which were previously never eroded, creating the river wider and shallower, thus highly braided. Hence, the original research performed in this study provide evidence to support the argument that attempts to 'train' the great river and protect its northern bank from erosion have not only proved inadequate (see below) but appear to have even made matters worse.

The 'protection' provided by the porcupine screens, spurs and dampeners constructed in 2004 have proved inadequate and short-lived and, in December 2017, the Brahmaputra Board framed a new scheme for the protection of Majuli Island from flooding and erosion by the Brahmaputra. The major elements of this new scheme include construction of further hard engineering structures including:

(i) Bank revetments made of geo-bags filled with earth/sand.

(ii) More RCC porcupines;

(iii) A sluice gate at the mouth of the Tuni river.

(iv) A pilot channel with a length of 3.5 km (not much detail given on the pilot channel which was published in Press Information Bureau Government of India, Ministry of Water Resources, 28th December, 2017).

Based on these proposals it may be concluded that the Board are intent on sticking with conventional bank protection and river training approaches, even despite experience gained since the 2004 works. In this context, the forecasting models developed in this research could be rerun, with the effects of these newly proposed works simulated through changes to bathymetry and bank erosion resistance, to predict the likely dynamic-response of the thalweg channel migration and width in the Brahmaputra. This could assist future decision making with respect to the need to move from conventional to sustainable flood and erosion management approaches, like those described below in Section 8.4.4.

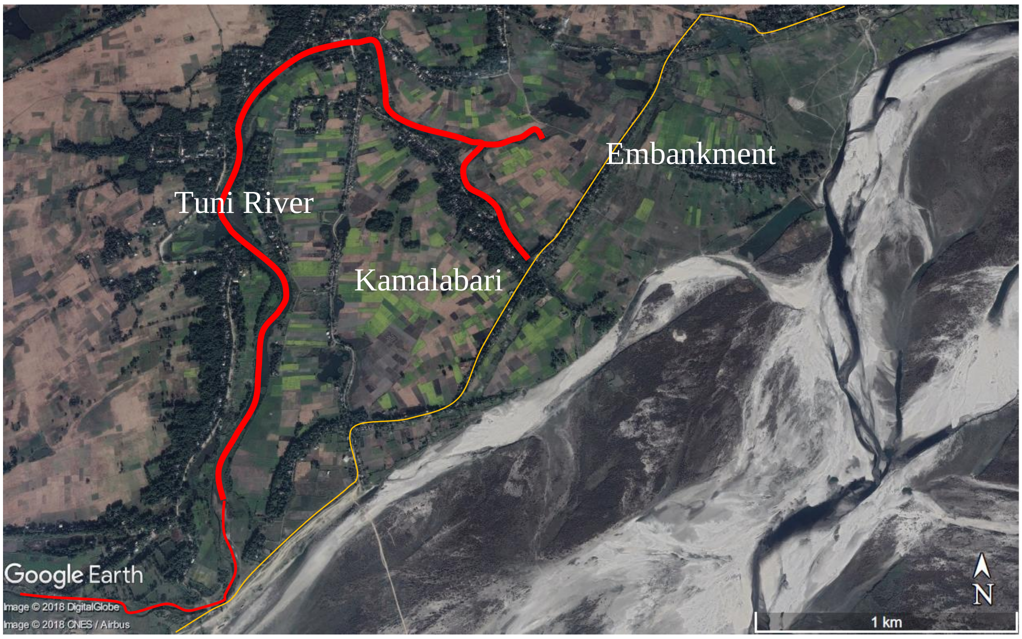

Figure 7.11. Image showing the River Tuni, which has been blocked at its outlets.

Notwithstanding these comments regarding renewed attempts to stabilise the north bank of the Brahmaputra and train its course away from the flood embankments at critical locations, one aspect of the newly-proposed works that may be advantageous is the plan to build a sluice at the mouth of the River Tuni.

During fieldwork, while interacting with local people, it emerged that they do not support of creating continuous embankments to prevent flooding to keep out the river. According to them, when floods overtop or breach the embankments (which often happens) standing water is trapped on the landward side, inundating the land for periods of 10 to 15 days even after water levels in the river have subsided. This is due to the absence of spillways within the embankments to allow flood water to flow back out of the island after a flood.

Historically, the River Tuni (which is an inland river on Majuli Island draining to the Brahmaputra near Kamalabari) used to fulfil the function of draining floodwater back to the main river (Figure 7.11). This was the case because high monsoon floods in the Brahmaputra caused backflow in Tuni River, which inundated the interior of Majuli island. On these occasions, the Brahmaputra and Tuni became a single sheet of water with an average width of 9.5 km that inundated that part of the island to depths of 2 to 4 m. However, on the falling limb of Brahmaputra floods (as well as during locally-generated rainwater floods), the Tuni used to efficiently convey floodwater out from the Island and into the Brahmaputra. In recent years, the inlet and outlet of River Tuni have been blocked by embankments, creating longer-lasting floods because inland floodwater is unable to drain from the island and inundates it for longer periods. In this regard, the proposal to build a sluice gate at the mouth of the River Tuni is welcome and will be supported by the local population.

8.5.4 Sustainable flood and erosion management based on creating a green buffer strip around Majuli Island.

As set out in the preceding sub-sections, the results of the medium-term forecasts of future morphological evolution in the Brahmaputra made as part of this research project using the C-L + H08 model combination imply that risks associated with flooding, bank retreat and damage to key infrastructure located close to the southern edge of Majuli Island are likely to increase in the medium-term future. They further imply that attempts to protect the island and its key flood defence infrastructure using conventional bank protection and river training structures have not only been unsuccessful but may have made matters worse.

Consideration of the sheer scale, the complex nature of the multiple hazards posed by the huge river, and the failure of conventional measures (reviewed above) suggest that a new and radical approach may be required. One sustainable approach to reducing future flood and erosion risks, or at least maintaining them at current levels, could be to create a 500 m wide ‘green buffer’ between the River Brahmaputra and homes, properties and key infrastructure on Majuli Island (Figures 7.13, 7.14 and 7.15).

While, this approach differs radically from the conventional bank protection and river training measures employed to date, there is a precedent for flood and erosion buffering. The Ministry of Forest and Environment, Govt. of India, has created the Coastal Regulation Zone (CRZ), which is intended to prevent damage to coastal plains from coastal flooding and erosion driven by waves and extreme high sea levels associated with spring tides, storm surges and tropical cyclones. The CRZ occupies coastal land up to 500m from the normal High Tide Line (HTL). The CRZ extends in land along coastal creeks, estuaries, backwaters, and rivers in the form of 100 m wide zones on both banks. Within these demarcated areas, special steps are taken to safeguard the people, property and wildlife living in all the coastal plains of India.

During fieldwork on Majuli Island, interactions with local people revealed that the great majority would be in favour of the introduction of this kind of zonation in river floodplains along the margins of the island, which in terms of topography, physical scale and exposure to flood and erosion hazards, are actually not that different to coastal floodplains. That said, this kind of zonation has never been adapted to or applied in an inland river in India.

Based on the sheer size of the Brahmaputra, the huge volume of floodwater it discharges during high monsoon runoff years, and its capacity for extensive bank erosion, even during normal runoff year, the width of the 'River Regulation Zone' (RRZ) should be no less than that of the CRZ (500 m). Development of a 'green buffer' on the floodplain, braid bars and islands within the RRZ will not only help to safeguard the island from flooding and reach-scale bankline retreat, but will also reduce rates of local bank erosion and deformation in near-bank and bank-attached sandbars. Based on the propensity of the planform of the Brahmaputra to switch from wide, unstable and intensely braided to narrower, more stable and anastomosed in sub-reaches with more resistant banks (e.g. compare sub-reaches 2 (braided) and 1 (anastomised) as described in Chapter 3), an increase in erosion resistance in the southern part of Majuli Island should reduce braiding intensity, sub-channel instability and the rate of northward migration of the thalweg sub-channel. Specifically, evidence collected in this study suggests that broad-scale planting of trees and the herbaceous plants on a sandy braid bar like A1, which is currently very volatile in nature, could help convert it into a vegetated braid bar like A3, which is much more stable.

Further empirical evidence to support the proposal that a 500 m buffer strip could be effective comes from a study conducted by Biwas et al. (2000). An area was selected for experimental planting of herbaceous plants to reduce or eliminate bank erosion between Botiamari village and the mouth of River Tuni, which is an inland river on Majuli Island that drains to the Brahmaputra. The selected site was in the southern part of Majuli Island, which has been subject to serious erosion in recent years. As mentioned above in this chapter the mouth of river Tuni is blocked in recent years by extending the Kamalabari embankment stabilising this area.

The experimental site was a fragile section of bank extending 1.7 km along the margin of the Brahmaputra. In the test reach, the herbaceous species native to Majuli Island that were planted were: Indian doab (*cynodon dactylon*), wild sugarcane (*saccharum spontaneum*) and vetiver (*chrysopogon zizanioides*). As native species, these plants are well adapted to local conditions, being able to thrive in infertile, sandy soils, survive long-term inundation, and withstand extreme drought conditions, all of which are prevalent on Majuli Island. These plants are also known to be able to be able to resist high velocity water flows and to have excellent soil binding characteristics (Biswas et al., 2000). For example, doab and munja (*saccharum munja*) have soil binding capacities of 90 to 97%, and 92 to 96%, respectively and both of these species have proven highly effective in checking erosion through other experients performed along the Rivers Ganga and Varuna (Biswas et al., 2000).

Additional, practical evidence of the potential for vegetation to stabilise banks and bars at Majuli Island comes from the work of a dedicated individual named Jadav Payeng, who has devoted 30 of his 55 years of life to the cause of using trees to create habitat and protect part of Majuli Island from erosion by the Brahmaputra. He has almost single-handedly created the *Molai kathoni* (Molai forest), which is a 550 ha woodland near Kokilamukh in the Jorhat District which is a part of A 3 sandbar in this study. His success in creating the forest and stabilising the sand bar on which it stands was recognised at the highest level in 2015, when Payeng was the awarded the title 'Forest man of India' by the President of India.

Drawing on experience like that at *Molai kathoni (Figure 7.12)* and considering the results of historical analyses, hindcasting modelling and forecast modelling performed as part of this study, it is further recommended that the possibility of using planted vegetation to help stabilise bars in the study reach should be further explored.

The aim would be to divide the braided river into management zones with erosion hazard management within each zone being selected to be appropriate to the dominant trajectory of morphological evolution in that zone. As a first step, stable and unstable braid bars would be mapped, as indicated in Figure 7.13. It might and should be possible, through time, to improve the stability of naturally-vegetated islands and convert some of the unstable sandbars in braided pattern into stable, vegetated bars and islands. Pursuing this approach over decades, especially south of the thalweg channel, could result in transforming the unstable, braided planform into a more stable, anastomosed pattern, as indicated in Figure 7.14.

Figure 7.12: Map showing Molai Forest which is also a part of A 3 sandbar.

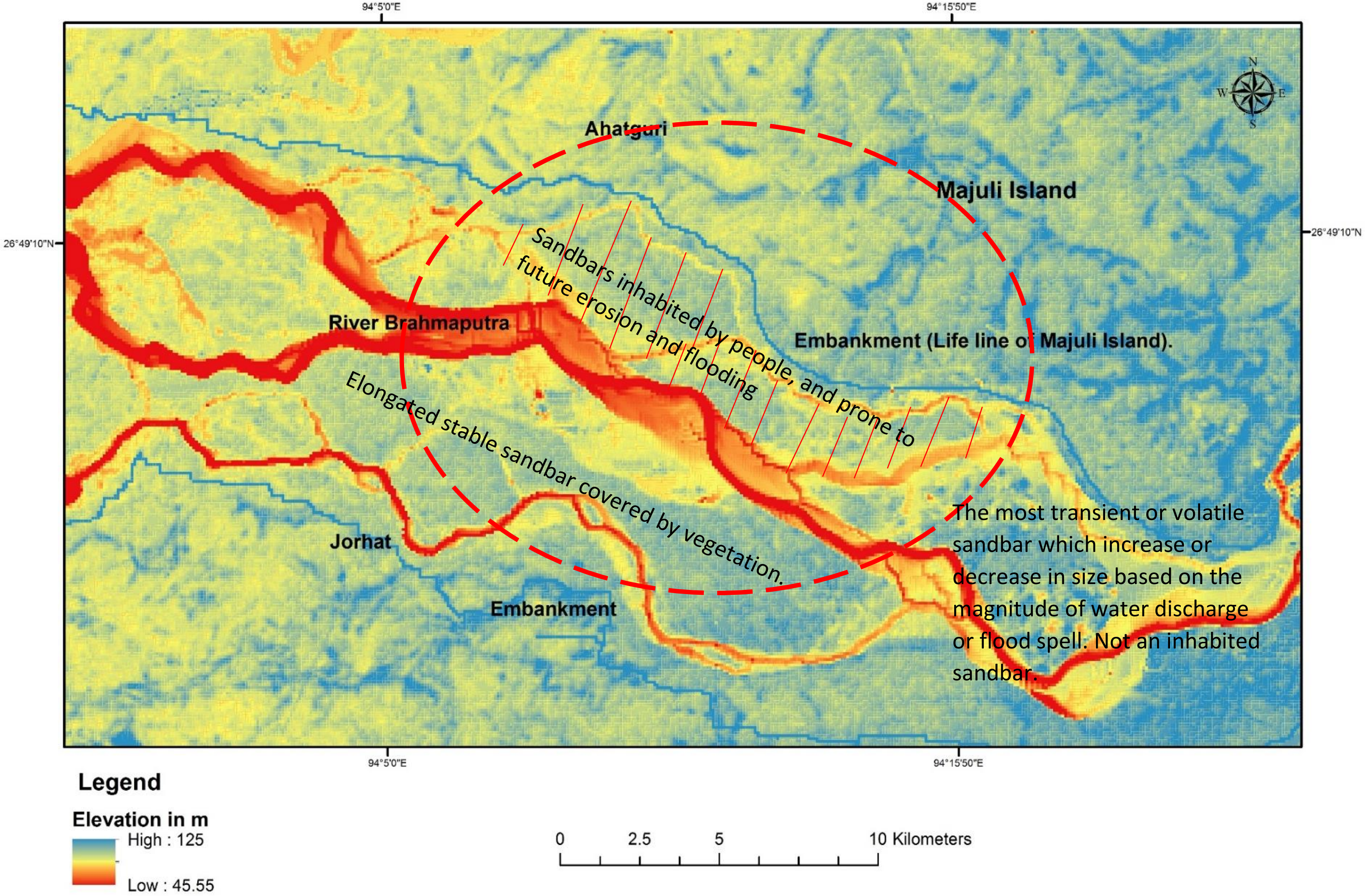

Figure 7.13. Stable and unstable braid bars in Brahmaputra near Majuli Island, based on C-L + H08 model forecasts.

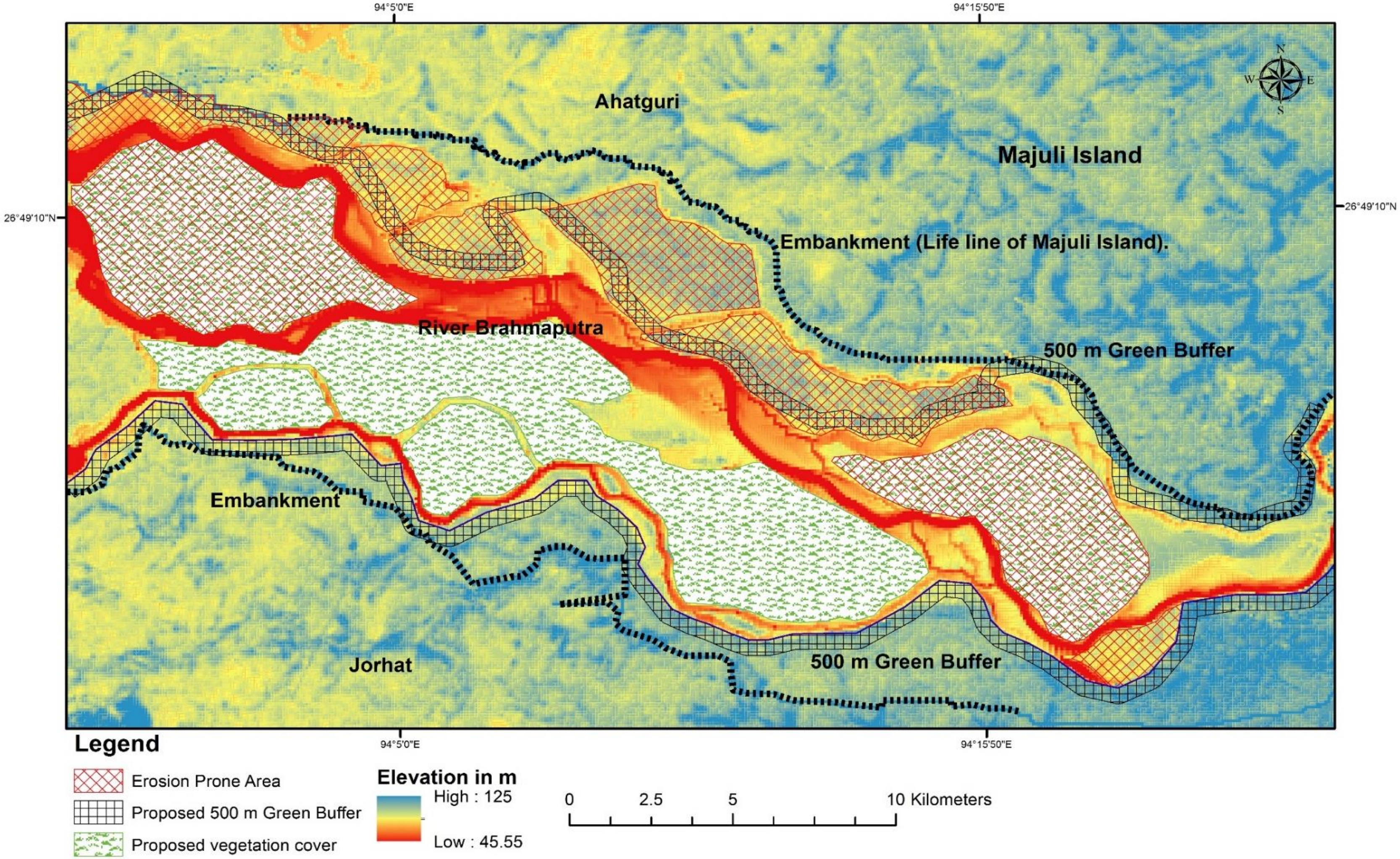

Figure 7.14: Indicative proposal for using planted vegetation to stabilise selected braid bar and banklines in the Brahmaputra near Majuli Island, based on interpretation of historical trends, hindcast modelling and morphological forecasting using the C-L + H08 model.

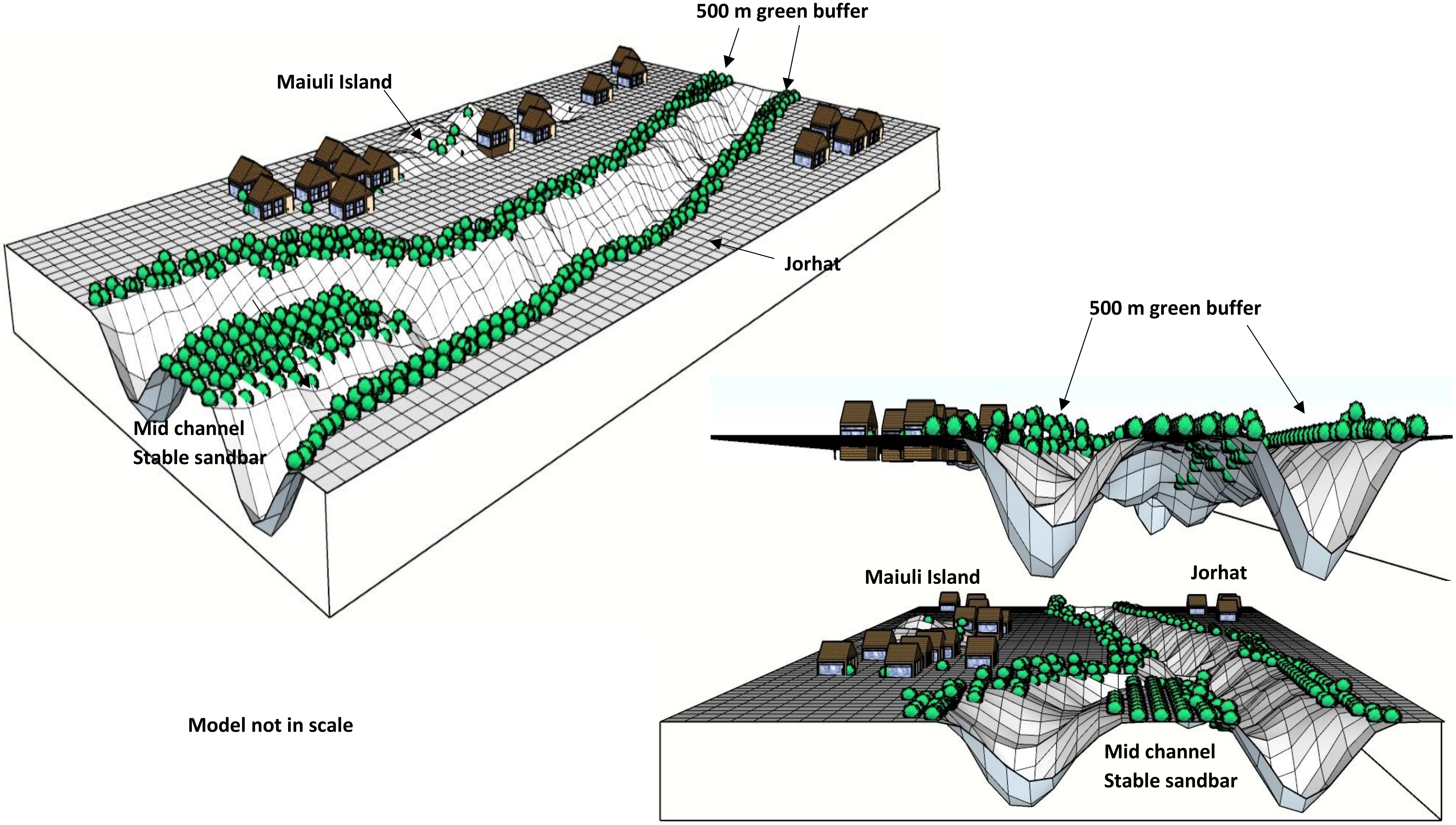

Figure 7.15: 3D view of the proposal for stabilizing the sandbar and the banks of river Brahmaputra near Majuli Island (based on forecasted C-L Model).

8.5.5 Comments on plans to channelise the River Brahmaputra in Assam

Notwithstanding on-going plans by the Brahmaputra Board to deploy new, conventional bank protection and river training measures at Majuli island, these approaches may be replaced by a much more extensive proposal to channelise the river. This is possible because the World Bank has approved a loan of US$ 15 *billion* to the Government of Assam to fund dredging of the Brahmaputra throughout its course in Assam, a length of river of 700 km (Figure 7.16). The plan is to channel the Brahmaputra into a single, 2 km wide waterway, bordered by embankments formed from the dredged material and each carrying a super-highway. The aim is to develop waterborne access from Assam to markets in West Bengal, Bangladesh, and beyond, boosting trade and industry in the State.

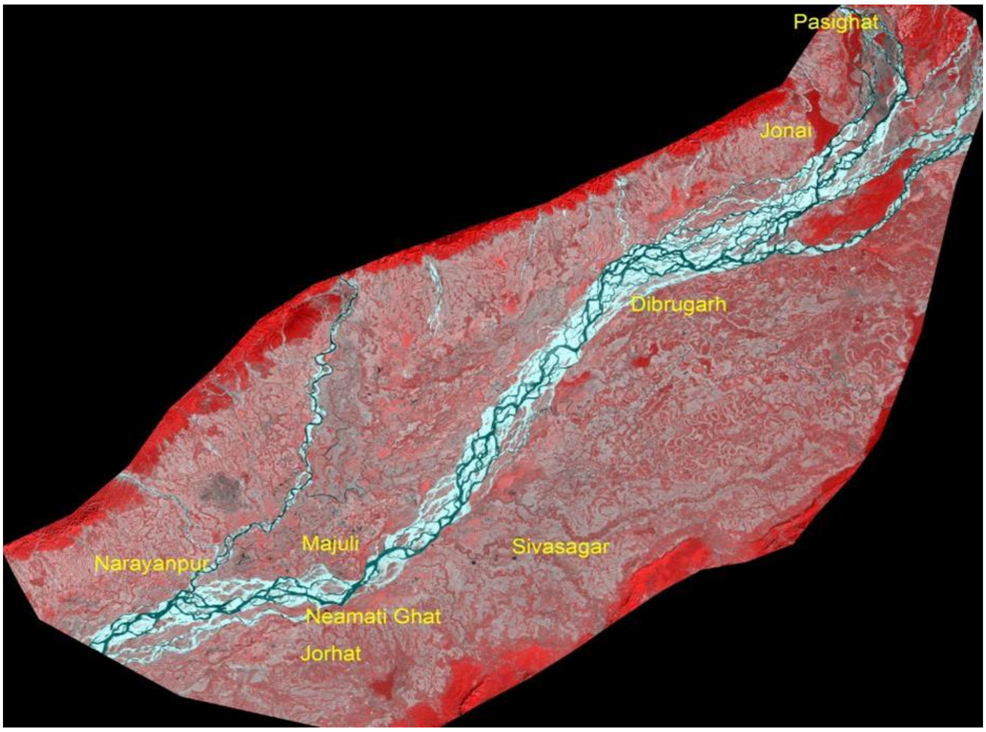

Figure 7.16: Satellite image of the Brahmaputra River between Neamatighat and the Chinese border (a distance of 200 km). The current braid plain visible in the image is over 20 km wide. The proposed scheme would reduce that width to just 2 km.

If the initial dredging is performed, hydraulic and morphological impacts within the reach will spread up and downstream, with impacts and responses that cannot currently be predicted with any confidence. The C-L models have forecasted lateral migration of the thalweg and channel capture of the thalweg channel by chute channels using a simplified modelling approach. Chute channel head-cutting in generally occurs during the falling stage of the monsoon flood, when high flows that inundate the entire braid plain (and the floodplain beyond) divide between the sub-channels and anabranches. These are profound processes, inherent to the braided nature of the river. As discussed in Chapter 7 a chute channel may dissect an island or become a major channel (see Figure 6.7) and it might capture the thalweg sub-channel, which switches its position every 5 – 10 years in the Brahmaputra. Beside this, tectonic influences such as northward tilting of the valley floor and the depression near the confluence of the river Brahmaputra and its tributary the Subansiri (see Figure 3.1) near Majuli Island can manifestly alter the rate and direction of lateral migration of the thalweg channel. For these and other reasons, it is highly unlikely that the river will continue to follow the narrow confines of a channel that is only 2 km wide for any prolonged period. In the area around Majuli Island, it is likely that flow would veer towards north bank, for example.

Based on consideration of the outcomes of research reported here, an attempt to train such a powerful and volatile river by dredging and embanking it is likely to invite disaster in terms of extreme morphological instability, which has the probability to create multiple local channel bank and embankment failures. In addition, dredging and embanking the river would have catastrophic impacts on life and habitats in the river corridor. Finally, to contain extreme monsoon floods within such a narrow floodplain would require very high embankments. Experience shows that the river will, at sometime, find weak spots and burst through these high embankments, with disastrous consequences. The risks associated with failure of an embankment would be very high, due to the severity of the consequence, even if the probability of a failure were very low. Finally, if the project does proceed and extensive embanking is to be undertaken, lessons learned from other rivers must be taken into account. The course of the River Brahmaputra has been mapped for more than 100 years and thorough surveys of these maps should be undertaken to identify channel courses in the floodplain. This is necessary because, as demonstrated by Gilvear et al. (1994) for the rivers Tay and Earn, Scotland, the risks of sudden embankment breaching or collapse are greatest where it crosses a buried channel.

Table 8.4: Summary of the challenges, approach and key contribution to knowledge of this research.

Challenges	Others approach	This research approach	Key contributions to knowledge
1. Restricted hydrological data for public use.	2. 2D Mike 21C (CFD) model to model channel morphological change for 12 km for two consecutive flood season in 2007 and 2008 (Karmakar et al., 2016).	1. Simplified reduced complexity model was used to model 40 k reach and for 20 years.	1. This is the first research undertaken to hindcast and forecast medium-term landscape evolution of the river Brahmaputra. The reduced complexity landscape evolution model was performed in the river Brahmaputra near Majuli Island which can be replicated in other parts of the river Brahmaputra to model the morphological changes occurring in the channel.
2. Lack of bathymetry data.	2. Acoustic Doppler current profiler (ADCP) was used to generate bathymetry data and hydrological data	1. Estimate hydrological and bathymetric data was used. The use of ADCP for a PhD project will be expensive there bathymetry data were generated	2. A simplified modelling approach was formulated to model large wide complex braided river system for long-term scale.

		using surveyed cross-section data of Water Resource Department and SRTM data.	
3. Lack of information of bed-load data to validate the model.	3. To predict the alignment of the thalweg channel for navigation purpose and determine best groyne field based on scouring, deposition and channel alignment and dredging volume.	3. To predict medium-term channel evolution of the river which encompasses thalweg migration, braiding intensity if the channel and bar formation and deformation.	3. An alternative technique was adopted to validate the landscape evolution model of the large complex braided river where there is the absence of bedload data.
	4. The channel alignment was validate using satellite images.	4. Application of planform indices using satellite images to validate the model in absence of bedload data.	4. Introduced new braiding indices to measure and validate braiding intensity of the landscape evolution models.

Chapter 9: Conclusions and Recommendations

9.1 Conclusions

In its middle reach, the River Brahmaputra flows through the Assam Valley, India in a multithread channel system which constantly adjusts its position and planform pattern, generating morphological changes that are semi-continuous and, on occasion, rapid. Generally, great braided rivers like the Brahmaputra are characterised by very large and highly variable discharges, huge sediment loads that include a considerable proportion of bedload, easily-eroded, non-cohesive banks and multiple secondary flow cells that generate multiple primary flow-threads, mid-channel deposition and anabranching (Bathurst et al., 1979; Richards, 1982; Richardson and Thorne, 2000).

In the Brahmaputra in Assam, long-term morphological evolution is driven by both processes of erosion and deposition in the braided channel. However, the long-stream profile of the river is extremely concave and the slope decreases markedly at the upstream boundary of the valley, where the river leaves its steep, upper course in the Himalayas. Consequently, in the Assam valley in general, and near Majuli Island in particular, morphological evolution and change is dominated more by deposition than erosion (Mahanta and Saikia. 2017).

A tendency for long-term, net deposition in this reach of the Brahmaputra, favours the creation of new sand bars (some of which are subsequently stabilised by vegetation) and consequent division of the flow into more braiding sub-channels, which then results in bank erosion and widening of the braid plain. Bank retreat and erosion of braid bars and islands as well as the mainland floodplain itself, pose serious hazards to people, property and key infrastructure such as flood embankments.

This research was set in the context of the River Brahmaputra near Majuli Island, Assam, India. Morphologically, this part of the river is particularly volatile, increased braiding intensity of the river is believed by many to be responsible for severe erosion in the southern part of Majuli Island that seems to be getting worse.

Based on a review of the literature, it can be discerned that to date there has been no comprehensive, quantitative study of the recent and future morphological evolution of the River Brahmaputra in the Vale of Assam (Sharma, 2004; Kotoky et al., 2005; Das and Saraf, 2007; Lahiri and Sinha, 2012). More specifically, there has been a negligible amount of attention paid to the use of numerical modelling of the morphological behaviour of very large, complex braided river systems like the River Brahmaputra, at reach space-scale and over the medium time-scales relevant to understanding and attempting to manage or mitigate the adverse impacts of morphological change (Mosselman, 1995; Schuurman et al., 2013).

To address this research gap, this study has evaluated the capacity of a reduce complexity model to simulate morphological change in the braided River Brahmaputra near Majuli Island, Assam, India.

The aim of the research, as set out in Chapter 1, was to answer the following research question:

To what extent can a cellular automaton, landscape evolution model be used to simulate medium-term channel evolution in a large complex braided river? A case study of Majuli Island, in the River Brahmaputra, Northeast India.

Nine objectives formulated to answer the research question:

Objective 1: To undertake a literature review to characterise the major hydrologic, hydraulic and geomorphologic processes driving landscape evolution in Majuli Island, and also undertake a review of the literature on channel evolution modelling in very large, complex rivers.

Chapter 2 outlines the history of geomorphological changes occurring in the River Brahmaputra near Majuli Island. The Brahmaputra is a very large braided river, with wide, shallow anabranches between which the flow is distributed and within which the river builds, deforms and dissects numerous braid bars and islands. During annual monsoon floods, high discharges and sediment loads drive a wide range of fluvial processes responsible for morphological adjustments. Processes include anabranching, anastomosing, lateral migration of anabranches and smaller sub-channels, sub-channel capture by head-cutting, and sandbar formation, deformation, erosion and dissection. Other, non-fluvial processes that affect channel morphology and behaviour include neotectonic movements that affect the topography of the floor of the Assam Valley, and colonisation of sandbars by vegetation, which tends to stabilise them (sometimes leading to the formation of mega-scale bars and islands). Collectively, it processes of fluvial, tectonic and bio-geomorphology that change the morphology of the River Brahmaputra.

Due to their complex geomorphological behaviours, it is very important to study the evolution of very large, braided rivers at the scale of the riverine landscape and over for medium time-scales. However, the length of the river in India is 918 km and its width varies between 9 and 23 km. To study the landscape evolution of the whole reach is computationally impossible. Instead, a study reach near Majuli Island was selected, because this area is very important both geomorphological and culturally. Majuli is the largest riverine island in the world and the Island has been nominated as the UNESCO cultural heritage site (The Majuli Island Cultural Landscape Region Act, 2006).

Therefore, a study reach near Majuli Island was selected for this research on the medium-term, morphological evolution of the River Brahmaputra.

<u>Objective 2</u>: To develop new braiding indices that better describe braided river morphology and that can be used to derive morphological performance metrics for validation and interpretation of numerical models.

Chapter 3 addresses the study of the existing braid parameters as the basis for developing new ones to quantitatively define changes in the braided channel. New indices were developed to quantify lateral shifting of the thalweg (Thalweg Migration Index, TMI), braiding intensity (Modified Plan Form Index, MPFI), cross-sectional disposition of anabranch channels (Modified Flow Geometry Index, MFGI) and change in bar area (Bar Deformation Index, BDI).

In classified rivers or rivers located in remote areas, where accessibility to hydrological data is restricted; these newly developed planform indices are suitable for quantifying landscape change occurring in the river channel using satellite images and, if available, surveyed cross-sections. The new indices were calculated for the River Brahmaputra near Majuli Island, to evaluate historical and current trends of morpho-dynamic change.

The findings have established, on a rational basis, that the reach alongside the southern part of Majuli Island is particularly volatile, morphologically. They reveal, for the first time, the extent to which braiding intensity has increased. Trends in the new indices also indicate that the frequencies with which braid bars form, deform and erode are increasing, which is accelerating the rate at which channel morphology evolves near Majuli Island.

Calibration and validation of river sediment and morphology models can be conducted using various techniques, including comparing model outputs to field data/observations of water surface profiles, inundated areas, sediment yields etc. (Murray and Paola, 2003, Thomas and Nicholas, 2002, Coulthard et al., 2007, Meadows, 2014). Model validation for the River Waitaiki, New Zealand demonstrated how limited calibration and validation opportunities are in braided rivers. The Waitaki sediment model was validated by comparing modelled to measured bedload yield. But for very large, braided rivers like the Brahmaputra, where bedload is not measured, this type of approach cannot be used to calibrate or validate a sediment and morphological model.

An alternative approach to calibration and validation applicable in braided river models is use of braiding indices like those developed in this research. In this context, planform based indices are especially useful as their values, and time-changes therein, can be derived using chronological satellite images (Hooke, 1984, Nicholas, 2005). According to Coulthard et al. (2007) models of braided system channel planform change can be calibrated and evaluated by comparing modelled braiding indices to reality. In case of classified or remotely located global rivers, this method may be ideal, as there are inadequate opportunities to calibrate or validate models using data intensive methods.

In developing the new braiding indices reported here, it was borne in mind that application of remote sensing techniques coupled with use of braiding indices that characterise the planform morphology of a braided river provides a viable method not only to evaluate morphological change quantitatively, but also to calibrate and validate models of large, complex, braided rivers for which access to data is limited.

Objective 3: To identify an appropriate modelling approach and a specific tool for simulating channel evolution processes near Majuli Island at a reach-scale and over the medium-term.

Chapter 4 deals with identification of an appropriate modelling approach. There is a limited number of morphological models that can model the landscape evolution of braided rivers. For example, 3D, CFD models are only suitable for modelling a small part of the river for relatively short time periods (for specific flood periods or a short period of high fluvial change). Hence, CFD models are unsuitable for application to complex, braided rivers over medium time-scales. Conversely, 1D models run fast but lack the capacity to simulate the lateral processes pivotal to generating and adjusting the morphology of a braided channel. This makes them unsuitable as well. 2D hydraulic and sediment transport models can simulate braiding, but their run times are too slow to support medium-term simulations at the reach-scale. Beside this, there is high cost and difficulty in collecting the hydrological, hydraulic, morphometric and sediment data needed to run a 2D, physics-based model in a very large, complex braided river, particularly as data for such rivers is often sensitive and therefore classified. Therefore, little attention has been paid to modelling channel evolution and change in very large, complex braided rivers over anything but small space and time scales.

The best alternative for modelling complex, braided rivers with limited data availability, is to use a form of simplified morphological model which is known as a reduced complexity model or RCM (Murray and Paola, 1994; Coulthard et al., 2002; Thomas and Nicholas, 2002). These are cellular automaton models, which allow computer simulations to run over wide spatial and medium to long time scales, albeit is at the expense of some physical explanation and morphological reliability (Nicholas and Quine, 2007; Thomas et al., 2007; Zilani et al., 2013).

For these reasons, the CAESAR-Lisflood (C-L) model was selected for use in this research project.

Objective 4: To understand the performance and limitations of cellular automaton models in braided river modelling.

Chapter 5 and section 8.2 of Chapter 8 addressed the performance and limitations of cellular automata models. Cellular automata, landscape evolution models are ideal for exploring long-term and large-scale river systems where there is an interaction between tectonics, climate, fluvial and slope processes. They are, however, less appropriate for small-scale (1- 5 km) and short-term (1-2 years) river models beacuse these models do not simulate the physics of the fluvial processes actually responsible for channel changes and, in any case, a simplified 50-100 m grid of the type suitable for a RCM will be too coarse to represent the necessary detail in floodplain and channel topography in a small-scale reach or over a short time scale (Coulthard et al., 2007).

Most cellular models applied in the context of braided rivers have been used to hindcast and forecast sediment yields at the catchment or reach-scale (Coulthard et al., 2002; Zilani et al., 2013; Meadows, 2014). A limited amount of research has been undertaken on feasibility of using a C-L model to hindcast and forecast morphological evolution of braided river systems that exhibit intense morphological changes, braiding patterns, and a complex, evolutionary trajectory. Hence, such an application would be novel.

The study of braided channel, sandbar and island morphodynamics in large, nationally or internationally important rivers is also limited by the difficulties of obtaining data quantifying flow, sediment transport and bathymetry change over the necessary time and spatial scales (Amsler et al., 2005). The simpler data needs of the reduced complexity, cellular models like C-L model becomes a significant advantge in this context.

Based on careful consideration of the capabilities and limitations of cellular automaton models, it was decided that C-L was suitable for modelling the Brahmaputra in the study reach becase it is sufficiently wide for a 100 m cellular grid to be used, because a twenty-year model run is long enough for changes to be modelled despite the limited physical basis for simulating the processes responsible and because it is a complex braided river for which there little data exists and limited access to what data do exist.

Objective 5: To identify the data sources and pre-processing requirements for parameterisation of the CAESAR-Lisflood model and to assemble the data required for CAESAR Lisflood to undertake hindcasting of channel evolution.

Chapter 5 recounts data compilation and model parameterisation. In this research, a reach-scale, C-L model was applied to hindcast and forecast landscape evolution of the river Brahmaputra near Majuli Island. The data required were: daily mean discharge, daily mean suspended sediment load, initial bathymetry, vegetation parameters, stream bank and terrace slope parameters. If available, bedload data can be used by the C-L model, but none are available for the Brahmaputra and so simuation of sediment trasnport was limited to suspended load.

In the reach mode, precipitation data are not required to run C-L model, as discharge is fed into the modelled channel at the upstream boundary. Sediment is also fed in at the upstream boundary, with sediment leaving the model at the downstream boundary being recirculated and fed in again at the upstream boundary in the next iteration.

According to the laws of the Government of India, the river Brahmaputra is categorised as a classified river. These are rivers whose hydrological data are restricted for public use. In this study, special permission was obtained to use hydrological data collected by the Water Resource Department, Govt. of Assam. However, daily mean discharge and suspended sediment load for the Brahmaputra in India is measured only at the Pandu gauge discharge site (GDS), which is 200 km downstream of Majuli Island. Therefore, to run C-L for the study reach near Majuli Island, local daily discharges had to be estimated from those measured at Pandu. Similarly, local daily suspended sediment load data had to be generated by applying the sediment rating curve for measurements made at Pandu, using the estimated daily discharges near Majuli Island. Suspended sediment measured at Pandu is classified into just three size classes and so, although C-L can handle up to 9 size classes, just three were used.

While discharge and sediment load data are limited, there is no bathymetry data that can be used to run a C-L model. Therefore, the initial bathymetry was generated by using cross-section data and a SRTM-based, 90 m resolution DEM in both the hindcasting and forecasting models.

Primary data on bank and terrace soils and critical slope angles were collected during fieldwork in 2016 and sued to interpret slope data calculated from the available DEM for Majuli Island and the adjacent Brahmaputra river channel.

Vegetation cover was assessed using Landsat imagery based on thematic mapping in ArcGIS.

Although data availability was were limited, it was possible to assemble all the data needed to parametrise a reach mode, C-L landscape evolution model of the River Brahmaputra near Majuli Island suitable for hindcasting morphological changes between 1998 and 2014.

<u>Objective 6</u>: To develop a method for calibrating CAESAR-Lisflood.

Chapter 6 dealt with model calibration. It was noted there are two methods that can be applied in calibrating the models: the generalised likelihood uncertainty estimation or GLUE method (Beven and Bingley, 1992) and the blind testing method (Ewen and Parkin, 1996). GLUE is numerically and computationally intensive. When applied to a model with multiple parameters representing a complex system, applying GLUE requires a large number of model runs, a high power/capacity computing facility and a comprehensive data set to define probability distributions for model parameters (Bathurst et al., 2004), none of which were feasible for this river and this study. Therefore, the alternative blind testing method was used in this research. In this method, a small number of calibrations are applied to final bounds of parameter values based on expert judgment, values known from the relevant literature and field measurements (Bathurst et al., 2004).

In this study, fifteen versions of C-L for the study reach were run initially, with different combinations of reasonable estimates for parameter values based on expert judgement, the literature and field measurements. Of these, ten models were able to produce the correct flow route for the thalweg sub-channel, taking into consideration the sensitivity of the parameters and the need for a practically-feasible model runtime.

These ten C-L test models were then evaluated with respect to three attributes of morphological change (thalweg migration, local-scale planform change, and bar deformation) that were derived using observed and modelled values of the new braiding indices (development of which was reported in Chapter 3). The performance of each model in producing outcomes that matched observed parameters of morphological change was then quantified and ranked using an Analytic Hierarchy Process (full details of this procedure are provided in Section 6.8 of Chapter 6). The AHP established that C-L models 3 and 4 performed the best (see Table 6.12), according to the blind testing approach to calibration adopted in this study, with C-L model 3 slightly outperforming model 4.

On the basis of these findings, it was decided to use C-L models 3 and 4 to forecast the morphological evolution of the channel in the study reach of the River Brahmaputra near Majuli Island for next 20 years.

Objective 7. To assess changes in medium-term river morphological forecasts by the cellular model.

Model forecasting is reported in Chapter 7. To make morphological forecasts for the next 20 years using the C-L models with the best calibration performances, it was necessary first to forecast future mean daily discharges in Brahmaputra near Majuli Island. To do this, recourse was made to the ISIMIP Fast track global hydrological models (GHM). Among the 34 GHM models, four models appropriate for representing the hydrological characteristics of the Brahmaputra (H08, LPJmL, JULES, MacPDM) were tested for possible use in this research. H08 and LPJmL were found to be the best model to provide future hydrological inputs to the C-L models, and the model combination C-L 3 + H08 was found to be the most reliable with which to forecast the morphological evolution of the River Brahmaputra between 2015 and 2035.

Trends and changes in the four braiding indices that were forecast by the C-L 3 + H08 combination of models indicated that the Brahmaputra in the study reach is likely to remain volatile morphologically for the next two decades. Forecast morphological changes in the study reach may be summarised as follows:

1. deposition is very likely to continue to exceed erosion, with net deposition increasing through time due to increased sediment inputs associated with greater monsoon runoff;

2. the Brahmaputra may widen its primary channel (braid plain) in response to increased runoff and net depsoition;
3. the thalweg may continue migrating northwards towards Majuli Island, possibly at an accelerating rate;
4. the number of sandbars is likely to increase and rates at which sandbars are formed, deformed and destroyed are likely to rise;
5. braiding intensity will most probably increase;
6. bank erosion and loss of floodplain land may become more severe, especially in the southern part of Majuli Island.

Objective 8. Compare the trends and changes forecast using the C-L + H08 model combination with the results of previous studies to assess their plausibility and validate the modelled forecasts of morphological changes responsible for medium-term landscape evolution in Majuli Island.

Chapter 8 presents in-depth discussion of the model results. This research represents the first attempt undertaken to date to model medium-term landscape evolution the River Brahmaputra. This makes it difficult to validate the results. Nothwithstanding this, some confidence can be drawn from comparision of the hindcast model braiding indices with braiding indices calculated using historical satellite images and the results of the few previous studies that have investigated braiding intensity in the River Brahmaputra in Assam. For example, Sharma (2004) calculated values of his plan form index (PFI) for the entire length of the river in India. His findings indicate a high degree of braiding in the study reach which is consistent with MPFI and MFGI values output by the hindcast models in that MFPI values indicate moderate/high braiding intensity in the planform and MFGI values indicate high braiding intensity in the wetted cross-section.

Forecast C-L model outputs compare favourably with those of Mahanta and Saikai (2017) in that both indicate that there is currently and will in future be more deposition than erosion in the study reach. This forecast is consistent with the general principle that net deposition in the reach is likely to create more sandbars, sub-channels and, ultimately, more bank erosion.

Lahri and Sinha (2012) put forward the hypothesis that geo-tectonically-driven, northward tipping of the floor of the Assam valley floor may affect channel migration and the pattern of valley sedimentation. Both measurements model and hindcasting indicate that northward migration of the thalweg has been accelerating, and model forecasts have those trends continuing. However, acceleration occurred following attempts to stabilise the southern bank of Majuli Island in 2004, offering an alternative explanation for the rise in the rate of migration, which tectonic effects are not actually included in the reach mode version of CAESAR-Lisflood. In that respect, which model outcomes are consistent with the hypothesis of Lahri and Sinha (2012), they neither prove nor disprove their explanation for northward shifting of the thalweg towards Majuli Island.

Objective 9. To evaluate the applicability of landscape evolution modelling and interpret research findings in the context of future river and land management at Majuli Island.

The research reported in this thesis has outlined the utility of a reduced complexity, cellular automaton model for medium-term forecasting of morphological changes in the Brahmaputra and other large, braided rivers. Such models are, however, unsuitable for modelling micro-scale features over short periods of time (i.e. changes in sub-100 m scale features, over periods of a year or two). This kind of small-scale modelling requires the high computational model to deliver detail morphological change in a fine-resolution DEM. It is in the context of a wide, complex (intensely braided/anastomosed) river (like the Brahmaputra), and at medium-term model durations that cellular and other RCM models come to the fore as being the only feasible way to hindcast and forecast morphological channel evolution and change.

The two key benefits of using the C-L + H08 model combination rather than relying on expert opinion or prediction that were identified during this research are:

1. The capacity to forecast change at least indicatively, and, to an extent, quantifiably, over wide spatial and long time scales despite the well know limitations of cellular models to provide physical explanation and morphological reliability (Zilani et al., 2013).

2. The capabilities to identify the most vulnerable areas, communities and infrastructure at risk of erosion and the areas more likely to remain stable using the forecasting models, opening up the possibility of using model outcomes to inform decision makers with respect to development, bank protection, and flood risk management strategies.

The potential for applying the resuts of using 20-year forecasts of future evolution in the morphology of the Brahmaputra near the southern part of Majuli island is illustrated in the final section of Chapter 8.

The implications of the forecasts developed in this thesis are that the Brahmaputra will become more highly braided, implying growing volatility in rates of bar sedimentation, channel widening, accelerated rates of shifting and headcutting by small sub-channels that become a major anabranches in the longer-term, and continued lateral shifting of the river towards Majuli Island. If morphological response to increased monsoon runoof and increased variability between years in the manner forecast by the C-L + H08 models, it will be necessary to make alternative arrangements for flood risk and erosion management at Majuli island and many other locations within and along the River Brahmaputra because 'holding the line' with ever heavier defences may not be affordable or even feasible in engineering terms. This is why alternative approaches, such as permanent relocation of the most vulnerable communities, planting of vegetation on semi-stable bars to consolidate them into stable isalnds and creation of a 500 m wide green buffer strip within a new 'Regulated River Zone' may be necessary. It is likely that such radical changes can only come about if forecasts provide decision makers with the foresight they need to embrace innovation and move away from technical and institutional lock-in to conventional approaches to bank protection and river training.

9.2 Limitations of the research:

1. CAESAR Lisflood model lacks in vegetation colonisation and development function in the hydrological model. Future climate change may increase/ decrease the temperature and precipitation, which will result in higher/ lower evapotranspiration rates and high/low groundwater recharge which will impact on water balance. Vegetation indicators such as leaf area index, rooting depth

and stomatal conductance etc. can calculate the water balance. Most of the hydrological models do not consider vegetation as a dynamic component in hydrological modelling. Therefore it is essential to consider the role of vegetation in hydrological modelling in future research.

2. The forecasting models of landscape evolution change of the River Brahmaputra was run using the suspended sediment load extrapolated from the sediment rating curve of Pandu gauge station (1998- 2015). Therefore the forecasting models lack in catchment-scale sediment delivery under climate change function. Climate models forecast change in the behaviour of precipitation extremes. Therefore, there is an additional uncertainty in modelling sediment production and transport processes. Climate change is likely to alter sediment transport processes. According to Nearing et al. (2004), the main climate change related stressors are changes in precipitation and temperature and there interaction with land-use and landcover which is likely to affect future sediment flow.

9.3 Recommendations

A number of issues that emerged during the course of this study should be addressed as a part of further research on medium-term landscape evolution modelling of the large complex braided rivers like the Brahmaputra. These are:

1. Using the same sets of parameter coefficients, but with finer-resolution bathymetric data and directly measured hydrological and sediment data in reach-scale C-L models would support enhanced calibration to produce improved morphological reliability. That would be a step on from what the C-L models produced in this research have achieved. Using these enhanced C-L models, the new braiding indices developed here will be able to compute representative, local-scale planform and cross-sectional changes and better forecast channel migration in complex braided rivers like the Brahmaputra.
2. Based on the sensitivity of model outputs and parameter specifications there is need for further C-L models to be tested to increase confidence in morphological changes forecast in the River Brahmaputra.

3. Instead of a single, 40 km reach, this could be sub-divided into two, 20 km sub-reaches to improve model resolution and make the simulation run faster or for a longer period.
4. There is need for a FORTRAN of the C-L model, which can model complex braided rivers using a High Performance Computing (HPC) cluster to increase the number of simulations and hence, confidence in the outcomes.
5. Some fluvial features that are known to be important to the river environment, such as in-channel bars, pools and riffles, as well as their evolutionary trends, are lacking from the current version of the C-L model. If these processes are added in the C-L models it will enhance the capacity of the model for simulating morphology and change in rivers.
6. River Subansiri is one of the largest tributaries of the River Brahmaputra which joins the main channel near the southern tip of the Majuli Island. This river hugely contributes towards the changing morphology of the River Brahmaputra near Majuli Island. The confluence of these two rivers is situated near the depression (see Figure 3.1) where the riverbed is northward tilting. Therefore there is a need for a combined landscape evolution model for both the rivers to see the implication of the future channel process change near Majuli Island for a medium or long term.

Reference:

Abernethy, B., and Rutherford, I. D., 2001; The distribution and strength of riparian tree roots in relation to riverbank reinforcement, Hydrological Processes, Vol.15, pp. 63–79, doi:10.1002/hyp.152

Akhtar, M.P., Sharma, N., and Ojha, C.S.P., 2001; Braiding process and bank erosion in the Brahmaputra River, International Journal of Sediment Research, Vol. 26, pp. 431 – 444.

Aichouri, I., Hani, A., Bougherira, N., Djabri, L., Chaffai, H., and Lallahem, S., 2015; River flow model using artificial neural networks, Energy Procedia, Vol. 74, pp. 1007- 1014.

Arnell, N. W., 1999; A Simple Water Balance Model for the Simulation of Streamflow over a Large Geographic Domain. Journal of Hydrology, Vol. 217, pp.314-335.

ASCE, 1993; Criteria for evaluation of watershed models, Journal of irrigation and Drainage Engineering, Vol. 119 (3), pp. 429 – 442.

Ashworth, P.J., and Lewin, J., 2012; How do big rivers come to be different? Earth- Science Reviews, Vol. 114, pp. 84- 107.

Baptist, M. J., 2003; A flume experiment on sediment transport with flexible, submerged vegetation, paper presented at International Workshop on Riparian Forest Vegetated Channels: Hydraulic, Morphological and Ecological Aspects, Int. Assoc. for Hydraul. Res., Trento, Italy.

Bates, P. D., Horritt, M. S. and Fewtrell, T. J., 2010; A simple inertial formulation of the shallow water equations for efficient two-dimensional flood inundation modelling, Journal of Hydrology, Vol. 387, pp. 33-45.

Bathrust, J.C., Ewen, J., Parkin, G., O’Connell, P.E., and Cooper, J.D., 2004; Validation of catchment models for predicting land-use and climate change impacts. 3. Blind validation for internal and outlet responses, journal of Hydrology, Vol. 287, pp. 74- 94.

Bennett, S. J., Alonso, W. Wu, C. V., and Wang, S. S. Y., 2008; Modeling fluvial response to in-stream woody vegetation: Implications for stream corridor restoration, Earth Surface Processes Landforms, Vol. 33, pp. 890–909, doi:10.1002/esp.1581.

Bertoldi, W., and Tubin. M., 2005; Bed and bank evolution of bifurcating channels. Water Resource Research, Vol. 41.

Best, J.L., and Bristow, C.S, (eds), 1993; Braided Rivers: perspectives and problems, Geological Society Special Publication, Vol.75, pp. 1- 11.

Beven, K.J., and Binley, A., 1992; The future of distributed models: model calibration and uncertainty prediction, Hydrological Processes, Vol. 6, pp, 279 – 298.

Boruah, S., Gilvear, D., Hunter, P. and Sharma, N., 2008; Quantifying channel planform and physical habitat dynamics on a large braided river using satellite data- The Brahmaputra, India, River Research and Application, Vol. 24, pp. 650 – 660.

Bowden, G. J., Maier, H. R. and Dandy, G. C., 2002; Optimal Division of Data for Neural Network Models in Water Resources Applications. Water Resources Research, Vol.38, pp. 2-1-2-11.

Braudrick, C. A., Dietrich, W. E., Leverich, G. T., and Sklar, L. S., 2009; Experimental evidence for the conditions necessary to sustain meandering in coarse bedded rivers, Proc. Natl. Acad. Sci. U. S. A., Vol. 106(40), pp. 16,936–16,941, doi:10.1073/pnas.0909417106.

Brice, J.C. 1960; Index for description of channel braiding, Geological Society of America Bulletin 71.

Brice. J.C., 1964; Channel patterns and terraces of the Loup Rivers in Nebraska. Geological Survey Professional Paper 422-D.

Brice, J.C., 1982; Stream Channel Stability Assessment, Final Report U.S. Department of Transportation, Federal Highway Administration, Washington, DC.

Bridge, J. S., 1993; The interaction between channel geometry, water flow, sediment transport and deposition in braided rivers, in Briaded River. In:

Bristow, J. L. B. A. C. S. (ed.) Special Publication Geological Society House. Bath, UK.

Bristow, C.S., 1999; Gradual avulsion, river metamorphosis and reworking by underfit streams: a modern example from the Brahmaputra River in Bangladesh and a possible ancient example in the Spanish Pyernees.

Bristow, C.S., Best, J.L. and Ashworth, P.J., 2000; The use of GPR in developing a facies model for large sandy braided river, Brahmaputra River, Bangladesh. In: Noon, D.A., Stickley, G.F. and Longstaff, D. (eds.) Gpr 2000: Proceedings of the Eight International Conference on Ground Penetrating Radar.

Carter, G. S. and Shankar, U., 1997; Creating rectangular bathymetry grids for environmental numerical modelling of gravel-bed Rivers, Applied Mathematical Modelling, Vol. 21, pp. 699-708.

Charlton R.O., 2008; Fundamentals of Fluvial Geomorphology. 2 Park Square, Milton Park, Abingdon, Oxon, OX14 4RN: Routledge.

Chew, L.C., Ashmore, P.E., 2001; Channel adjustment and a test of rational regime theory in a proglacial braided stream, Geomorphology, Vol. 37. Pp. 43–63

Church, M., 2007; Multiple scales in rivers, Dev. Earth Surface Processes, Vol. 11, pp. 3-28.

Coulthard, T. J., Hicks, D. M. and Van De Wiel, M. J., 2007; Cellular modelling of river catchments and reaches: Advantages, limitations and prospects, Geomorphology, Vol. 90, pp.192-207.

Coulthard, T. J., Macklin M.G. and Kirkby, M.J. 2002. A cellular model of Holocene upland river basin and alluvial fan evolution, Earth Surface Processes Landforms, Vol. 27,pp. 269-288.

Coulthard, T.J., Krikby, M.J. and Macklin, M.G., 1998; Non-linearity and spatial resolution in a cellular automaton model of a small upland basin, Hydrology and earth System Sciences, Vol. 2. Pp. 257 – 264.

Coulthard, T.J., Krikby, M.J. and Macklin, M.G., 2000; Modelling geomorphic response to environmental change in an upland catchment, Hydrological Processes, Vol. 14, pp. 2031 – 2045.

Coulthard, T.J., Lewin, J. and Macklin, M.G., 2008; Non-stationarity of basin scale sediment delivery in response to climate change. In: Habersack, H., Piegay, H. and Rinaldi, M. (eds.), Gravel-Bed Rivers Vi: from Process Understanding to River Restoration.

Coulthard, T. J., Neal, J. C., Bates, P. D., Ramirez, J., De Almeida, G. A. M. and Hancock, G. R., 2013; Integrating the LISFLOOD-FP 2D hydrodynamic model with the CAESAR model: implications for modelling landscape evolution, Earth Surface Processes and Landforms, Vol. 38, pp. 1897-1906.

Coulthard, T.J. and Skinner, C.J., 2016; The sensitivity of landscape evolution models to spatial and temporal rainfall resolution, earth Surface Dynamics, Vol. 4, pp. 757- 771.

Coulthard, T.J. and Van De Wiel, M.J., 2006; A cellular model of river meandering. Earth Surface Processes and landforms, Vol. 31, pp. 123 – 132.

Coulthard, T.J. and Van De Wiel, M.J., 2007; Quantifying fluvial non-linearity and finding self-organized criticality? Insights from simulations of river history and evolution, Geomorphology, Vol. 91, pp. 216- 235.

Coulthard,T.J. and Van De Wiel, M. J., 2007; Cellular modelling of river catchments and reaches: Advantages, limitations and prospects, Geomorphology, Vol. 90, pp. 192- 207.

Coulthard, T. J. and Van De Wiel, M. J., 2012; Modelling river history and evolution. Philosophical Transactions of the Royal Society a-Mathematical Physical and Engineering Sciences, Vol. 370, pp. 2123-2142.

Coulthard, T.J. and Van Dei Wiel, M.J., 2017; Modelling long term basin scale sediment connectivity, driven by spatial landuse changes, Geomorphology, Vol. 277, pp. 265- 281.

Cox, P., Betts, R., Bunton, C., Essery, R., Rowntree, P. and Smith, J., 1999; The Impact of New Land Surface Physics on the Gcm Simulation of Climate and Climate Sensitivity. Climate Dynamics, Vol.15, pp.183-203.

Das, J.D. and Saraf, A.K., 2007; Remote sensing in the mapping of the Brahmaputra? Jamuna River channel patterns and its relation to various landforms and tectonic environment, International Journal of Remote Sensing, Vol. 28. Pp. 3619 – 3631.

Dawson, C.W., Abrahart, R.J., and See, L.M., 2005; Hydro Test: A web-based toolbox of evaluation metrics for the standardised assessment of hydrological forecasts, Environmental Modelling & Software, Vol. 22, pp. 1034 – 1054.

Dewan, A., Corner, R., Saleem, A., Rahman, M.M., Haider, M.R., Rahman, M.M. and Sarker, M.H., 2017; Assessing channel changes of the Ganges- Padma River system in Bangladesh using Landsat and hydrological data, Geomorphology, Vol. 276, pp. 257 – 279.

Doeschl-Wilson, A. B., and Ashmore, P.E., 2005; Assessing a numerical cellular braided-stream model with a physical model, Earth Surface Processes Landforms, Vol. 30, pp. 519-540.

Doeschil-Wilson, A.B., and Davison, M., 2006; Methods for assessing exploratory computational models of braided rivers, in Braided Rivers. In: Smith, G.H.S (ed.) IAS Special Publication, Oxford, UK: Blackwell Publishing.

Dos Santos, V.C., Stevaux, J.C. and Assine, M.L., 2017; Fluvial Processes in Attachment Bars in the Upper Parana River, Brazil, Revista Brasileria De Geomorfologia, Vol. 18, pp. 483 – 499.

Dubey, A.K., Gupta, P., Dutta, S. and Kumar, B., 2014, Evaluation of satellite – altimetry- derived river stage variation for the braided Brahmaputra River, International Journal of Remote Sensing, Vol 35, pp. 7815 – 7827.

Eaton, B. C., 2006; Bank stability analysis for regime model of vegetated gravel bed rivers, Earth Surf. Processes Landforms, 31, 1438–1444, doi:10.1022/esp.1364.

Egozi, R., and Ashmore P.E., 2008; Defining and measuring braiding intensity Earth Surface Processes and Landforms, Vol. 33, pp. 2121-2138.

Einstein, H.A., 1950; The bedload function for sediment transportation in open channel flows: Technical Bulletin. Vol. 1026. Washington, DC: US Department of Agriculture.

Elshorbagy, A., Simonovic, S.P., and Panu, U.S., 2000; Performance evaluation of neural networks for runoff prediction, Journal of Hydrologic Engineering. Vol. 5(4), pp.424-427.

Ewen, J., and Parkin, G., 1996; Validation of catchment models for predicting land-use and climate change impacts. 1. Method. Journal of Hydrology, Vol. 175, pp. 583- 594.

Fischer, G., Tubiello, F.N., Van Velthuizen, H., and Wiberg, D.A., 2007; Climate change impacts on irrigation water requirements: effects of mitigation. Technol Forecast Soc Change, Vol. 74(7). pp. 1083–1107.

Ferguson, R. I., 2007; Gravel-bed Rivers at the reach scale, in Gravel-Bed Rivers VI: From Process Understanding to River Restoration, Developments in Earth Surface Processes, Vol. 11. pp. 33- 51.

Galappati, R., Olesen, K.W. and Khan, A.S., 2004; Schematizing large active rivers for morphological computations: Experience from Bangladesh.

Gaurav, K., Tandon, S.K., Devauchelle, O., Sinha, R. and Metivier, F., 2017; A single width-discharge regime relationship for individual threads of braided and meandering rivers from the Himalayan Foreland, Geomorphology, Vol. 295, pp. 126- 133.

Germanoski, D., Schumm, S.A., 1993; Changes in braided river morphology resulting from aggradation and degradation. Journal of Geology, Vol.101. pp. 451–466.

Gilfellon, G.B., Sarma, J.N. and Gohain, K., 2003; Channel and bed morphology of a part of the Brahmaputra river in Assam, Journal of the Geological Society of Indian, Vol. 62, pp. 227- 235.

Gilvear, D.J., Davis, J.R. and Winterbottom, S.J.,1994; Mechanisms of floodbank failure during large flood events on the rivers Tay and Earn, Scotland, Journal of Engineering Geology, Vol. 27, pp. 319- 332.

Gilvear, D., Winterbottom, S., and Sichingabula, H., 2000; Character of channel planform change and meander development: Luangwa river, Zambia, Earth Surface Processes and Landforms, Vol. 25, pp. 421 – 436.

Goswami, D. C., 1985; Brahmaputra River, Assam, India: physiography, basin denudation and channel aggradation, Water Resource, Vol. 21. Pp. 959- 978.

Gosling, S. N., and Arnell, N. W., 2011; Simulating Current Global River Runoff with a Global Hydrological Model: Model Revisions, Validation and Sensitivity Analysis. Hydrological Processes, Vol.25, pp. 1129-1145.

Gran, K. and Paola, C., 2001; Riparian vegetation controls on braided stream dynamics, Water Resources Research, Vol. 37, pp. 3275-3283.

Green, I.R.A., Stephenson, D., 1986; Criteria for comparison of single event models; Hydrological sciences Journal, Vol. 31 (3), pp. 395 – 411.

Gurnell, A. M., Petts, G. E., Hannah, D. M., Smith, B. P. G., Edwards, P. J., Kollman, J., Ward, J. V., and Tockner, K., 2001; Riparian vegetation and island formation along the gravel-bed fiume Tagliamento, Italy, Earth Surface Processes Landforms, Vol. 26, pp. 31–62, doi:10.1002/1096–9837(200101)26:1<31::AID-ESP155>3.0.CO;2-Y.

Gurnell, A. M., and Petts, G.E., 2006; Trees as riparian engineers: Tagliamento River, Italy, Earth Surf. Processes Landforms, Vol. 31, pp. 1558–1574, doi:10.1002/esp.1342.

Gupta, A., 1995; Magnitude, frequency and special factors affecting channel form and processes in the seasonal tropics. In Natural and Anthropogenic Influences in fluvial Geomorphology, Geophysical Monograph, Vol. 89, pp. 125 – 136.

Gurnell, A.M., Bertoldi, W. and Corenblit, D., 2012; Changing river channels: The roles of hydrological processes, plants and pioneer fluvial landforms in humid temperate, mixed load, gravel bed rivers, Earth-Science review, Vol. 111, pp. 129- 141.

Haddeland, I., Clarke, D., Franssen, W., Ludwig, F., Voß, F., Arnell, N. W., Bertrand, N., Best, M., Folwell, S., Gerten, D., Gomes, S., Gosling, S., Hagemann, S., Hanasaki, N., Harding, R., Heinke, J., Kabat, P., Koirala, S., Oki, T., Polcher, J., Stacke, T., Viterbo, P., Weedon, G. P. and Yeh, P. (2011); Multimodel Estimate of the Global Terrestrial Water Balance: Setup and First Results, Journal of Hydrometeorology, Vol. 12, pp. 869-884.

Hanasaki, N., Kanae, S., Oki, T., Masuda, K., Motoya, K., Shirakawa, N., Shen, Y. and Tanaka, K. 2008; An Integrated Model for the Assessment of Global Water Resources - Part 1: Model Description and Input Meteorological Forcing, Hydrology and Earth System Sciences, Vol. 12, pp. 1007-1025.

Hazarika, D., Baruah, S., Gogoi, N.K., 2009; Attenuation of coda waves in the North-Eastern region of India, Journal of Seismology, Vol. 13, pp. 141 -160.

Haff, P. K., Limitations on predictive modelling in geomorphology in The Scientific Nature of Geomorphology In: Thorne, C.R., (ed). Proceedings of the 27th Binghamton Symposium in Geomorphology 1996 Chichester, UK. John Wiley & Sons Ltd, pp. 337-358.

Hancock, G. R., Lowry, J. B. C. and Coulthard, T. J., 2015; Catchment reconstruction - erosional stability at millennial time scales using landscape evolution models, Geomorphology, Vol. 231, pp. 231, 15-27.

Hancock, G.R., Verdon- Kidd, D. and Lowry, J.B.C, 2017; Soil erosion predictions from a landscape evolution model- An assessment of a post- mining landform using spatial climate change analogues, Science of the Total Environment, Vol. 601, pp. 109- 121.

Hassan, A., Martin, T.C. and Mosselman, E., 1999; Island topography mapping for the Brahmaputra – Jamuna Rivers using remote sensing and GIS. In: Marriott, S. and Alexander, J. (eds.) Floodplains: Interdisciplinary Approaches.

Hunter, N.M., Bates, P.D., neelz, S., pender, G., Villanueva, I., Wright, N.G., Liang, d., Falconer, R.A., Lin, B., and Waller, S., 2008; Benchmarking 2D hydraulic models for urban flooding, proceedings of the ICE-Water management, Vol. 161, pp. 13- 30.

Hooke, J.M., 1984; Changes in river meanders: review of techniques and results of analyses, Progress in Physical Geography, Vol. 8, pp. 473-508.

Hong, L.B., Davies, T.R.H., 1979; A study of stream braiding. Geological Society of America Bulletin 90(Part II).pp 1839–1859.

Howard, A.D., Keetch, M.E., Vincent, C.L., 1970; Topological and geometrical properties of braided streams, Water Resources Research, Vol. 6pp. 1674 –1688.

Jordan, R. L., Caro, E. R., Kim, Y., Kobrick, M., Shen, Y. S., Stuhr, F. V. and Werner, M. U., 1996; Shuttle radar topography mapper (SRTM), Bellingham, Spie - Int Soc Optical Engineering.

Jung,H.C., Hamski, J., Durand, M., Alsdorf, D., Hossain, F., H., Hossain, A., Hasan, K., Khan, A.S. and Hoque, A., 2010; Characterization of complex fluvial systems using remote sensing of spatial and temporal water level variations in the Amazon, Congo, and Brahmaputra Rivers, Earth Surface Processes and Landforms, Vol. 35, pp. 294 – 304.

Karmaker, T. and Dutta, S., 2016; Prediction of short-term morphological change in large braided river using satellite 2D numerical model, Journal of Hydraulic Engineering, Vol. 142.

Karmaker, T., Medhi, H. and Dutta, S., 2017; Study of channel instability in the braided Brahmaputra river using satellite imagery, Current Science, Vol. 112, pp. 1533- 1543.

Karunanithi, N., Grenney, W., Whitley, and D., Bovee, K., 1994; Neural networks for river flow prediction, Journal of Computing in Civil Engineering, Vol. 8 (2), pp. 201-220.

Kasper, A., Brasington, J., Hafen, K., Williams, R.D., and Wheaton, J.M., 2018; Modelling braided river morphodynamics using a particle travel length framework, Earth Surface Dynamics, Vol.13, pp. 1- 53, https://doi.org/10.5194/esurf-2018-17.

Keylock, C.J., 2007; Identifying linear and non-linear behaviour in reduced complexity modelling output using surrogate data methods, Geomorphology, Vol. 90, pp. 356 – 366.

Khalil, M., Panu, U.S., and Lennox, W.C., 2001; Groups and neural networks based streamflow data infilling procedures, Journal of Hydrology, Vol. 241 (3-4), pp. 153-176.

Kirkby, M., 1995; Modelling the links between vegetation and landforms, Geomorphology, Vol. 13, pp. 319 – 335.

Kleinhans, M.G., Weerts, H.J.T., Cohen, K.M., 2010; Avulsion in action: reconstruction and modelling sedimentation pace and upstream flood water levels following a medieval tidal- river diversion catastrophe (Biesbosch, The Netherlands, 1421- 1750 AD), Geomorphology, Vol. 18 (12). pp. 65- 79.

Klingeman, P.C., Kehe, S.M., and Owusu, Y.A., 1984; Streambank erosion protection and channel scour manipulation using rockfill dikes and gabions. Technical Rep. WRRI- 98, Water Resource Research Institute, Oregon State University, Corvallies, O.R.

Kotoky, P., Bezbaruah, D., Baruah, J., and Sarma, J.N., 2003; Erosion activity on Majuli – the largest river island of the world, Current Science, Vol. 84, pp. 929 – 932.

Kuo, C.W., Chen, C.F., Chen, S.C., Yang, T.C., and Chen, C.W., 2017; Channel Planform Dynamics Monitoring and Channel Stability Assessment in Two Sediment – Rich Rivers in Taiwan, Water, Vol. 9.

Lahiri, S.K., and Sinha, R., 2012; Tectonic controls on the morphodynamics of the Brahmaputra River system in the upper Assam valley, India, Geomorphology, Vol. 169, pp. 74 – 85.

Lahiri, S.K., and Sinha, R., 2014; Morphotectonic evolution of the Majuli Island in the Brahmaputra valley of Assam, India inferred from geomorphic and geophysical analysis, Geomorphology, Vol. 227, pp. 101- 111.

Lancaster, S.T., and Bras, R.L., 2002; A simple model of river meandering and its comparison to natural channels, Hydrological Processes, Vol. 16, pp. 1- 26.

Lane, S., and Richards, K.S., 1997; Linking river channel form and process: time, space and causality revisited, Earth surface processes and landforms, Vol. 22, pp. 249- 260.

Lane, S. N., 2006; Approaching the system-scale understanding of braided river behaviour, in braided rivers. In: Smith, G. H. S. (ed.) IAS Special Publication Oxford, UK: Blackwell Publishing.

Mahanta, C., and Saikia, L., 2017; Sediment Dynamics in a Large Alluvial River: Characterization of Materials and Processes and Management Challenges, (eds) Sharma, River system Analysis and Management, Springer, Singapore. pp 47 – 72.

Martin-Vide, J.P., Frrer-Box, and Ollero, A., 2010; Incision due to gravel mining: Modelling a case study from the Gallego River, Spain geomorphology, Vol. 90, pp. 261- 271.

Mackin, J. H., 1956; Causes of braiding by a graded river, Geol. Soc. Am. Bull., Vol.67, pp. 1717 – 1718.

Meadows, T., 2014; Forecasting long-term sediment yield from the Upper North Fork Toutle River, Mount St Helens, USA. Phd Thesis, University of Nottingham.

Millar, R. G., 2000; Influence of bank vegetation on alluvial channel patterns, Water Resource. Research, Vol. 36, pp. 1109 – 1118, doi:10.1029/1999WR900346.

Mosley, P.M., 1982; Analysis of the effect of changing discharge on channel morphology in stream uses in a braided River, Ohau River, NewZealand. Water Resources Research, Vol. 18. pp. 800–812.

Mosley, M. P., 1983; Response of braided rivers to changing discharge, Journal of Hydrology, New Zealand, Vol. 22, pp. 18-67.

Mosselman, E., 1995; A review of mathematical – models of river planform changes, Earth Surface Processes and Landforms, Vol. 20, pp. 661- 670.

Mosselman, E., 2012; Modelling sediment transport and morphodynamics of gravel-bed rivers, In: Church. M., Biron, P. M., Roy, A.G., (ed.) Gravel-Bed Rivers. Chichester, UK: John Wiley.

Mosselman, E., Shisshikura, T., and Kalassen, G.J., 2000; Effect of bank stabilization on bend scour in anabranches of braided rivers, Physics and Chemistry of the Earth Part B- Hydrology Oceans and Atmosphere, Vol. 25, pp. 699- 704.

Mount, N.J., Tate, N.J., Sarker, M.H., and Thorne, C.R., 2013; Evolutionary, multi-scale analysis of river bank line retreat using continuous wavelet transforms: Jamuna River, Bangladesh, Geomorphology, Vol. 183, pp. 82- 95.

Mukul, M., Srivastava, V, and Mukul, M., 2015; Analysis of the accuracy of Shuttle Radar Topography Mission (SRTM) height models using International Global Navigation Satellite Sysytem Service (IGS) Network, Journal of Earth System, Vol. 124, pp. 2579 – 2587.

Murray, A. B. and Paola, C., 1996; A new quantitative test of geomorphic models, applied to a model of braided streams. Water Resources Research, Vol. 32, pp. 2579-2587.

Murray, A.B., 2007; Two paradigms in landscape dynamics: Self- similar processes and emergence.

Murray, A.B., and Paola, C., 1994; A cellular model of braided rivers, Nature, Vol. 371, pp. 54- 57.

Murray, A.B., and Paola, C., 1996; A new quantitative test of geomorphic models, applied to a model of braided streams, Water Resource Research., Vol. 32, pp. 2579 – 2587.

Murray, A.B., and Paola, C., 1997; Properties of a cellular braided –stream model, Earth Surface Processes and Landforms, Vol. 22, pp. 1001 – 1025.

Nakagawa, H., Zahang, H., Baba, Y., Kawaike, K. and Teraguchi, H., 2013; Hydraulic characteristic of typical bank- protection works along the Brahmaputra/ Jamuna River, Bangladesh, Journal of Flood Risk Management, Vol. 6, pp. 345 – 359.

Narula, P.L., Acharyya, S,K., Banerjee, J., 2000; Seismotectonic atlas of India and its environs. Special publication.

Nanson, G. C., and Knighton, A. D., 1996; Anabranching rivers: Their cause, character and classification, Earth Surface Processes Landforms, Vol. 21, pp. 217–239, doi:10.1002/(SICI)1096-9837(199603)21:3<217::AID-ESP611> 3.0.CO;2-U

Nicholas, A. P., 2005; Cellular modelling in fluvial geomorphology, Earth Surf. Processes & Landforms, Vol, 30, pp. 645-649.

Nicholas, A.P., 2010; Reduced complexity modelling of free bar morphodynamics in alluvial channels, Journal of Geophysical Research –Earth Surface, Vol. 115. Pp. 1- 16.

Nicholas, A. P. and Quine, T. A., 2007; Crossing the divide: Representation of channels and processes in reduced-complexity river models at reach and landscape scales, Geomorphology, Vol. 90, pp. 318-339.

Nicholas, A. P., Walling, D. E., Sweet, R. J. and Fang, X., 2006; New strategies for upscaling high-resolution flow and overbank sedimentation models to quantify floodplain sediment storage at the catchment scale, Journal of Hydrology, Vol. 329, pp. 577-594.

Nicholas, A.P., Ashworth, P.J., Sambrook Smith, G.H., and Sanbach, S.D., Numerical simulation of bar and island morphodynaimcs in anabranching mega rivers, Journal of Geophysical Research: Earth Surface, Vol. 118 (4), pp. 2019 – 2044.

Paola, C., and Georgiou, E.F., 2001; Statistical geometry and dynamic of braided rivers. In: Mosley, M.P., (ed.) Gravel-Bed Rivers. Wellington, New Zealand: Hydrological Society.

Pollen, N., and Simon, A., 2005; Estimating the mechanical effects of riparian vegetation on stream bank stability using a fibre bundle model, Water Resource. Research, Vol. 41, W07025, doi:10.1029/2004WR003801.

Prosser, I.P., and S.J. Winchester (1996); History and processes of gully initiation and development in eastern Australia, Zeitschrift Fuer Geomorphology, Vol. 105, pp. 91- 109.

Rhoads, B. L., 1992; Statistical models of fluvial systems, Geomorphology, Vol. 5, pp. 433-455.

Riahi, K., Rao, S., Krey, V., Cho, C., Chirkov, V., Fisher, G., Kindermann, G., Nakicenovic, N., and Rafaj, P., 2011; RCP 8.5 – A senerio of comparatively high greenhouse gas emissions, Climate change, Vol. 109, pp. 33- 57.

Richardson, W.R., 1997; Secondary Flow and Channel Change in Braided Rivers, Unpublished PhD Thesis, School of Geography, University of Nottingham, UK.

Richardson, W. R. and Thorne, C. R., 2000; Multiple thread flow and channel bifurcation in a braided river: Brahmaputra-Jamuna River, Bangladesh, Geomorphology, Vol. 38, pp. 185-196.

Rust, B.R., 1978; A classification of alluvial channel systems. In Fluvial Sedimentology, Miall AD (ed). Canadian Society of Petroleum Geologist: Alberta; pp.187–198

Satty, R.W., 1987; The analytic hierarchy process – what it is and how it is used, Mathematical Modelling, Vol. (3-5), pp. 161-176.

Satty, T.J., 1994; How to make a decision: the Analytic Hierarchy Process., Interfaces, Vol. 24 (6), pp. 19 -43.

Sarkar, M.H., 2008; Morphological response of the Brahmaputra- Padma-Lower Meghna river system to the Assam earthquake of 1950, PhD thesis, University of Nottingham.

Sarker, M. H., Thorne, C. R., Aktar, M. N. and Ferdous, M. R., 2014; Morpho-dynamics of the Brahmaputra-Jamuna River, Bangladesh, Geomorphology, Vol. 215, pp. 45-59.

Sarma, J.N, and Phukan, M.K, 2004; Origin and some geomorphological changes of Majuli Island of the Brahmaputra River in Assam, India, Geomorphology, Vol 60 (1), pp.1-19.

Salo,J Kalliola R hakkinen I Makinen Y Niemala P Puhakka M Coley P D. 1986; River in the Vientaine- Nong Khai reach, LAO PDR and Thailand. Report to the Mekong River Commission.

Salttelli, A., Chan, K., and Scott, M., editors, 2000; Sensitivity Analysis, Probability and Statistic series, New York: John Wiley and Sons.

Sapozhnikov, V., Murray, A.B., Paola, C., and Foufoula-Georgiou, E., 1998; Validation of braided-stream models: Spatial state-space plots, self -affine scaling and island shape comparison, Water Resour. Research, Vol. 34, pp. 2353-2364.

Schuurman, F., and Kleinhans, M.G., 2015; Bar dynamics and bifurcation evolution in a modelled braided sand-bed rivers, Earth surface processes landforms, Vol. 40, pp. 1318- 1333.

Schuurman, F., Kleinhans, M.G., Marra, W.A., 2013; Physics- based modelling of large braided sand-bed rivers: bar pattern formation, dynamics and sensitivity, Journal of Geophysical Research, Vol. 118 (4), pp. 2509 – 2527.

Schuurman, F., Ta, W., Post, S., Sokolewicz, M., Busnelli, M., and Kleinhans, M., 2018; doi:10.1002/esp.4344.

Sharma, N., 2004; Mathematical modelling and Braid Indicators, The Brahmaputra Basin Water Resources, pp. 229-260, Kluwer Academic Publishers, Dordrecht, The Netherlands.

Sharma, N., Sarkar, A., Akhter, P., and Kumar, N., 2012; Study of Brahmaputra river erosion and its control, Department of Water Resource Development and Management, India Institute of Technology.

Singh, B., and Goswami R.K., 2011; Influnce of Landform and Geomorphic Process on Topographic Evolution of a River Island, International Journal of Engineering Science and Technology, Vol. 3 (7), pp. 5562- 71.

Simon, A., 1989; A model of channel response in disturbed alluvial channels, Earth Surface Processes Landforms, Vol 14. Pp. 11- 26.

Simon, J.D., Geogory, H.S., James, L.B., Andrew, P.N., Jon, M.B., mark, E.V., Maminul, H.S., and Steven, G., 2018; The planform mobility of river channel confluences: Insights from analysis of remotely sensed imagery. Earth- Science Reviews, Vol. 176, pp. 1- 18.

Stephenson, D., 1979; Direct optimization of Muskingum routing coefficients, Journal of Hydrology, Vol. 41 (1-2), pp. 161 – 165.

Surian, N., 2015; Fluvial Processes in Braided Rivers, In: Rowinski, P., ans Radeckipawlik,A., (eds.) River-Physical, Fluvial and Environmental Processes.

Tal, M., Gran, K., Murray, A. B., Paola, C. and Hicks, D. M., 2004; Riparian vegetation as a primary control on channel characteristics in multi-thread rivers, Riparian Vegetation and Fluvial Geomorphology, Vol. 1, pp . 43- 58.

Tal, M. and Paola, C., 2010; Effects of vegetation on channel morphodynamics: results and insights from laboratory experiments. Earth Surface Processes and Landforms, Vol. 35, pp. 1014-1028.

Teegavarapu, R., and Elshorbagy, A., 2005; Fuzzy set based error measure for hydrologic model evaluation, Journal of Hydroinformatics, Vol. 7 (3), pp. 199-207.

Thorne, C. R., 1990; Effects of vegetation on riverbank erosion and stability, in Vegetation and Erosion, edited by J. B. Thornes, pp. 125–144, John Wiley, Chichester, U. K

Thorne, C. R., Russell, A. P. G. and Alam, M. K., 1993; Planform pattern and channel evolution of the Brahmaputra River, Bangladesh, Geological Society, London, Special Publications, Vol. 75, pp. 257-276.

Van De Wiel, M. J., Coulthard, T. J., Macklin, M. G. and Lewin, J., 2007; Embedding reach-scale fluvial dynamics within the CAESAR cellular automaton landscape evolution model, Geomorphology, Vol. 90, 283-301.

Vargas, L.G., 1990; An overview of the Analytic Hierarchy Process and its applications, European Journal of operational research, Vol. 48, pp. 2-8.

WAPCOS, INDIA, 1993; Morphological Studies of River Brahmaputra. In: North Eastern Council. Govt. of India (ed.) New Delhi.

Watson, R. L., 1969; Modified Rubey's law Accuratley Predicts Sediment Settling Velocities, Water Resources Research, Vol. 5, pp. 1147-1150.

Wilcock, P.R., and Crowe, J.C., 2003; Surface –based transport model for mixed – size sediment. Journal of Hydraulic Engineering, Vol. 129, pp. 120- 128.

Woldemichael, A. T., Degu, A. M., Siddique-E-Akbor, A. H. M., and Hossain, F., 2010; Role of Land-Water Classification and Manning's Roughness Parameter in Space-Borne Estimation of Discharge for Braided Rivers: A Case Study of the Brahmaputra River in Bangladesh, Journal of Selected Topics in Applied Earth Observations and Remote Sensing, Vol. 3, pp. 395-403.

Ziliani, L., Surian, N., Coulthard, T. J. and Tarantola, S., 2013; Reduced-complexity modeling of braided rivers: Assessing model performance by sensitivity analysis, calibration, and validation, Journal of Geophysical Research-Earth Surface, Vol. 118, pp. 2243-2262.

https://web.archive.org/web/20120722144718/http://www.assamtribune.com/aug2411/at096.txt

https://thenortheasttoday.com/assam-state-eyes-world-heritage-site-tag-for-majuli-river-island/

Appendix 1: Comparison of the observed TMI with the five modelled TMI of the river Brahmaputra near Majuli Island.

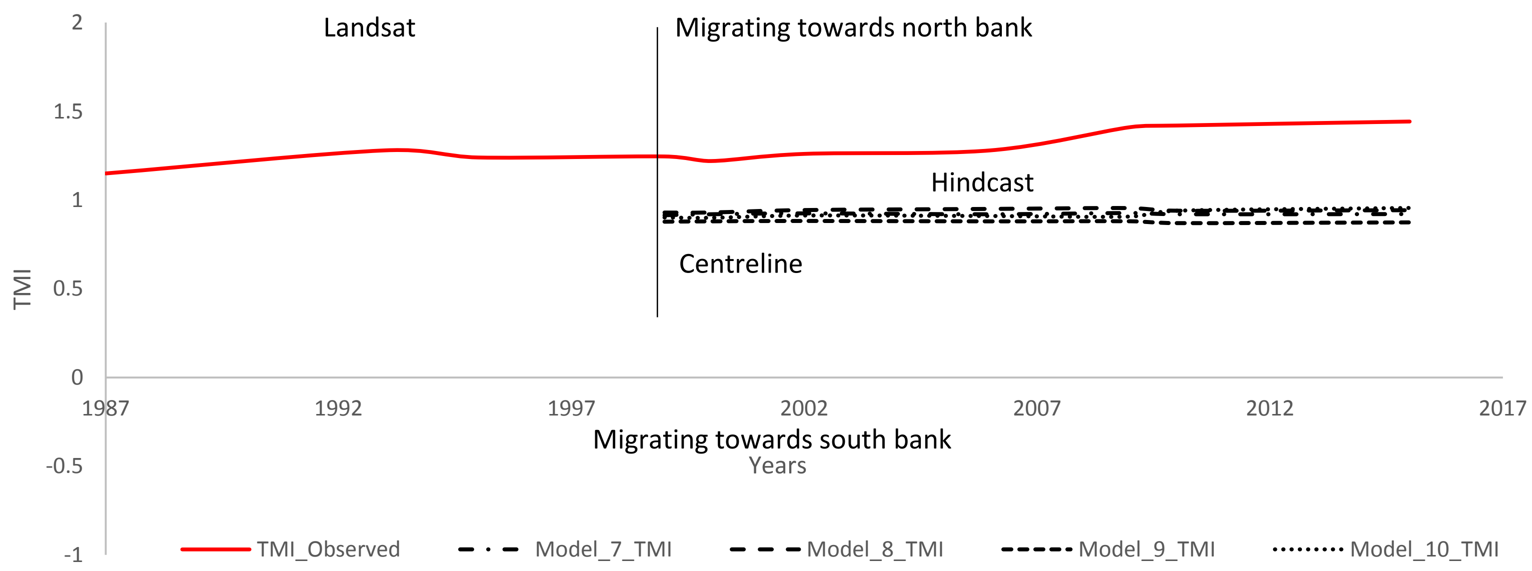

Appendix 2: MPFI value of the four C-L model of the sub-reach.

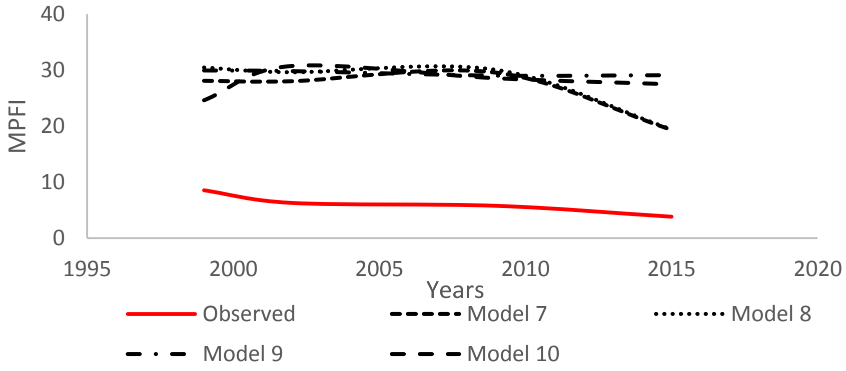

Figure 9.1: MPFI value of the four C-L model of the sub-reach 1.

MPFI Thresholds
MPFI < 6 – High braiding
6 > MPFI < 18 - Moderate braiding
MPFI > 18 - less braiding

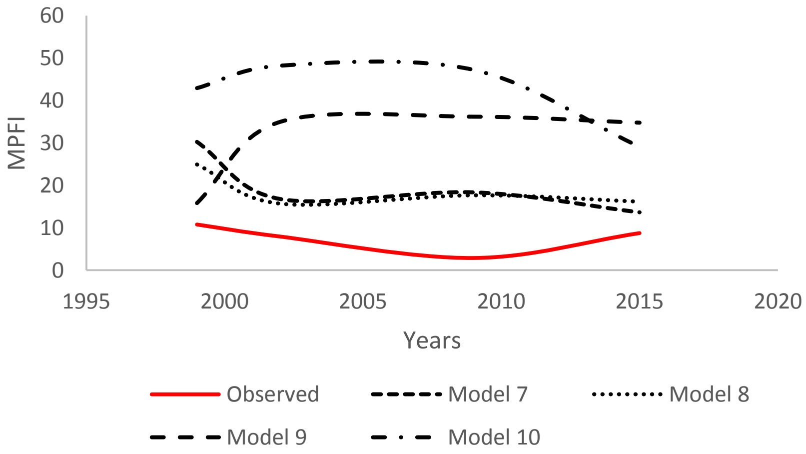

Figure 9.2: MPFI value of the four C-L model of the sub-reach 2.

Appendix 3: Bar Deformation of A -1, A 2, A 3 of C-L models

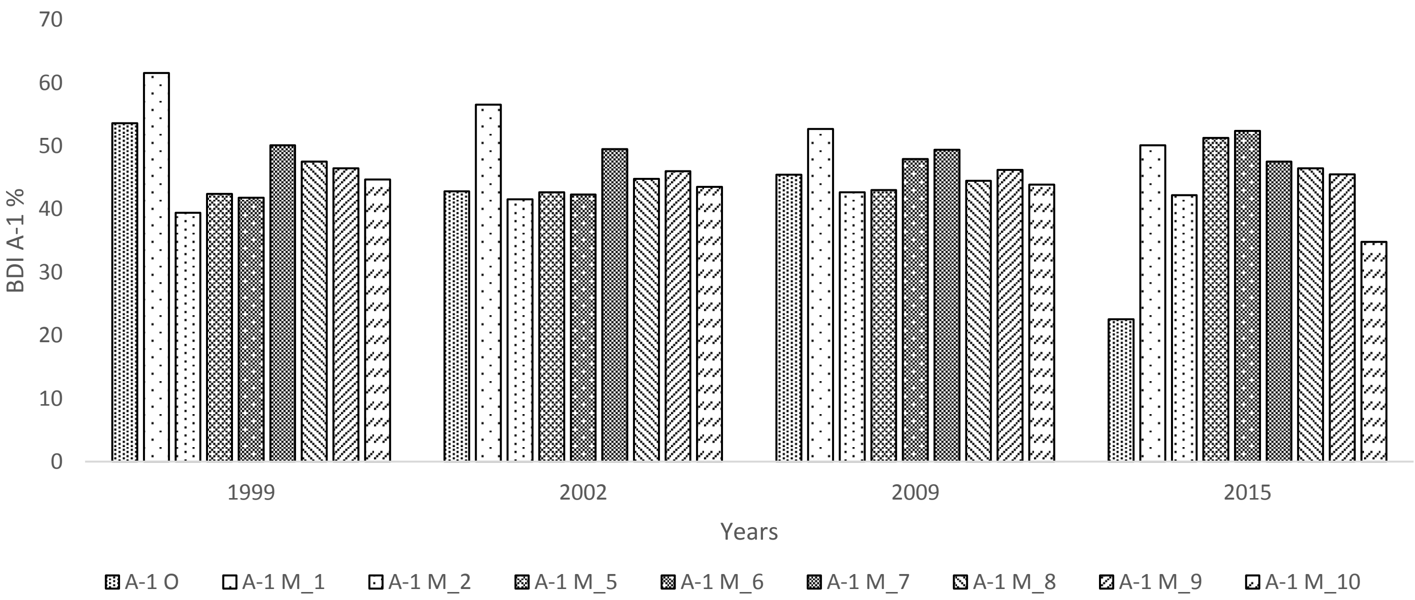

Figure 9.3: Bar Deformation of A -1 of C-L models

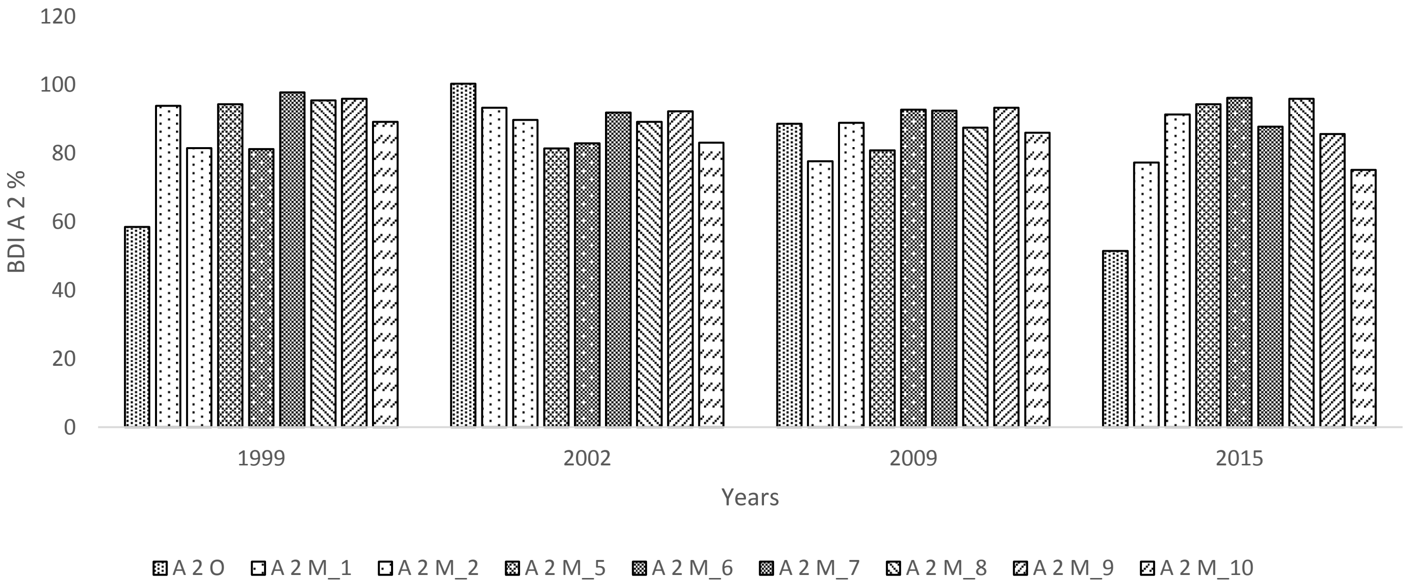

Figure 9.4: Bar Deformation of A 2 of C-L models

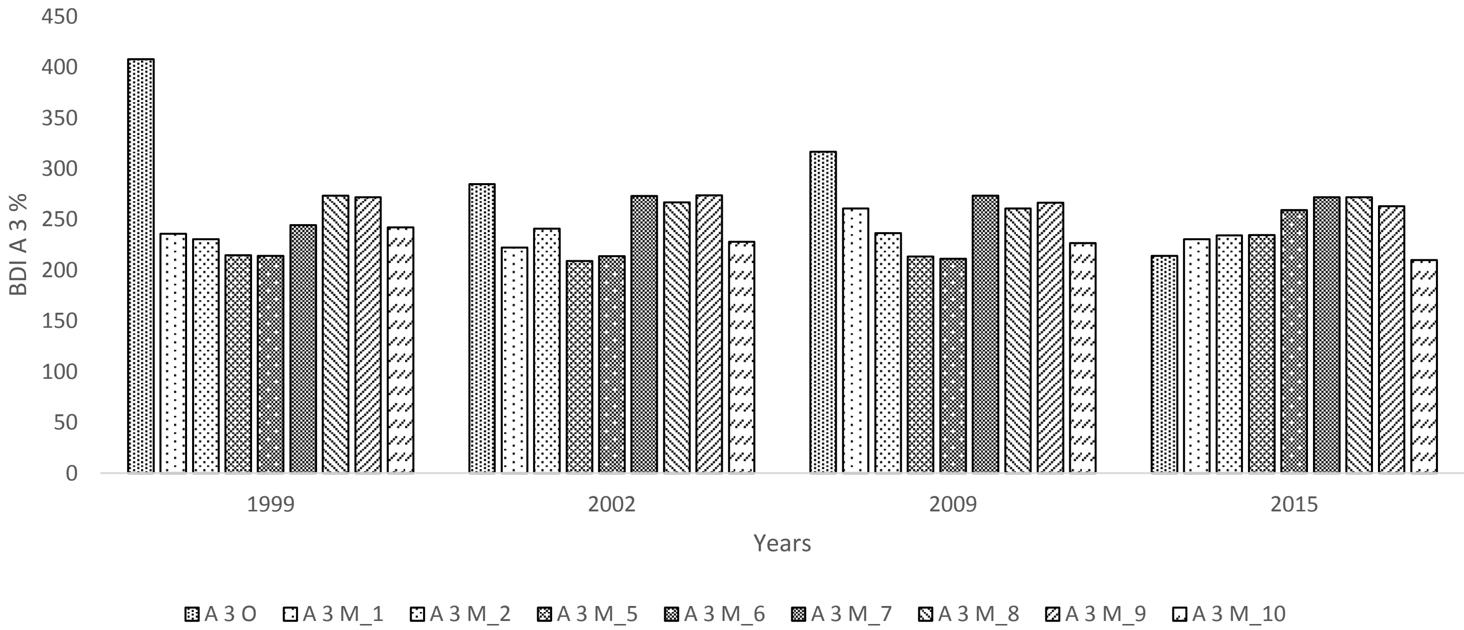

Figure 9.5: Bar Deformation of A 3 of C-L models

Appendix 4: Modelled and Observed cross-section 49 (1998 and 2007).

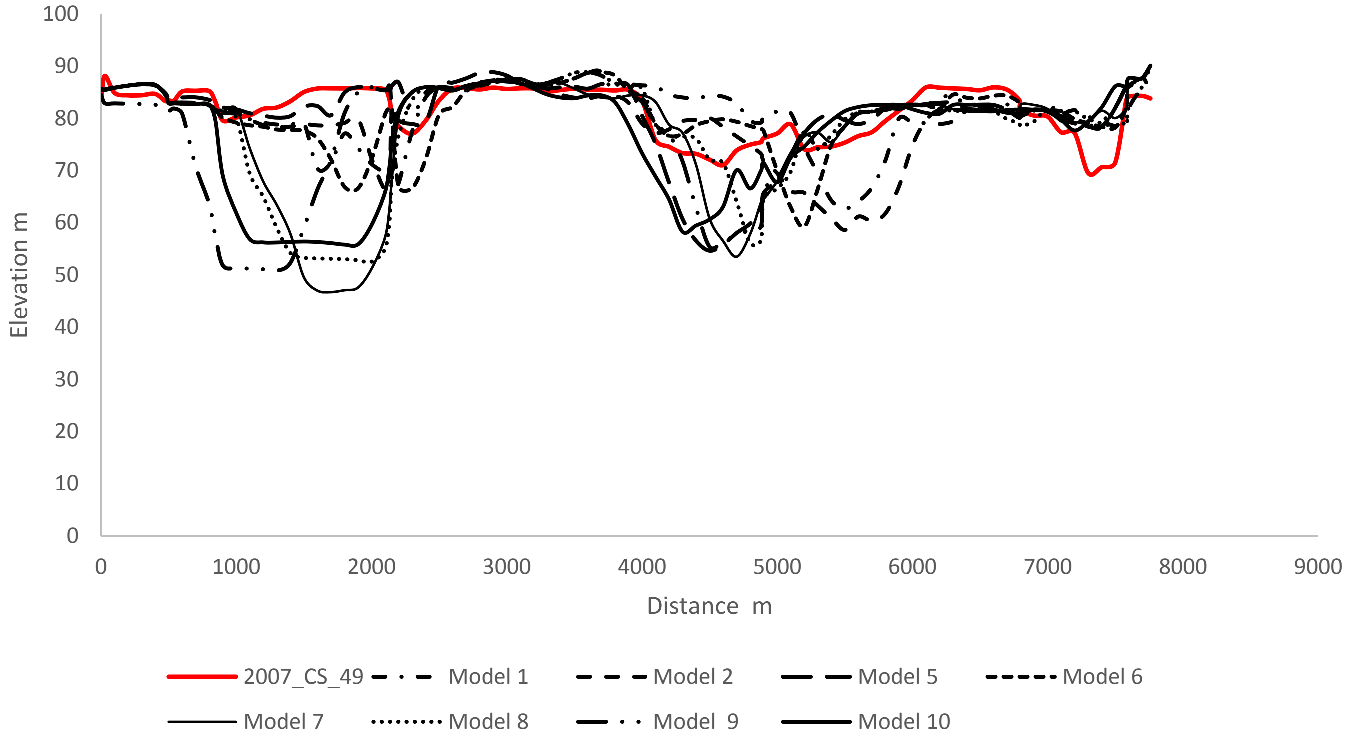

Figure 9.6: Modelled and Observed cross-section 49 (1998 and 2007).

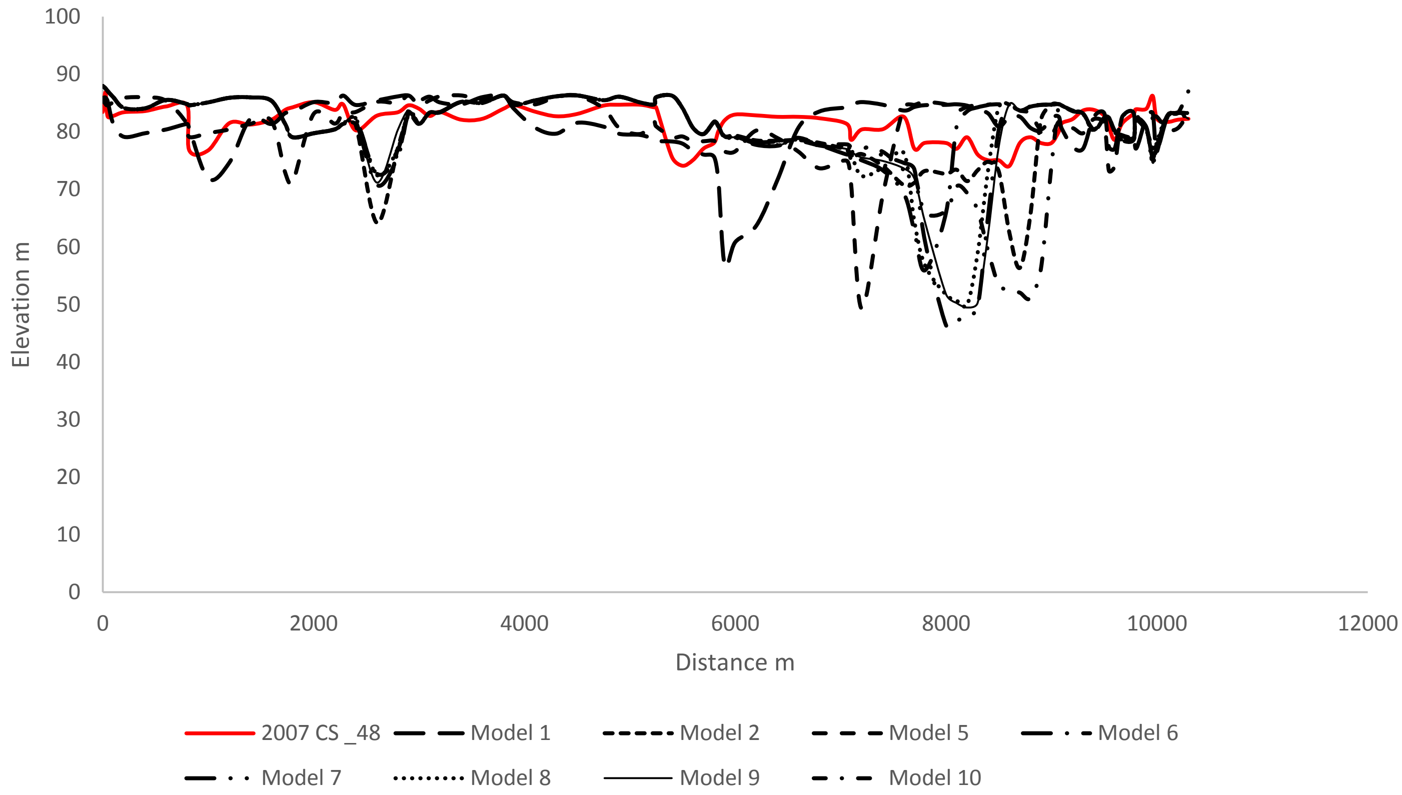

Figure 9.7: Modelled and Observed cross-section 48 (1998 and 2007).

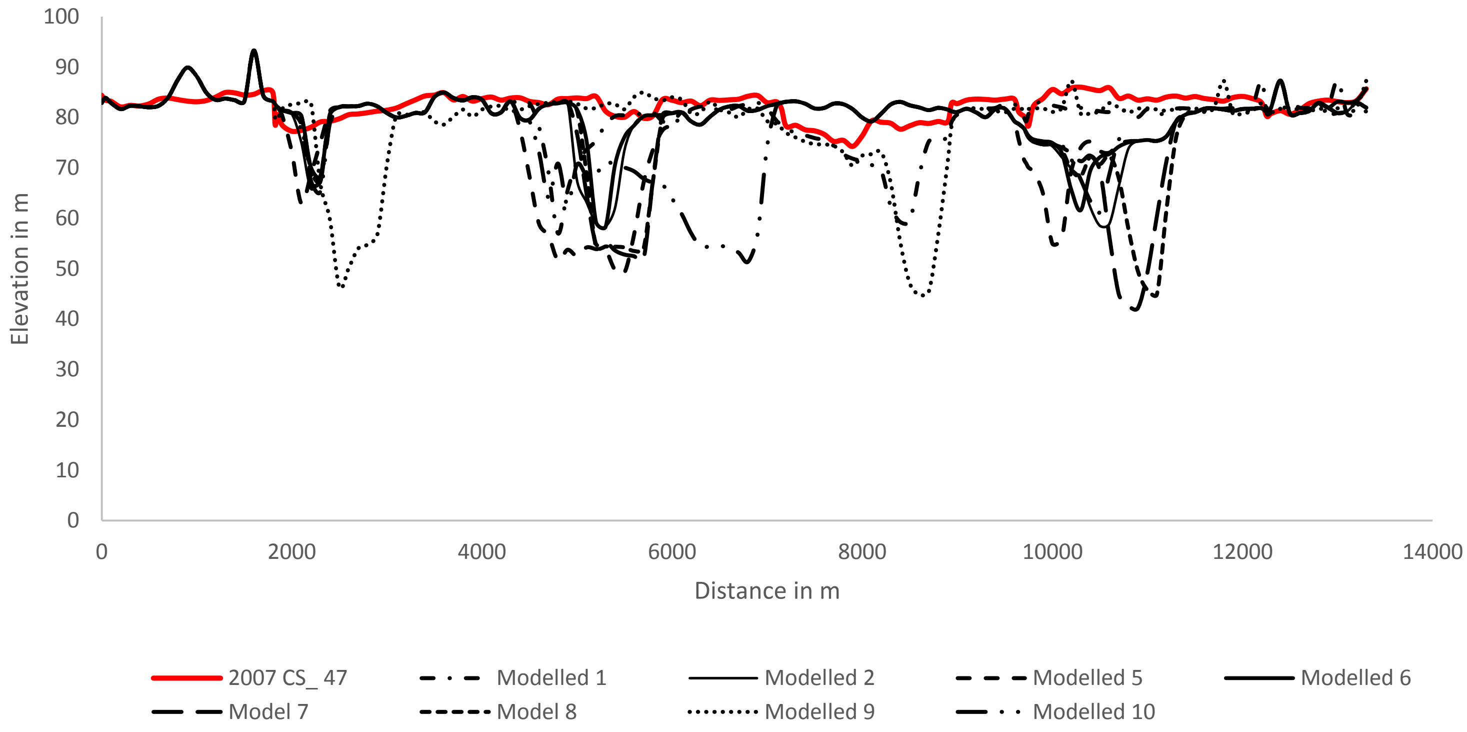

Figure 9.8: Modelled and Observed cross-section 47 (1998 and 2007).

Appendix 5: TMI of the two models of C-L+ (MacPDM and JULES).

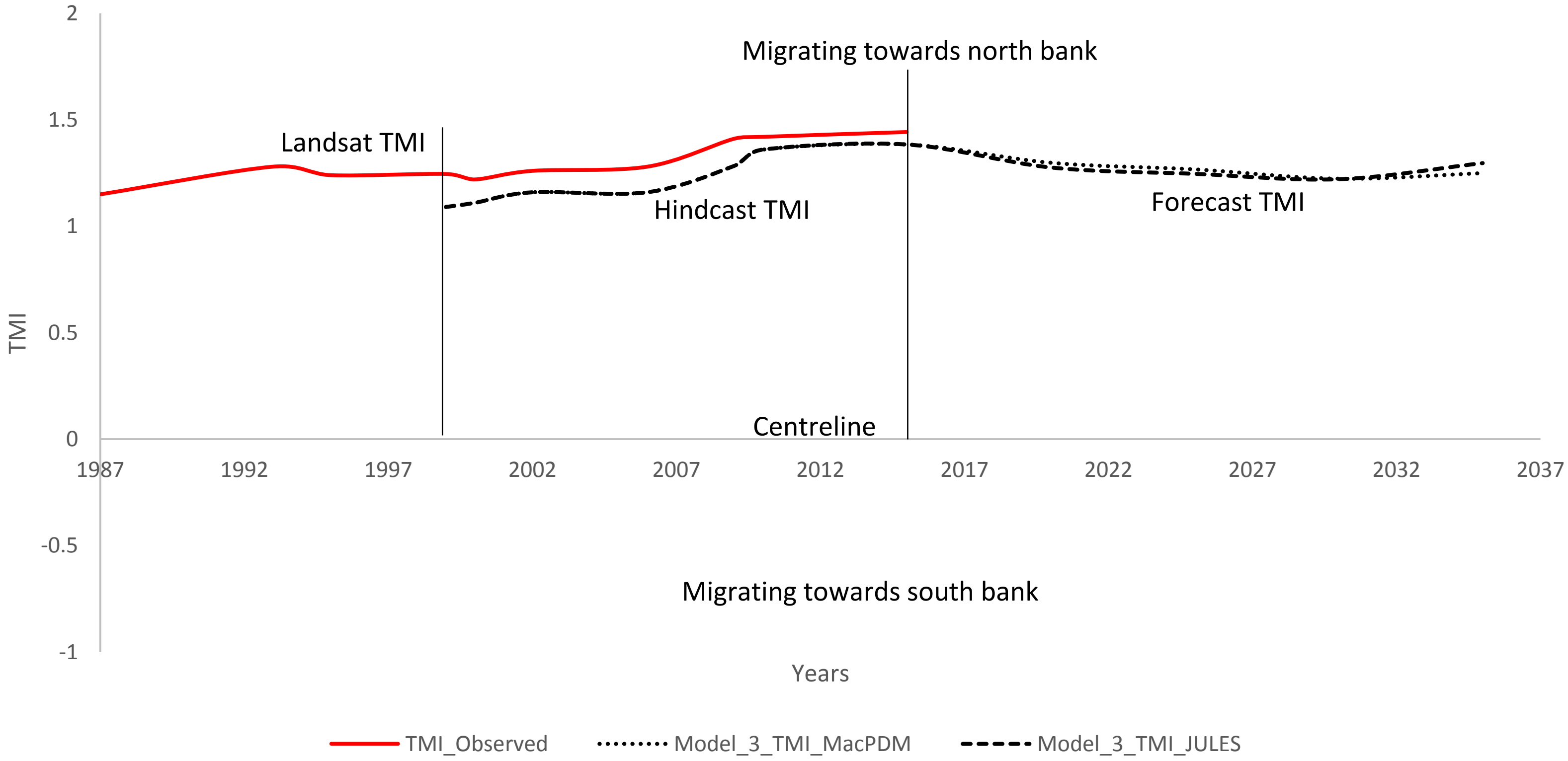

Figure 9.9: TMI of the two models of C-L+ (MacPDM and JULES).

Appendix 6: MPFI of sub reach 1 of MacPDM and JULES C-L+ models.

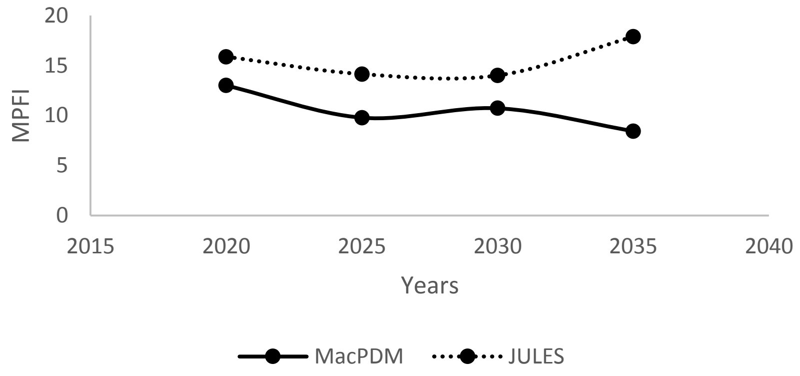

Figure 9.10: MPFI of sub reach 1 of MacPDM and JULES C-L+ models.

MPFI Thresholds
MPFI < 4 – High braiding
4 > MPFI < 19 - Moderate braiding
MPFI > 19 - less braiding

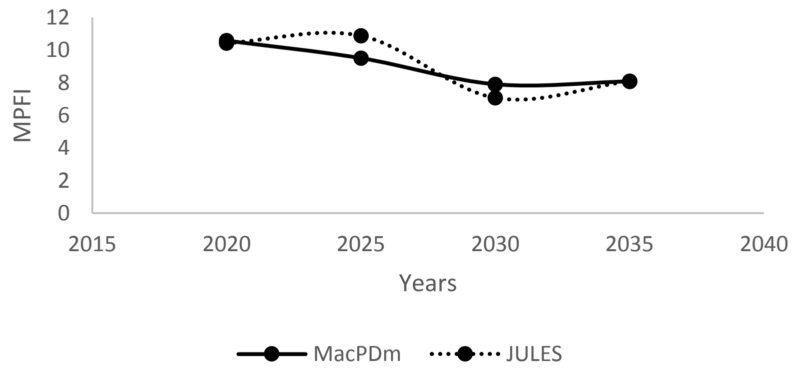

Figure 9.11: MPFI of sub reach 2 of MacPDM and JULES C-L+ models.

Appendix 7: MFGI of CS 49,48 and 47 of JULES and MacPDM C-L+ model.

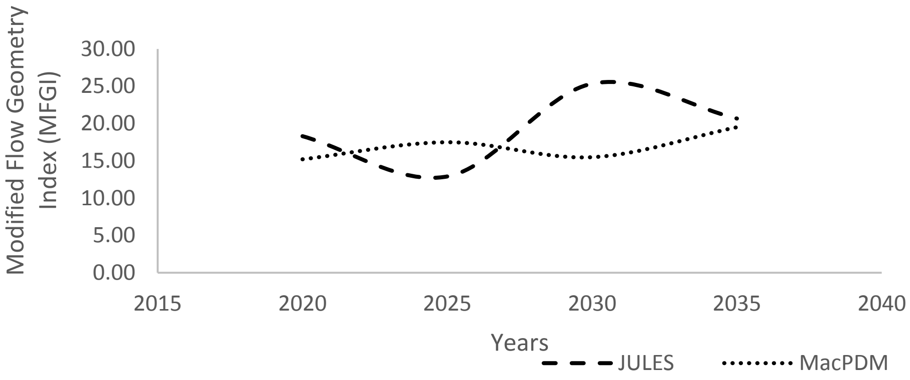

Figure 9.12: MFGI of CS 49 of JULES and MacPDM C-L+ model.

MFGI Thresholds
MFGI > 5 - Low Braided Intensity

5 > MFGI < 15 - Moderate Braiding

MFGI > 15 - High Braiding Intensity

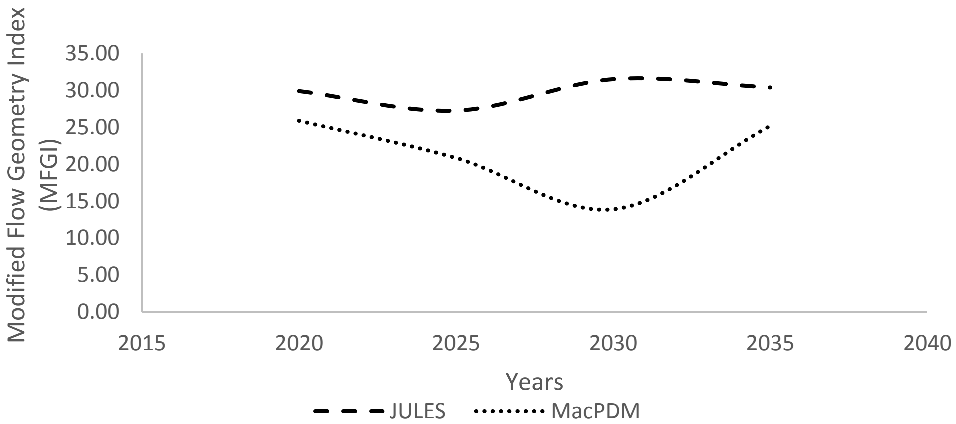

Figure 9.13: MFGI of CS 48 of JULES and MacPDM C-L+ model.

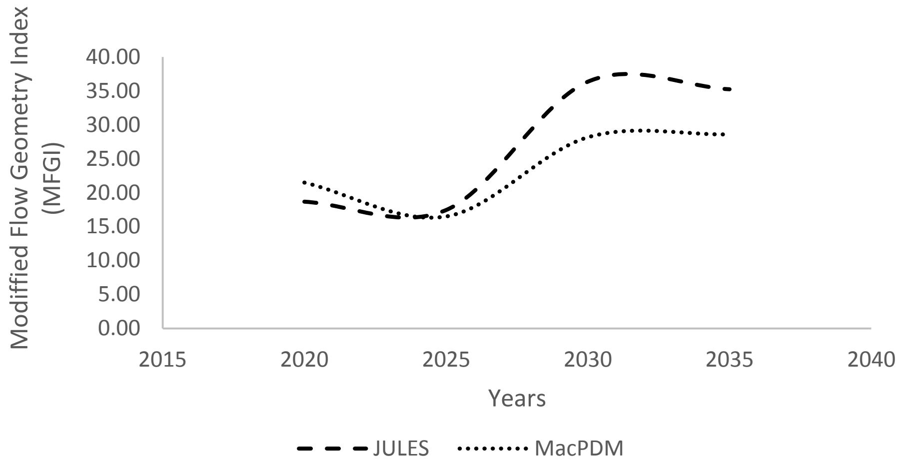

MFGI Thresholds
MFGI > 5 - Low Braided Intensity

5 > MFGI < 15 - Moderate Braiding

MFGI > 15 - High Braiding Intensity

Figure 9.14: MFGI of CS 47 JULES and MacPDM CL+ model.

Appendix 8: BDI of A-1 (a), A 2 (b), A 3 (c) of C-L+ model.

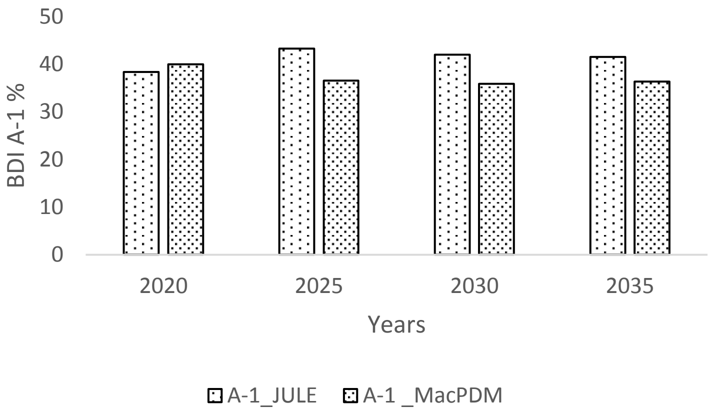

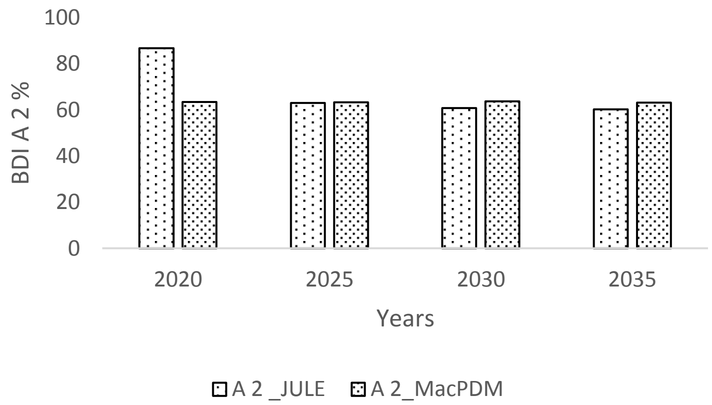

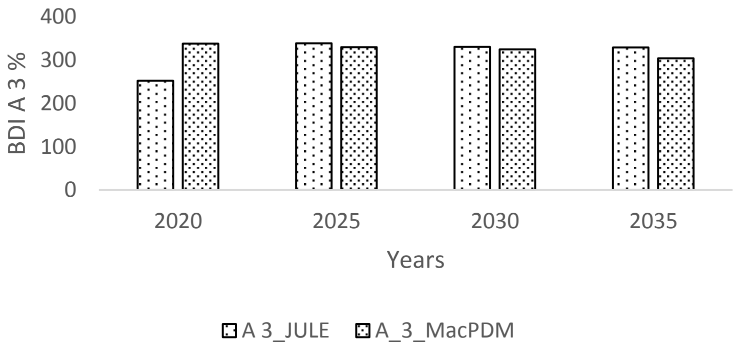

Figure 9.15: BDI of A-1 (a), A 2 (b), A 3 (c) of C-L+ model

Appendix 9: Forecasted cross-section 49 of the river Brahmaputra near Majuli Island (JULES and MacPDM).

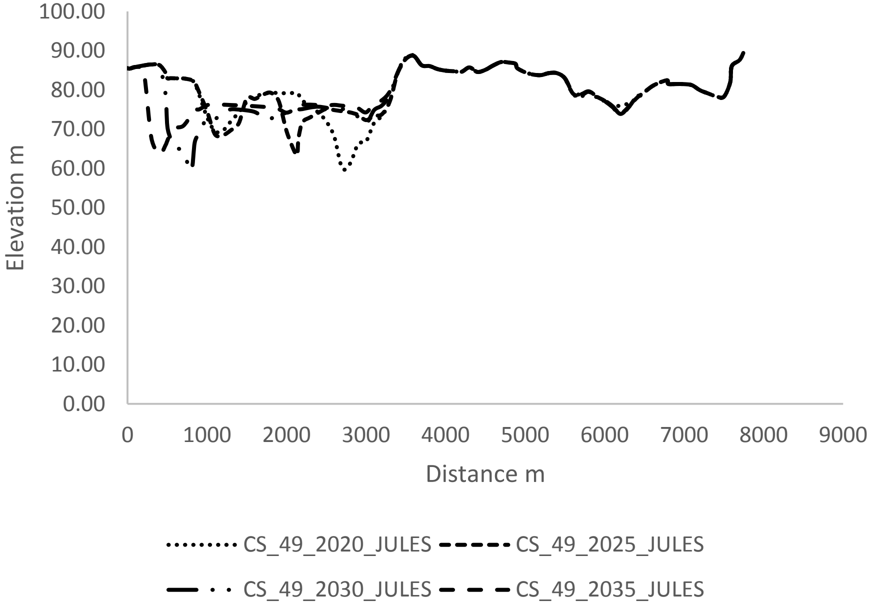

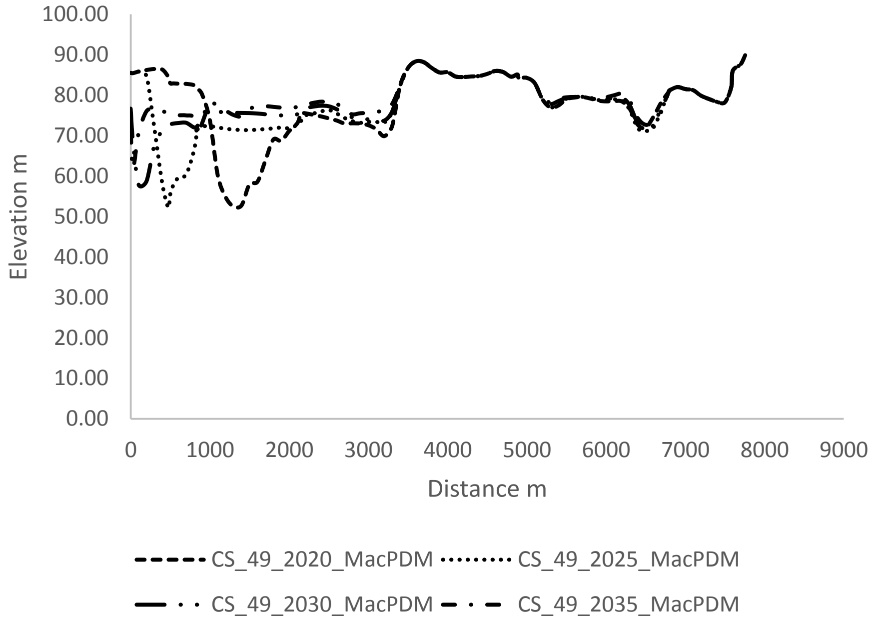

Figure 9.16: Forecasted cross-section 49 of the river Brahmaputra near Majuli Island (JULES and MacPDM).

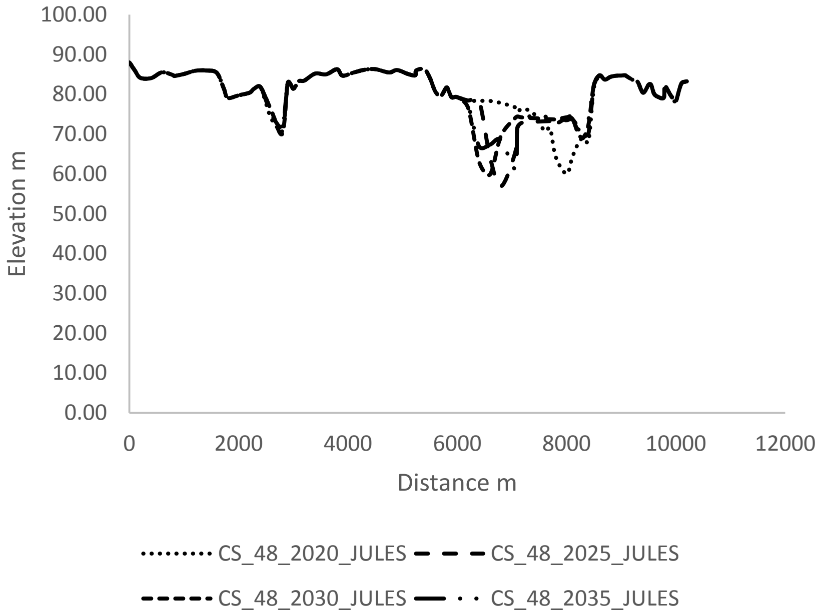

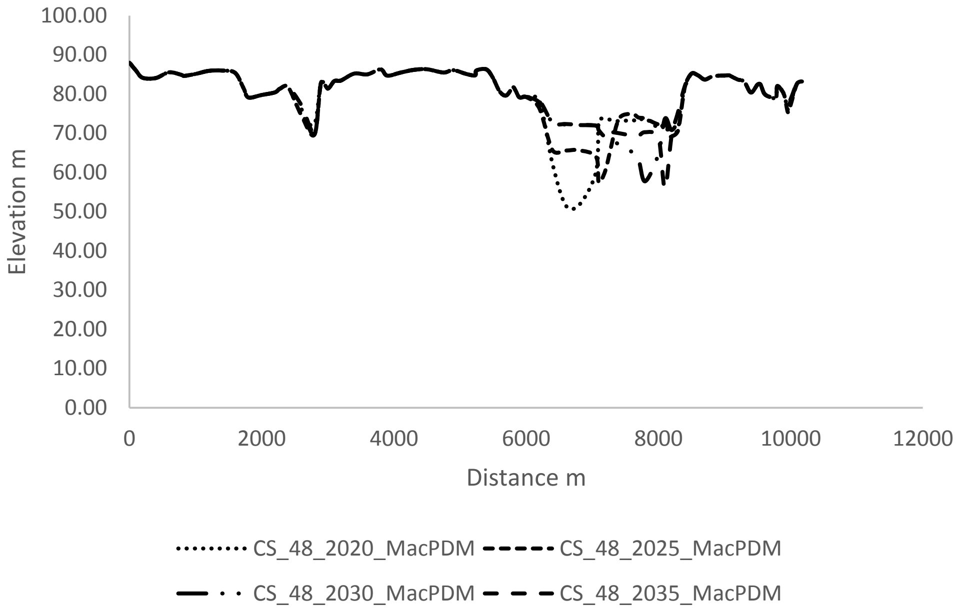

Figure 9.17: Forecasted cross-section 48 of the river Brahmaputra near Majuli Island (JULES and MacPDM).

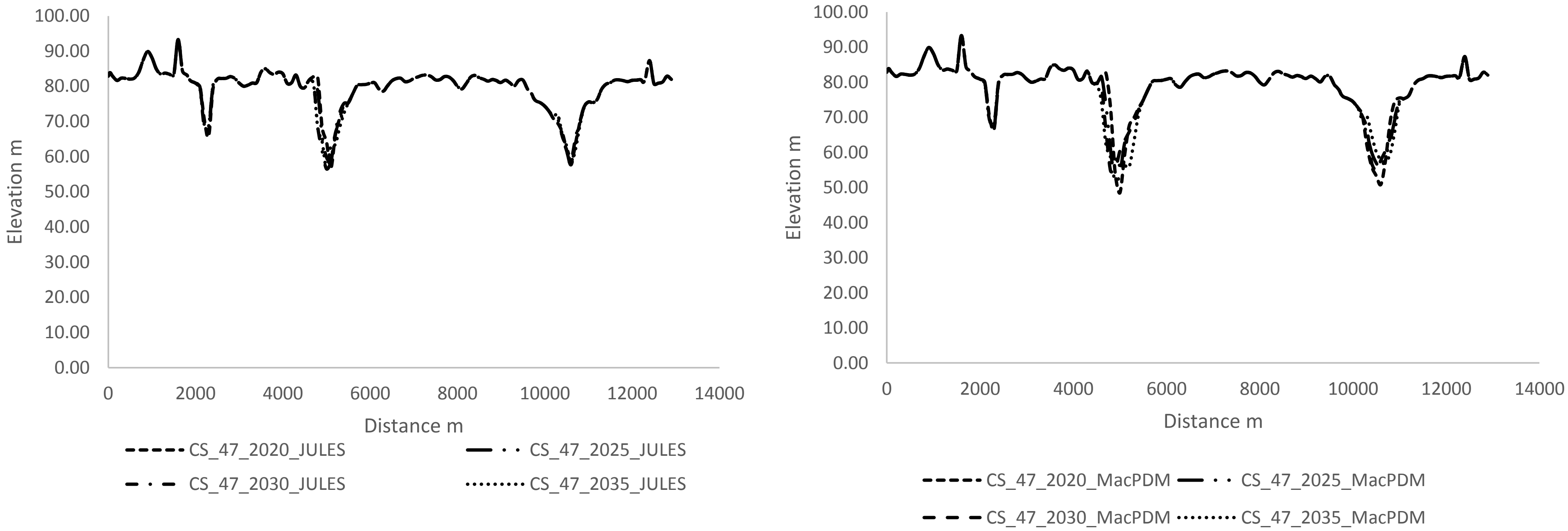

Figure 9.18: Forecasted cross-section 47 of the river Brahmaputra near Majuli Island (JULES and MacPDM).